TECHNISCHE UNIVERSITÄT MÜNCHEN

Fakultät für Chemie

WACKER-Lehrstuhl für Makromolekulare Chemie

Polyvinylphosphonates: The Next Generation of Smart Materials in Biomedical Applications

---

Christina Eva Schwarzenböck

Vollständiger Abdruck der von der Fakultät für Chemie der Technischen Universität München zur Erlangung des akademischen Grades eines

Doktors der Naturwissenschaften

genehmigten Dissertation.

Vorsitzender:	Priv.-Doz. Dr. Gerd Gemmecker
Prüfer der Dissertation:	1. Prof. Dr. Dr. h.c. Bernhard Rieger
	2. Prof. Dr. Ralf Huss
	3. apl. Prof. Dr. Wolfgang Eisenreich (mündliche Prüfung)
	3. Prof. Dr. Alexander L. Gerbes (schriftliche Beurteilung)

Die Dissertation wurde am 20.06.2018 bei der Technischen Universität München eingereicht und durch die Fakultät für Chemie am 09.11.2018 angenommen.

„Es ist nicht genug zu wissen, man muß auch anwenden;

es ist nicht genug zu wollen, man muß auch tun."

Johann Wolfgang von Goethe

Die vorliegende Arbeit wurde in der Zeit von Juni 2015 bis Juni 2018 am WACKER-Lehrstuhl für Makromolekulare Chemie, Technische Universität München, unter Betreuung von Herrn Prof. Dr. Dr. h.c. Bernhard Rieger angefertigt.

Acknowledgements

Zuerst möchte ich Ihnen, Professor Rieger, für Ihre Unterstützung bei meiner – vor allem anfänglich – ziemlich schwierigen Arbeit, für das interessante Thema, das ich bearbeiten durfte und Ihre allzeit offene Art danken. Als Chef haben Sie mir alle Freiheiten gelassen, die ich gebraucht habe, um das Beste aus meiner Forschung zu machen.

Professor Huss, Professor Nelson und Professor Nößner gilt ebenfalls mein Dank, da ohne Sie der biologische Teil meiner Arbeit und somit der sehr spannende Anwendungsbereich, unmöglich gewesen wäre. Anke und Sylke ihr wart tolle Laborkolleginnen und habt mir immer geholfen oder mich aufgemuntert, wenn es mal nicht so lief.

Carsten und Sergei möchte ich für die Organisation unseres manchmal etwas chaotischen Laboralltags danken. Ihr beide helft immer, wenn eines unserer vielen Geräte streikt, habt aber auch ein offenes Ohr für jegliche Probleme mit denen ich mich in meiner Zeit als Doktorandin auseinandersetzen musste. Vielen Dank dafür! Das ist wirklich nicht selbstverständlich. Mein herzlicher Dank geht auch an Frau Bauer, die immer alle organisatorischen Probleme spielend löst und einem so das Leben deutlich erleichtert. Ich möchte außerdem allen anderen Doktoranden und Mitarbeitern des Wacker-Lehrstuhls danken, die mich so nett aufgenommen haben und die Zeit dort so angenehm gemacht haben.

Besonders meine Laborkollegen Rike, Marina, Martin, Markus, Basti und Andi haben für eine allzeit gute Stimmung im Labor und eine entspannte Atmosphäre im Alltag gesorgt. Desweiteren möchte ich Daniel, Philipp, Bene, Peter und Alex für die vielen fachlichen Diskussionen, das mehrfache Korrekturlesen und die große Hilfe bei der Publikation meiner Manuskripte danken. Außerdem konnte man mit euch auch in den Pausen und bei der ein oder anderen Feier viel Spaß haben!

Ein weiterer großer Dank gilt all meinen Studenten und Azubis. Besonders sollten Kerstin, Philipp, Anna und Caro erwähnt werden, die alle längere Zeit mit mir gearbeitet haben und meine Arbeit in dieser Form erst ermöglicht haben.

Mama und Papa, Pezi und Tom, ihr habt alle keinerlei Interesse an Naturwissenschaften, aber ihr habt mich, egal was ich machen wollte, immer unterstützt. Ihr seid eine tolle Familie und ihr habt mich zu der gemacht, die ich heute bin. Es ist wirklich schön euch zu haben. Alex und Maria, ihr versteht mich da schon ein bisschen besser und ich freue mich wirklich sehr, dass ihr ein Teil unserer wachsenden Familie geworden seid.

Stefan, du begleitest mich jetzt schon seit der Kollegstufe durch all meine Ausbildungsebenen. Ich war in diesen neun Jahren sicher nicht immer einfach und gut drauf, aber wir haben gemeinsam immer einen Weg gefunden. Ich bin sicher, dass das auch noch lange so bleibt. Danke für deine immerwährende Unterstützung!

Table of Content

List of Abbreviations

2VP	2-vinylpyridine
CMC	critical micelle concentration
Cp	cyclopentadienyl
DCM	dichloromethane
DAlVP	diallyl vinylphosphonate
DAVP	dialkyl vinylphosphonate
DEEP	diethyl ethylphosphonate
DEVP	diethyl vinylphosphonate
DIVP	diisopropyl vinylphosphonate
DLS	dynamic light scattering
DMEM	*Dulbecco's* modified eagle medium
DMF	*N,N*-dimethylformamide
DMVP	dimethyl vinylphosphonate
DNA	desoxyribonucleic acid
DOX	doxorubicin
DSC	differential scanning calorimetry
ESI-MS	electrospray ionization mass spectrometry
FCS	fetal calf serum
i.e.	that is (*latin: id est*)
IPOx	2-isopropenyl-2-oxazoline
LCST	lower critical solution temperature
MAA	methacrylamide
Me	methyl
MMA	methyl methacrylate
PBS	phosphate buffered saline

PDI	polydispersity index
PDAVP	poly-DAVP
PEG	poly(ethylene glycol)
PNIPAAm	poly(*N*-isopropylacrylamide)
PPE	poly(phosphoester)
PVPA	poly(vinylphosphonic acid)
RNA	ribonucleic acid
r.t.	room temperature
THF	tetrahydrofuran
TMS	trimethylsilyl
TMSBr	bromotrimethylsilane
TOF	turn-over frequency
UCST	upper critical solution temperature

Publication List

- C. Schwarzenböck, A. Schaffer, P. Pahl, P. J. Nelson, R. Huss, B. Rieger, *Polym. Chem.* **2018**, *9*, 284-290, rewarded with cover page. „Precise Synthesis of Thermoresponsive Polyvinylphosphonate-Biomolecule Conjugates *via* Thiol-ene Click Chemistry."
- C. Schwarzenböck, A. Schaffer, E. Nößner, P. J. Nelson, R. Huss, B. Rieger, *Chem. Eur. J.* **2018**, *24*, 2584-2587. „Fluorescent Polyvinylphosphonate Bioconjugates for Selective Cellular Delivery."
- C. Schwarzenböck, P. J. Nelson, R. Huss, B. Rieger, *Nanoscale* **2018**, *10*, 16062-16068. „Synthesis of Next Generation Dual-Responsive Cross-Linked Nanoparticles and their Application to Anti-Cancer Drug Delivery."

Publications beyond the Scope of this Thesis:

- C. Schwarzenböck, S. I. Vagin, W. R. Heinz, P. J. Nelson, B. Rieger, *Macromol. Rapid Commun.* **2018**, *39*, 1800259, rewarded with cover page. „Studies on the Biocompatibility of Poly(diethyl vinylphosphonate) with a New Fluorescent Marker".
- P. Pahl, C. Schwarzenböck, F. A. D. Herz, B. S. Soller, C. Jandl, B. Rieger, *Macromol.* **2017**, *50*, 6569-6576. „Core-First Synthesis of Three-Armed Star-Shaped Polymers by Rare Earth Metal-Mediated Group Transfer Polymerization."
- P. T. Altenbuchner, P. D. L. Werz, P. Schöppner, F. Adams, A. Kronast, C. Schwarzenböck, A. Pöthig, C. Jandl, M. Haslbeck, B. Rieger, *Chem. Eur. J.* **2016**, *22*, 14576-14584. "Next Generation Multiresponsive Nanocarriers for Targeted Drug Delivery to Cancer Cells."

1 Introduction

Human history is divided into epochs based on the material mainly employed for devices of daily use. Thousands of years ago, every chair, weapon, and tool was made from stone. Fortunately, a pioneering chemist found out how to reduce iron oxide, with the help of coke, into iron, inducing a new age. Novel tools, machines and transport vehicles were invented and the daily life changed dramatically, with the advancing industrial development.[1] The next foundation stone, toward a new era, was laid by pioneer *Hermann Staudinger* in the 1920s. He introduced the concept of the covalent bond formation between small monomers, to receive a macromolecule, with a large molecular weight. The field of polymer chemistry was born.[2] In 1953 *Hermann Staudinger* was awarded with the Nobel Prize.[3] And already in the 1980s the world's annual steel production by volume was outperformed by polymers.[4] The global production of plastics is steadily growing with a yearly expansion of 8.7% from 1950 to 2012 (Figure 1.1) and reached the enormous mass of 335 million tons in 2016.[5, 6]

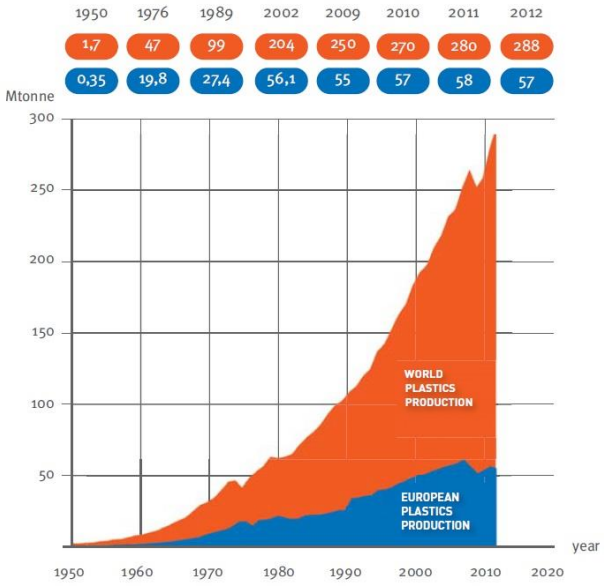

Figure 1.1: World plastics production 1950-2012.[6]

Nowadays, plastics are an essential material in our modern society. We drink from polyethylene bottles, build poly(vinylchloride) floors, windows and pipes in our houses. Poly(propylene) is used for many automotive parts, touch screens are made from poly(methylmethacrylate), disposable cups consist of polystyrene and low density polyethylene is indispensable for agricultural films.[5] More and more complex materials like poly(para-phenyleneterephthalamide) are explored, which have a higher tensile strength than steel. Furthermore, this polymer has a strength-to-weight ratio six-fold higher than steel. Under its trade name Kevlar® it is especially known as the material of bullet proof vests, but its main field of application is in airplanes where weight reduction is of enormous value.[1]

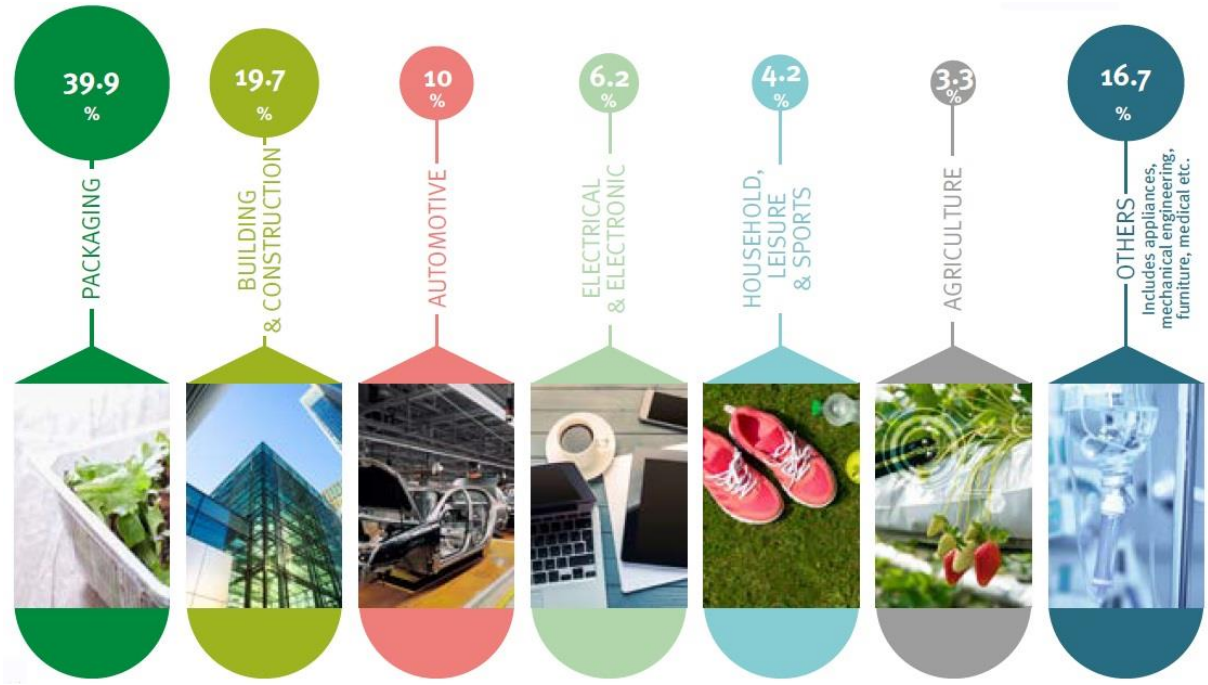

Figure 1.2: Main market sectors of the plastics converter demand in 2016.[5]

Without plastics, we would not have all the electronic devices that connect us around the globe each and every day. Also our leisure time would be very different without the modern balls, skis, helmets, sportswear and all other sorts of equipment, we are used to since so many years. However, these are all commodity articles, which belong to our lives, but the really life changing developments happened and are still ongoing in the health care industry. Plastic prostheses replace body parts and enable athletes to participate in the Paralympic Games. Plastics can unblock blood vessels, enable hearing impaired people to live normal lives and build the matrix for tissue implants.[6] All these data present how much development was already done in polymer science in the last few decades. This could imply that not much effort toward more sophisticated materials is made anymore. But in contrast, the plastics sector is one of the top five most innovative industries in Europe. One of 25 non-academic patents between 2003 and 2012 can be attributed to this manufacturing branch.[7] In the 21st century, new tasks in important fields like tissue engineering, cancer research, and nanotechnology require more complex and sophisticated materials than the commonly used techniques could deliver (*i.e.* step and chain polymerizations). Living polymerizations are the most promising candidates for the production of future functional materials. Over the last 20 years, a lot of research was done on living radical polymerizations. The living character of these reactions can only be enforced through low radical concentrations and results rather low propagation rates. Consequently, radical reactions cannot be the optimal choice for the next generation polymerization techniques. Only catalytic precision polymerizations can result in the multi-responsive functional polymer materials of tomorrow.[4]

2 Theoretical Background

2.1 Rare Earth Metal-Mediated Group Transfer Polymerization

The development of a non-radical living-type polymerization was in the 1980s mainly achieved through the American chemist *Owen W. Webster* and his coworkers.[8] He introduced the concept of group transfer polymerization (GTP) in 1983. The polymerization was driven by a silyl ketene acetal (SKA) as initiator and a *Lewis* acid to activate the monomer. At this time the polymerization was supposed to follow an associative mechanism, where the SKA group is transferred from the initiator to the monomer, *via* repeated conjugate addition.[8] The mechanism underlying this polymerization type had to be investigated and was a hot topic of scientific discussions, in the first years of its development.[9] Experimental studies revealed the dissociative nature of the underlying reaction mechanism of GTP.[10-13] Ensuing it is generally accepted that nucleophiles reversibly remove the silyl group from the chain end to form the active enolate, which attacks the next unreacted monomer (Scheme 2.1).[14] However, the misleading term of group transfer polymerization remains in literature.[15, 16]

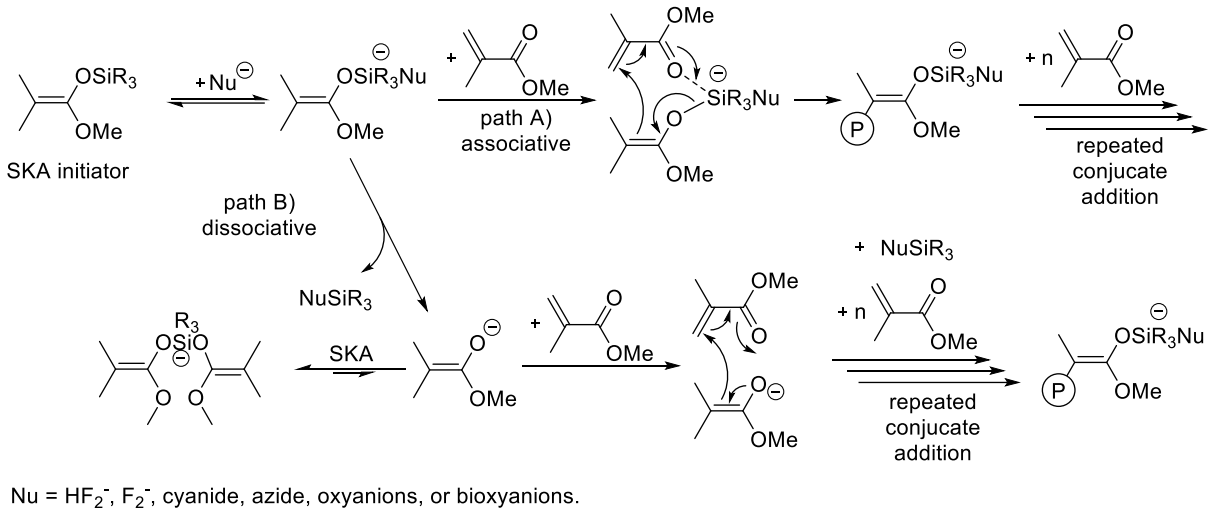

Scheme 2.1: A) Associative and B) dissociative mechanism of SKA-GTP of methyl methacrylate. Reprinted with permission from ref. [4]. Copyright 2016 American Chemical Society.

SKA-GTP can be conducted at elevated temperatures, leading to dispersing agents for pigmented inks and automobile finishes.[15] A great variety of *Michael*-type monomers could be polymerized with SKA-GTP protocols, to yield (co)polymers with specific properties. The obtained dispersions and rheology additives are of interest for academia as well as industry.[17-21] One of the less successful applications was the copolymerization of methyl methacrylate (MMA) and diethyl vinylphosphonate (DEVP). In this example, a maximal incorporation of DEVP of less than 2 mol% was reached. This leads to the conclusion that an insufficient activation of the monomer was reached and that subsequently another polymerization method

needs to be applied for this copolymerization.[22] Rare earth metal-mediated group transfer polymerization (REM-GTP) renders this copolymerization possible.

REM-GTP is a potent tool toward the precise synthesis of tailor-made functional materials. This method succeeds in the generation of polymers, with defined molecular weights and narrow polydispersities (PDI < 1.1). It combines the best characteristics of the living anionic and the coordinative polymerization type. Figure 2.1 indicates the living character and the, throughout the polymerization reaction, constantly narrow molecular weight distribution.[4]

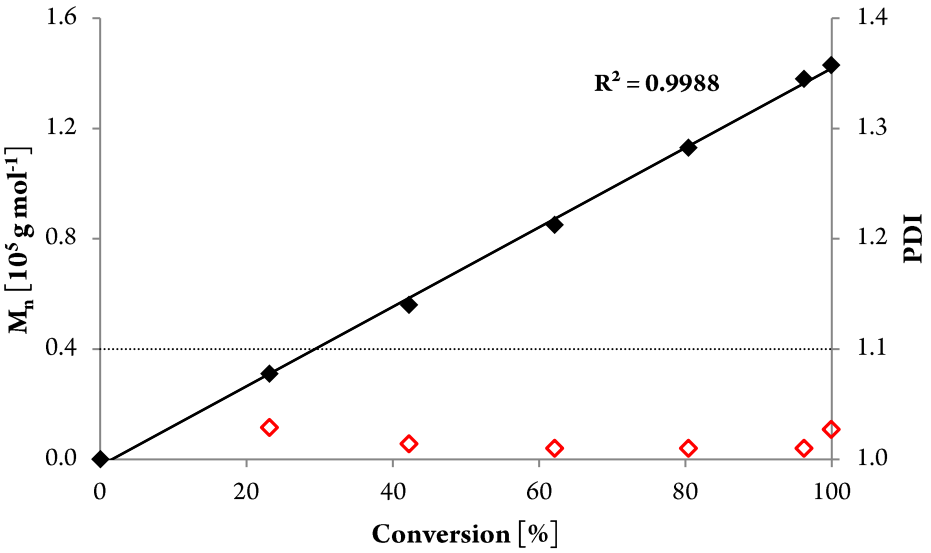

Figure 2.1: Molecular weight and molecular weight distribution of PDEVP as a function of conversion, produced with $Cp_2Y(CH_2(C_5H_2Me_2N))$ as catalyst. Adapted with permission from ref. [23]. Copyright 2015 American Chemical Society.

The first reports on the living polymerization of MMA catalyzed with metallocene complexes were published of two independent groups in 1992. The neutral $[(C_5Me_5)_2SmH]_2$ was the catalyst of choice for the *Yasuda* group,[24] whereas *Collins* and *Ward*[25] used the cationic Cp_2ZrMe_2 system (Cp = cyclopentadienyl, Me = methyl). The samarium complex showed an applicability over the enormous temperature range of –95 to 40 °C. The obtained polymers had low polydispersities (PDI < 1.05) and syndiotacticities of up to 95%.[24, 26] *Yasuda et al.* proposed a similar mechanism like the discussed dissociative one, *via* repeated conjugate addition in case of the SKA initiators. The initiation step proceeds through the attack of the hydride on the first MMA monomer. The propagation was demonstrated with the help of the crystal structure of the MMA adduct. It showed an eight-membered monometallic ester enolate species consisting of the catalyst with two coordinated monomers (Scheme 2.2). The tacticity is thought to be caused by the repulsion of the two methyl groups in the eight-membered transition state.[24, 27]

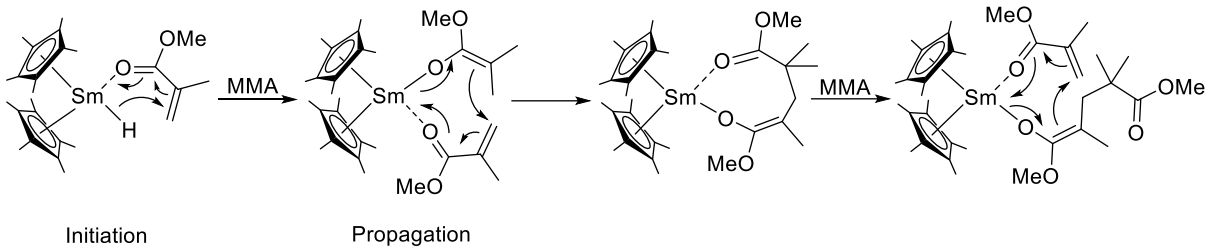

Scheme 2.2: *Yasuda*-type mechanism of the polymerization of MMA.[27] Adapted with permission from ref. [14]. Copyright 2018 John Wiley and Sons.

The polymerization catalyzed by the cationic zirconocene follows the same reaction mechanism. This was already proven by *Collins* and *Ward* through ^{13}C-labelled initiators in 1992.[25] In the first years of GTP mainly acrylates and acrylamides were polymerized. However, this living polymerization type can be used for a variety of *Michael*-type acceptor monomers, like MMA, DEVP, 2-vinylpyridine (2VP), 2-isopropenyl-2-oxazoline (IPOx), and many more (Figure 2.2).

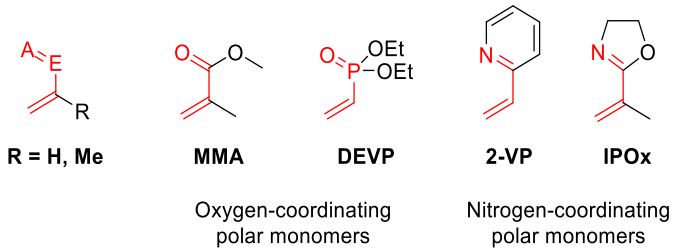

Figure 2.2: Most commonly used *Michael*-type monomers for REM-GTP. Adapted with permission from ref. [4]. Copyright 2016 American Chemical Society.

The properties of the obtained materials depend mainly on the functional groups of the polymers. Today a broad range of polymers consisting of a multiplicity of monomers is known, however most of them consist of carbon, hydrogen, oxygen, nitrogen, silicon, sulfur or halogens. Surprisingly only few synthetic macromolecules comprising phosphorus exist.[4]

2.2 Phosphorus-Containing Polymers

In contrast, in nature omnipresent phosphorus-containing polymers are the deoxyribonucleic acid (DNA) and the ribonucleic acid (RNA). These macromolecules store the genetic information required in the growth, evolution, operation, and reproduction of all living organisms.[28, 29] Nevertheless synthetic poly(phosphates) are prone to hydrolysis and, are therefore, not very stable. Examples for the most prominent phosphorus-containing polymers are presented in Scheme 2.3.

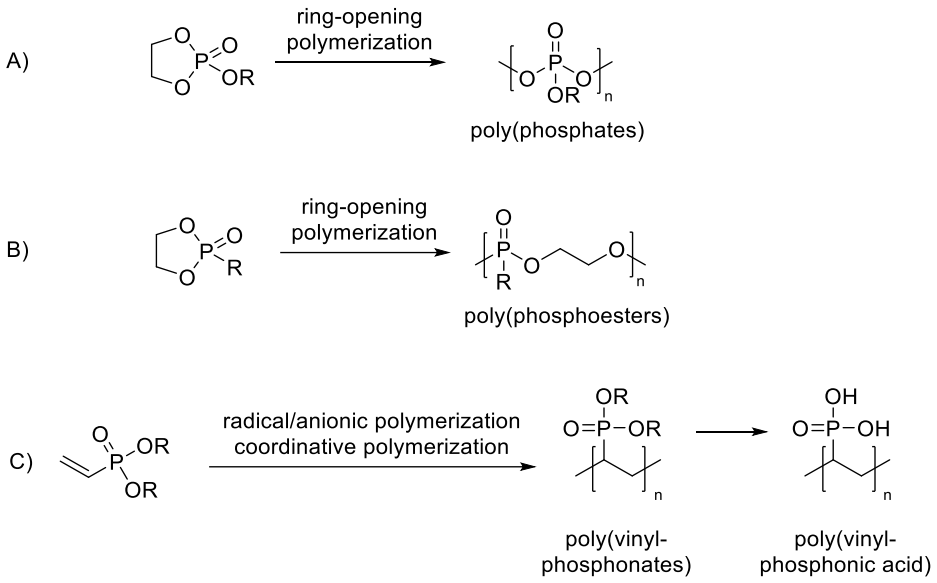

Scheme 2.3: Phosphorus-containing polymers and their monomers. A) Poly(phosphates), B) poly(phosphoesters) and C) poly(vinylphosphonates).[4]

One well-studied polymer class are the poly(phosphoesters) (PPEs), which are promising candidates for biomedical applications, due to their biocompatibility and structural analogy to naturally occurring biopolymers. Additionally, these polymers show a biodegradability through hydrolytic or enzymatic decay. The physicochemical properties of PPEs can be tailored, through adjusting its constitution. Many side chain modifications are feasible, which renders the PPEs to be structurally versatile. PPE can be used for a plurality of applications from drug and gene delivery to tissue engineering.[30-32] The most prominent method to produce PPEs is the ring-opening polymerization of cyclic phosphoesters as presented in Scheme 2.3. These monomers are easily accessible, *via* the condensation of the commercially available 2-chloro-2-oxo-1,3,2-dioxaphospholane with alcohols.[33] In one recent study improved paclitaxel delivery *in vitro* and *in vivo* could be shown with poly(phosphoester)-based nanocarriers. Both biodegradable polymeric micelles and shell cross-linked particles were prepared and successfully applied.[34]

Another important group of phosphorus-containing polymers are polyvinylphosphonates. They are, like PPE, biocompatible and water soluble, but the phosphorus is located in the side chain in contrast to PPE.

2.3 Polyvinylphosphonates

Besides their water solubility and biocompatibility, polyvinylphosphonates exhibit a tunable lower critical solution temperature. They are therefore classified as responsive or smart materials. To date many different vinylphosphonate monomers exist, which allows the synthesis of an exceptional spectrum of polymers with unique characteristics.[35-37]

2.3.1 Monomers

Vinylphosphonate monomers were already developed in the 1940s. Starting materials for the synthesis are triethyl or triisopropyl phosphite, which react in a *Michaelis-Arbusov* rearrangement, followed by an $E1_{cb}$ elimination to the desired products (Scheme 2.4 A). The monomers can be obtained in good yields and high purities.[38, 39] For diaryl vinylphosphonates an alternative three step synthetic route has to be used. It starts with the *Kabachnik* rearrangement of tris(2-chloroethyl)phosphite to yield bis(2-chloroethyl)(2-chloroethyl) phosphonate. Following, a chlorination with thionyl chloride is performed to gain (2-chloroethyl)phosphonic dichloride. The dichloride can be esterified with an alcohol like 4-methylphenol and followed by a base induced elimination toward the vinylphosphonate product (Scheme 2.4 B).[40-42]

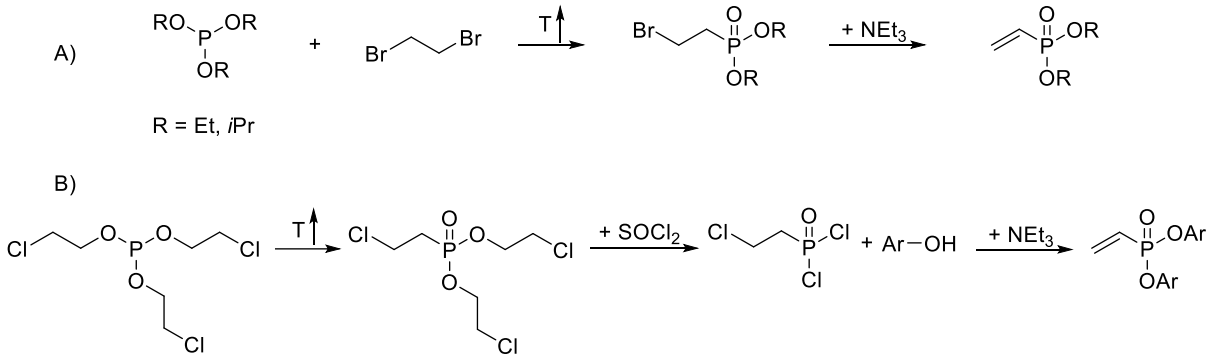

Scheme 2.4: A) Synthesis of dialkyl vinylphosphonates *via Michaelis-Arbusov* reaction. B) Synthesis of diaryl vinylphosphonates *via Kabachnik* rearrangement.

Vinylphosphonates can be used for *Diels-Alder* cyclizations, 1,4-additions, thiol-ene click reactions and polymerizations.[43-45] The following chapters will focus on polymerization of vinylphosphonates and the characteristics of the obtained polymers.

2.3.2 Polymerization of Vinylphosphonates

Polymers with a saturated hydrocarbon backbone and phosphoester side chains, are yielded through the homopolymerization of dialkyl vinylphosphonates (DAVPs). This structural motif makes the macromolecules stable toward hydrolysis in contrast to, for example, the above described, PPEs. Therefore, it is surprising that for a long time only a few studies regarding the polymerization of vinylphosphonates were published. The main cause for this observation might be the poor results, obtained through the application of classical polymerization methods. Already short time after the synthesis of the monomers, first radical polymerization attempts were made yielding only oligomers. There are many reasons for this outcome. One is the intramolecular scission of the polymer backbone, caused by the hydrogen transfer of the backbone to the side chain, which forms a thermolabile –P–O–C– bond, through the insertion of the next monomer, leading to chain fragmentation (Scheme 2.5).[46]

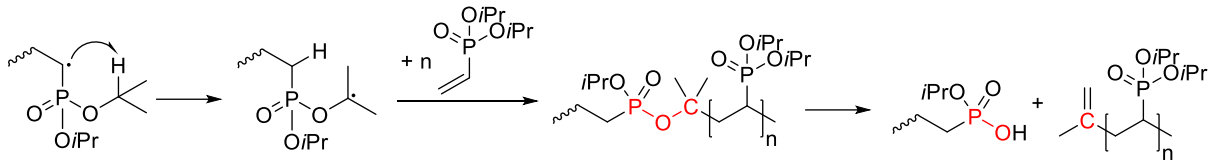

Scheme 2.5: Intramolecular chain scission of PDIVP during radical polymerization.[36, 41] Adapted with permission from ref. [4]. Copyright 2016 American Chemical Society.

Another drawback of the radical polymerization of DAVPs is the high stability of the formed radicals, leading to a slow propagation. In combination with the chain scissions, this results in materials with low molecular weight, low conversions, high polydispersities and an irregular structure of the polymer backbone. Thus far, none of the numerous attempts to overcome these major issues was successful.[46-48]

In the 1960s and 70s DAVPs were polymerized with anionic protocols for the first time. The applied lithium and magnesium alkyls were linked to low conversions and the formation of oligomeric materials.[49, 50] Similar to the radical polymerization, the anionic pathway suffers from a plurality of side reactions. This leads to polyvinylphosphonates with high polydispersities.[51] The major drawback of the anionic mechanism is the facile abstraction of the α–acidic proton of the double bond, through initiating molecules (Scheme 2.6 A).[36] A nucleophilic attack at the phosphorus atom, with subsequent elimination of an alcoholate, is presented in pathway B of Scheme 2.6.[52] The third side reaction can proceed *via* a nucleophilic attack at the double bond (Scheme 2.6 C). Long reaction times are necessary to reach full monomer conversion, which indicates low polymerization rates. A resonance stabilization of the anionic chain end, through the phosphonate moiety, decreases the reactivity of the chain and the poor initiator efficiency of the applied metal salts, may be the main reasons for the low activity.[40]

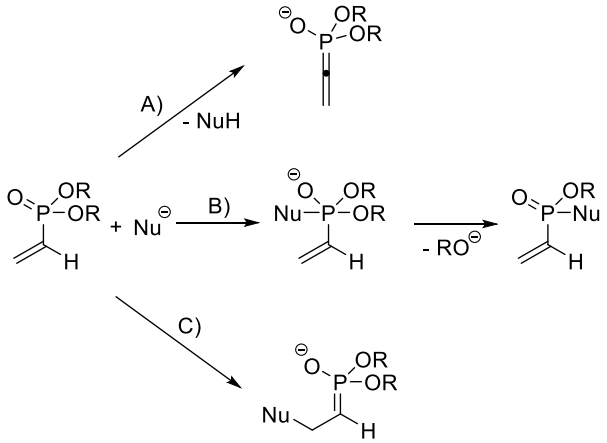

Scheme 2.6: Possible reaction pathways of the anionic polymerization of DAVPs: A) Abstraction of the α–acidic proton, B) nucleophilic attack at the phosphorus atom with subsequent elimination of an alcoholate and C) nucleophilic attack at the double bond. Adapted with permission from ref. [36]. Copyright 2012 John Wiley and Sons.

Through the above described issues, high molecular weight polyvinylphosphonates were inaccessible for a long time. However, the promising properties of phosphorus-containing polymers, the insufficient polymerization techniques and the structural similarity of vinylphosphonates to other *Michael*-type

monomers, like the omnipresent (meth)acrylates (Scheme 2.7), motivated our group to conduct some initial studies.

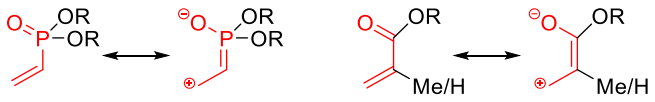

Scheme 2.7: Structural and electronic similarity of vinylphosphonates and (meth)acrylates.[36, 53] Adapted with permission from ref. [36]. Copyright 2012 John Wiley and Sons.

Simple rare earth metal alkyl precursors (Figure 2.3) were tested for the polymerization of dimethyl vinylphosphonate (DMVP) and diisopropyl vinylphosphonate (DIVP) and oligomers were obtained.[40, 54]

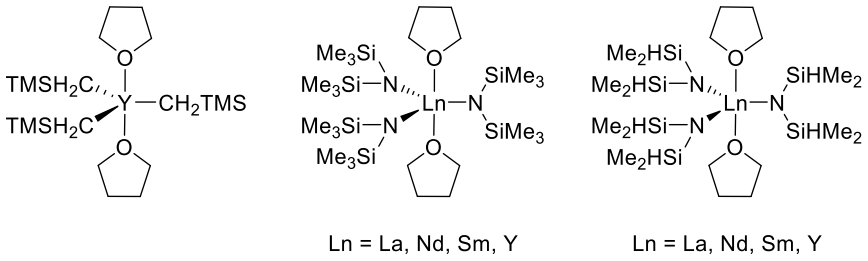

Figure 2.3: First rare earth metal alkyl complexes for the oligomerization of DMVP and DIVP. Adapted with permission from ref. [36]. Copyright 2012 John Wiley and Sons.

The major limitation in case of DMVP polymerization was the poor solubility of PDMVP in applicable solvents like toluene or tetrahydrofuran (THF). NMR studies could show that the oxygen atom of DMVP coordinates to the metal center during oligomerization and not the double bond. This observation indicates, that polyvinylphosphonates can possibly be obtained *via* a group transfer mechanism.[54] In 2010 the group of *Rieger* could successfully solve this complex task.[35] Simple late rare earth metal complexes (Cp_2YbCl, Cp_2YbMe) were employed to obtain, for the first time, poly(diethyl vinylphosphonate) with a molecular weight of 10^5-10^6 g/mol. Already in this first study a group transfer mechanism was suggested, for the synthesis of block copolymers of MMA and DEVP. A follow-up work proposed the coordination of one DEVP moiety to the metal center, leading to a rearrangement of one Cp group from η^5 to η^1 coordination. This Cp group attacks the vinyl group in a conjugate addition step, followed by the coordination of the next monomer to the metal center (Scheme 2.8).[55]

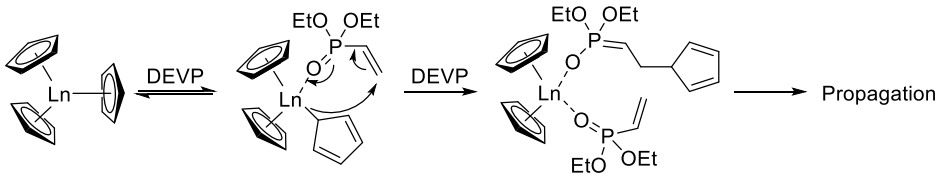

Scheme 2.8: Postulated initiation mechanism of metallocene catalysts in DEVP polymerization. Adapted with permission from ref. [55]. Copyright 2011 American Chemical Society.

The same report could show a contrary trend in the influence of the ionic radius of the metal center on the polymerization rate, compared to *Yasuda's* report (activity: Sm > Y > Yb > Lu).[26] For the metallocene complexes used in DEVP polymerization, the initiator efficiency *I** increased with decreasing ionic radius of the late lanthanides. At that time, no clear explanation could be found for this observation. Only a more comprehensive study published two years later, gave a deeper insight into the on-going initiation and propagation mechanisms.[56]

One distinctive characteristic of the GTP of DAVP is its initiation *via* a chloro ligand. For other *Michael*-type monomers this is impossible, due to an insufficient nucleophilicity.[57] In contrast to the expectations, Cp_2LnCl complexes showed a successful initiation of DAVP polymerization after a certain initiation period. Through the presence of the α–acidic proton three reaction pathways are rendered: deprotonation, nucleophilic transfer of the ligand X or a ligand exchange (Scheme 2.9).[56]

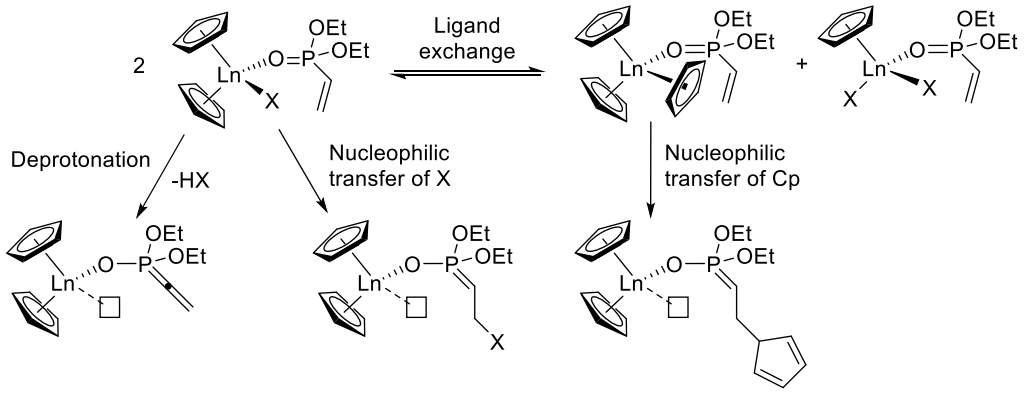

Scheme 2.9: Complex network of reactions taken place during the initiation of DEVP group transfer polymerization. Adapted with permission from ref. [56]. Copyright 2013 American Chemical Society.

To obtain a deeper insight into the complex reaction network of the REM-GTP of DAVPs, NMR spectroscopic studies with diethyl ethylphosphonate (DEEP) were conducted. DEEP is structurally similar to DEVP, but has no vinyl group, which prevents polymerization. Therefore, it is the ideal candidate for mechanistic studies. DEEP was added to Cp_2LnX complexes to yield a monomer-induced ligand exchange with an equilibrium of $Cp_2Ln(DEEP)$ and $CpLnX_2(DEEP)_n$ (Scheme 2.10).

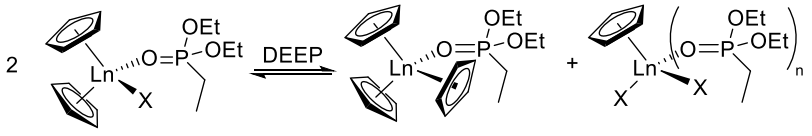

Scheme 2.10: Ligand exchange of Cp_2LnX through addition of DEEP. Adapted with permission from ref. [56]. Copyright 2013 American Chemical Society.

Furthermore, the single crystals of $Cp_3Y(DEEP)$ and also of Cp_2LnCl (Ln = Ho, Yb) could be analyzed, to find exclusively the coordination *via* the oxygen atom of the vinylphosphonate and not *via* the double bond. The structures also demonstrate, that the *Michael*-system of the coordinated monomer is retained, which

renders a repeated conjugate addition polymerization.[35, 56] All these investigations proved the mediation of the mechanism by a Cp_2Ln moiety.

Experimental data led to the conclusion that DAVP polymerization proceeds *via* an S_N2-type associative mechanism. Herein, the polymer phosphonate ester is displaced by the monomer with a pentacyclic intermediate (Scheme 2.11). The monomer coordination is the rate-determining step of the polymerization. Smaller metal centers lead to a higher steric crowding in the eight-membered metallacycle, which leads to a destabilization of the propagation and its acceleration. Also larger side chains of the monomers lead to higher steric demand of the growing polymer chain in the transition state.[4, 56]

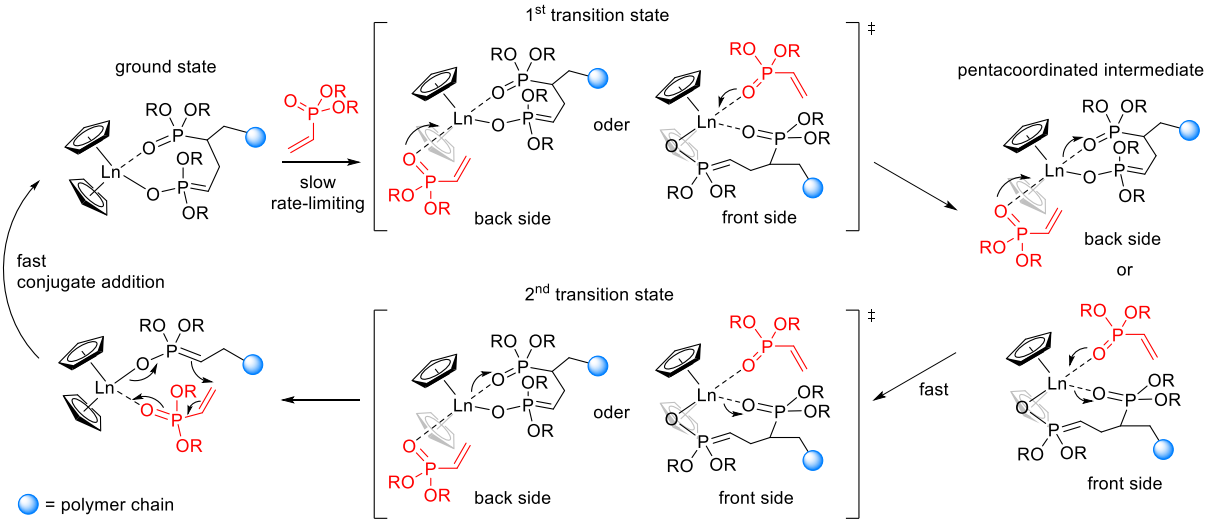

Scheme 2.11: Reaction mechanism of the REM-GTP of DAVPs. Adapted with permission from ref. [56]. Copyright 2013 American Chemical Society.

To get a deeper insight into the mechanism of REM-GTP of DAVPs, a plethora of catalysts with varying metal centers, ligand systems and initiators were synthesized. They were applied in the polymerization to compare their activities and efficiencies. The structural motif of Cp_2LnX, with X as the initiator moiety, was demonstrated to be suitable for this polymerization type. However, the activity depends to a great extent on the initiating group and its initiation mechanism (Figure 2.4). The thiolato compounds were found to be the most active ones, however they bear several drawbacks. These complexes render end-group elimination, weaker monomers cannot be polymerized due to the formation of $[Cp_2LnStBu]_2$ dimers and their smell is excruciating.

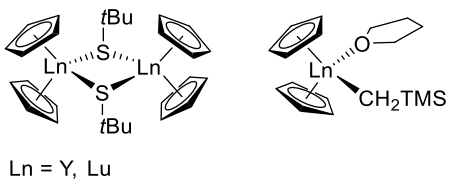

Figure 2.4: Most active Cp_2LnX catalyst structures.[56]

Consequently, a new class of initiators had to be discovered that outperforms the thiols.

2.3.3 C–H Bond Activation through σ–Bond Metathesis

In the REM-GTP of methacrylates strongly basic initiator systems like hydrides or alkyls are applied. These initiating ligands do not lead to a nucleophilic transfer to the coordinated monomer, in case of vinylphosphonates, but to an abstraction of the α–acidic proton (see Scheme 2.9).[24, 56] Hence, long initiation periods and low initiator efficiencies are observed. The group of *Collins* developed enolate-type initiators to overcome the limitations of alkyl ligands in zirconium catalyzed GTP of acrylates.[58] According to the successful application of enolates in the GTP of acrylates, *Rieger et al.* tried to synthesize a variety of enolate and enamide lanthanide complexes (Scheme 2.12).[23]

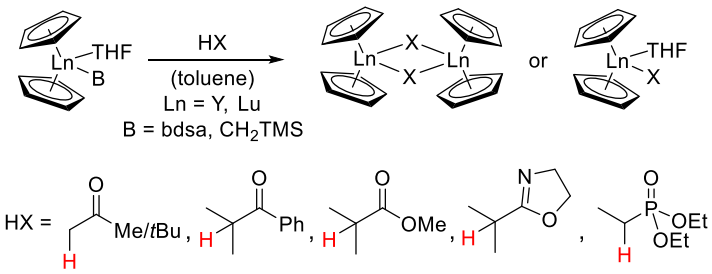

Scheme 2.12: Attempted synthesis of enolate and enamide initiators for application in REM-GTP (bdsa = bis(dimethylsilylamide, $N(SiMe_2H)_2$). Adapted with permission from ref. [23]. Copyright 2015 American Chemical Society.

These complexes are supposed to favor nucleophilic transfer over the abstraction of the α–acidic proton and therefore avoid the long initiation periods. However, the synthesis of most structures did not work without the formation of numerous side products, like for example a starting decomposition under the necessary reaction conditions. Therefore, another synthetic method had to be found – the σ–bond metathesis. As early as 1983, studies about the σ–bond metathesis of cyclopentadienyl lutetium complexes were published.[59, 60] σ–Bond metathesis enables lanthanoids as well as d^0-transition metals to activate intramolecular substrates without any change in their oxidation state. A concerted reaction mechanism *via* a four-membered transition state takes place. The $(2\sigma + 2\sigma)$-cycloaddition can lead to hydrogenolysis or alkanolysis depending on the activated substrate (Scheme 2.13).[61, 62]

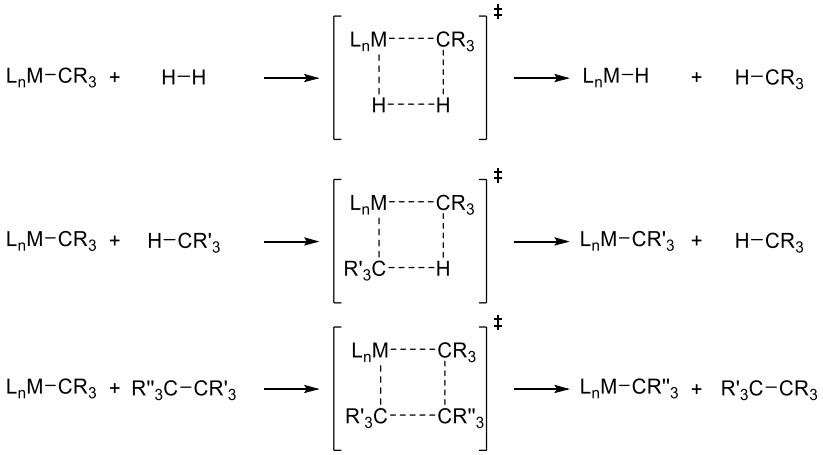

Scheme 2.13: H–H, C–H and C–C bond activation *via* σ–bond metathesis.[61]

The C–H bond activation of heteronuclear structures, like pyridines, and also alkynes was well studied by the *Teuben* group.[63-67] *Mashima et al.* investigated the application of C–H bond activated yttrium complexes on the polymerization 2VP (Scheme 2.14).[68]

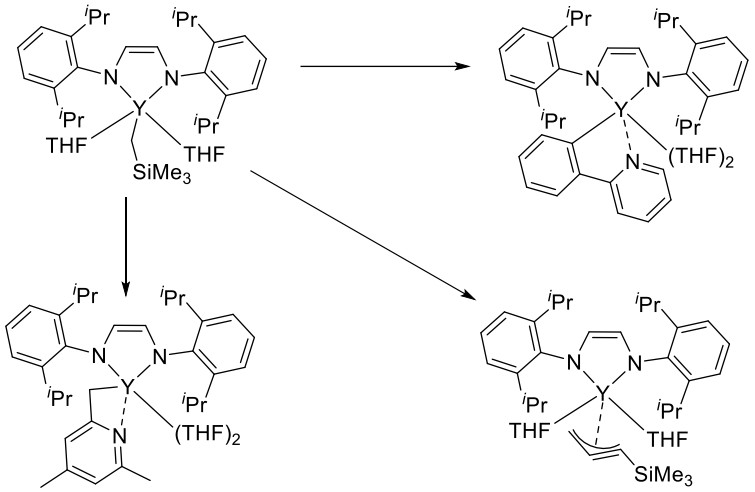

Scheme 2.14: C–H bond activated Yttrium-ene-diamido complexes applied by *Mashima et al.* for 2VP polymerization. Adapted with permission from ref. [68]. Copyright 2011 American Chemical Society.

All these reports gave rise to the idea of 2,4,6-trimethylpyridine (*sym*-collidine) as potential initiator for REM-GTP of DAVPs. The activation of *sym*-collidine with $Cp_2Y(CH_2TMS)(THF)$ showed full conversion at room temperature after only 30 minutes (Scheme 2.15).[23]

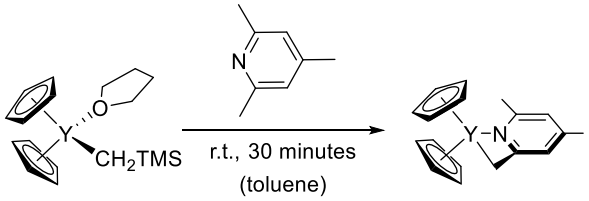

Scheme 2.15: C–H bond activation of *sym*-collidine with $Cp_2Y(CH_2TMS)(THF)$. Adapted with permission from ref. [23]. Copyright 2015 American Chemical Society.

The coordination of *sym*-collidine can be in the form of a carbanion as well as an enamide (Scheme 2.16). Therefore, deprotonation and nucleophilic transfer as visualized in Scheme 2.9 are possible for the initiating step.

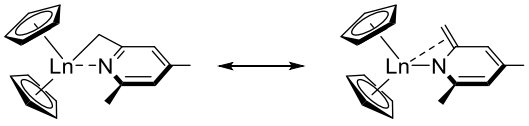

Scheme 2.16: Mesomeric equilibrium of the carbanion and the enamide of the activated catalyst. Adapted with permission from ref. [23]. Copyright 2015 American Chemical Society.

Electrospray ionization mass spectrometry (ESI-MS) studies showed an end-group functionalization of oligomeric DEVP with (4,6-dimethylpyridin-2-yl)methyl. This is the first indication toward a nucleophilic transfer mechanism, as well as the high initiation rates. The final evidence for this theory is the dimeric crystal

structure of the activated metal complex, suggesting a partial double bond character of the Ln coordinating *C–C* bond. Subsequently, an initiation mechanism with an eight-membered ring transition state can be proposed (Scheme 2.17).[23]

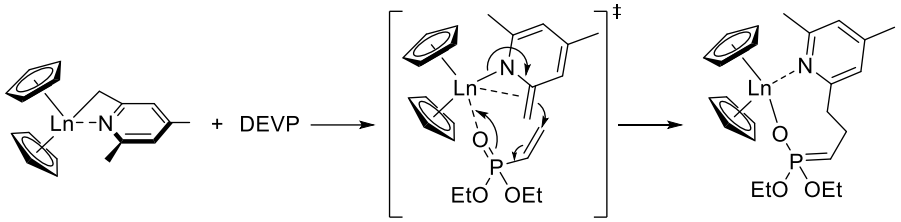

Scheme 2.17: Initiation of DEVP *via* the proposed eight-membered transition state. Adapted with permission from ref. [23]. Copyright 2015 American Chemical Society.

Especially the yttrium complex proved to be highly active in the polymerization of DEVP. High initiator efficiencies, low polydispersities and a living character were determined. Additionally, this new initiator class gives rise, to the synthesis of end-group functionalized materials through the formation of a stable C–C bond (see chapter 4). Besides, the activation of polar monomers is rendered possible, which leads to new materials with various properties.[23]

2.3.4 Thermoresponsive Behavior of Polyvinylphosphonates

After the development of a polymerization method toward high molecular mass poly-DAVPs (PDAVPs) their properties had to be investigated. Interestingly, all polyvinylphosphonates exhibit thermoresponsive behavior. In the field of temperature-dependent solubility, two types are defined: macromolecules with a lower critical solution temperature (LCST) versus polymers with an upper critical solution temperature (UCST). The LCST describes the temperature below which the system is homogenously dissolved, whereas the UCST represents the point above which the polymer is in solution (Figure 2.5).[69]

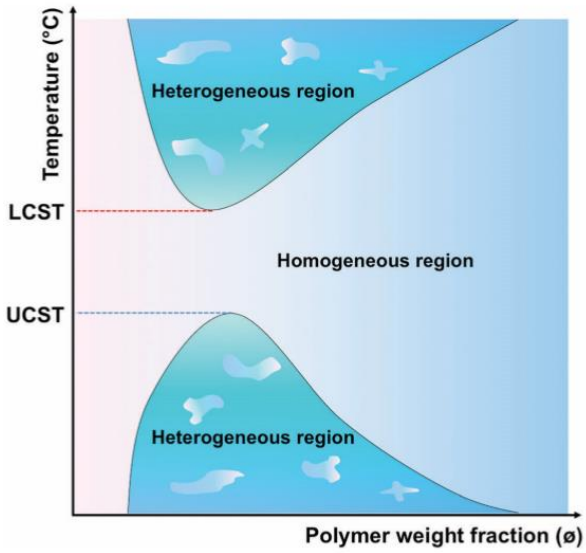

Figure 2.5: Phase diagram of LCST and UCST polymers in aqueous solution. Reprinted with permission from ref. [69]. Copyright 2017 The Royal Society of Chemistry.

The sharp and fully reversible phase transition follows a coil–globule transition mechanism (Scheme 2.18). Increased temperatures induce an entropic driven precipitation for LCST polymers according to *Gibbs-Helmholtz* ($\Delta G = \Delta H - T\Delta S$).

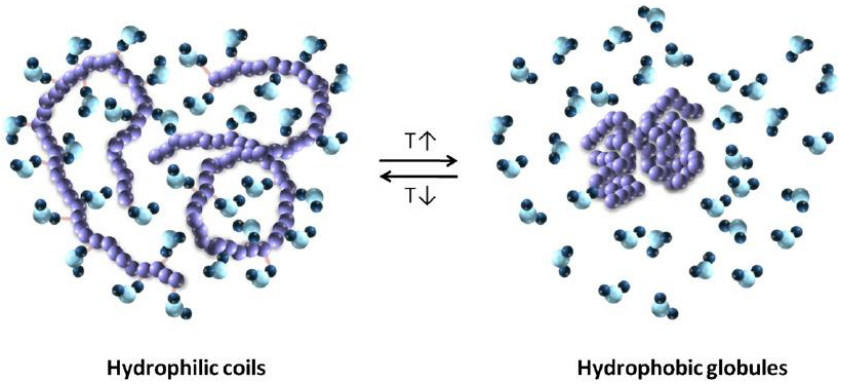

Scheme 2.18: Temperature dependent coil-to-globule transition of responsive polymers. Reprinted with permission from ref. [70]. Copyright 2012 Elsevier.

The differential scanning calorimetry (DSC), of a 30 wt% aqueous PDEVP solution, verified the endothermic process as a very sharp phase transition, at 46 °C for this polymer sample. Hence, the observation of an endothermic phase separation by DSC analysis reflects the cleavage of the hydrogen bonds, between water molecules and the dissolved polymer, clearly proving the occurrence of the before described coil–globule transition mechanism. During the cooling cycle an exothermic phase transition at 45 °C was measured, which is in good accordance with the turbidimetry results.[37]

Many factors influence the characteristics of polyvinylphosphonates. One factor with a high impact is the type of side group that is present in the polymer. PDMVP is hydrophilic and therefore almost exclusively water soluble. In contrast, PDIVP shows a good solubility in most organic solvents. Whereas, PDEVP, as middle course between the two, reveals amphiphilic properties. Aqueous PDEVP solutions have a lower critical solution temperature close to the physiological range ($T_{LCST} = 40 - 46$ °C) (Figure 2.6). This is an interesting property for various applications.[55]

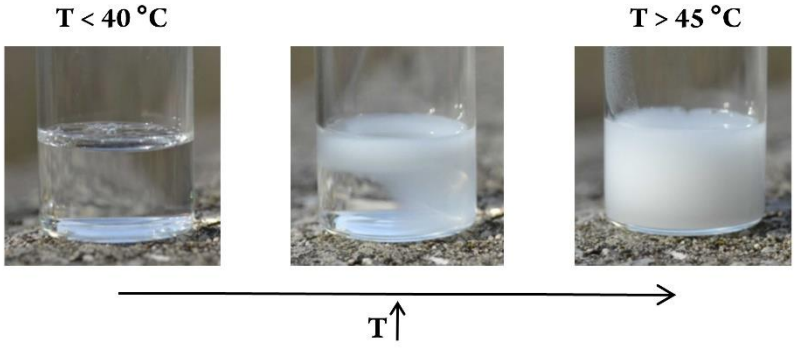

Figure 2.6: Temperature dependent solubility of PDEVPs in water.[4]

The cloud point of polyvinylphosphonates is dependent on many factors. There are influences like the polarity of the solvent, the polymer concentration and additives in the solvent that have an impact on the LCST of a macromolecule of a certain composition. However, also the composition and the molecular weight are of great importance for the thermoresponsive characteristics of polyvinylphosphonates. In case of PDEVP, the cloud point rises with an increasing molecular weight. This dependence is presented in the following Figure 2.7.[55]

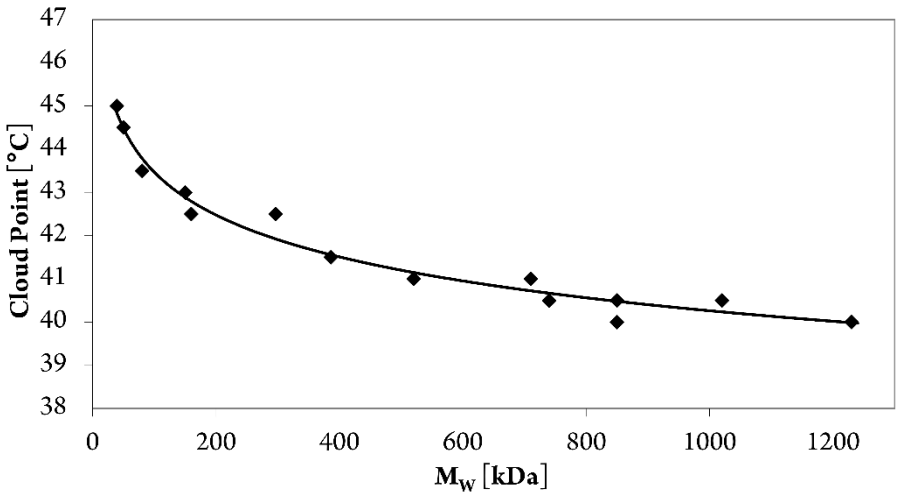

Figure 2.7: Dependence of the cloud point of PDEVP on the molecular weight. Adapted with permission from ref. [55]. Copyright 2011 American Chemical Society.

The insertion of comonomers into the PDEVP chain enlarges the temperature range of the phase transition tremendously. By varying the comonomer composition, the LCST can be adjusted between 5 and 92 °C (Figure 2.8). The LCST correlates to the ratio of hydrophobic to hydrophilic monomer and can be precisely tuned.[37]

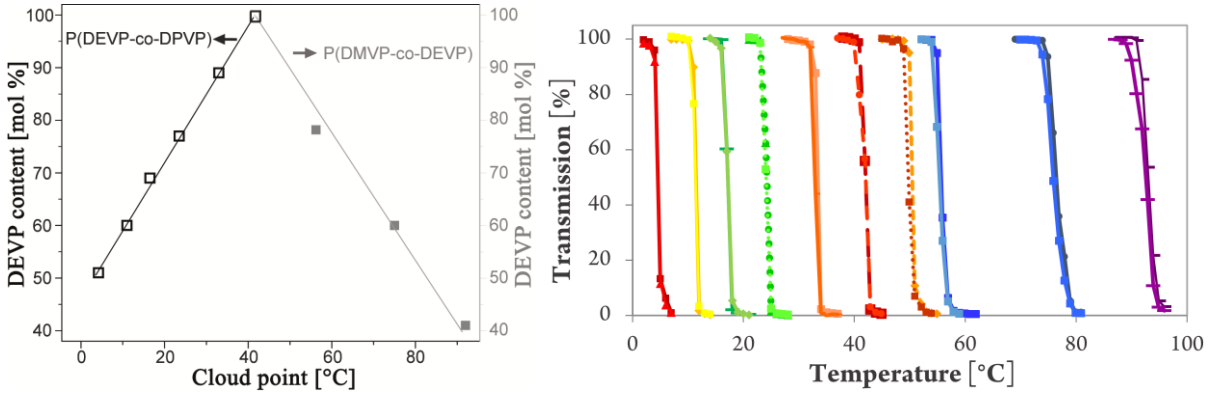

Figure 2.8: Left: Linear dependence of the LCST on the comonomer ratio of DEVP and DPVP/DMVP. Reprinted with permission from ref. [37]. Copyright 2012 American Chemical Society. Right: Aqueous PDAVP solutions exhibit thermoresponsive behavior with a tunable LCST between 5 and 92 °C (DEVP–DPVP ≙ 0 – 35 °C, DEVP ≙ 42 °C and DEVP–DMVP ≙ 50 – 95 °C homo/copolymers). Adapted with permission from ref. [4]. Copyright 2016 American Chemical Society.

These properties, as well as their water solubility and their biocompatibility make these polymers very promising candidates for biomedical utilization, like in controlled cell growth and cell release. For these

applications, the influence of additives on the thermoresponsive behavior had to be investigated, since the polymers must be employable in complex media. Therefore, sodium chloride, calcium chloride, phosphate buffered saline (PBS) as well as fetal calf serum (FCS) were tested on their influence on the turbidimetry measurements (Figure 2.9).[37] As expected, salting-out effects were monitored, however they were smaller than those for the standard polymers in the biomedical research field, poly(ethylene glycol) (PEG) or poly(*N*-isopropylacrylamide) (PNIPAAm).[37, 71]

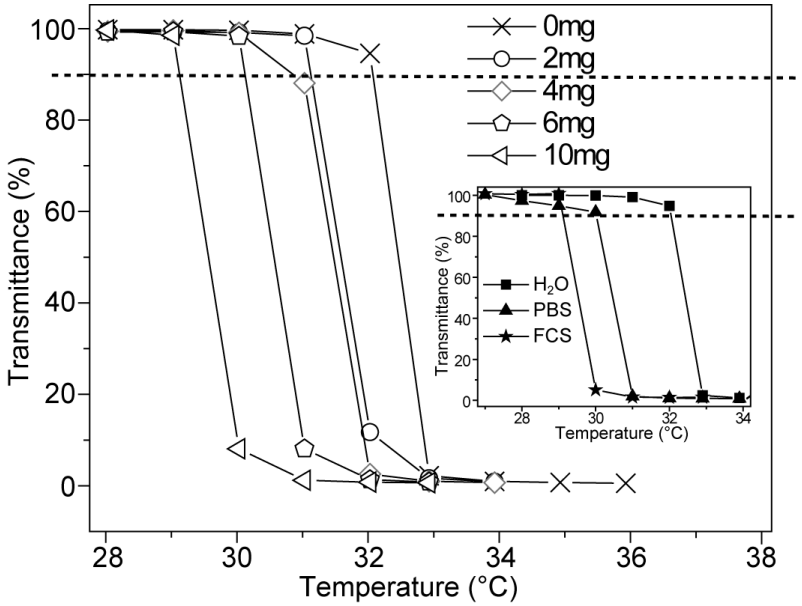

Figure 2.9: Determination of cloud points of P(DEVP$_{0.89}$-*co*-DPVP$_{0.11}$) in 1.0 wt% aqueous solution at varying sodium chloride concentrations upon heating (Inlet: determination of cloud points of the same polymer in deionized water, PBS and FCS)). Reprinted with permission from ref. [37]. Copyright 2012 American Chemical Society.

2.3.5 Post-Polymerization Functionalizations

To use polyvinylphosphonates in biomedicine or in other areas of application, post-polymerization modification is a potent tool to create very sophisticated systems. In general, there are three ways of addressing this task: Modifications on 1) the initiating group, 2) the terminating group or 3) the side groups.

The first steps toward the functionalization of the initiating group was made through the application of complex functional molecules like allyls or 2-(4-vinylphenyl)pyridine, which are presented in Scheme 2.14. The later molecule attaches a free vinyl group to one end of the polymer and makes it prone to functionalization reactions. A suitable method that can accomplish a coupling reaction on a specific position of a complex macromolecule is a click reaction. In the specific case of a vinyl group, the very fast, high-yielding and selective thiol-ene click reaction must be the method of choice. There are different pathways of the thiol-ene click reaction, but addressing a vinyl group attached to an aromatic system only radical couplings are feasible. The general mechanism of such a click reaction is illustrated in Scheme 2.19.[72, 73]

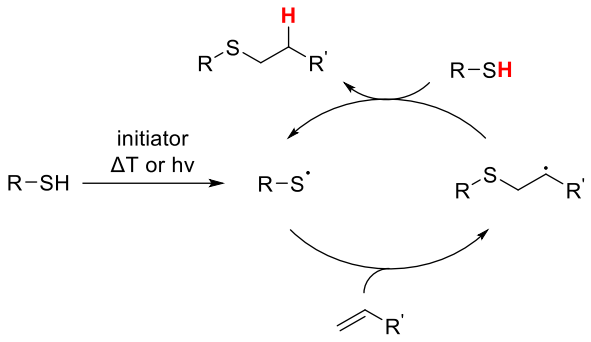

Scheme 2.19: General reaction pathway of a radical thiol-ene click reaction.[73]

In addition, modifications of polyvinylphosphonates *via* functional terminating groups are imaginable. It could be possible to add a new functionality to the polymer through the quenching reaction. To date, alcohols are used to terminate the polymerization with the addition of a proton to the anionic chain. *Via* the coupling of electrophiles such as anhydrides, acyl chlorides or sulfonates to the polymer chain reactive groups could be attained, whereupon modifications, with for example biologically active molecules, would come into reach. So far these are only options that were applied to other polymer classes, but never before to polyvinylphosphonates.

The first trials on the modification of polyvinylphosphonates were made at the ester side groups, with the goal to obtain poly(vinylphosphonic acid) (PVPA). The intension behind the hydrolysis of PDAVPs to PVPAs is that vinylphosphonic acid cannot be polymerized *via* group transfer or anionic protocols, due to the catalysts' sensitivity toward protic impurities. The hydrolysis can be achieved through thermal treatment (Scheme 2.20 C) or refluxing the polymer in a concentrated, strong acid like hydrochloric acid. However, these harsh conditions can lead to the degradation of the substrate (Scheme 2.20 A).[36]

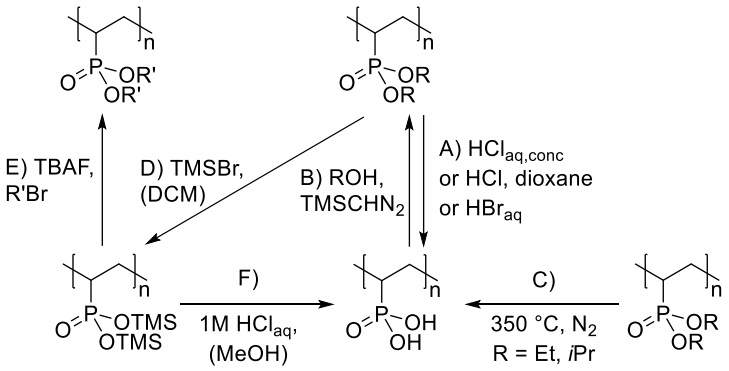

Scheme 2.20: Transesterification of polyvinylphosphonates (A/C/D+B/E) and hydrolysis to obtain PVPA (A, C, D+F). Adapted with permission from ref. [36]. Copyright 2012 John Wiley and Sons.

Therefore, *Wagner et al.* investigated this reaction pathway more closely and found a way to gain PVPA through the refluxation of PDIVP with bromotrimethylsilane (TMSBr) in dichloromethane (DCM) (Scheme 2.20 D + F).[51] Following this procedure, the group of *Rieger* could reach full conversion to the TMS ester for PDEVP but not for PDIVP, presumably due to the higher steric demand of the side chain. With this method,

the very sensitive TMS ester could be isolated and besides its hydrolysis, it was feasible to transesterify the side groups. In this report, benzyl bromide and tetra-*n*-butylammonium fluoride were used to yield poly(dibenzyl vinylphoshphonate), which could not be purified at this stage.[55] This functionalization technique could lead to a plethora of different polymers, especially when only partial transesterification is applied to obtain macromolecules with mixed side groups. Another route to yield polymers with a variety of side groups is the copolymerization of monomers in the desired order and exact amounts. Especially, block copolymers become feasible in contrast to the transesterification methods.

2.3.6 Copolymerization of various Monomers *via* REM-GTP

The REM-GTPs unique character allows the synthesis of copolymers consisting of a plurality of *Michael*-type monomers. To obtain block copolymers, the coordination strength to the metal center is essential for the order of the monomer addition. The weaker binding monomer has to be added first, otherwise it cannot be polymerized, since its coordination to the metal cannot be established due to the strong interaction of the growing chain to the active center. The monomer sequence for full conversion of all monomers has to be the following: 2VP – IPOx – (R)MA – (R)MAA – DAVP (R = any substituent, MAA = methacrylamide).[74, 75] Through the sequential addition of these monomers block copolymers with AB-, ABC- or multiblock-copolymers can be synthesized. Statistical copolymers are possible among monomers of the same coordination strength. These random copolymers are synthesized *via* the addition of a premixed monomer blend (Figure 2.10).[14]

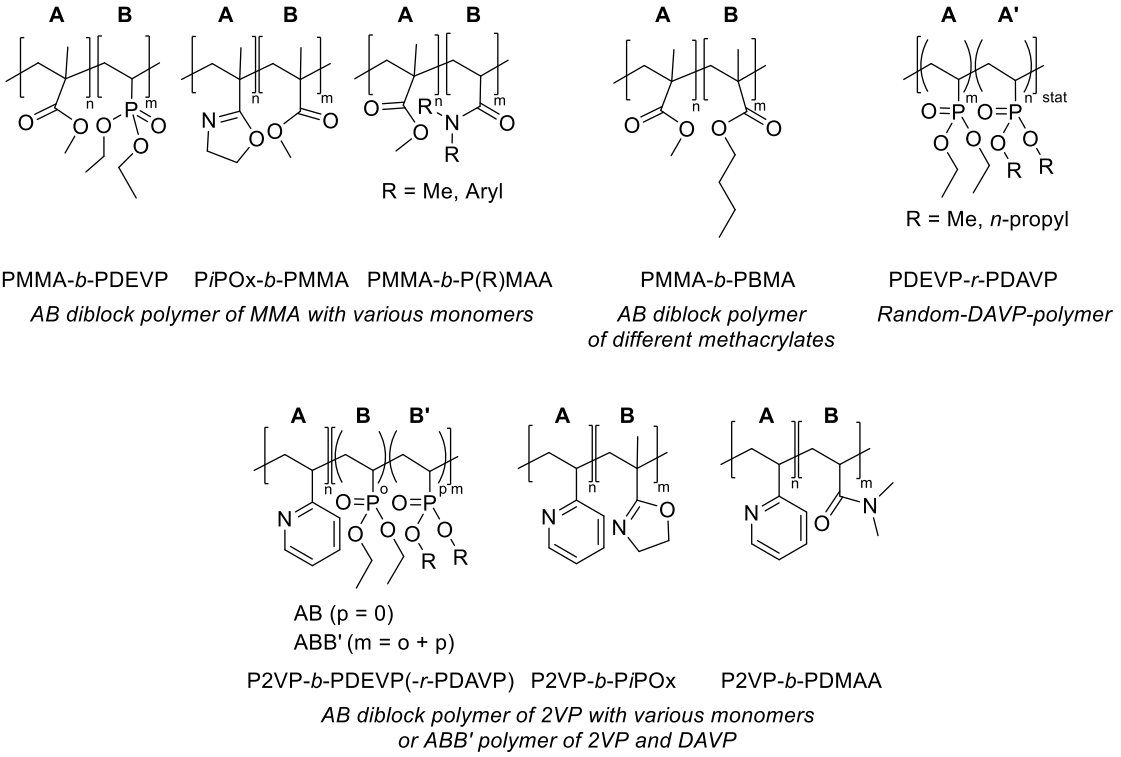

Figure 2.10: Copolymers obtained through REM-GTP of *Michael*-type monomers. Reprinted with permission from ref. [14]. Copyright 2018 John Wiley and Sons.

Consequently, REM-GTP enables the synthesis of copolymers of different vinylphosphonates, as well as the introduction of for example 2VP. This is especially interesting, since this constellation renders block copolymers with hydrophilic and hydrophobic blocks. This polymer structure leads to micelle formation above a certain polymer concentration in solution (critical micelle concentration (CMC)). AB as well as BAB structures can assemble into micellar structures.[76, 77] The following Figure 2.11 indicates the catalyst structure and the reaction pathway toward BAB block copolymers consisting of 2VP and DEVP.[77]

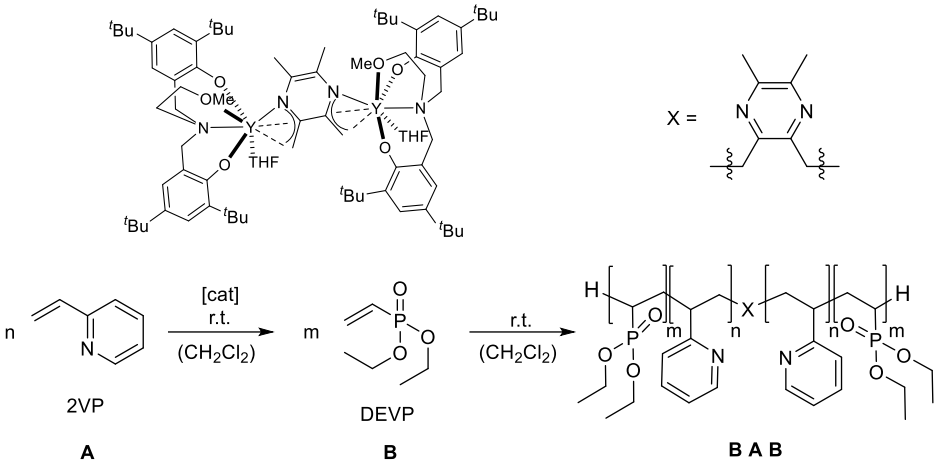

Figure 2.11: Sequential REM-GTP of 2VP and DEVP. Adapted with permission from ref. [77]. Copyright 2016 John Wiley and Sons.

These micelles were found to have CMCs of 0.1 – 0.3 mg/mL (Figure 2.13 B) and they still showed thermo-responsive behavior with nearly no hysteresis. Furthermore, a sharp phase transition could still be measured in more complex media like PBS buffer. Usually a salting-out effect is observed under these conditions, but not in case of the examined BAB micelles. (Figure 2.12).[77] Only a shift in the phase transition temperature of about four degree could be detected.

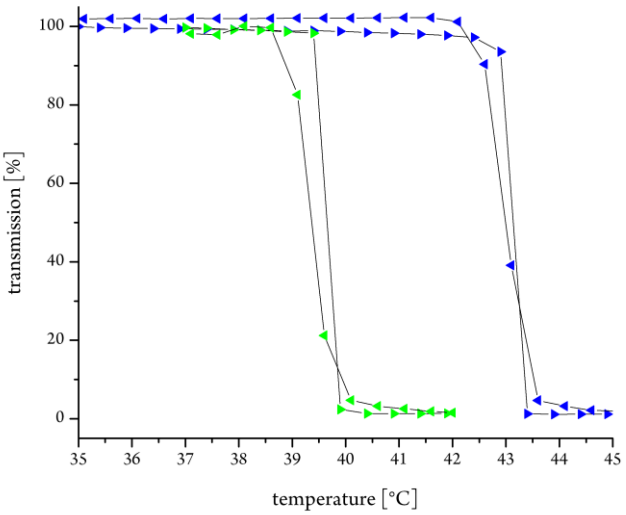

Figure 2.12: LCST measurement of a block copolymer BAB ($2VP_{200}/DEVP_{400}$).The cloud point was determined at 10% decrease of transmittance for 2.5 wt% aqueous polymer solution (blue: deionized water, green: PBS buffer). Reprinted with permission from ref. [77]. Copyright 2016 John Wiley and Sons.

These properties render the BAB micelles promising candidates for future biomedical applications, however also their physical properties, like shape and uniformity are of great importance. Figure 2.13 shows *via* TEM (C) and DLS (D) that monodisperse, round micelles were formed. This is desirable for their use in drug delivery, since round particles are endocytosed efficiently.[78] Additionally, the micelle dimensions ranged from 54 – 88 nm, which is ideal for delivery vehicles, since they should measure 30 – 100 nm. Previous reports found that particles from this size accessed tumor tissue best through an enhanced permeability and retention effect, and in contrast, do not appear to penetrate normal vessel walls. Within this size range, vehicles can usually escape non-specific clearance through the reticuloendothelial system (RES) and are also too big for renal clearance.[79, 80] Consequently, the loading and release characteristics were investigated, as last hurdle toward *in vitro* experiments. The micelles were loaded with fluorescein and the cargo was successfully released pH or temperature triggered and also untriggered, but to a much lower extent (Figure 2.13 A). Hence, water solubility, stability, shape, uniformity and loading and release characteristics argue for the application of these BAB micelles *in vitro*.[77]

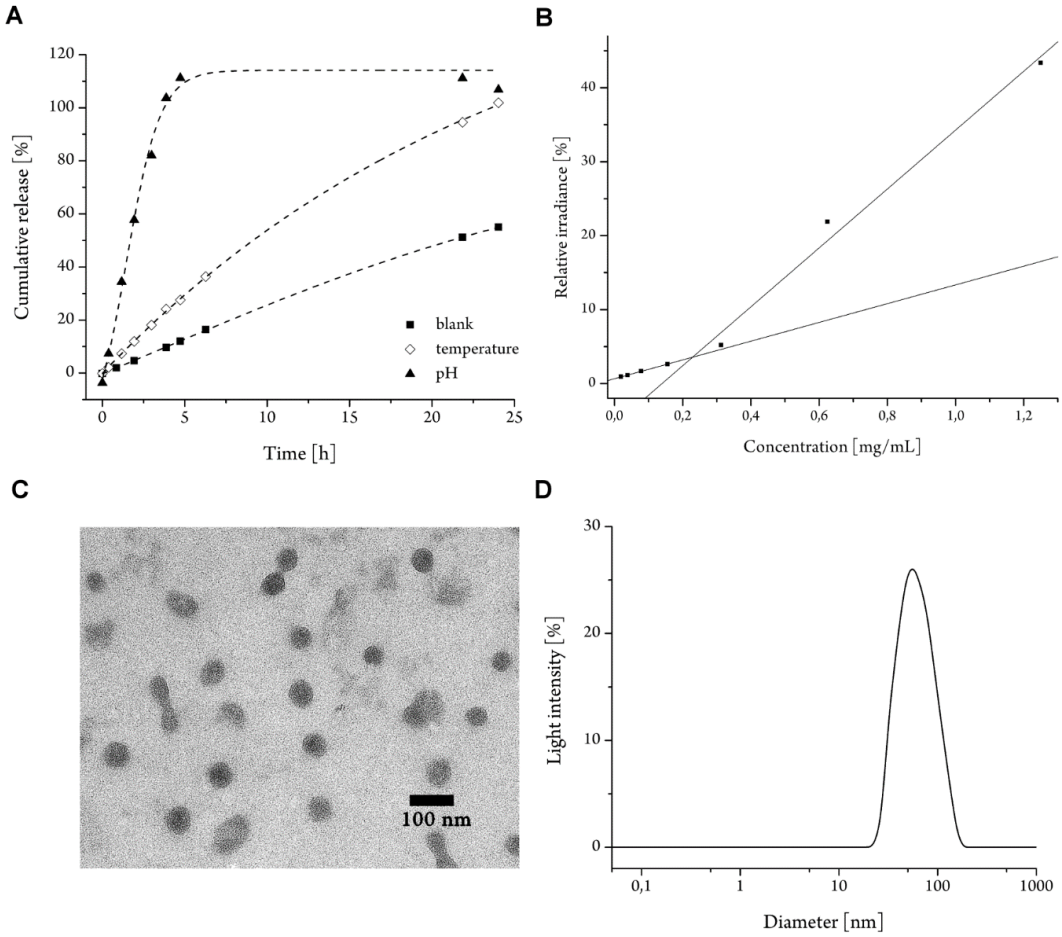

Figure 2.13: A: Cumulative release of fluorescein from loaded micelles: untriggered and triggered with pH (4.5 buffer solution) and temperature (44 °C). B: Determination of critical micelle concentration (CMC) with Nile red. C: TEM-image of micelles. D: Light-scattering measurement of micelles (2.5 mg/mL) in H_2O. Reprinted with permission from ref. [77]. Copyright 2016 John Wiley and Sons.

2.3.7 Drug Delivery with Polyvinylphosphonates

Only recently, our group succeeded to apply the fascinating properties of polyvinylphosphonates and develop a new type of multi-responsive nanocarriers for the use in the field of targeted drug delivery. We synthesized novel temperature and pH sensitive drug delivery vehicles as a potent tool in cancer therapy as depicted in Figure 2.11, Figure 2.12 and Figure 2.13. In case of polyvinylphosphonates, it is possible to adjust the temperature sensitivity *via* variation of the used monomer ratios. Furthermore, we could prove a desired pH response. These highly tunable properties make these smart polymers very attractive for a broad range of drug delivery applications and are therefore a fascinating opportunity for a tailor-made cancer therapy. To investigate their cargo release behavior under physiological conditions, *in vitro* studies were performed.

Figure 2.14 exhibits a cell viability study of HeLa cells as a function of increasing DOX-loaded BAB micelles (red) and non-encapsulated DOX (black) concentrations. All calculated cell viability values are means of at least three independent measurements. Toxicity is measured in both cases. As expected the decrease in viability is higher for free DOX, since no release has to take place. The IC_{50} value (half-maximal inhibitory concentration) was determined to be 1.9 µg/mL compared to 3.7 µg/mL in DOX-loaded micelles. These results are in good agreement with the literature data.[81-83] In comparison to for example nanopolymersomes four-fold higher toxicities combined with a higher biocompatibility was achieved.[81] Possibly, similar cytotoxicites, for both samples, would be measured after longer incubation times, since a prolonged release is assumed in case of the loaded micelles. This can be proven with fluorescence microscopic studies.

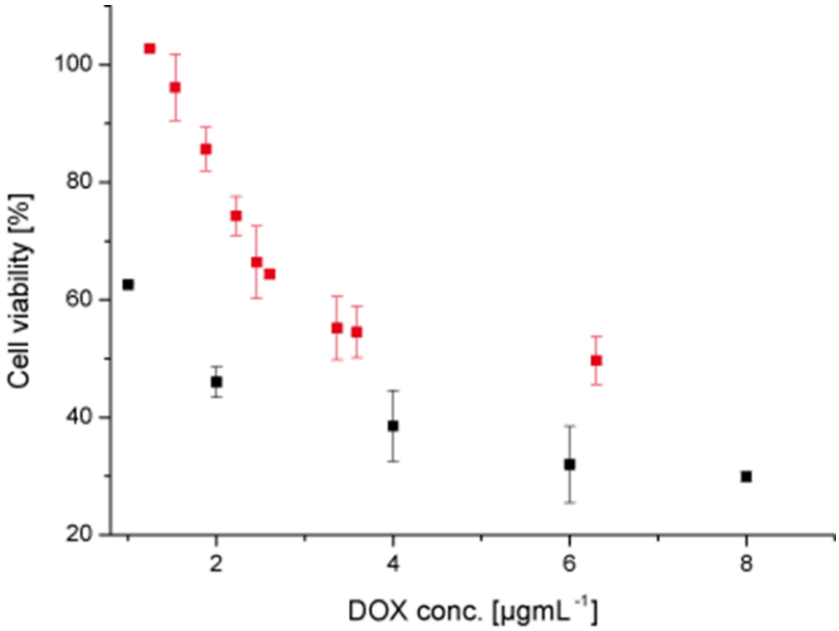

Figure 2.14: Analysis of the cell viability of DOX-loaded BAB and non-encapsulated DOX treated HeLa cells. Reprinted with permission from ref. [77]. Copyright 2016 John Wiley and Sons.

Localization studies of HeLa cells treated with DOX-loaded BAB micelles (A, B) or non-encapsulated DOX (C, D) for three hours (A, C) or six hours (B, D), were performed, respectively (Figure 2.15). After three hours of incubation time, a colocalization in the nucleus, was measured only for the free DOX sample. Incubating another three hours led to the desired colocalization in all samples. This is important, because DOX exhibits its cytotoxic effect when it reaches the nucleus, as it needs to intercalate into DNA where it inhibits topoisomerase II, leading to a suppression of replication and the subsequent death of tumor cells.[83-85] Consequently, this study supports the findings already indicated in the cytotoxicity screen. The free DOX transport is faster than the micellar transport. Thus, our micelles may enable a sustained release, which is desired for long-term treatments in patients. In conclusion, it can be stated that a polyvinylphosphonate based drug delivery system with the desired properties, for future applications, was developed. There is still room for improvements, but it is the basis for studies on the utilization of these systems in more complex *in vitro* and in the future also in *in vivo* studies.

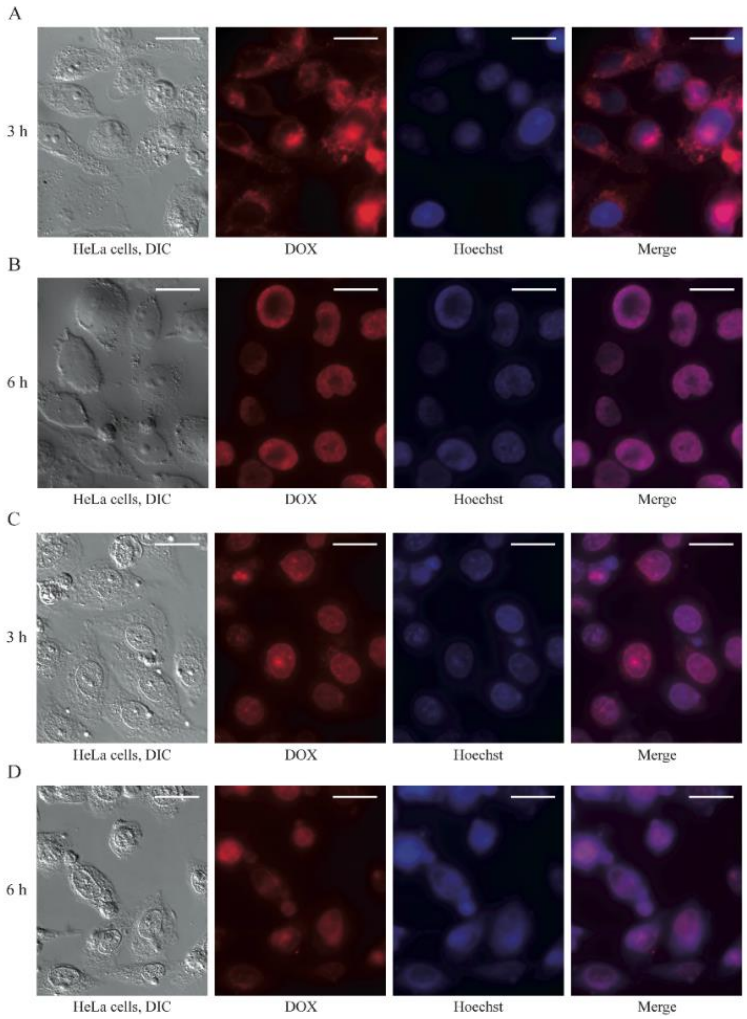

Figure 2.15: Localization studies of intracellular DOX release of DOX-loaded BAB micelles and non-encapsulated DOX followed by fluorescence microscopy. Reprinted with permission from ref. [77]. Copyright 2016 John Wiley and Sons.

3 Aim of this Thesis

Polyvinylphosphonates are phosphorus-containing polymers that remained unexplored for a long time. The reason was the inaccessibility of high molecular weight polyvinylphosphonates, through the classical anionic and radical polymerization techniques.[4] From 2010 on our group succeeded in the synthesis of high molecular weight PDEVP and copolymers, consisting of a broad variety of *Michael*-type monomers, *via* REM-GTP.[35] Since this time the properties of the polymers have been examined closely to find possible application fields like as halogen-free flame-retardant additives,[42] as non-amide kinetic hydrate inhibitors[86] or as delivery vehicles in biomedical research.[77]

A promising route toward the application of polyvinylphosphonates in medicine might be the specific end-group functionalization of each polymer strand. The C–H bond activation is expected to be the right tool for this task. The successful utilization of *sym*-collidine in DEVP activation is the foundation of future end-group functionalization studies. *sym*-Collidine is, before this thesis, the most efficient initiator in DEVP polymerization.[23] One goal of this thesis was to find an initiating molecule with an initiator efficiency similar or higher, than the gold standard *sym*-collidine, in combination with an additional functional group for post-polymerization functionalization. For this purpose two structures were planned, whereas one was unprecedented, 2,6-dimethyl-4-(4-vinylphenyl)pyridine (Figure 3.1).

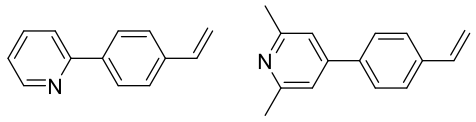

1 **2**

Figure 3.1: Possible initiating molecules with vinyl functional groups: 2-(4-vinylphenyl)pyridine (**1**) and 2,6-dimethyl-4-(4-vinylphenyl)pyridine (**2**).

Initially, a C–H bond activation with the catalyst $Cp_2Y(THF)(CH_2TMS)$ (**3**) was planned. The activated complexes (**4** and **5**) shall than be utilized in DEVP polymerization, to obtain PDEVP with the initiator **1** or **2** as end-groups (Scheme 3.1).

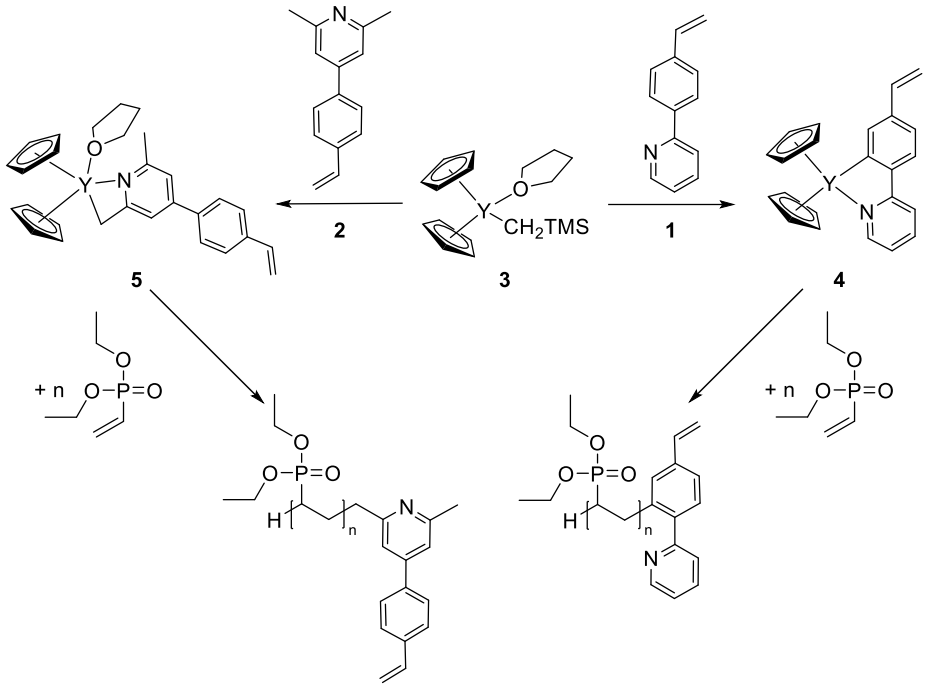

Scheme 3.1: C–H bond activation of **1** and **2** with following DEVP polymerization. Reprinted with permission from ref. [87] "Precise Synthesis of Thermoresponsive Polyvinylphosphonate-Biomolecule Conjugates *via* Thiol–ene Click Chemistry". Copyright 2018 The Royal Society of Chemistry.

After the careful evaluation of the structural characteristics of **4** and **5**, their abilities in DEVP polymerization, have to be examined. Important factors are the turn-over frequency (TOF), the initiator efficiency I^* and also the activation *via* one selective route, to obtain polymers with one specific end-group. The vinyl group can be conjugated in a subsequent step with biomolecules like folic acid or cholesterol. The method of choice for such a conjugation is the selective, efficient and rapid thiol-ene click reaction (Scheme 3.2).

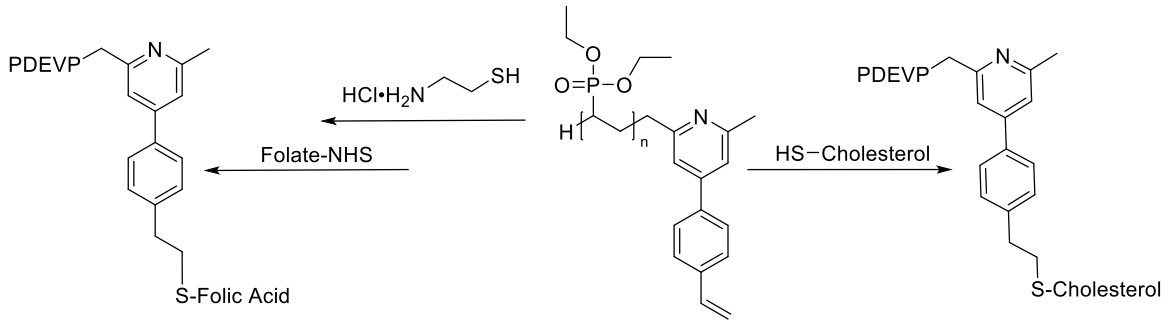

Scheme 3.2: Thiol-ene click reaction of PDEVP toward folic acid and cholesterol conjugates.

After the evaluation of the full conversion of the conjugation reaction, the polymer properties have to be examined. Water solubility, a lower critical solution temperature in media close to the physiological conditions, as well as the cytotoxicity of the polymers are important for future biomedical applications. (Ref. [87] "Precise Synthesis of Thermoresponsive Polyvinylphosphonate-Biomolecule Conjugates *via* Thiol–ene Click Chemistry") However, it is impossible to examine the localization of the polymers *in vitro*, since there is no method of imaging specifically polyvinylphosphonates inside or on top of cells. Therefore, as next step, the fluorescent labeling has to follow. Labeling of polymers can be achieved *via* multiple routes, such

as using fluorescent initiators, post-polymerization functionalization of the end-group or the utilization of fluorescent monomers. Certainly, all these techniques could lead to success, but all methods would change the structure significantly compared to the non-fluorescent ones, a fact that is not desirable. Consequently, the partial transesterification of the side groups will be the method of choice (Scheme 3.3). Through this approach only very little change of the polymer architecture is made and the comparability to the unlabeled version is higher.

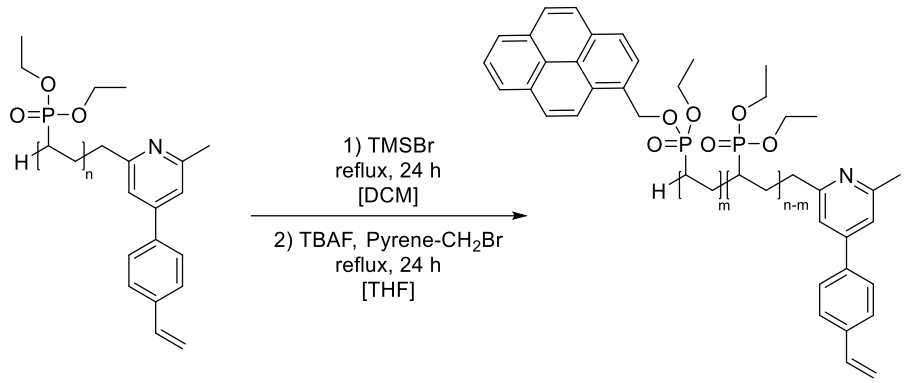

Scheme 3.3: Pyrene labeling of PDEVP through partial transesterification. Reprinted with permission from ref. [88] "Fluorescent Polyvinylphosphonate Bioconjugates for Selective Cellular Delivery". Copyright 2018 John Wiley and Sons.

To accomplish this complex task, a strategy employed by our group for the hydrolysis of PDEVP can be adapted.[36, 55] This functionalization proceeds *via* the trimethylsilyl ether intermediate. The consecutive deprotection is rendered by tetra-*n*-butylammonium fluoride (TBAF) and followed by the addition of pyrene to the activated positions (Scheme 3.3). The fluorescent labeling opens the door toward the biological evaluation of the obtained constructs and enables localization experiments to study the impact of the anchor units on the biological functions of the novel conjugates. In this context especially folic acid, as ligand that renders receptor-mediated uptake into cells[89, 90] and cholesterol, as component of the cellular membrane, [91, 92] are antithetic end-groups. This is important to provide an insight into the complex cellular transport mechanisms. (Ref. [88] "Fluorescent Polyvinylphosphonate Bioconjugates for Selective Cellular Delivery")

Subsequent to the investigation of targeting ligands on the localization of polyvinylphosphonates after cell treatment, drug delivery applications have to be taken into the focus of our research. For this challenge, new and stable nanoparticles have to be developed. The, to date available, micelles are an important basis for all following synthetic approaches.[76, 77] However, they have to be optimized for systemic applications, since they are formed in a concentration dependent manner, which would lead to immediate, unspecific cargo release after intravenous injection. Therefore, a new monomer with functional side group has to be implemented, to facilitate the cross-linking of micelles to gain stable nanoparticles. This monomer can be the diallyl vinylphosphonate (DAlVP), which is to date mainly used as linker unit for tRNA synthesis on solid supports.[93] DAlVP can be copolymerized with DEVP as the hydrophilic and 2VP as the hydrophobic block (Scheme 3.4).

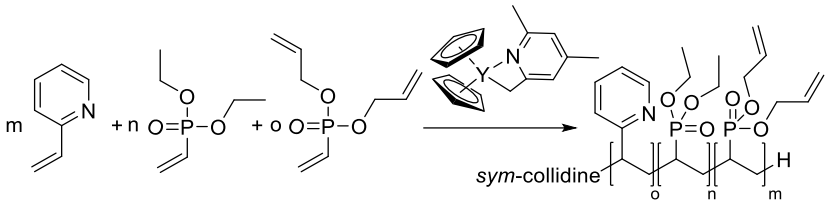

Scheme 3.4: Copolymerization procedure of 2VP, DEVP and DAlVP with Cp_2Y(*sym*-collidine) as catalyst. Reprinted with permission from ref. [94] "Synthesis of Next Generation Dual-Responsive Cross-Linked Nanoparticles and their Application to Anti-Cancer Drug Delivery". Copyright 2018 The Royal Society of Chemistry.

After the evaluation of all polymer parameters like polydispersity and molecular weight, the cross-linking reaction has to be performed. Again, the thiol-ene click reaction is the route to go, due to its favorable characteristics (Scheme 3.5).

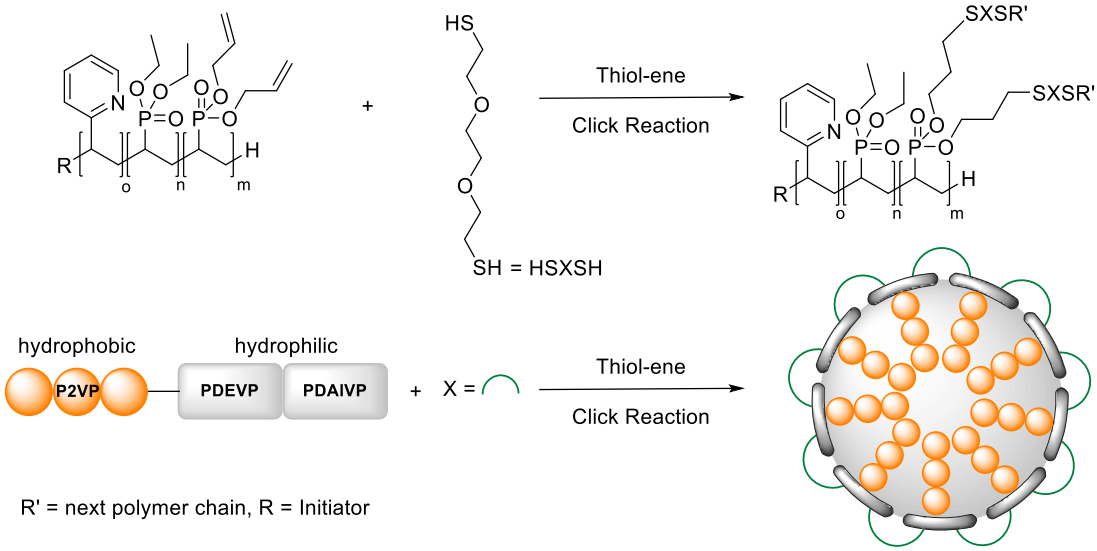

Scheme 3.5: Particle synthesis *via* thiol-ene click reaction. Adapted with permission from ref. [94] "Synthesis of Next Generation Dual-Responsive Cross-Linked Nanoparticles and their Application to Anti-Cancer Drug Delivery". Copyright 2018 The Royal Society of Chemistry.

Moreover, the particle characteristics have to be evaluated, to ensure monodispersity and examine shape as well as surface charge. Additionally, surface tension, loading and release experiments have to be conducted, to investigate the stability and behavior upon a change in the setting conditions. In case satisfying results are obtained, *in vitro* experiments can follow. First, cytotoxicity of the pure particles has to be measured and thereupon loaded samples can be applied. Colocalization studies have to be performed to analyze the cargo release and its transport into and within the cell. Especially the time is an important factor in these microscopic set-ups. To ensure the statistical accuracy of the localization results, flow cytometry has to be consulted as tool to complete the analytical picture about the novel drug delivery vehicles. (Ref. [94] "Synthesis of Next Generation Dual-Responsive Cross-Linked Nanoparticles and their Application to Anti-Cancer Drug Delivery".)

After this multiplicity of experiments, a clear conclusion about the qualification of polyvinylphosphonates for complex biomedical applications should be feasible. This is the comprehensive defiance of the following thesis.

4 Precise Synthesis of Thermoresponsive Polyvinylphosphonate-Biomolecule Conjugates *via* Thiol–ene Click Chemistry

4.1 Bibliographic Data

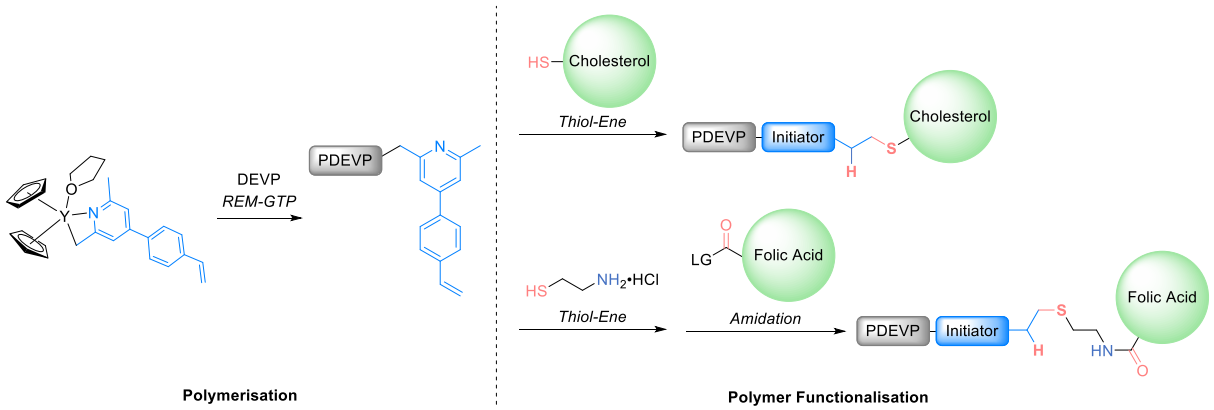

Title: "Precise Synthesis of Thermoresponsive Polyvinylphosphonate-Biomolecule Conjugates *via* Thiol–ene Click Chemistry"

Status: Full paper, Accepted 7th November 2017, Rewarded with Cover Page

Journal: Polymer Chemistry, 2018, 9, 284-290

Publisher: Royal Society of Chemistry

Link/DOI: https://doi.org/10.1039/C7PY01796K

Authors: Christina Schwarzenböck, Andreas Schaffer, Philipp Pahl, Peter J. Nelson, Ralf Huss and Bernhard Rieger

4.2 Summary

A polymerization type only recently attracting attention is the rare earth metal-mediated group transfer polymerization. This living-type polymerization is able to overcome the constraints faced by classical anionic and radical polymerizations. REM-GTP renders the synthesis of biocompatible, water-soluble and thermoresponsive polymers with narrow polydispersities and controlled molecular weights. Furthermore, this technique enables the introduction of a functional end-group *via* the initiating molecule. Our group was able to synthesize a novel multi-functional pyridine derivative and utilize it as a highly active and efficient initiator in the polymerization of DEVP. The structure comprises the beneficial motifs of the well-established initiating molecules, *sym*-collidine and 2-(4-vinylphenyl)pyridine. Using the C–H bond activated Cp_2Y complex, the, to date, highest TOF and I^* values in the REM-GTP of DEVP were measured, resulting in a remarkably rapid and efficient catalysis. This new end-group opens the door to various post-polymerization functionalizations. In the present study, the thiol–ene click reaction, a fast, high-yielding, stereospecific and well-established coupling strategy, was employed to conjugate PDEVP and a thiolated biomolecule. The motive for this study was to create a polymer platform that can easily address a plethora of applications through facile variations of the linked biomolecule units. Herein, we present for the first time the modification of polyvinylphosphonates with biologically relevant structures, namely cholesterol and folic acid. These novel conjugates are of great interest for many applications, since they were found to be water-soluble, thermoresponsive and biocompatible. In addition, they might have gained a biological function. Cholesterol is an inalienable constituent of the cell walls, whereas folic acid is recognized by the folic acid receptor and in consequence transported into cells. Ongoing studies in our laboratory will further examine the assignment of these biological functions onto the conjugates.

4.3 Manuscript

Volume 9 | Number 3 | 21 January 2018 | Pages 251–390

Polymer Chemistry

rsc.li/polymers

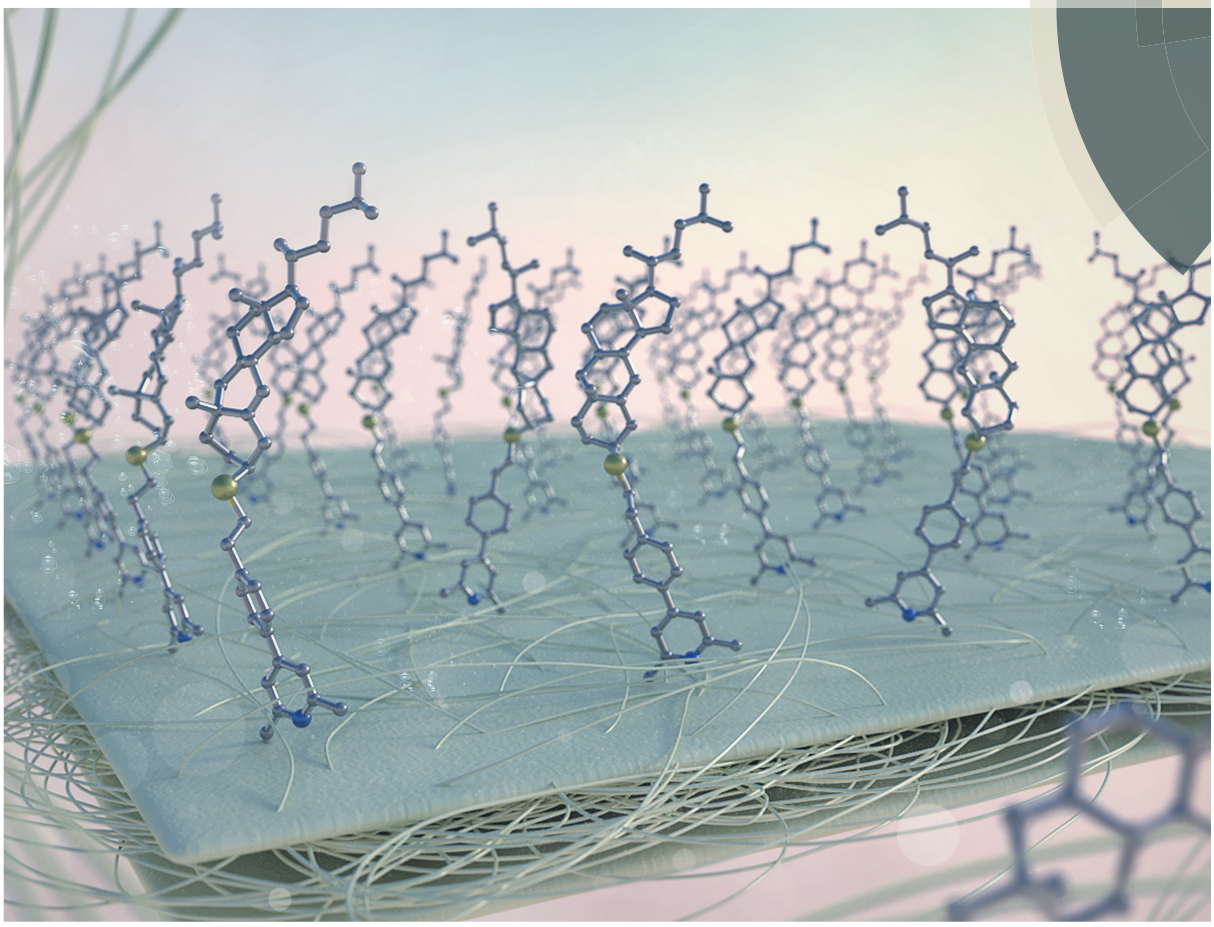

ISSN 1759-9962

ROYAL SOCIETY OF CHEMISTRY

PAPER
Bernhard Rieger *et al.*
Precise synthesis of thermoresponsive polyvinylphosphonate-biomolecule conjugates *via* thiol–ene click chemistry

Polymer Chemistry

PAPER

Cite this: *Polym. Chem.*, 2018, **9**, 284

Precise synthesis of thermoresponsive polyvinylphosphonate-biomolecule conjugates *via* thiol–ene click chemistry†

Christina Schwarzenböck,[a] Andreas Schaffer,[a] Philipp Pahl,[a] Peter J. Nelson,[b] Ralf Huss[c] and Bernhard Rieger *[a]

Received 25th October 2017,
Accepted 7th November 2017

DOI: 10.1039/c7py01796k

rsc.li/polymers

A polymerisation type only recently attracting notice is the rare earth metal-mediated group transfer polymerisation (REM-GTP). This living-type polymerisation is able to conquer the limitations faced by classical anionic and radical polymerisations. REM-GTP enables the synthesis of biocompatible, water-soluble and thermoresponsive polymers with narrow polydispersities and controlled molecular weights. Furthermore, this technique renders the introduction of a functional end-group *via* the initiating molecule. Our group was able to synthesise a new multi-functional pyridine derivative and apply it as a highly active and efficient initiator in the polymerisation of diethylvinylphosphonate (DEVP). This novel end-group opens the door to various post-polymerisation modifications. In the present study, the thiol–ene click reaction, a fast, selective and well-established coupling method, was applied to link poly-DEVP and a biomolecule. The incentive for this investigation was to create a polymer platform, that can easily address a multiplicity of applications through facile alterations of the coupled biomolecule entities. Herein, we present for the first time the functionalisation of polyvinylphosphonates with biologically relevant motifs, namely cholesterol and folic acid.

Introduction

Rare earth metal-mediated group transfer polymerisation (REM-GTP) is a potent tool towards the precise synthesis of tailor-made functional materials. This living method succeeds in the generation of polymers with defined molecular weights and narrow polydispersities. REM-GTP combines the best characteristics of living anionic as well as coordinative polymerisations and can be used for a variety of Michael-type acceptor monomers.[1] Especially, the phosphorus-containing vinylphosphonates have attracted interest, because their polymers exhibit water solubility, a tuneable lower critical solution temperature (LCST) and good biocompatibility. To date, various vinylphosphonate monomers exist, that allow for the synthesis of an exceptional spectrum of polymers with unique characteristics.[2–4] For the efficient synthesis of these materials, a profound understanding of the polymerisation mechanism is necessary. Rieger *et al.*[5] found the widely used system of strongly basic, methyl, CH_2TMS (TMS = trimethylsilyl) and hydride initiators to be restricted to the polymerisation of only certain types of monomers.

For vinylphosphonates, no efficient initiating ligands were known until 2,4,6-trimethylpyridine (*sym*-collidine) was evaluated to be a promising candidate for this complex task. *sym*-Collidine was reacted with $Cp_2YCH_2TMS(THF)$, where Cp = cyclopentadienyl and THF = tetrahydrofuran, *via* C–H bond activation to form the most active complex for polymerisation of diethylvinylphosphonate (DEVP) known to date.[6] However, this initiator carries only two free, but chemically inert, methyl groups on its aromatic ring. These methyl groups are not prone to post-polymerisation functionalisation. Therefore, we aimed at finding a pyridine derivative, which is capable of initiating the polymerisation of DEVP efficiently and, in addition, bears a reactive group not interfering with the catalytic process. We found 2-(4-vinylphenyl)pyridine (**1**) to be the ideal candidate for detailed examinations. The group of Mashima[7] presented the activation of **1** with an yttrium enediamido complex. The resultant catalyst was used in the polymerisation of 2-vinylpyridine (2VP). They also showed, that *sym*-collidine in 2VP polymerisation is superior to **1**. Consequently, we decided to not only activate the known substrate **1**, but also to synthesise a new molecule **5** carrying the

[a]*WACKER–Lehrstuhl für Makromolekulare Chemie, Technische Universität München, Lichtenbergstraße 4, 85748 Garching bei München, Germany. E-mail: rieger@tum.de*
[b]*Medizinische Klinik und Poliklinik IV, Nephrologisches Zentrum und Arbeitsgruppe Klinische Biochemie, University of Munich, Munich, Germany*
[c]*Definiens AG, Bernhard-Wicki-Strasse 5, 80636 Munich, Germany*
†Electronic supplementary information (ESI) available. See DOI: 10.1039/c7py01796k

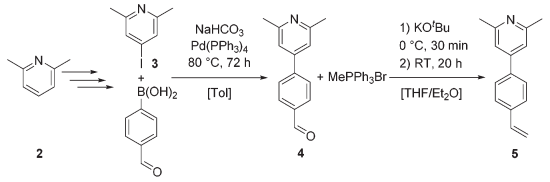

Scheme 1 Synthesis of 2,6-dimethyl-4-(4-vinylphenyl)pyridine (**5**) starting from 2,6-dimethylpyridine (**2**).

advantageous motifs of both *sym*-collidine and **1** (Scheme 1). With these two new initiators for the REM-GTP of DEVP, we established a platform for various end-group functionalisation reactions.

Herein, we focus on the thiol–ene click chemistry of the C–C double bond of the pyridine derivatives. The term 'click' chemistry was entrenched by Sharpless and co-workers in 2001.[8] They defined it as '... a set of powerful, highly reliable and selective reactions for the rapid synthesis of useful new compounds and combinatorial libraries through heteroatom links (C–X–C) ...'. This definition describes exactly what scientists care about, when finding new coupling strategies.[9–11] Fast, modular, high-yielding and stereospecific are the most important attributes for click chemistry, particularly when it comes to linking complex structures like polymers and biomolecules.[12,13] The classic form of click chemistry is the copper-catalysed azide–yne reaction.[14] However, copper is a toxic metal and in case of using the resulting compounds in biological applications, avoidance of toxic reagents is favourable.[15,16] The thiol–ene click reaction is a fast and efficient conjugation method, bearing all of the positive characteristics of click reactions without the need for a metal catalyst and at the same time using naturally occurring biological functional groups, like thiols and alkenes.[17,18] Therefore, we decided to apply this advantageous strategy for the aspired addition reaction. Thiocholesterol and an activated folic acid were synthesised and efficiently coupled to the polymer end-group of poly-DEVP (PDEVP), giving access to a new type of PDEVP-biomolecule conjugate. These two biomolecules were chosen, due to their opposing properties. Cholesterol is an essential component of cellular membranes,[19–22] while folic acid is recognised by the corresponding folic acid receptor (FR-α) and is consequently taken up into the cell *via* endocytosis.[23–27] In summary the intention was to add varying biological functions to the polymers *via* post-polymerisation modifications.

Results and discussion

Complex synthesis

For the end-group functionalisation of PDEVP, it was necessary to synthesise pyridine derivatives with an additional functional group. We selected the C–C double bond, because thiol–ene click chemistry is a very efficient and elegant way to connect two molecules. Our first choice was the known molecule **1**. It was obtained *via* a Wittig reaction.[28] The subsequent C–H bond activation at the phenyl ring worked out well (Scheme 2). The ^{1}H-NMR and the elemental analysis (EA) confirmed the structure expected from literature known yttrium phenyl pyridyl complexes.[29] Furthermore, we decided to synthesise a new initiator bearing the two desired motifs of **1** and the very fast and effective *sym*-collidine. 2,6-Dimethyl-4-(4-vinylphenyl) pyridine was successfully synthesised *via* a five-step route starting from 2,6-dimethylpyridine (Scheme 1). The 3-step synthesis of 4-iodo-2,6-dimethylpyridine followed literature procedures[30,31] whereof the transhalogenation was published only recently.[32]

To obtain 4-(2,6-dimethylpyridin-4-yl)benzaldehyde (**4**), a Suzuki coupling of **3** with 4-formylphenylboronic acid was performed in high yields. The final product, 2,6-dimethyl-4-(4-vinylphenyl)pyridine (**5**), was obtained through a Wittig reaction and fully characterised by EA, electrospray ionisation mass spectrometry (ESI-MS), ^{1}H- and ^{13}C-NMR spectroscopy. Subsequently, the C–H bond activation was studied (Scheme 2). As expected, immediately after the addition of the initiator to the dissolved catalyst, the solution turned red. Full conversion was reached after 90 minutes. With NMR spectroscopy and EA, we proved, that one methyl group of **5** was turned into a methylene group *via* C–H bond activation and that the THF molecule was still coordinated to the yttrium.

Kinetic investigations on the new Cp_2Y complexes (7 and 8) in DEVP polymerisation

To evaluate the characteristics of the novel catalysts **7** and **8**, kinetic measurements were performed as the first step. Fig. 1 shows the conversion-time plot for the polymerisation of DEVP using complex **7** in black. The turn-over frequency (TOF) was 47 900 h^{-1}, which was about 20% lower compared to the value of 59 400 h^{-1} of *sym*-collidine.[6] The initiator efficiency (I^*) was found to be only 8% at the beginning and 7% at the end of the reaction. We assume, that the initiation of the DEVP poly-

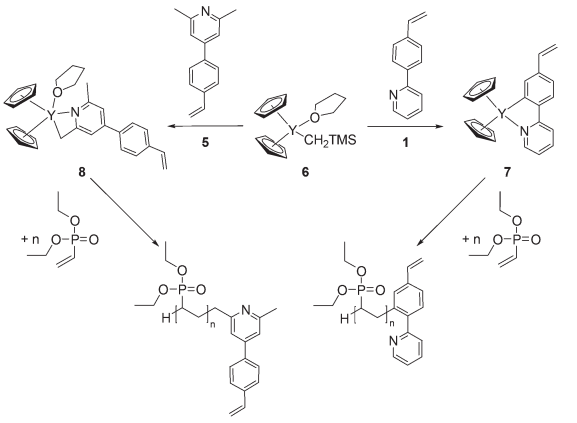

Scheme 2 C–H bond activation of **1** and **5** followed by polymerisation of DEVP.

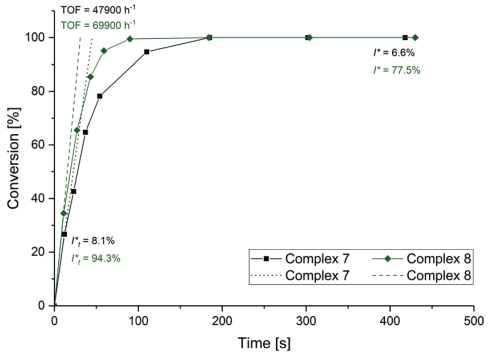

Fig. 1 Conversion–time plot for the polymerisation of DEVP using complex **7** (black squares) and complex **8** (green diamonds) (21.7 μmol catalyst, 600 eq. DEVP in 10.0 mL toluene at 30 °C).

merisation is more sterically hindered at the phenyl ring compared to the methyl group in case of *sym*-collidine. Furthermore, the polymerisation reaction starts heterogeneously, since the activated complex precipitated partially during the activation in toluene. Performing the activation reaction in dichloromethane and hexane did not improve the solubility. In tetrahydrofuran and acetone, conversions remained incomplete and decomposition was observed. The precipitate was not soluble in any common solvent. A clear solution is obtained only after the addition of DEVP. This might lead to a prolonged initiation period which results in a lower I^* and TOF. M_n and the polydispersity indices (PDIs) are plotted against conversion in Fig. S1† to proof the living character of the polymerisation.

Subsequently, the novel complex **8** was used for the polymerisation of DEVP. Fig. 1 shows the conversion-time plot for the polymerisation of DEVP catalysed by complex **8** in green. The living character, as well as the polydispersity indices (PDIs) as a function of the conversion of this polymerisation reaction, are presented in Fig. 2. To the best of our knowledge, the TOF of 69 900 h^{-1} is the highest TOF reported to date for the polymerisation of DEVP. The initiator efficiency, especially at the steepest slope of the reaction, was exceptionally high. *sym*-Collidine shows a lower TOF (factor 10 500 h^{-1}) and I_t^* (73%) compared to complex **8** (I_t^* of 94%).[6] This indicates, that the newly developed complex **8** has no initiation period, is highly active and efficient in the polymerisation of DEVP. Therefore, it is the perfect candidate for the synthesis of PDEVP, leading to narrow PDIs and to the desired molecular weights for subsequent end-group functionalisation. For the following investigations, **5** was the initiator of choice.

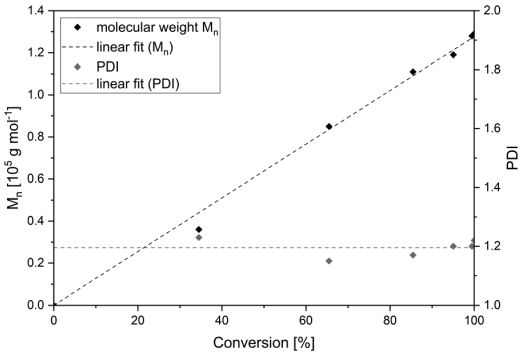

Fig. 2 Conversion–dependent plot of M_n and the respective PDI of the polymer aliquots generated during kinetic investigations using complex **8** (21.7 μmol catalyst, 600 eq. DEVP in 10.0 mL toluene, 30 °C).

End-group analysis *via* NMR and ESI-MS

To start with the post-polymerisation functionalisation, the presence of the end-group had to be proven. The expected ^{1}H-NMR signals of **5** were found and assigned. For the subsequent thiol–ene click reactions, the vinyl group signals are the most important. These are visible as a doublet of doublets at 6.80 ppm and as doublets at 5.88 and 5.32 ppm in CD_3OD (Fig. 4 in black). ESI-MS analysis further corroborated the presence of the covalently bound initiator. Fig. 3 shows a representative spectrum of oligomeric DEVP proving, that the desired end-group is attached to the chain. The found *m*/*z* values corresponded to initiator **5** ionised with H^+ (210 g mol^{-1}) and its oligomers ionised either with H^+ (374, 538 and 702 g mol^{-1}) or with Na^+ (560 and 724 g mol^{-1}). These findings clearly confirmed the presence of the initiating group at the chain end.

Synthesis of activated biomolecules

For the coupling of cholesterol and folic acid to the polymers, activated derivatives had to be synthesised. Thiocholesterol was obtained *via* a high-yielding and well-established two step route starting from the chloro derivative.[33]

For the coupling of folic acid to the polymer chain, another route had to be chosen, since thiofolic acid prevented the radical thiol–ene click reaction. The group of Mukherjee[34] demonstrated, that folic acid acts as a scavenger, thereby preventing radical reactions (Scheme 3). Consequently, we coupled cysteamine to the double bond of initiator **5** *via* a

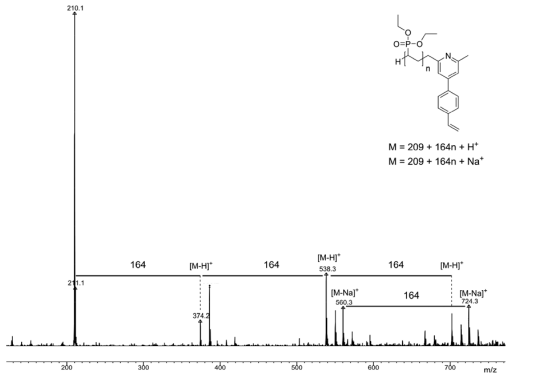

Fig. 3 ESI-MS of oligomeric DEVP measured in methanol/acetonitrile.

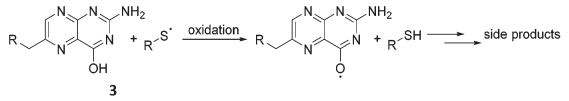

Scheme 3 Radical oxidation of folic acid.[34]

thiol–ene click reaction. Afterwards, the free amine group was reacted with a *N*-hydroxysuccinimide (NHS)-activated folic acid to form an amide bond (Scheme 4). The synthesis of the NHS-activated folic acid was performed in accordance to literature procedures.[35,36]

Ahead of starting the functionalisation reactions, two polymers with varying chain lengths were produced (Table 1). M_n and PDI were determined *via* gel permeation chromatography multi-angle light scattering (GPC-MALS). The cloud point (T_c) was defined as the temperature corresponding to a 10% decrease in optical transmittance. These turbidity measurements were performed on a UV/Vis device with 2.5 mg mL^{-1} in water. The data are shown in Fig. S8.†

Thiol–ene click reaction towards PDEVP-biomolecule conjugates

Adjacently, thiocholesterol was attached to the polymers in a temperature-induced thiol–ene click reaction started by the initiator azobisisobutyronitrile (AIBN) (Scheme 4). The reaction yielded full conversion after 24 hours at 70 °C. Fig. 4 shows exemplary ^{1}H-NMR excerpts of PDEVP before (black) and after functionalisation with cholesterol (green). The signals from the vinyl group of **5** disappear and the singlet of the cholesterol double bond comes up at 5.34 ppm. The chemical shifts of the functionalised polymers are summarised in Table S1† and the whole spectra are presented in Fig. S9 and S10.†

Table 2 entries 1 and 2 list the polymer data after the successful coupling to cholesterol. UV/Vis measurements of the coupled structures revealed the preservation of the LCST near the physiological range, similar to those of the homopolymers (Fig. S11 and S12†). Ensuing, the coupling of cysteamine to PDEVP was conducted successfully. The amidation reaction showed full conversion after 48 hours at 50 °C (Scheme 4). The received polymer-biomolecule conjugates were analysed and

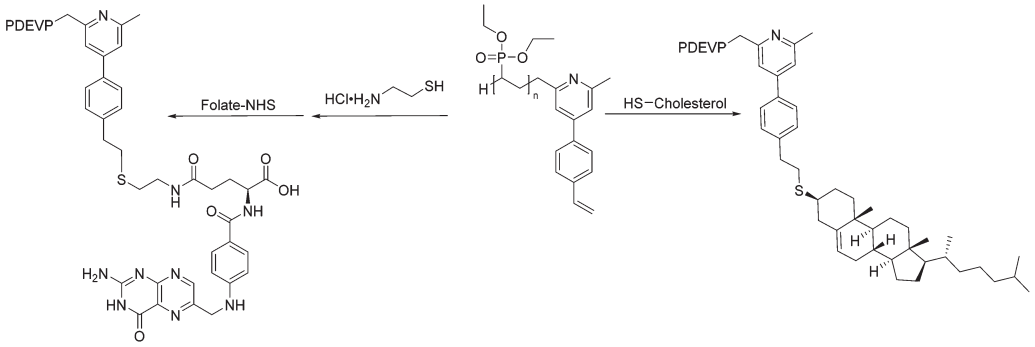

Scheme 4 Conjugation of the activated biomolecules to polymer.

Table 1 Molecular weight (M_n), PDI, signals in ^{1}H- and ^{31}P-NMR, initiator efficiency (I*) and cloud point (T_c) of PDEVP in aqueous solutions

	$[M]_0/[Cat]_0$	M_n [kg mol^{-1}]	PDI	^{1}H-NMR (500 MHz, CD_3OD, 300K) δ [ppm]	^{31}P-NMR (203 MHz, CD_3OD, 300 K) δ [ppm]	I* [%]	T_c [°C]
1	100	18.7	1.09	7.75 (qd, J_3 = 7.7, 4.0 Hz, 2H, H_{arom}), 7.60–7.39 (m, 4H, H_{arom}), 6.80 (dd, J_3 = 17.6, 10.8 Hz, 1H, H_{vinyl}), 5.88 (d, J_3 = 17.6 Hz, 1H, H_{vinyl}), 5.32 (d, J_3 = 10.8 Hz, 1H, H_{vinyl}), 4.18 (s, POCH_2), 3.07–0.97 (m, PDEVP), 1.38 (s, $POCH_2CH_3$)	33.2	89	48.0
2	600	158	1.01	7.79–7.70 (m, 2H, H_{arom}), 7.59–7.38 (m, 4H, H_{arom}), 6.80 (dd, J_3 = 17.6, 10.9 Hz, 1H, H_{vinyl}), 5.88 (d, J_3 = 17.6 Hz, 1H, H_{vinyl}), 5.32 (d, J_3 = 10.9 Hz, 1H, H_{vinyl}), 4.18 (s, POCH_2), 3.09–0.74 (m, PDEVP), 1.38 (s, $POCH_2CH_3$)	33.2	62	43.0

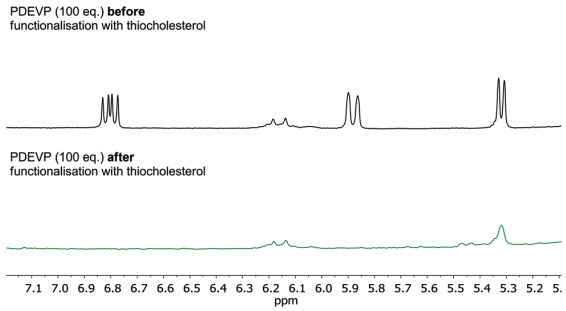

Fig. 4 ^{1}H-NMR spectra in MeOD of PDEVP (100 eq.) before (black) and after (green) functionalisation with thiocholesterol.

Table 2 Molecular weight (M_n), PDI, yield and cloud points (T_c) of cholesterol- (entries 1 and 2) and folic acid-functionalised PDEVP (entries 3 and 4)

	Substrate	M_n [kg mol^{-1}]	PDI	Yield [%]	T_c [°C] (H_2O)
1	PDEVP (100 eq.)	25.1	1.08	100	40.5
2	PDEVP (600 eq.)	178	1.05	100	40.5
3	PDEVP (100 eq.)	24.8	1.13	100	52.0
4	PDEVP (600 eq.)	184	1.10	100	43.0

the resulting data are presented in Table 2 entries 3 and 4. These new compounds as well exhibited thermal responses visible in Fig. S13 and S14.† Finally, the cytotoxicity of the polymers on cells was tested. This is an essential criterion for future applications in the biomedical field. Two cell lines were used for this screening: HEK-293 is a human embryonic renal cell line,[37,38] while HMEC-1 are immortalised human microvascular endothelial cells.[39,40] Both cell lines were originally obtained from the American Type Culture Collection, ATCC.

Cytotoxicity screening

The cytotoxicity was measured *via* the colorimetric 3-(4,5-dimethylthiazol-2-yl)-2,5-diphenyltetrazolium bromide (MTT) assay. This analysis of the cell metabolic activity represents the number of viable cells.[41–43] For the cell viability assays, cells were plated on 96 well plates, cultured for 24 hours and then treated with the polymer samples (dissolved in phosphate-buffered saline) for varying time periods and at differing concentrations. The resulting graphs of the MTT assay are shown in Fig. 5. Outside of a few instances, all of the measured viabilities were above 50%. This was surprising, since, in certain cases, very high amounts of polymer were applied to the cells. Moreover, some data points exist above 100% and were interpreted to indicate, that the polymers were beneficial for cell

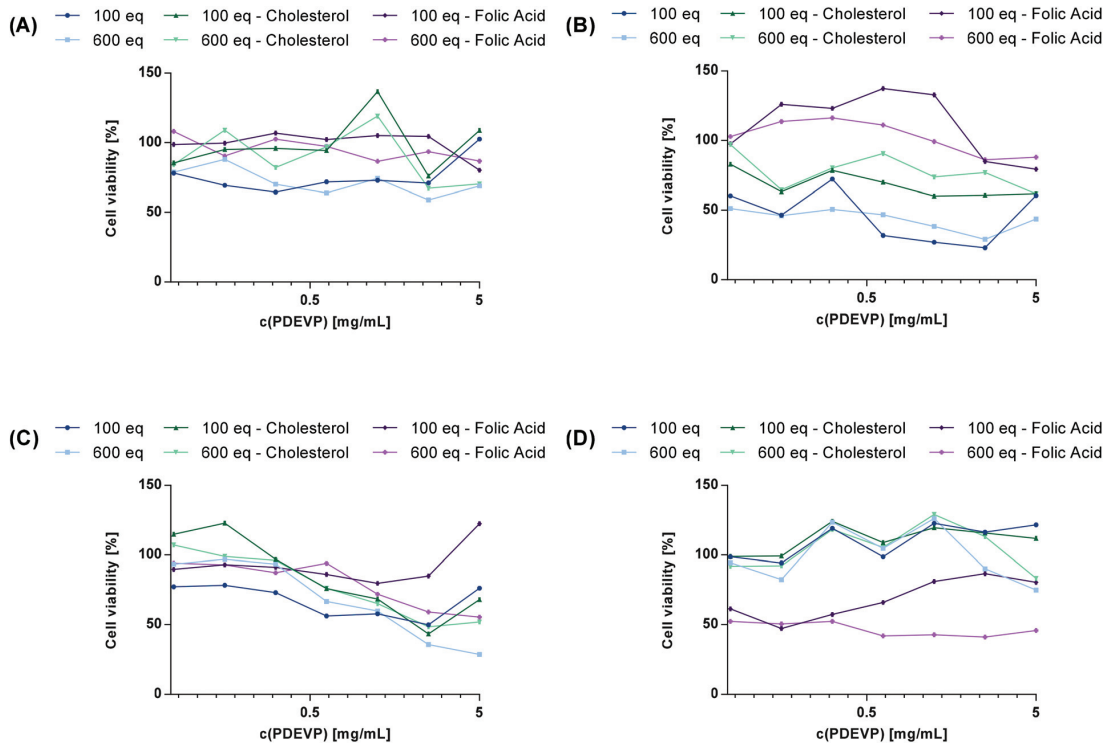

Fig. 5 Cell viability of (A) HEK-293 cells after 24 h and (B) 48 h, and (C) HMEC-1 cells after 24 h and (D) 48 h of incubation with polymer samples (measured in triplicate, standard error of the mean indicated).

growth. To conclude, the toxicity of the polymers towards renal cells and endothelial cells appears to be low. In most cases, the two anchor units seem to be advantageous with regards to the toxicity compared to polymers without functionalisation.

Conclusions

In summary, it was feasible to synthesise a novel initiator for the REM-GTP of DEVP. The structure contained the beneficial motifs of *sym*-collidine and 2-(4-vinylphenyl)pyridine. Using the C–H bond activated Cp_2Y complex, the highest TOF and I^* values in DEVP polymerisation were achieved, to date, resulting in an exceptionally fast and efficient catalysis. *Via* the thiol–ene click reaction on the new end-group, cholesterol and folic acid were coupled to the polymer chain. These novel conjugates are interesting for many applications, because they are water-soluble, thermoresponsive and biocompatible. Furthermore, they might have gained a biological function. Cholesterol is an inalienable constituent of cellular membranes, whereas folic acid is recognised by the folic acid receptor and taken up into the cell. Ongoing studies in our laboratory will investigate further the retention of these biological functions in the conjugates.

Conflicts of interest

There are no conflicts to declare.

Acknowledgements

The authors thank Philipp Güllich for performing the kinetic measurements and Dr Peter Altenbuchner for proof reading.

References

1 B. S. Soller, S. Salzinger and B. Rieger, *Chem. Rev.*, 2016, **116**, 1993–2022.
2 U. B. Seemann, J. E. Dengler and B. Rieger, *Angew. Chem., Int. Ed.*, 2010, **49**, 3489–3491.
3 N. Zhang, S. Salzinger and B. Rieger, *Macromol.*, 2012, **45**, 9751–9758.
4 S. Salzinger and B. Rieger, *Macromol. Rapid Commun.*, 2012, **33**, 1327–1345.
5 S. Salzinger, B. S. Soller, A. Plikhta, U. B. Seemann, E. Herdtweck and B. Rieger, *J. Am. Chem. Soc.*, 2013, **135**, 13030–13040.
6 B. S. Soller, S. Salzinger, C. Jandl, A. Pöthig and B. Rieger, *Organometallics*, 2015, **34**, 2703–2706.
7 H. Kaneko, H. Nagae, H. Tsurugi and K. Mashima, *J. Am. Chem. Soc.*, 2011, **133**, 19626–19629.
8 H. C. Kolb, M. G. Finn and K. B. Sharpless, *Angew. Chem., Int. Ed.*, 2001, **40**, 2004–2021.
9 R. Hoogenboom, *Angew. Chem., Int. Ed.*, 2010, **49**, 3415–3417.
10 A. B. Lowe, C. E. Hoyle and C. N. Bowman, *J. Mater. Chem.*, 2010, **20**, 4745–4750.
11 J. Justynska, Z. Hordyjewicz and H. Schlaad, *Polymer*, 2005, **46**, 12057–12064.
12 B. S. Sumerlin and A. P. Vogt, *Macromol.*, 2010, **43**, 1–13.
13 A. B. Lowe, *Polym. Chem.*, 2010, **1**, 17–36.
14 H. C. Kolb and K. B. Sharpless, *Drug Discovery Today*, 2003, **8**, 1128–1137.
15 H. H. Sandstead, *Am. J. Clin. Nutr.*, 1995, **61**, 621S–624S.
16 J. M. Baskin, J. A. Prescher, S. T. Laughlin, N. J. Agard, P. V. Chang, I. A. Miller, A. Lo, J. A. Codelli and C. R. Bertozzi, *Proc. Natl. Acad. Sci. U. S. A.*, 2007, **104**, 16793–16797.
17 B. Colak, J. C. S. Da Silva, T. A. Soares and J. E. Gautrot, *Bioconjugate Chem.*, 2016, **27**, 2111–2123.
18 Y. Liu, W. Hou, H. Sun, C. Cui, L. Zhang, Y. Jiang, Y. Wu, Y. Wang, J. Li, B. S. Sumerlin, Q. Liu and W. Tan, *Chem. Sci.*, 2017, **8**, 6182–6187.
19 P. L. Yeagle, *Biochimie*, 1991, **73**, 1303–1310.
20 S. Heino, S. Lusa, P. Somerharju, C. Ehnholm, V. M. Olkkonen and E. Ikonen, *Proc. Natl. Acad. Sci. U. S. A.*, 2000, **97**, 8375–8380.
21 X.-M. Liu, Y.-Y. Yang and K. W. Leong, *J. Colloid Interface Sci.*, 2003, **266**, 295–303.
22 H. Mizuno, M. Abe, P. Dedecker, A. Makino, S. Rocha, Y. Ohno-Iwashita, J. Hofkens, T. Kobayashi and A. Miyawaki, *Chem. Sci.*, 2011, **2**, 1548–1553.
23 S. D. Weitman, R. H. Lark, L. R. Coney, D. W. Fort, V. Frasca, V. R. Zurawski and B. A. Kamen, *Cancer Res.*, 1992, **52**, 3396–3401.
24 D. J. O'Shannessy, E. B. Somers, E. Albone, X. Cheng, Y. C. Park, B. E. Tomkowicz, Y. Hamuro, T. O. Kohl, T. M. Forsyth, R. Smale, Y.-S. Fu and N. C. Nicolaides, *Oncotarget*, 2011, **2**, 1227–1243.
25 S. Gorle, M. Ariatti and M. Singh, *Int. Proc. Chem., Biol. Environ. Eng.*, 2013, **52**, 1–4.
26 C. E. Wang, H. Wei, N. Tan, A. J. Boydston and S. H. Pun, *Biomacromolecules*, 2016, **17**, 69–75.
27 E. C. Calvaresi and P. J. Hergenrother, *Chem. Sci.*, 2013, **4**, 2319–2333.
28 M. C. DeRosa, D. J. Hodgson, G. D. Enright, B. Dawson, C. E. B. Evans and R. J. Crutchley, *J. Am. Chem. Soc.*, 2004, **126**, 7619–7626.
29 B. N. Williams, D. Benitez, K. L. Miller, E. Tkatchouk, W. A. Goddard and P. L. Diaconescu, *J. Am. Chem. Soc.*, 2011, **133**, 4680–4683.
30 H. P. Kokatla, P. F. Thomson, S. Bae, V. R. Doddi and M. K. Lakshman, *J. Org. Chem.*, 2011, **76**, 7842–7848.
31 B. Singh, G. Y. Lesher and P. O. Pennock, *J. Heterocycl. Chem.*, 1990, **27**, 1841–1842.
32 P. Pahl, C. Schwarzenböck, F. A. D. Herz, B. S. Soller, C. Jandl and B. Rieger, *Macromol.*, 2017, **50**, 6569–6576.

33 G. L. O'Connor and H. R. Nace, *J. Am. Chem. Soc.*, 1953, **75**, 2118–2123.
34 R. Joshi, S. Adhikari, B. S. Patro, S. Chattopadhyay and T. Mukherjee, *Free Radical Biol. Med*, 2001, **30**, 1390–1399.
35 C. M. Alexander, K. L. Hamner, M. M. Maye and J. C. Dabrowiak, *Bioconjugate Chem.*, 2014, **25**, 1261–1271.
36 A. F. Trindade, R. F. Frade, E. M. Macoas, C. Graca, C. A. Rodrigues, J. M. Martinho and C. A. Afonso, *Org. Biomol. Chem.*, 2014, **12**, 3181–3190.
37 F. L. Graham, J. Smiley, W. C. Russell and R. Nairn, *J. Gen. Virol.*, 1977, **36**, 59–72.
38 N. Louis, C. Evelegh and F. L. Graham, *Virology*, 1997, **233**, 423–429.
39 E. W. Ades, F. J. Candal, R. A. Swerlick, V. G. George, S. Summers, D. C. Bosse and T. J. Lawley, *J. Invest. Dermatol.*, 1992, **99**, 683–690.
40 V. A. Nguyen, C. Fürhapter and N. Sepp, *Microvasc. Res.*, 2001, **62**, 204–207.
41 T. Mosmann, *J. Immunol. Methods*, 1983, **65**, 55–63.
42 F. Denizot and R. Lang, *J. Immunol. Methods*, 1986, **89**, 271–277.
43 M. V. Berridge, P. M. Herst and A. S. Tan, *Biotechnol. Annu. Rev.*, 2005, **11**, 127–152.

4.4 Reprint Permission of Copyrighted Content

Dear Ms Schwarzenböck

The Royal Society of Chemistry (RSC) hereby grants permission for the use of your paper(s) specified below in the printed and microfilm version of your thesis. You may also make available the PDF version of your paper(s) that the RSC sent to the corresponding author(s) of your paper(s) upon publication of the paper(s) in the following ways: in your thesis via any website that your university may have for the deposition of theses, via your university's Intranet or via your own personal website. We are however unable to grant you permission to include the PDF version of the paper(s) on its own in your institutional repository. The Royal Society of Chemistry is a signatory to the STM Guidelines on Permissions (available on request).

Please note that if the material specified below or any part of it appears with credit or acknowledgement to a third party then you must also secure permission from that third party before reproducing that material.

Please ensure that the thesis states the following:

Reproduced by permission of The Royal Society of Chemistry

and include a link to the paper on the Royal Society of Chemistry's website.

Please ensure that your co-authors are aware that you are including the paper in your thesis.

Best wishes,

Chloe Szebrat
Contracts and Copyright Executive
Royal Society of Chemistry
Thomas Graham House
Science Park, Milton Road
Cambridge, CB4 0WF, UK
Tel: +44 (0) 1223 438329
www.rsc.org

5 Fluorescent Polyvinylphosphonate Bioconjugates for Selective Cellular Delivery

5.1 Bibliographic Data

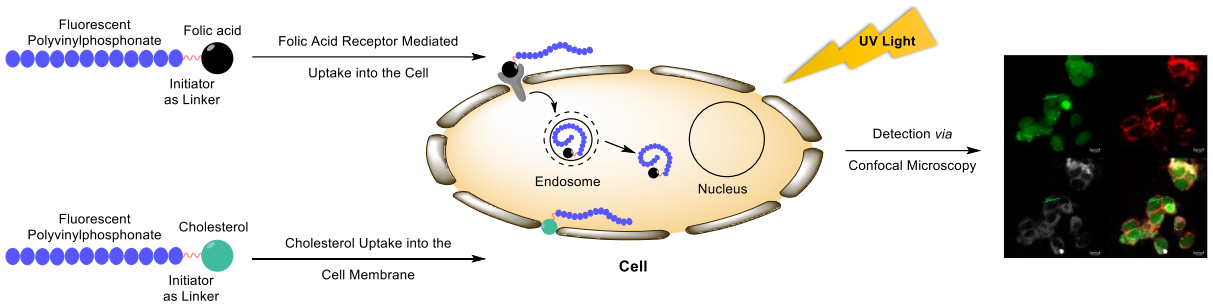

Title: "Fluorescent Polyvinylphosphonate Bioconjugates for Selective Cellular Delivery "

Status: Communication, Accepted manuscript online: January 8, 2018

Journal: Chemistry – A European Journal, 2018, 24, 2584 – 2587

Publisher: John Wiley and Sons

Link/DOI: https://doi.org/10.1002/chem.201706034

Authors: Christina Schwarzenböck, Andreas Schaffer, Elfriede Nößner, Peter J. Nelson, Ralf Huss and Bernhard Rieger

5.2 Summary

Thus far, numerous poly(ethylene glycol) (PEG) and poly(N-isopropylacrylamide) (PNIPAAm) biomolecule conjugates have been synthesized, but they often show long response times, are not bio-inert, or lose function in biological fluids. Herein, we present a modular synthesis route towards polyvinylphosphonate biomolecule conjugates. It was feasible to fluorescently label PDEVP–cholesterol and folic acid constructs *via* a partial transesterification approach. The modifications proceeds *via* the trimethylsilyl ether intermediate. The subsequent deprotection is enabled by tetra-*n*-butylammonium fluoride (TBAF) and followed by the addition of pyrene to the activated positions. The new macromolecules remained water-soluble despite the linkage of the hydrophobic pyrene side groups. These conjugates exhibit an exact lower critical solution temperature even in biological fluids, where only few other examples with this property have been reported thus far. Of capital importance was the ascertainment that the biological functions of the polymers depend on their anchor units, which were linked through the thiol-ene click conjugation step. The bound biomolecules can govern the localization of the polymer in the cell. The PDEVP–cholesterol constructs are attached to the cellular membrane, whereas the folic acid anchored polymers are shuttled into the cells. This is an exceptional finding through a straightforward synthetic approach. Consequently, this modular synthetic strategy opens the door to a plurality of applications and facilitates multiple modifications.

5.3 Manuscript

ChemPubSoc Europe

DOI: 10.1002/chem.201706034

CHEMISTRY A European Journal Communication

Polymers

Fluorescent Polyvinylphosphonate Bioconjugates for Selective Cellular Delivery

Christina Schwarzenböck,[a] Andreas Schaffer,[a] Elfriede Nößner,[b] Peter J. Nelson,[c] Ralf Huss,[d] and Bernhard Rieger*[a]

Abstract: To date, many poly(ethylene glycol) (PEG) and poly(*N*-isopropylacrylamide) (PNIPAAm) biomolecule conjugates have been described, but they often show long response times, are not bio-inert, or lose function in biological fluids. Herein, we present a modular synthetic approach to generate polyvinylphosphonate biomolecule conjugates. These conjugates exhibit a sharp phase transition temperature even under physiological conditions where few other examples with this property have been described to date. Furthermore, it was feasible to add biological functions to the polymers via the conjugation step. The polyvinylphosphonate cholesterol constructs are attached to the cellular membrane and the folic acid anchored polymers are shuttled into the cells. This is an exceptional finding through a straightforward synthetic approach.

Targeting of therapeutic agents to specific cells, or even to compartments in the cells, promises the optimization of therapeutic efficacy, along with minimizing the systemic side effects. Two main targeting strategies exist, of which the active targeting is mostly preferred to the less specific, passive targeting. Active targeting can be driven by antibodies, polysaccharides, biomolecules and manifold other structures.[1] Folic acid is a widely used ligand for the folic acid receptor alpha (FR-α).[2] The binding of folic acid to its receptor drives the uptake via endocytosis and therefore can be used to transport agents into a cell.[3] In addition, folic acid is essential for the synthesis of nucleic acids and for the metabolism of amino acids, which are required for cell division.[4] Consequently FR-α is overexpressed on many cancer cells, since they divide rapidly and have an enormous folic acid consumption.[5,6] By contrast, the anchoring of molecules to the cellular membrane represents a less specific method for cellular engineering. The lipid cholesterol is an important component of the cell wall.[7] It is required for the structure of the cellular membrane and modulates its fluidity.[8] Additionally, a cholesterol homeostasis is maintained in the blood stream. This is mainly regulated by the lipoprotein receptors, which govern cholesterol uptake.[9]

In an earlier study we were able to connect these two disparate biomolecules, via thiol-ene click chemistry, to the water-soluble, biocompatible and thermoresponsive polyvinylphosphonates.[10] It was shown that the new conjugates have low toxicities and that the thermoresponsive behavior was maintained in water. However, at this stage it was not possible to report on the biological functions of the novel compounds, since there was no way of monitoring their uptake into cells. Herein, we present the fluorescent labeling of the conjugates via the partial transesterification of the polymer side chains. To accomplish this complex task, a strategy employed by our group for the hydrolysis of poly(diethyl vinylphosphonate) (PDEVP) was adapted.[11,12] The functionalization proceeds via the trimethylsilyl ether intermediate. The consecutive deprotection is rendered by tetra-*n*-butylammonium fluoride (TBAF) and followed by the addition of pyrene to the activated positions (Scheme 1). Functionalization degrees vary from 0.38 to 1.13% with 2.00% addressed and are highly dependent on the

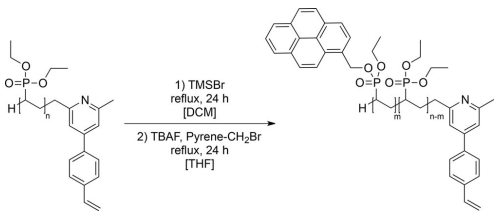

Scheme 1. Partial transesterification of side chain groups of poly(diethyl vinylphosphonates).

[a] *C. Schwarzenböck, A. Schaffer, Prof. Dr. B. Rieger*
WACKER-Lehrstuhl für Makromolekulare Chemie
Technische Universität München
Lichtenbergstraße 4, 85748 Garching bei München (Germany)
E-mail: rieger@tum.de

[b] *Prof. Dr. E. Nößner*
Immunoanalytics: Research Group Tissue Control of Immunocytes & Core Facility
Deutsches Forschungszentrum für Gesundheit und Umwelt
Helmholtz Zentrum München
Marchioninistraße 25, 81377 München (Germany)

[c] *Prof. Dr. P. J. Nelson*
Medizinische Klinik und Poliklinik IV
Nephrologisches Zentrum und Arbeitsgruppe Klinische Biochemie
Ludwig-Maximilians-Universität München
Schillerstraße 42, 80336 München (Germany)

[d] *Prof. Dr. R. Huss*
Definiens AG
Bernhard-Wicki-Straße 5, 80636 München (Germany)

Supporting information and the ORCID identification number(s) for the author(s) of this article can be found under https://doi.org/10.1002/chem.201706034.

ChemPubSoc Europe

CHEMISTRY A European Journal Communication

polymer chain length. The reason for this finding can be attributed to a lower conversion of the side groups in case of long chain PDEVP during the initial ester cleavage with trimethyl silyl bromide (TMSBr). This can be explained by a higher hygroscopy of the long chain polymer resulting in the degradation of TMSBr and therefore in a lower conversion.

The thermoresponsive properties were then characterized. All fluorescent samples and polymers from our recent publication were measured in water, and in a medium/phosphate buffer saline solution (DMEM/PBS) containing 1% antibiotics (PS) and 10% fetal bovine serum (FBS) (Table 1).[10] This composition was used in subsequent cell culture experiments. Intriguingly, the lower critical solution temperature (LCST) was retained for all tested polymers, even under these complex conditions. And all the more surprising, the three pyrene functionalized long chain polymers showed no LCST transition in water, whereas they have a sharp LCST in DMEM/PBS. The reason why, in case of the 600 equivalents fluorescent polymers no phase transitions in water can be measured are supposedly the π–π stacking interactions between the pyrene units and the resulting difficulties in the conformation change necessary for the LCST.[13] The heavy polymers contain more pyrene per chain and therefore pyrene interactions become more likely and their influence gets more prominent than for the lighter polymers. In not presented investigations we could observe a phase transition already in PBS and also in PBS/DMEM without PS and FBS, however the sharp reversible phase transition was only monitored in the presence of FBS. Consequently the main component affecting the thermoresponsive behaviour of the pyrene functionalized polymers is BSA, which was shown in a study of Xu et al.[14] to bind to pyrene. Therefore BSA can break up the interactions between the hydrophobic side groups of the functionalized PDEVPs and restore the precise thermoresponse that is known from this polymer class. To the best of our knowledge, the thermoresponsive nature of polymers in complex biological solutions has only been previously investigated by the groups of Kanazawa and Yang.[15,16] These groups studied the effect of electrolytes and serum on the LCST of poly(*N*-isopropylacrylamide), but DMEM/PBS with antibiotics and FBS was never used before. Consequently, the LCST of our PDEVP conjugates was measured in a fluid that strongly reflects physiological conditions and is also suitable for UV/Vis measurements.

Table 1. Comparison of cloud points (T_c) of PDEVP substrates in aqueous solution and DMEM/PBS (2:1)

Entry	Substrate	T_c [°C] (H_2O)	T_c [°C] (DMEM/PBS)
Non-fluorescent polymer substrates			
1	100 equiv. DEVP	48.0	48.0
2	600 equiv. DEVP	43.0	40.0
3	100 equiv. DEVP–cholesterol	40.5	40.5
4	600 equiv. DEVP–cholesterol	40.5	39.5
5	100 equiv. DEVP–folic acid	52.0	49.0
6	600 equiv. DEVP–folic acid	43.0	41.0
Fluorescent polymer substrates			
7	100 equiv. DEVP	46.0	38.0
8	600 equiv. DEVP	n.a	45.0
9	100 equiv. DEVP–cholesterol	50.5	41.0
10	600 equiv. DEVP–cholesterol	n.a.	42.5
11	100 equiv. DEVP–folic acid	54.0	45.0
12	600 equiv. DEVP–folic acid	n.a	42.5

Adjacent photophysical properties were studied. Figure 1 shows the absorbance spectra of all six fluorescent samples. The absorbance of short chain polymers is stronger than of the long ones. This finding is in accordance with the obtained functionalization degrees, which are higher in case of the polymers with lower molecular weight. The absorbance spanned from 200 to a maximal 450 nm. Consequently, all excitation experiments were conducted within this UV light range.

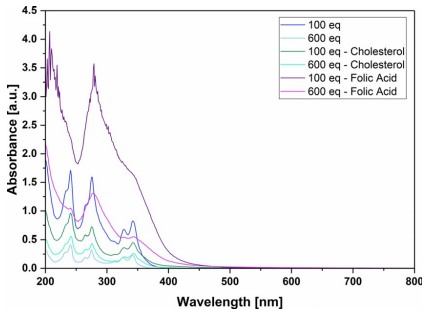

Figure 1. UV/Vis spectra of the fluorescent polymers in aqueous solution (2.5 mg mL^{-1}).

The second relevant photophysical property is the emission followed by irradiation, in this case at a 365 nm wavelength. The resulting spectra are presented in Figure 2. The first high peak for most polymers results from the irradiation. Their maximum emission was measured between 450 and 500 nm, which corresponds to blue fluorescence.

In the next phase of the study, the location of the polymers in the treated cells was investigated. To this end, the toxicity of

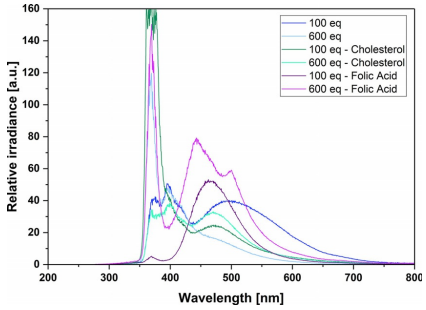

Figure 2. Photoluminescence spectra of the fluorescent polymers in aqueous solution (2.5 mg mL^{-1}).

ChemPubSoc Europe

CHEMISTRY A European Journal Communication

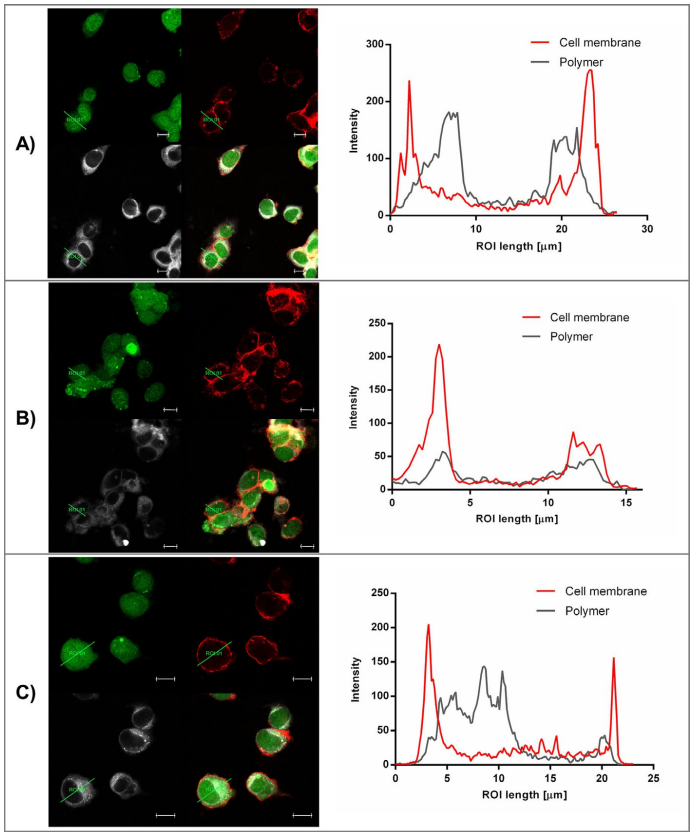

Figure 3. Confocal microscopy images and region of interest (ROI) analysis of HMEC-1 cells treated with A) polymer without anchor, B) polymer with cholesterol and C) polymer with folic acid. Scale bar represents 10 µm.

the fluorescent samples was first evaluated in comparison to the probes lacking pyrene. Pyrene and its metabolites are known to be cytotoxic.[17] The endothelial cell line HMEC-1, and the renal cell line HEK-293 showed reduced viability after treatment with fluorescent PDEVP for 24 or 48 hours (Figure S5–10). For cellular localization studies, a concentration of 1.25 mg mL^{-1} and an incubation time of four hours were selected as optimal conditions reflecting low cytotoxic effects and high fluorescence signals. The endothelial cells were treated with the polymers in the localization studies, since the HEK-293 cells grow in foci and are therefore less suitable for microscopic investigations. The most important localization findings are presented in Figure 3. Additional images and graphs are shown in Figures S11–S13.

The three cellular imaging techniques using confocal microscopy are shown in Figure 3. They represent green for the cellular cytoplasm, red for the cell membrane and grey for the polymer samples. Green staining was achieved with 5-chloromethylfluorescein diacetate (CMFDA)[18,19] and red with W6/32, a major histocompatibility complex I specific monoclonal antibody[20] and a rhodamine red™-X (RRX) fluorescent-labeled secondary antibody. CMFDA enters cells through the plasma membrane where it is converted into its fluorescent derivative. W6/32 was chosen as primary antibody, since the group of Sepp[21] showed expression of MHC I antigens on the surface of HMEC-1 cells. The graphs on the right side of each image in Figure 3 are the region of interest (ROI) plots of RRX and the polymers fluorescence to quantify, and locate, the fluorescence intensity of the applied polymer samples. Figure 3A shows that PDEVP without a targeting molecule can reach the inside of the cell. This is an important finding, consistent with our previous observation that micelles from 2-vinylpyridine–DEVP block copolymers can be taken up by HeLa cells.[22] A crucial observation was the localization of the cholesterol functionalized polymers at the cellular membrane demonstrated by the fluorescence co-localization of the plasma membrane stain

ChemPubSoc Europe

CHEMISTRY A European Journal Communication

W6/32-RRX and the polymer (Figure 3B, right panel). They are located to the cell wall and on its inner face of the membrane (See Figure 3B, S12, and 13). To the best of our knowledge, this is the first report of such an anchoring of thermoresponsive polymers to the plasma membrane. Many examples exist where cholesterol is the hydrophobic block of a polymeric micelle,[23–25] or where it has been added to liposomes for enhanced stability or uptake,[26–28] whereas our novel fluorescent PDEVP–cholesterol conjugates could be localized directly in the cellular membrane. The only studies existing about polymer–cholesterol conjugates are PEG and chitosan based ones, which are not thermoresponsive.[29–31] In contrast, the folic acid conjugates showed direct uptake into the cells (Figure 3C). Thus, it is possible to regulate the localization of PDEVP through the conjugation of one single biomolecule to the polymer chain. Consequently, a diverse potential application spectrum can be envisioned from targeted drug delivery in cancer research to the engineering of the cell membrane, including the selective addition of chemical functions to cells.

To conclude, it was possible to fluorescently label PDEVP–cholesterol and folic acid conjugates. The new macromolecules remained water-soluble and their LCST behavior was retained in biological fluids. Of capital importance was the observation that the polymer characteristics depend on their anchor unit. The attached biomolecules can regulate the localization of the polymer in the cell. Hence, this modular synthetic strategy opens the door to manifold applications and a plurality of functionalization options.

Acknowledgements

The authors thank Philipp Pahl for proof reading. We thank Anke Fischer and Sylke Rohrer for their support with the in vitro experiments.

Conflict of interest

The authors declare no conflict of interest.

Keywords: delivery · fluorescent polymer bioconjugate · selective cellular targeting · thermoresponsive polymer · thiolene click chemistry

[1] Y. Zhong, F. Meng, C. Deng, Z. Zhong, *Biomacromolecules* **2014**, *15*, 1955 – 1969.
[2] D. J. O'Shannessy, E. B. Somers, E. Albone, X. Cheng, Y. C. Park, B. E. Tomkowicz, Y. Hamuro, T. O. Kohl, T. M. Forsyth, R. Smale, Y.-S. Fu, N. C. Nicolaides, *Oncotarget* **2011**, *2*, 1227 – 1243.
[3] S. Gorle, M. Ariatti, M. Singh, *Int. Proc. Chem. Biol. Environ. Eng.* **2013**, *52*, 1 – 4.
[4] I. o. Medicine, *Dietary Reference Intakes for Thiamin, Riboflavin, Niacin, Vitamin B6, Folate, Vitamin B12, Pantothenic Acid, Biotin, and Choline*, The National Academies Press, Washington, DC, **1998**.
[5] S. D. Weitman, R. H. Lark, L. R. Coney, D. W. Fort, V. Frasca, V. R. Zurawski, B. A. Kamen, *Cancer Res.* **1992**, *52*, 3396 – 3401.
[6] E. C. Calvaresi, P. J. Hergenrother, *Chem. Sci.* **2013**, *4*, 2319 – 2333.
[7] P. L. Yeagle, *Biochimie* **1991**, *73*, 1303 – 1310.
[8] P. L. Yeagle, *Biochim. Biophys. Acta Rev. Biomembr.* **1985**, *822*, 267 – 287.
[9] M. S. Brown, P. T. Kovanen, J. L. Goldstein, *Science* **1981**, *212*, 628 – 635.
[10] C. Schwarzenböck, A. Schaffer, P. Pahl, P. J. Nelson, R. Huss, B. Rieger, *Polym. Chem.* **2017**.
[11] S. Salzinger, U. B. Seemann, A. Plikhta, B. Rieger, *Macromolecules* **2011**, *44*, 5920 – 5927.
[12] S. Salzinger, B. Rieger, *Macromol. Rapid Commun.* **2012**, *33*, 1327 – 1345.
[13] H. Ringsdorf, J. Venzmer, F. M. Winnik, *Macromolecules* **1991**, *24*, 1678 – 1686.
[14] C. Xu, J. Gu, X. Ma, T. Dong, X. Meng, *Spectrochim. Acta Part A* **2014**, *125*, 391 – 395.
[15] Y. Hiruta, Y. Nagumo, Y. Suzuki, T. Funatsu, Y. Ishikawa, H. Kanazawa, *Colloids Surf. B* **2015**, *132*, 299 – 304.
[16] C.-S. Chaw, K.-W. Chooi, X.-M. Liu, C.-w. Tan, L. Wang, Y.-Y. Yang, *Biomaterials* **2004**, *25*, 4297 – 4308.
[17] T. Yoshikawa, L. P. Ruhr, W. Flory, D. Giamalva, D. F. Church, W. A. Pryor, *Toxicol. Appl. Pharmacol.* **1985**, *79*, 218 – 226.
[18] R. G. Breuls, A. Mol, R. Petterson, C. W. Oomens, F. P. Baaijens, C. V. Bouten, *Tissue Eng.* **2003**, *9*, 269 – 281.
[19] V. Lulevich, Y.-P. Shih, S. H. Lo, G. – *y.* Liu, *J. Phys. Chem. B* **2009**, 113, 6511 – 6519.
[20] P. Parham, C. J. Barnstable, W. F. Bodmer, *J. Immunol.* **1979**, *123*, 342 – 349.
[21] V. A. Nguyen, C. Fürhapter, N. Sepp, *Microvasc. Res.* **2001**, *62*, 204 – 207.
[22] P. T. Altenbuchner, P. D. L. Werz, P. Schöppner, F. Adams, A. Kronast, C. Schwarzenböck, A. Pöthig, C. Jandl, M. Haslbeck, B. Rieger, *Chem. Eur. J.* **2016**, *22*, 14576 – 14584.
[23] W. Y. Seow, J. M. Xue, Y.-Y. Yang, *Biomaterials* **2007**, *28*, 1730 – 1740.
[24] S. Sevimli, F. Inci, H. M. Zareie, V. Bulmus, *Biomacromolecules* **2012**, *13*, 3064 – 3075.
[25] H.-T. Jiang, K. Ding, F.-N. Meng, L.-L. Bao, Y.-D. Chai, Y.-K. Gong, *J. Mater. Chem. B* **2016**, *4*, 5464 – 5474.
[26] K. Kusumoto, H. Akita, A. El-Sayed, H. Harashima, *Biol. Pharm. Bull.* **2012**, *35*, 445 – 448.
[27] H. Yin, H. C. Kang, K. M. Huh, Y. H. Bae, *Colloids Surf. B* **2014**, *116*, 128 – 137.
[28] C. Martin, N. Marino, C. Curran, A. P. McHale, J. F. Callan, B. Callan, *Int. J. Pharm.* **2016**, *511*, 570 – 578.
[29] H.-R. Jia, H.-Y. Wang, Z.-W. Yu, Z. Chen, F.-G. Wu, *Bioconjugate Chem.* **2016**, *27*, 782 – 789.
[30] X. Chen, X. Zhang, H.-Y. Wang, Z. Chen, F.-G. Wu, *Langmuir* **2016**, *32*, 10126 – 10135.
[31] H.-Y. Wang, J. Sun, L.-Y. Xia, Y.-H. Li, Z. Chen, F.-G. Wu, *ACS Biomater. Sci. Eng.* **2017**, *3*, 2570 – 2578.

Manuscript received: December 20, 2017
Accepted manuscript online: January 8, 2018
Version of record online: January 25, 2018

5.4 Reprint Permission of Copyrighted Content

Thank you for your order!

Dear Ms. Christina Schwarzenböck,

Thank you for placing your order through Copyright Clearance Center's RightsLink® service.

Order Summary

Licensee:	WACKER-Lehrstuhl für Makromolekulare Chemie
Order Date:	May 4, 2018
Order Number:	4341910482116
Publication:	Chemistry - A European Journal
Title:	Fluorescent Polyvinylphosphonate Bioconjugates for Selective Cellular Delivery
Type of Use:	Dissertation/Thesis
Order Total:	0.00 EUR

View or print complete details of your order and the publisher's terms and conditions.

Sincerely,

Copyright Clearance Center

6 Synthesis of Next Generation Dual-Responsive Cross-Linked Nanoparticles and their Application to Anti-Cancer Drug Delivery

6.1 Bibliographic Data

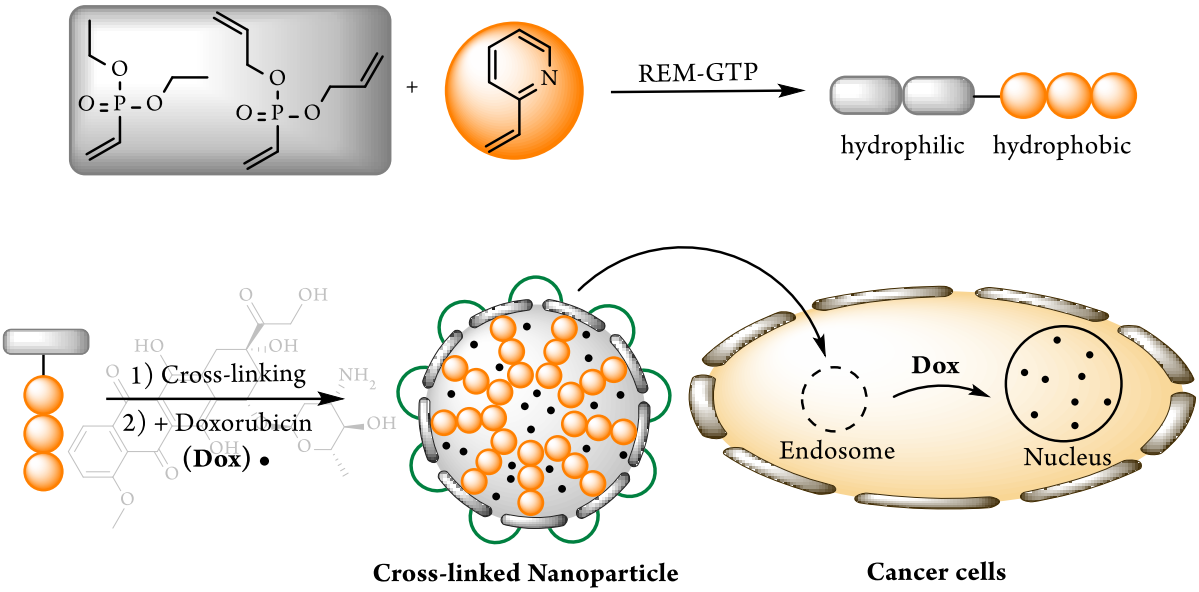

Title: "Synthesis of Next Generation Dual-Responsive Cross-Linked Nanoparticles and their Application to Anti-Cancer Drug Delivery"

Status: Full paper, Accepted 7th August 2018

Journal: Nanoscale, 2018, 10, 16062-16068

Publisher: Royal Society of Chemistry

Link/DOI: https://doi.org/10.1039/C8NR04760J

Authors: Christina Schwarzenböck, Peter J. Nelson, Ralf Huss and Bernhard Rieger

6.2 Summary

Rare earth metal-mediated group transfer polymerization renders the synthesis of previously inaccessible block copolymers of 2-vinylpyridine, diethyl vinylphosphonate and the novel diallyl vinylphosphonate monomer. This catalytic precision polymerization and the specific cross-linking of allyl side groups *via* thiol-ene click chemistry leads to the generation of well-defined dual-responsive nanoparticles. In the present study, three novel nanocarriers were synthesized and characterized. The copolymer substrates exhibited narrow polydispersities as well as controlled molecular weights. The particles, obtained after the successful thiol-ene click conjugation, are spherical, highly monodisperse and did not form concentration dependently. We evidenced that these next generation drug delivery vehicle show a sharp pH- and temperature-response as well as promising loading and release profiles. High anti-cancer activity could be demonstrated *via* cytotoxicity tests on breast cancer (MCF-7) and cervical cancer (HeLa) cells. Their biocompatibility appeared to depend on the monomer ratio of the block copolymer substrate applied for the conjugation step. The three types of particles each exhibited a fast and efficient release of their cargo *in vitro*. The vehicles are capable of delivering doxorubicin into the nucleus of cancer cells within only one hour of incubation time. To give the full picture of the transport characteristics of the nanocarriers, flow cytometry measurements were conducted. These experiments bring the statistical point of view into the analysis and showed, already after ten minutes, positive uptake results. After three hours very high DOX fluorescence signals could be detected. In consequence a high absorption, of the loaded particles, into the cells was achieved for a large number of cells. The microscopy results are therefore no artefacts, they represent the true transport characteristics of the polyvinylphosphonate particles into the cancer cells. These results validate this modular synthetic approach as an ideal platform for the evolution of sophisticated nanocarriers for future drug delivery applications.

6.3 Manuscript

Nanoscale

PAPER

View Article Online
View Journal | View Issue

Cite this: *Nanoscale*, 2018, **10**, 16062

Synthesis of next generation dual-responsive cross-linked nanoparticles and their application to anti-cancer drug delivery†

Christina Schwarzenböck,[a] Peter J. Nelson,[b] Ralf Huss[c] and Bernhard Rieger *[a]

Received 11th June 2018,
Accepted 7th August 2018

DOI: 10.1039/c8nr04760j

rsc.li/nanoscale

Rare earth metal-mediated group transfer polymerisation enables the synthesis of previously inaccessible block copolymers of 2-vinylpyridine, diethyl vinylphosphonate and the new diallyl vinylphosphonate monomer. This precision polymerisation and the selective cross-linking of allyl side groups *via* thiol–ene click chemistry leads to the formation of well-defined dual-responsive nanoparticles. We demonstrate that these next generation nanocarriers are pH- and temperature-responsive and are capable of efficiently delivering doxorubicin into the nucleus of cancer cells. High anti-cancer activity could be demonstrated *via* cytotoxicity tests on breast cancer (MCF-7) and cervical cancer (HeLa) cells. These results validate this modular synthesis route as an ideal platform for the development of sophisticated nanocarriers for future drug delivery applications.

Introduction

Responsive drug delivery vehicles have the potential to revolutionise future anti-cancer therapies. The most potent drugs in this field still have major issues that include an inefficient systemic distribution, hydrophobicity, low targeting efficiency and resulting toxicity towards all tissue types.[1] The so-called molecular target therapy approach, which focuses on targeting specific overexpressed receptors on the tumour cell surface have yielded less than optimal results in clinical studies.[2,3] This has underscored the clinical need for novel carriers that minimise side effects and maximise dose efficacy of chemotherapy.[4–6] Due to their auspicious characteristics polymeric nanoparticles represent a promising platform for targeted and controlled drug delivery.[7–11] Multiple reports have shown that 24 h after intravenous injection, the accumulation of most macromolecular therapeutics was 10–200 times higher in malignant as compared to healthy tissues and organs.[12–16] Currently, on-going clinical studies have suggested an emerging acceptance of this field of research in the pharma industry. The early studies have demonstrated positive effects from the application of polymeric nanoparticles as drug delivery vehicles, *e.g.*, reduced side effects, enhanced drug uptake into the tumour tissue and prolonged systemic circulation times.[17–19] However, the vehicles tested, comprising non-responsive polymers like poly(ε-caprolactone), poly(lactide) or poly(lactide-*co*-glycolide), lack important properties linked to stability upon injection and therefore target specific release behaviours.[20,21] Thus far, approved nanotherapeutics, such as Doxil, DaunoXome, Abraxane and Genexol-PM have exhibited only limited progress as compared with free drugs.[8] While these nanotherapeutics are capable of reducing adverse therapeutical effects, patient survival rates have been only marginally prolonged.[22,23] These findings highlight the importance of developing stimuli-responsive materials for biomedical applications. There are two general approaches used for stimulating the release of nanocarrier cargo: the use of either internal or external stimuli.[24] Cancer tissue and therapy methods have unique properties with regards to temperature and pH (pH < 6, T = 40–43 °C), which can be exploited for internal or external stimuli-targeted delivery applications.[11,25–28] Thus, pH- and temperature-responsive systems are of special interest for the selective delivery of agents, in part, due to the naturally occurring pH gradients in cancer tissues as well as along the endocytic pathway (physiological pH = 7.4 and T = 37 °C, endosomal pH = 5.5–6.0, lysosomal pH = 3.5–5.5).[29–32] For thermo-responsive polymers used in concert with regional hyperthermia, poly(*N*-isopropylacrylamide) (PNIPAam) represents the current gold standard in the biomedical field.[28,33,34] However, drawbacks linked to the application of PNIPAam, are seen. These include their broad range of phase transitions, copolymerisation must attain a lower critical solution temperature in

[a]*WACKER Lehrstuhl für Makromolekulare Chemie, Technische Universität München, Lichtenbergstraße 4, 85748 Garching bei München, Germany. E-mail: rieger@tum.de*
[b]*Medizinische Klinik und Poliklinik IV, Nephrologisches Zentrum und Arbeitsgruppe Klinische Biochemie, University of Munich, Munich, Germany*
[c]*Definiens AG, Bernhard-Wicki-Strasse 5, 80636 Munich, Germany*

†Electronic supplementary information (ESI) available. See DOI: 10.1039/c8nr04760j

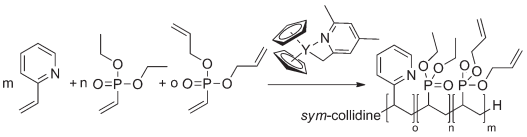

Scheme 1 Block copolymerisation of 2VP, diethyl vinylphosphonate (DEVP) and the new DAlVP with $Cp_2Y(CH_2(C_5H_2Me_2N))$ as catalyst.

the physiological range, and they show functional loss in biological fluids.[35,36] Thermoresponsive materials, with suitable properties for application under physiological conditions linked to therapy, have been scarce.[37] Thus, the development of new, water-soluble, thermo-responsive and biocompatible polymers is crucial for future applications of thermoresponsive polymer carriers in human medicine. One promising polymer class, with all these properties, are the polyvinylphosphonates. In 2016 our group proposed the application of AB block copolymer micelles, comprising polyvinylphosphonate and poly(2-vinylpyridine) (P2VP) as next generation nanocarriers.[38] The micelles displayed excellent loading and release properties and were responsive to pH as well as to temperature triggers. However, micelle formation was concentration dependent, limiting its application to local administration and rendering systemic dosing impossible. Therefore, it became important to develop stable, cross-linked nanoparticles with similar or improved delivery characteristics as compared to the micelles. The monomer diallyl vinylphosphonate (DAlVP) was found to address these complex criteria. This molecule was previously synthesised by the *Micura* group and used as an intermediate in the synthesis of a *t*RNA molecule on a solid support.[39] DAlVP polymerisation, thus far, has only been accomplished *via* undefined, radical cross-linking reactions. However, the vinyl group has never been selectively polymerised.[40,41] Scheme 1 depicts the structure of the three monomers used in the copolymerisation procedure. Rare earth metal-mediated group transfer polymerisation (REM-GTP) was the technique of choice to synthesise polymers with narrow polydispersities and the desired molecular weights. Bis(cyclopentadienyl)(4,6-dimethyl-pyridin-2-yl)methyl yttrium ($Cp_2Y(CH_2(C_5H_2Me_2N))$), developed by our group, was employed as catalyst complex for block copolymerisation.[42] The 2,4,6-trimethyl pyridine initiator used is also known as *sym*-collidine.

Results and discussion

The analytical data describing the three block copolymers discussed in this study are presented in Table 1. Monomer amounts of 100 or 200 eq. 2VP and DEVP in a 1/1 or 1/2 ratio were chosen. In each copolymerisation, 5 eq. of DAlVP were added to obtain samples with an appropriate number of double bonds in the side chains. The GPC traces and NMR spectra leading to the results presented in Table 1, can be found in the ESI Fig. S1–S9.† The table shows the success of

Table 1 Monomer feed, polymer composition, molecular weight (M_n [$\times 10^4$ g mol^{-1}]) and $Đ$ of block copolymer substrates

	Feed A_{eq}/B_{eq} B'_{eq} [a]	Composition A/B [2VP/DEVP][b]	M_n (A)[c]	$M_{n,\,NMR}$ (AB)[b]	$Đ$[c]
AB1	$2VP_{100}/DEVP_{100}$ $DAlVP_5$	1/1.3	1.3	4.1	1.17
AB2	$2VP_{100}/DEVP_{200}$ $DAlVP_5$	1/2.2	1.2	5.4	1.12
AB3	$2VP_{200}/DEVP_{200}$ $DAlVP_5$	1/1.4	2.5	7.9	1.10

[a] By weighing the monomer, [M]/[cat] = eq. [b] Calculated from ^{1}H-NMR spectrum. [c] Determined by GPC-MALS.

the block copolymerisation. Polymers with narrow polydispersities ($Đ$ = 1.10–1.17) and the desired molecular weights (M_n = 4.1–7.9 × 10^4 g mol^{-1}) were obtained. Most importantly, copolymers with molecular weights above 40 kDa could be produced, this represents the threshold for renal clearance. Carriers exceeding a mass of 40 kDa are desirable due to their selective accumulation and prolonged retention in tumour tissues.[19] These properties lead to prolonged circulation times, and a slow clearance from the body.[43] The disappearance of the monomer signal in ^{31}P-NMR in the course of polymerisation provided evidence for the full conversion of the new monomer. Additionally, the signals that referred to the double bond in the allyl side groups were clearly visible in the ^{1}H-NMRs as presented in Fig. S3, S6 and S9.† Through analysis of these spectra, the exact monomer composition could be determined.

The next step, visualised in Scheme 2, involved cross-linking *via* a thiol–ene click reaction. The signals from the double bond should vanish as a response to full conversion.

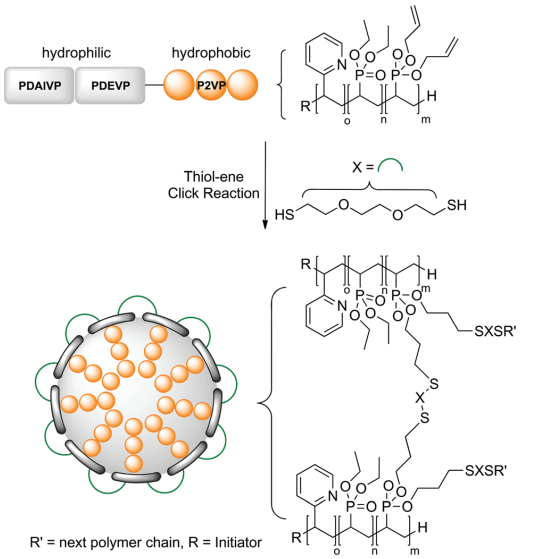

Scheme 2 Thiol–ene click reaction towards cross-linked P2VP-PDEVP-PDAlVP nanoparticles.

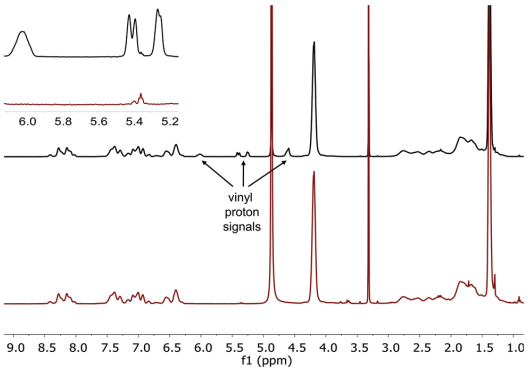

Fig. 1 ^{1}H-NMR spectra of AB1 (black) and NP1 (red) in MeOD.

As depicted in Fig. 1, the ^{1}H-NMR demonstrates the successful completion of the thiol–ene click reaction. Herein the disappearance of the vinyl proton signals is visible showing the full conversion of the reaction. However, it remained unclear if uniform particles were obtained through the cross-linking reaction. To verify uniformity electron microscopy and dynamic light scattering (DLS) techniques were employed.

The data presented in Fig. 2, and Table 2, verify that highly monodisperse, spherical particles were obtained through the cross-linking procedure described. Size values, obtained from microscopy and DLS, are in good accordance with each other. Depending on the 2VP content, the particle size varied from 35.6 to 66.0 nm in solution. This size range agrees with previous reports that found that particles of 30 to 100 nm best accessed tumour tissue through an enhanced permeability and retention effect, and in contrast, do not appear to penetrate normal vessel walls. Within this size range, vehicles can usually escape non-specific clearance through the reticuloendothelial system (RES) and are also too big for renal clearance.[12,44]

Measurements of the zeta potential show that the spheres obtained have a slight negative charge. A positive charge is more favourable for optimal cellular uptake, due to the anionic character of the cellular membrane.[45,46] However, cationic particles tend to exhibit higher cytotoxicity.[47] Furthermore, cationic polymers bind to vascular endothelial cells, as well as other anionic species in the circulation rendering them less attractive for *in vivo* applications. This potential binding can lead to rapid aggregation, a shorter half-life in the systemic circulation, and increased accumulation in the lungs, all of these effects result in a decreased dose efficacy upon intravenous injection.[48–50] For this reason, anionic or neutral carriers are thought to be more desirable for optimal pharmacokinetics. However, previous studies have found that the RES cleared anionic particles faster as compared with neutral particles, and therefore, surfaces with a charge near zero are advantageous for drug delivery applications.[51]

Table 2 Diameter, polydispersity and zeta potential ζ of the nanoparticles

	d [nm] (DLS)	*PDI* (DLS)	ζ [mV]	d [nm] (TEM)	PDI (TEM)
NP1	36.39 ± 1.09	0.030	−5.02 ± 0.10	32.54 ± 1.89	0.058
NP2	35.57 ± 2.31	0.065	−5.30 ± 0.35	28.70 ± 1.64	0.057
NP3	65.99 ± 7.65	0.116	−3.97 ± 0.21	53.19 ± 2.70	0.051

We performed surface tension measurements to demonstrate that the particles obtained do not form in a concentration dependent manner, in contrast to what was found in the micelles used prior to the thiol–ene click reaction approach. The critical micelle concentration (CMC) was studied using surface tension measurements. The absence of an inflexion point for NP1–NP3 verified the formation of stable particles after the functionalisation step. Fig. 3 shows differences in surface tension between all six samples over a range of concentration of 0.025 mg mL^{-1} to 1.000 mg mL^{-1}. Subsequent to the full physical characterisation of the newly synthesised particles, we examined their general loading and release properties. All six samples were loaded with fluorescein and their cumulative release was analysed using dialysis under varying conditions. Fig. 4 illustrates the comparison of P2VP$_{100}$-*block*-PDEVP$_{100}$-*block*-PDAlVP$_5$ (AB1) and its cross-linked nanoparticle (NP1). Particle fluorescein release was much higher than that seen from micelles. In both cases, a clear, pH and temperature-based triggering effect is visible

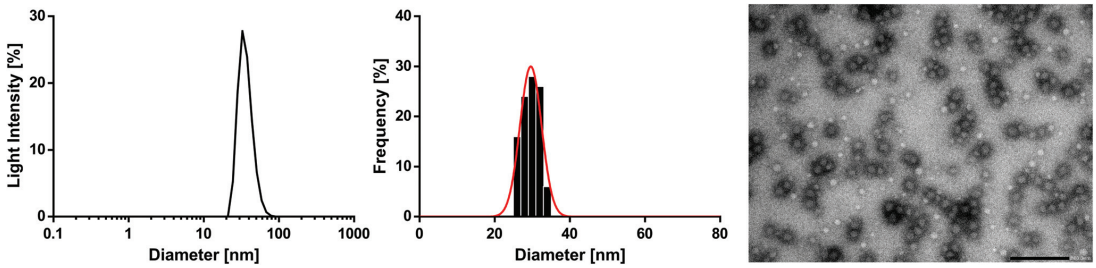

Fig. 2 Size distribution of NP1 determined *via* DLS measurements at a concentration of 2.5 mg mL^{-1} in water (left); histogram plot with a Gaussian regression fit (middle); and a TEM image of NP1 (right) with a scale bar of 200 nm.

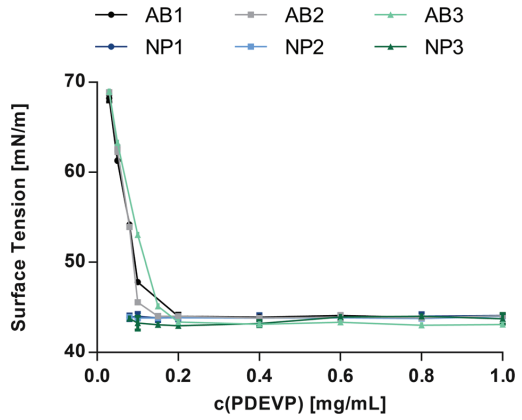

Fig. 3 Surface tension plot of the polymers (AB1, AB2, AB3) and the particles (NP1, NP2, NP3) (measured in triplicate, standard deviation indicated).

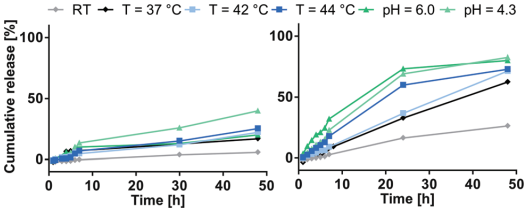

Fig. 4 Cumulative fluorescein release from AB1 (left) and NP1 (right) under varying conditions.

where NP1 exhibited a stronger response to the stimuli as compared to AB1.

Fig. 5 illustrates the cumulative release behaviour of the cross-linked nanoparticles made from $P2VP_{100}$-*block*-$PDEVP_{200}$-*block*-$PDAlVP_5$ (NP2) and $P2VP_{200}$-*block*-$PDEVP_{200}$-*block*-$PDAlVP_5$ (NP3). In this regard, NP3 represents a promising therapeutic delivery candidate as there is a very clear distinction between the curves seen for room temperature, 37 °C, 42 °C and 44 °C. Only acidic pH conditions featured faster hydrophobic cargo release from the carriers.

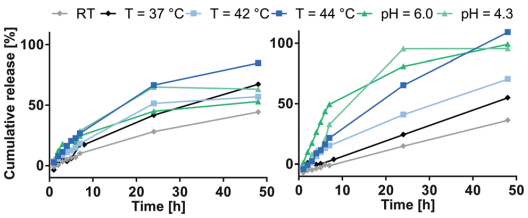

Fig. 5 Cumulative fluorescein release from NP2 (left) and NP3 (right) under varying conditions.

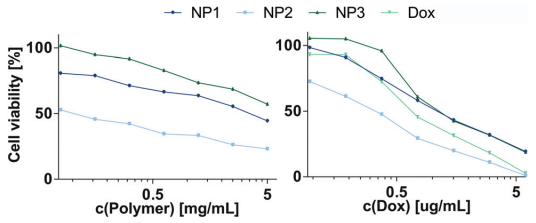

Fig. 6 MCF-7 cell viability after 24 h of incubation with unloaded (left, 0.08–5.00 mg mL^{-1}) and doxorubicin loaded nanoparticle samples (right, 0.09–6.00 μg mL^{-1}) (measured in triplicate, standard error of the mean indicated).

After evaluation of the general release characteristics, two human cancer cell lines, HeLa and MCF-7, were treated with particles for 24 h to monitor toxicity and release *in vitro*. Unloaded control carriers were compared to carriers loaded with doxorubicin (Dox) *in vitro*. The left graph in Fig. 6 indicates that NP2 is the most toxic construct for the breast cancer cells tested. Conversely, NP3 showed only minor toxicity even at very high polymer concentrations. The right graph presents the cell viability after incubation with loaded carrier samples for 24 h. The results fit very well with the earlier data presented. NP2 exhibited a higher level of toxicity than that seen with the same amount of doxorubicin, because the particles themselves were also found to be harmful to the cells. NP1 and NP3 exhibited similar profiles, suggesting that NP3 releases Dox more efficiently as compared to NP2, as NP2 is more toxic. The viability results for the rather robust HeLa cells, and for an incubation time of only 3 h are presented in the ESI.† The results described here can be indirectly compared to those reported for micelles. For example, through analysing the amount of time required for Dox to reach the nucleus after incubation with the loaded vehicles. Dox exhibits its cytotoxic effect when it reaches the nucleus, as it needs to intercalate into DNA where it inhibits topoisomerase II, leading to a suppression of replication and the subsequent death of tumour cells.[1,52,53] In micelles, it was described to take approximately 6 h to show the co-localisation of a nuclear dye and Dox.[38]

As illustrated in Fig. 7, using the nuclear dye DAPI, and fluorescence microscopy imaging, Dox was found to reach the nucleus of the MCF-7 cells for all tested samples after only 1 h. This result was also obtained with HeLa cells and after 3 h incubation equal images were taken, in case of both cell lines, as presented in the ESI.†

To obtain a complete picture of this new drug delivery vehicle, a more statistical approach was adopted. To this end, flow cytometry experiments were conducted to characterise the Dox uptake profile. Fig. 8 depicts the mean fluorescence intensities measured after 10 min of incubation of 500 000 MCF-7 cells treated with either the loaded carrier particles, free Dox or PBS. After 10 min an initial shift in fluorescence was seen as compared to the reference sample. Interestingly, the shift

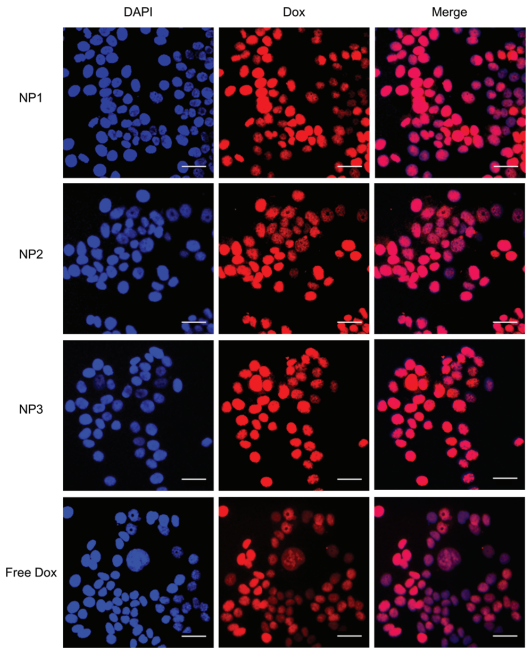

Fig. 7 Fluorescence microscopic images of MCF-7 cells incubated with NP1, NP2, NP3 and doxorubicin for 1 h at 37 °C (scale bar = 50 μm).

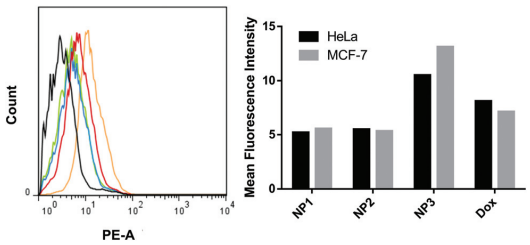

Fig. 8 Mean fluorescence intensities (MFIs) of MCF-7 cells incubated with PBS (black), NP1 (blue), NP2 (green), NP3 (orange) and doxorubicin (red) for 10 min at 37 °C (left). Comparison of MFIs of HeLa and MCF-7 cells after the same incubation conditions (right).

caused by NP3 was higher than that seen for free Dox treated cells, suggesting that Dox uptake is more efficient following encapsulation into NP3 particles. Similar effects have been observed in other settings. Tumour cells are able to actively pump small molecules, like Dox, out of the cells after their uptake in a process linked to their general sensitivity to toxic reagents.[54–56] When used to deliver chemotherapeutic agents, nanoparticles have been shown to generally exhibit better uptake dynamics than those seen with free chemotherapeutic agents, in part, because reagents loaded in nanoparticles are

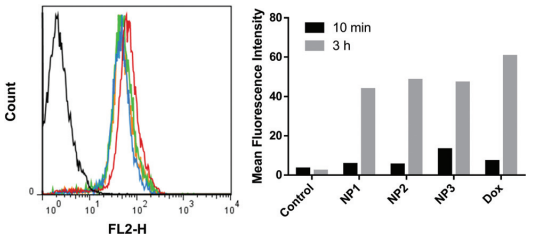

Fig. 9 Mean fluorescence intensities of MCF-7 cells incubated with PBS (black), NP1 (blue), NP2 (green), NP3 (orange) and doxorubicin (red) for 3 h at 37 °C (left) and comparison of 10 min and 3 h Dox uptake (right).

less available to the transporters that underlie this biology.[57] The results presented here show that our drug delivery vehicles exhibit a higher fluorescence intensity than that measured for free Dox treated cells. The right graph of Fig. 8 demonstrates that the same trend was seen for HeLa cells.

A second set of flow cytometry experiments were conducted using longer incubation times to determine if elevated uptake levels could be detected. Fig. 9 exhibits, that after a prolonged incubation time, increased Dox fluorescence was recorded and that free Dox has slightly higher or similar values to those measured with particles. This finding suggests that after a period of time, the effects influencing free Dox uptake, and its egress from cells, equal the processes underlying the nanoparticle uptake dynamics.

Conclusions

In the present study, three novel drug delivery vehicles were synthesised and characterised. The copolymers prepared exhibited narrow polydispersities, and the expected molecular weights. The particles are spherical, highly monodisperse and did not form concentration dependently. The carriers exhibited promising loading and release profiles, and their cytotoxicity appeared to depend on the monomer ratio of the cross-linked block copolymer. The three types of particles each showed a rapid and efficient release of their cargo *in vitro*. As these agents progress in their development, as a next step they will be evaluated in preclinical *in vivo* testing to empirically determine their systemic circulation time, renal clearance, target specificity and dose efficacy. Currently, we are working in parallel on more complex delivery vehicles with surficial targeting ligands (*e.g.* folic acid). These modifications will lead to more sophisticated and more specific nanocarriers for future drug delivery applications.

Conflicts of interest

There are no conflicts to declare.

Acknowledgements

The authors thank Andreas Schaffer for proof reading, Kerstin Halama for her participation in the release studies, Dr Stefanie Steiger and Anke Fischer for their help with the flow cytometry measurements. The authors are also grateful to Johannes Stecher for the opportunity to measure surface tension and Dr Carsten Peters for his valuable time and effort to get the best TEM pictures possible.

References

1 W. Chen, F. Meng, R. Cheng, C. Deng, J. Feijen and Z. Zhong, *J. Controlled Release*, 2015, **210**, 125–133.
2 T. Fojo and C. Grady, *JNCI J. Natl Cancer Inst.*, 2009, **101**, 1044–1048.
3 J. Tol, M. Koopman, A. Cats, C. J. Rodenburg, G. J. M. Creemers, J. G. Schrama, F. L. G. Erdkamp, A. H. Vos, C. J. van Groeningen, H. A. M. Sinnige, D. J. Richel, E. E. Voest, J. R. Dijkstra, M. E. Vink-Börger, N. F. Antonini, L. Mol, J. H. J. M. van Krieken, O. Dalesio and C. J. A. Punt, *N. Engl. J. Med.*, 2009, **360**, 563–572.
4 M. S. Shim and Y. J. Kwon, *Adv. Drug Delivery Rev.*, 2012, **64**, 1046–1059.
5 J. Zhuang, M. R. Gordon, J. Ventura, L. Li and S. Thayumanavan, *Chem. Soc. Rev.*, 2013, **42**, 7421–7435.
6 S. Mura, J. Nicolas and P. Couvreur, *Nat. mater.*, 2013, **12**, 991.
7 D. Peer, J. M. Karp, S. Hong, O. C. Farokhzad, R. Margalit and R. Langer, *Nat. Nanotechnol.*, 2007, **2**, 751.
8 M. E. Davis, Z. Chen and D. M. Shin, *Nat. Rev. Drug Discovery*, 2008, **7**, 771.
9 Y. Bae and K. Kataoka, *Adv. Drug Delivery Rev.*, 2009, **61**, 768–784.
10 R. Cheng, F. Meng, C. Deng, H.-A. Klok and Z. Zhong, *Biomaterials*, 2013, **34**, 3647–3657.
11 A. Alshememry, S. El-Tokhy and L. Unsworth, *Curr. Pharm. Des.*, 2017, 5358–5391.
12 Y. Matsumura and K. Kataoka, *Cancer Sci.*, 2009, **100**, 572–579.
13 R. Duncan, *Nat. Rev. Drug Discovery*, 2003, **2**, 347.
14 M. J. Vicent, H. Ringsdorf and R. Duncan, *Adv. Drug Delivery Rev.*, 2009, **61**, 1117–1120.
15 H. Maeda, *Adv. Drug Delivery Rev.*, 2001, **46**, 169–185.
16 J. Fang, T. Sawa and H. Maeda, in *Polymer Drugs in the Clinical Stage*, Springer, 2004, pp. 29–49.
17 J. Ding, L. Zhao, D. Li, C. Xiao, X. Zhuang and X. Chen, *Polym. Chem.*, 2013, **4**, 3345–3356.
18 S. R. Abulateefeh, S. G. Spain, K. J. Thurecht, J. W. Aylott, W. C. Chan, M. C. Garnett and C. Alexander, *Biomater. Sci.*, 2013, **1**, 434–442.
19 J. Fang, H. Nakamura and H. Maeda, *Adv. Drug Delivery Rev.*, 2011, **63**, 136–151.
20 F. Meng, R. Cheng, C. Deng and Z. Zhong, *Mater. Today*, 2012, **15**, 436–442.
21 C. Deng, Y. Jiang, R. Cheng, F. Meng and Z. Zhong, *Nano Today*, 2012, **7**, 467–480.
22 D. L. Stirland, J. W. Nichols, S. Miura and Y. H. Bae, *J. Controlled Release*, 2013, **172**, 1045–1064.
23 Y. Barenholz, *J. Controlled Release*, 2012, **160**, 117–134.
24 S. Kashyap, N. Singh, B. Surnar and M. Jayakannan, *Biomacromolecules*, 2016, **17**, 384–398.
25 Z. Ge and S. Liu, *Chem. Soc. Rev.*, 2013, **42**, 7289–7325.
26 Y. Li, J. Li, B. Chen, Q. Chen, G. Zhang, S. Liu and Z. Ge, *Biomacromolecules*, 2014, **15**, 2914–2923.
27 C.-Y. Chen, T. H. Kim, W.-C. Wu, C.-M. Huang, H. Wei, C. W. Mount, Y. Tian, S.-H. Jang, S. H. Pun and A. K. Y. Jen, *Biomaterials*, 2013, **34**, 4501–4509.
28 R. D. Issels, L. H. Lindner, J. Verweij, *et al.*, *JAMA Oncol.*, 2018, **4**, 483–492.
29 S. Wu, Z. Li, J. Han and S. Han, *Chem. Commun.*, 2011, **47**, 11276–11278.
30 C. Nilsson, K. Kågedal, U. Johansson and K. Öllinger, *Methods Cell Sci.*, 2004, **25**, 185–194.
31 Z. Fang, L.-Y. Wan, L.-Y. Chu, Y.-Q. Zhang and J.-F. Wu, *Expert Opin. Drug Delivery*, 2015, **12**, 1943–1953.
32 R. Haag and F. Kratz, *Angew. Chem., Int. Ed.*, 2006, **45**, 1198–1215.
33 C. Pietsch, R. Hoogenboom and U. S. Schubert, *Angew. Chem., Int. Ed.*, 2009, **48**, 5653–5656.
34 Y. Qu, J. Li, J. Ren, J. Leng, C. Lin and D. Shi, *Nanoscale*, 2014, **6**, 12408–12413.
35 L. Zha, B. Banik and F. Alexis, *Soft Matter*, 2011, **7**, 5908–5916.
36 E. Roux, M. Francis, F. M. Winnik and J.-C. Leroux, *Int. J. Pharm.*, 2002, **242**, 25–36.
37 J.-F. Lutz, Ö. Akdemir and A. Hoth, *J. Am. Chem. Soc.*, 2006, **128**, 13046–13047.
38 P. T. Altenbuchner, P. D. L. Werz, P. Schöppner, F. Adams, A. Kronast, C. Schwarzenböck, A. Pöthig, C. Jandl, M. Haslbeck and B. Rieger, *Chem. – Eur. J.*, 2016, **22**, 14576–14584.
39 L. Rigger, R. L. Schmidt, K. M. Holman, M. Simonović and R. Micura, *Chem. – Eur. J.*, 2013, **19**, 15872–15878.
40 W. Lüders, W. Herwig, U. Van Spankeren and K. Burg, Hoechst AG, *US* 4174340, 1979.
41 K.-H. Keil, F. Engelhardt, U. Greiner, K. Kuhlein, R. Keller, M. Schlingmann and G. Hess, Cassella AG, *US* 4576973, 1986.
42 B. S. Soller, S. Salzinger, C. Jandl, A. Pöthig and B. Rieger, *Organometallics*, 2015, **34**, 2703–2706.
43 Y. Matsumura and H. Maeda, *Cancer Res.*, 1986, **46**, 6387–6392.
44 J. Wang, W. Mao, L. L. Lock, J. Tang, M. Sui, W. Sun, H. Cui, D. Xu and Y. Shen, *ACS Nano*, 2015, **9**, 7195–7206.
45 R. Elul, *J. Physiol.*, 1967, **189**, 351–365.
46 A. Musyanovych, J. Dausend, M. Dass, P. Walther, V. Mailänder and K. Landfester, *Acta Biomater.*, 2011, **7**, 4160–4168.
47 E. Fröhlich, *Int. J. Nanomed.*, 2012, **7**, 5577–5591.

48 M. Nakamura, P. Davila-Zavala, H. Tokuda, Y. Takakura and M. Hashida, *Biochem. Biophys. Res. Commun.*, 1998, **245**, 235–239.
49 R. B. Campbell, D. Fukumura, E. B. Brown, L. M. Mazzola, Y. Izumi, R. K. Jain, V. P. Torchilin and L. L. Munn, *Cancer Res.*, 2002, **62**, 6831–6836.
50 W. Zhao, S. Zhuang and X.-R. Qi, *Int. J. Nanomed.*, 2011, **6**, 3087–3098.
51 S.-D. Li and L. Huang, *Mol. Pharm.*, 2008, **5**, 496–504.
52 E. S. Kim, C. Durairaj, R. S. Kadam, S. J. Lee, Y. Mo, D. H. Geroski, U. B. Kompella and H. F. Edelhauser, *Pharm. Res.*, 2009, **26**, 1155–1161.
53 Y.-M. Li, T. Jiang, Y. Lv, Y. Wu, F. He and R.-X. Zhuo, *Colloids Surf., B*, 2015, **132**, 54–61.
54 M. Nikolaou, A. Pavlopoulou, A. G. Georgakilas and E. Kyrodimos, *Clin. Exp. Metastasis*, 2018, 1–10.
55 R. W. Robey, K. M. Pluchino, M. D. Hall, A. T. Fojo, S. E. Bates and M. M. Gottesman, *Nat. Rev. Cancer*, 2018, 1.
56 K. McIntosh, C. Balch and A. K. Tiwari, *Expert Opin. Drug Metab. Toxicol.*, 2016, **12**, 633–644.
57 X. Wang, Z. Teng, H. Wang, C. Wang, Y. Liu, Y. Tang, J. Wu, J. Sun, H. Wang and J. Wang, *Int. J. Clin. Exp. Pathol.*, 2014, **7**, 1337.

6.4 Reprint Permission of Copyrighted Content

Dear Christina,

Many thanks for sending the permissions request below. I am copying the Copyright Clearance Center so that they are aware that you have had issues to submit your request.

I shall grant you permission via email in the meantime. The Royal Society of Chemistry (RSC) hereby grants permission for the use of your paper(s) specified below in the printed and microfilm version of your thesis. You may also make available the PDF version of your paper(s) that the RSC sent to the corresponding author(s) of your paper(s) upon publication of the paper(s) in the following ways: in your thesis via any website that your university may have for the deposition of theses, via your university's Intranet or via your own personal website. We are however unable to grant you permission to include the PDF version of the paper(s) on its own in your institutional repository. The Royal Society of Chemistry is a signatory to the STM Guidelines on Permissions (available on request).

Please note that if the material specified below or any part of it appears with credit or acknowledgement to a third party then you must also secure permission from that third party before reproducing that material.

Please ensure that the thesis states the following:

Reproduced by permission of The Royal Society of Chemistry

and include a link to the paper on the Royal Society of Chemistry's website.

Please ensure that your co-authors are aware that you are including the paper in your thesis.

Best wishes,

Chloe Szebrat
Contracts and Copyright Executive
Royal Society of Chemistry
Thomas Graham House
Science Park, Milton Road
Cambridge, CB4 0WF, UK
Tel: +44 (0) 1223 438329
www.rsc.org

7 Summary and Outlook

In 2010 the group of Professor *Rieger* succeeded in the synthesis of high molecular weight polyvinylphosphonates.[35] Since this major breakthrough a lot of work was done, to investigate the polymerization mechanism,[36, 56] possible monomer combinations,[37, 75] new catalysts and initiators[23, 76, 95]. Just since 2015, we are actively trying to use their auspicious properties to bring them into applications. Their utilization as halogen-free flame-retardant additives,[42] as non-amide kinetic hydrate inhibitors[86] or as delivery vehicles in biomedical research[77] were the first fields where polyvinylphosphonates were employed.

Medicinal applications seem to be very promising, since there is an enormous need of highly specialized materials in diverse fields from tissue engineering, to advanced cell culture techniques and drug delivery. This work was intended to rate the value of polyvinylphosphonates in these various applications. Therefore, first of all new, functional initiators had to be utilized for C–H bond activation and in the following step for end-group analysis. The known initiator 2-(4-vinylphenyl)pyridine was tested first, because its synthesis was published and it was applied before in 2VP polymerization.[68] However, its C–H bond activation with $Cp_2Y(CH_2TMS)(THF)$ yielded a complex that was insoluble in toluene and only the addition of DEVP brought it back into solution. This issue led to an initiator efficiency of only about 8% and consequently to polymers with a way higher molecular weight than the intended one. Therefore, an initiator had to be synthesized with the same activation motif as in *sym*-collidine and with the functional group. This molecule was found to be 2,6-dimethyl-4-(4-vinylphenyl)pyridine. The novel initiator showed an I^*_t of 94% and a TOF of 69900 h^{-1}, which is even higher than for *sym*-collidine (I^*_t = 73% and TOF = 59400 h^{-1}).[23] Polymers with low PDIs and the desired molecular weights were obtained. The presence of exclusively the functional end-group could be demonstrated with ESI-MS and NMR. In the following synthetic step, conjugation of the biomolecules, namely folic acid (using a cysteamine linking unit) and thio-cholesterol, could be achieved. This was the first step toward polyvinylphosphonate-biomolecule conjugates. All data are presented in Chapter 4 and 9.1.

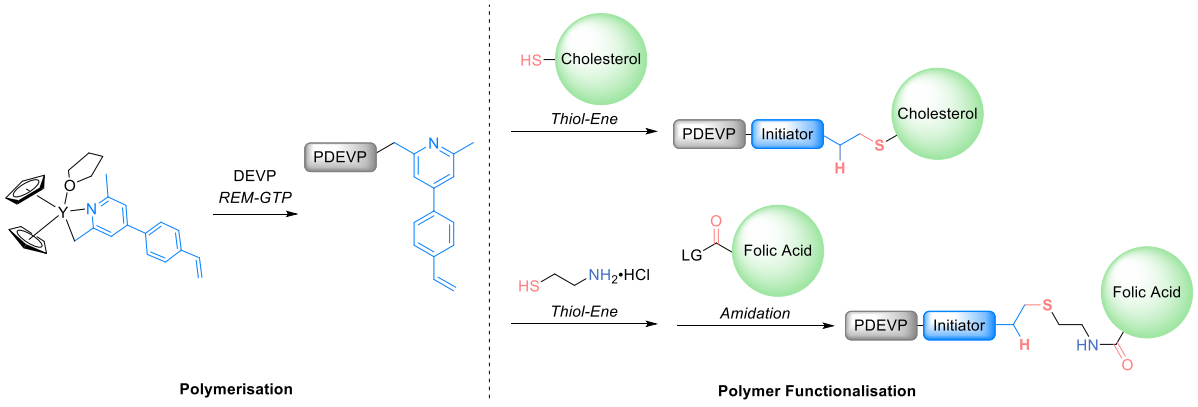

Scheme 7.1: Table of content of the publication presented in Chapter 4 and 9.1: "Precise Synthesis of Thermoresponsive Polyvinylphosphonate-Biomolecule Conjugates *via* Thiol–ene Click Chemistry".

To evaluate the biological function of the novel bioconjugates, a fluorescent labeling had to be accomplished. Therefore, a route, established at our chair, was adapted to partially transesterify the ethyl side groups of the polymers.[36] The functionalization proceeds *via* the trimethylsilyl ether intermediate. The consecutive deprotection is rendered by tetra-*n*-butylammonium fluoride (TBAF) and followed by the addition of pyrene to the activated positions. 2% functionalization degree were intended. The reached conversion was lower, but all functionalized polymers were fluorescent and applicable for *in vitro* experiments. These experiments showed a higher toxicity of the fluorescent polymers compared to the unlabeled ones. This is caused by the cytotoxic pyrene label.[96] This observation gives room for future optimizations. For *in vivo* applications a tag should be linked to the side chain of the polymers that does not cause any harm to the cells and consequently, also not to the animals in the more advanced studies. In the next step of this work, the localization of the fluorescent polymers was studied through confocal microscopy (Figure 7.1).

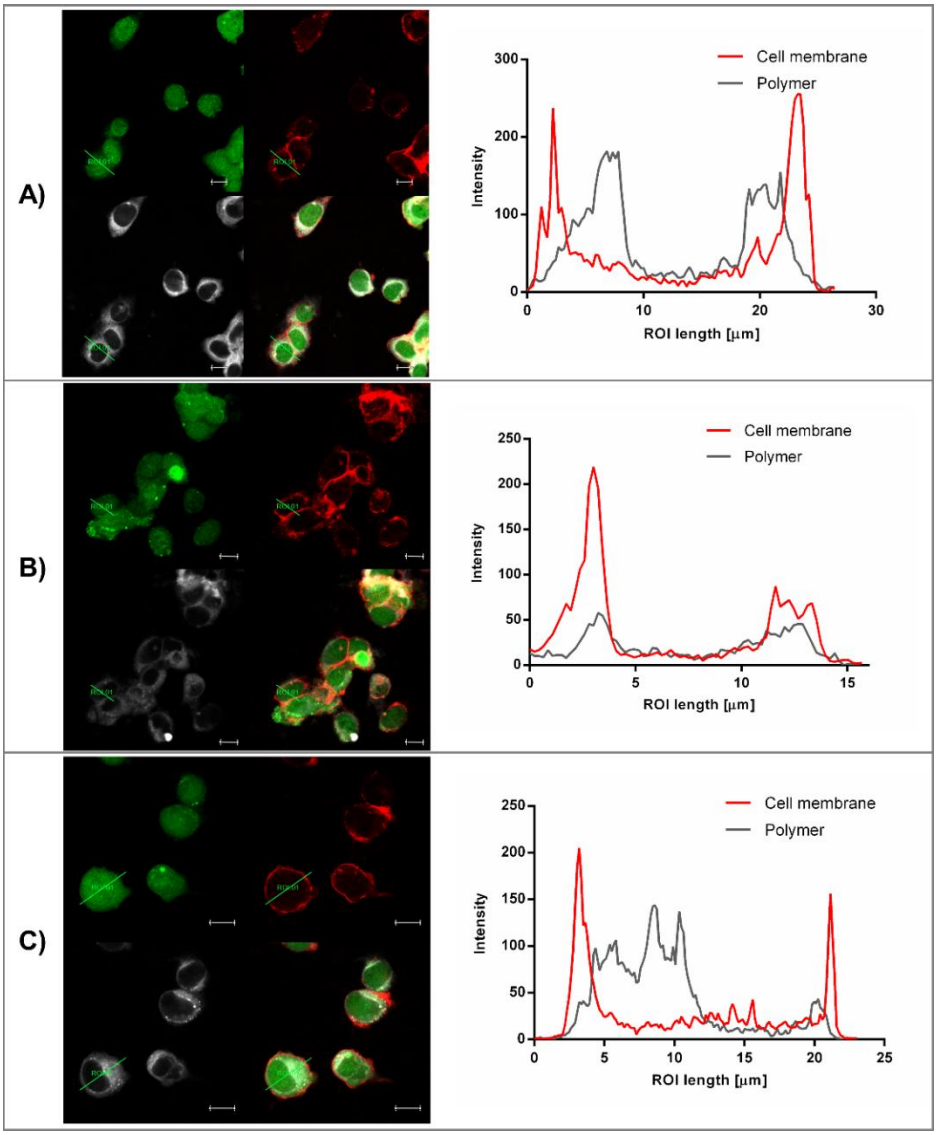

Figure 7.1: Confocal microscopy images and region of interest (ROI) analysis of HMEC-1 cells treated with A) polymer without anchor, B) polymer with cholesterol and C) polymer with folic acid. Scale bar represents 10 µm. Reprinted with permission from ref. [88]. Copyright 2018 John Wiley and Sons.

The region of interest plots quantify and locate the fluorescence of the polymers and the applied stains. These plots, presented on the right side of Figure 7.1, demonstrate the varying localization of the bioconjugates depending on their anchor unit. With folic acid or no anchor, the polymers reach the inside of the endothelial cells. The polymer fluorescence is visualized in grey, the antibody staining of the cellular membrane in red and the cytoplasm stained in green. The cholesterol unit directs the polymers into the cell wall and on its inner side. This observation proves that biological functions were added to the polyvinylphosphonates through the anchor molecule. All data concerning this work are presented in Chapter 5 and 9.2.

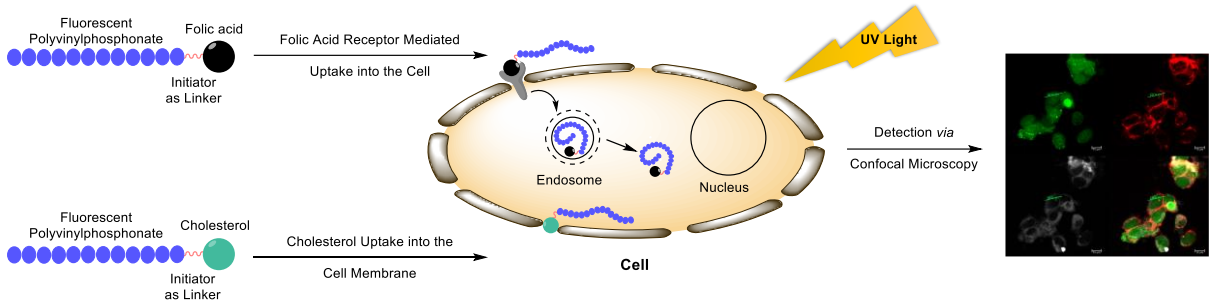

Scheme 7.2: Table of content of the publication presented in Chapter 5 and 9.2: "Fluorescent Polyvinylphosphonate Bioconjugates for Selective Cellular Delivery".

This modular synthetic approach opens the door toward a plurality of structures. Bioconjugates with various anchors and fluorescent side groups, for specific imaging applications can be envisioned. Also advanced cell culture or tissue engineering application are conceivable, with responsive polymers anchored to the cell surface. Consequently, it can be stated that a pathway toward promising polyvinylphosphonate constructs, for biomedical research, could be developed and some further experiments could lead to their utilization for advanced medicinal tasks.

Another important field in the medicinal research is the drug delivery section, especially for cancer research. The reason for that are the severe adverse effects, cancer patients suffer from the treatment with the commonly used chemotherapeutics. These issues are caused through the inefficient systemic distribution, hydrophobicity, low targeting efficiency and resulting toxicity toward all tissue types of the most potent drugs.[84] Consequently, it is important to find delivery vehicles that are able to transport their cargo to the target and provoke a strong response of the tumor tissue, as a result of an efficient drug uptake. Only water-soluble, biocompatible, *in vivo* stable and multi-responsive nanocarriers can accomplish this complex task. Therefore, the already promising polyvinylphosphonate micelles were developed into stable nanoparticles, to enable systemic applications. Diallyl vinylphosphonate could successfully be copolymerized with DEVP and 2VP. These copolymers were formed into stable, spherical and monodisperse nanoparticles *via* thiol-ene click chemistry. Depending on the 2VP content, the particle size differed from 35.6 to 66.0 nm in solution. This size range agrees with previous studies that found that particles of 30 to 100 nm best accessed tumor tissue through an enhanced permeability and retention effect, and in contrast, do not penetrate normal vessel walls. Within

this size area, vehicles can usually escape non-specific clearance through the reticuloendothelial system (RES) and are too big for renal clearance.[79, 80] These facts and the good loading and release behavior, made them ideal candidates for *in vitro* experiments. Cytotoxicity assays showed a high biocompatibility of the unloaded particles and an efficient cell dispatch with doxorubicin loaded carriers. To evaluate the time frame and prove the colocalization of DOX in the nucleus, fluorescence microscopic images were taken. These images demonstrated that already after one hour of incubation with the samples, DOX could migrate into the nucleus, where it exhibits its cytotoxic effect. When DOX reaches the nucleus, it intercalates into DNA, inhibits topoisomerase II, leading to a suppression of replication and the subsequent death of tumor cells.[83-85] With flow cytometry, a statistical aspect was added to the evaluation of the novel particles as drug delivery vehicles. These experiments showed that already after ten minutes of incubation, DOX uptake into the cells can be measured. In case of one particle sample, the fluorescence signal is even stronger, than for free DOX. After three hours, a really high uptake can be detected, which indicates the successful development of a new type of polyvinylphosphonate nanocarriers (Scheme 7.3). All data are presented in Chapter 6 and 9.3.

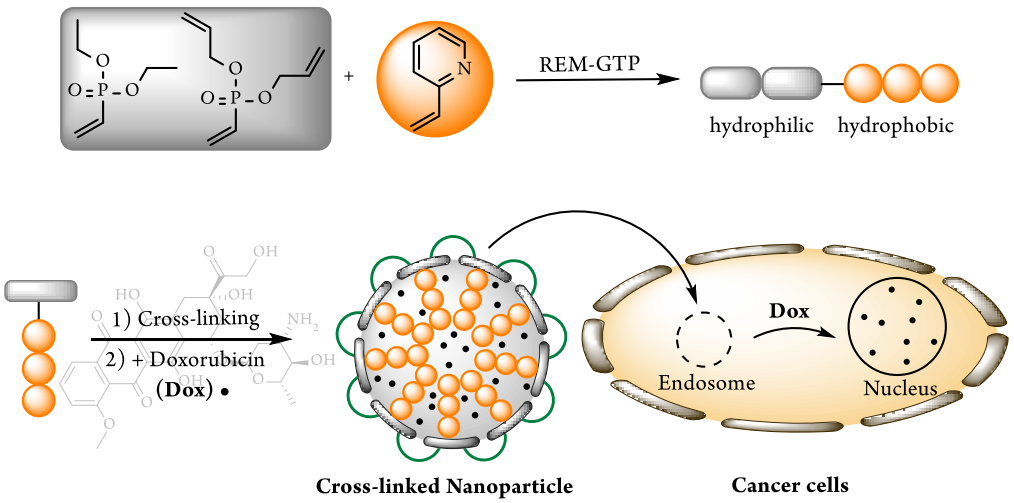

Scheme 7.3: Table of content of the publication presented in Chapter 6 and 9.3: "Synthesis of Next Generation Dual-Responsive Cross-Linked Nanoparticles and their Application to Anti-Cancer Drug Delivery".

These results demonstrate that polyvinylphosphonate nanocarriers are promising candidates for drug delivery applications. In the next step, their eligibility has to be tested in various *in vivo* set-ups to investigate their circulation times, their biocompatibility under these complex conditions and their renal clearance. If these pharmacokinetic characteristics are positive, target specificity and dose efficacy have to be evaluated in a second step.

Another future task is their synthetic optimization. With further studies, it could be possible to imply more or different monomers, depending on the required properties of the carriers. The specific applications might render other characteristics of the vehicle necessary, like for example higher LCSTs for hyperthermia treatments. On the other hand, for local injections less stable particles are favorable, in contrast to systemic

applications. Furthermore, is targeting another challenge that has to be conquered. Through the specific partial thiol-ene click conjugation in the particle formation step, free allyl side groups could be generated. These side groups are prone to functionalization reactions, for example with targeting ligands like folic acid. This modification would add another dimension to the already very complex and sophisticated system.

Overall, it can be stated that polyvinylphosphonates are smart materials and can for sure be entitled as the next generation in biomedical applications. Consequently, this work could lay the fundament toward the future employment of polyvinylphosphonates in galenics.

8 Zusammenfassung und Ausblick

2010 schaffte Professor *Riegers* Gruppe erstmals die Synthese hochmolekularer Polyvinylphosphonate.[35] Seit diesem Durchbruch wurde viel Arbeit in die Untersuchung des Polymerisationsmechanismus,[36, 56] möglicher Monomerkombinationen,[37, 75] sowie neuer Katalysatoren und Initiatoren[23, 76, 95] investiert. Erst seit 2015 wird versucht, die außergewöhnlichen Eigenschaften dieser Polymere für Anwendungen nutzbar zu machen. Zu Beginn wurden sie als halogenfreie Brandschutzadditive,[42] nicht amid-basierte kinetische Hydrat-inhibitoren[86] und als Transportvehikel im biomedizinischen Bereich verwendet.[77]

Besonders vielversprechend scheint der zukünftige Einsatz in medizinischen Anwendungen, da dort ein enormer Bedarf an hochspezialisierten Materialien in Feldern wie Gewebe-Engineering, fortgeschrittenen Zellkulturtechniken und dem gezielten Wirkstofftransport herrscht. Die vorliegende Arbeit sollte den Wert der Polyvinylphosphonate für diese vielfältigen Einsatzgebiete untersuchen. Dafür mussten zu allererst neue, funktionelle Initiatoren für die C–H-Bindungsaktivierung eingesetzt werden, um im folgenden Schritt die Endgruppenanalyse durchführen zu können. Zuerst wurde der bekannte Initiator 2-(4-Vinylphenyl)-pyridin untersucht, da dessen Synthese bekannt war und dieser auch schon für die Polymerisation von 2VP verwendet wurde.[68] Allerdings ergab die C–H-Bindungsaktivierung von 2-(4-Vinylphenyl)pyridin mit $Cp_2Y(CH_2TMS)(THF)$ einen in Toluol unlöslichen Komplex, der nur durch die Zugabe von DEVP wieder in Lösung gebracht werden konnte. Dieses Problem führte zu einer Initiatoreffektivität von nur 8% und somit zu einem viel zu hohen Molekulargewicht. Daher musste ein Initiator synthetisiert werden, der dasselbe Aktivierungsmotiv wie der derzeitige Goldstandard, *sym*-Collidin, hat und eine zusätzliche funktionelle Gruppe trägt. 2,6-Dimethyl-4-(4-vinylphenyl)pyridin war das Molekül der Wahl. Dieser neue Initiator erreichte mit einer I^*_t von 94% und einer TOF von 69900 h^{-1}, sogar noch bessere Werte als *sym*-Collidin (I^*_t = 73% und TOF = 59400 h^{-1}).[23] Somit konnten Polymere mit niedrigen PDIs und den gewünschten Molekulargewichten erhalten werden. Das ausschließliche Vorhandensein der funktionellen Endgruppe am Polymerkettenende wurde durch ESI-MS und NMR-Spektroskopie bewiesen. Im nächsten synthetischen Schritt sollte die Konjugation von Biomolekülen, in diesem Fall aktivierte Folsäure (unter Verwendung eines Cysteamin-Linkers) und Thiocholesterol, folgen. Dies war der erste Schritt um Polyvinylphoshonat-Biomolekülkonjugate zu erhalten. Alle Daten werden in den Kapiteln 4 und 9.1 dargestellt.

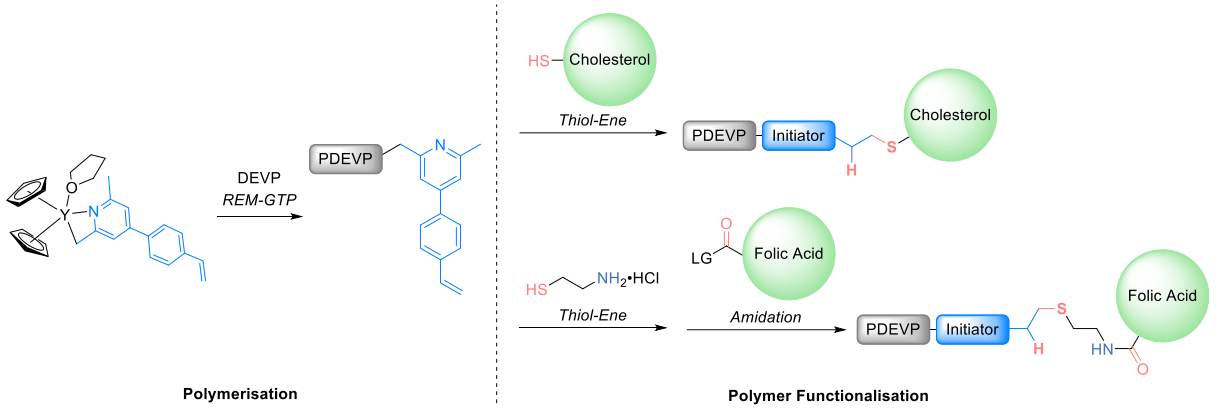

Schema 8.1: Graphische Zusammenfassung der Publikation mit dem Titel: "Precise Synthesis of Thermoresponsive Polyvinylphosphonate-Biomolecule Conjugates *via* Thiol–ene Click Chemistry". Diese wird in den Kapiteln 4 sowie 9.1 präsentiert.

Um die biologische Funktion der neuen Biokonjugate untersuchen zu können, mussten diese fluoreszent markiert werden. Dafür wurde eine Syntheseroute, die am Lehrstuhl entwickelt wurde, angepasst, um die Ethylseitengruppen der Polymere teilweise umzuestern.[36] Die Funktionalisierung verläuft über ein Trimethylsilyletherintermediat. Die anschließende Entschützung wird durch Tetra-*n*-butylammoniumfluorid (TBAF) ermöglicht wodurch Pyren an die aktivierten Positionen addiert werden kann. Ein Funktionalisierungsgrad von 2% wurde angestrebt. Die erreichte Umsetzung war zwar bei allen Polymeren geringer, aber sie waren fluoreszent und konnten für *in-vitro*-Studien eingesetzt werden. Diese Experimente zeigten eine hohe Toxizität der fluoreszenten Polymere gegenüber den nicht markierten Proben. Der Grund dafür ist die Giftigkeit des verwendeten Farbstoffs Pyren.[96] Dieser Befund schafft Raum für zukünftige Optimierungen des Systems. Vor allem für die geplanten *in-vivo*-Untersuchungen muss eine Markierung verwendet werden, die Zellen und somit auch den Tieren in fortgeschrittenen Studien, keinen Schaden zufügt. Im nächsten Schritt dieser Arbeit wurde die Lokalisation der fluoreszenten Polymere mit Hilfe von Konfokalmikroskopie untersucht (Abbildung 8.1).

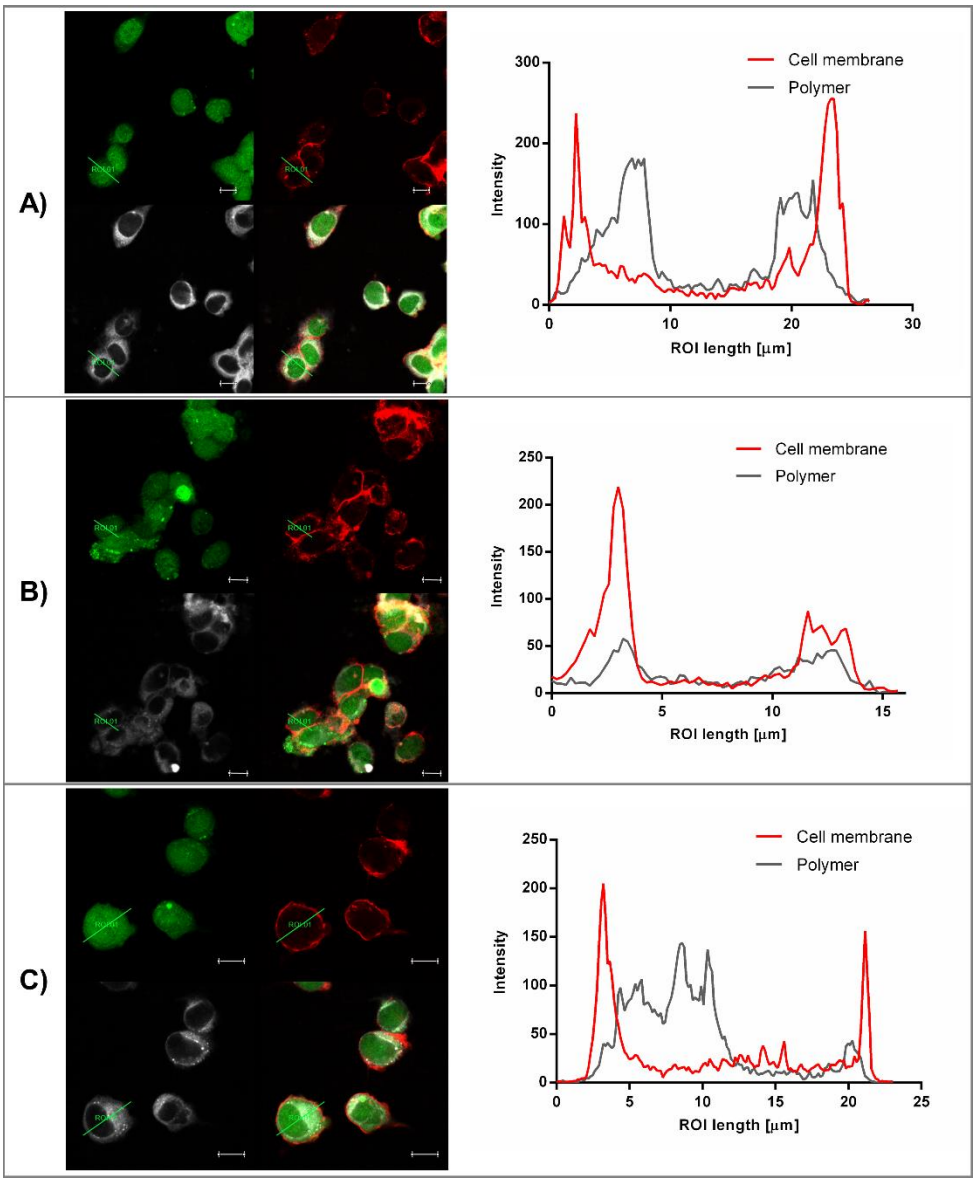

Abbildung 8.1: Konfokalmikroskopiebilder und Region von Interesse (ROI) Analyse von HMEC-1 Zellen, die mit A) Polymeren ohne Anker, B) Polymeren mit Cholesterol oder C) Polymeren mit Folsäure behandelt wurden. Maßstabsskala entspricht 10 µm. Mit Genehmigung nachgedruckt von Ref. [88]. Urheberrecht 2018 John Wiley and Sons.

Die ROI-Darstellungen quantifizieren und lokalisieren die Fluoreszenz der Polymere und der verwendeten Färbereagenzien. Diese Graphen, gezeigt jeweils auf der rechten Seite von Abbildung 8.1, veranschaulichen die unterschiedlichen Lokalisierungen der Biokonjugate in Abhängigkeit ihrer Ankereinheiten. Ohne Anker oder mit Folsäure erreichen die Polymere das Innere der Zellen. Zu sehen ist das durch die grau dargestellte Fluoreszenz der Polymere, wohingegen die Zellwand mittels einer Antikörpermarkierung rot und das Zytoplasma grün gefärbt ist. Die Cholesterol-Einheit verankert die Polymere in der Zellwand oder an deren Innenseite. Diese Beobachtung beweist, dass die Polyvinylphosphonate durch die Ankermoleküle unterschiedliche biologische Eigenschaften erhalten haben. Alle Daten zu dieser Arbeit sind in den Kapiteln 5 sowie 9.3 gezeigt.

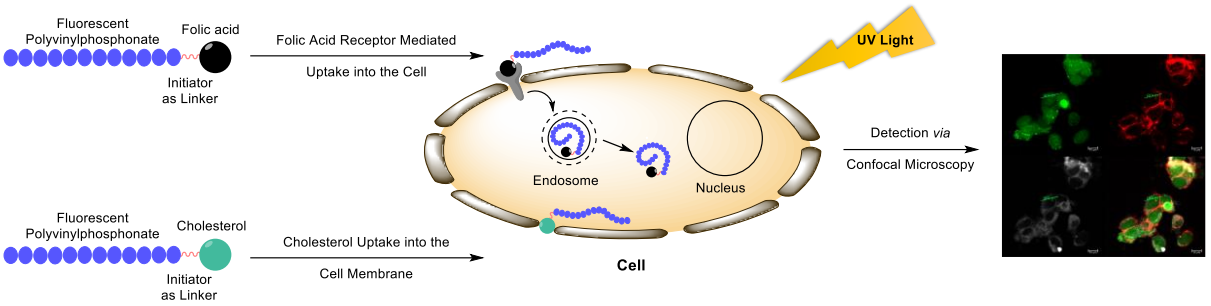

Schema 8.2: Graphische Zusammenfassung der Publikation mit dem Titel: "Fluorescent Polyvinylphosphonate Bioconjugates for Selective Cellular Delivery". Diese wird in den Kapiteln 5 sowie 9.2 präsentiert.

Diese modulare, synthetische Herangehensweise öffnet die Tür hin zu einer großen Vielfalt an Strukturen. Biokonjugate mit verschiedensten Ankern und fluoreszenten Seitengruppen für spezifische Bildgebungsanwendungen sind vorstellbar. Durch die Verankerung von responsiven Polymeren auf der Zelloberfläche sind auch Gewebe-Engineering oder fortgeschrittene Zellkulturanwendungen denkbar. Folglich kann festgestellt werden, dass ein Weg zur Darstellung vielversprechender Polyvinylphosphonatkonstrukte gefunden wurde. Diese könnten durch wenige weitere Experimente so entwickelt werden, dass deren Anwendung auf komplexe medizinische Aufgaben möglich ist.

Ein weiteres wichtiges Gebiet in der medizinischen Forschung, vor allem für die Krebstherapie, ist der Wirkstofftransport. Grund dafür sind die massiven Nebenwirkungen der Standardchemotherapeutika an welchen die Patienten leiden. Diese Probleme werden durch die ineffiziente systemische Verteilung, die Hydrophobizität, die zu geringe Freisetzung am Wirkort und die daraus resultierende Toxizität der wirksamsten Medikamente gegenüber allen Gewebetypen, verursacht.[84] Folglich ist es von großer Bedeutung Transportvehikel zu entwickeln, die den Wirkstoff zum Zielort transportieren, dort eine hohe Aufnahme und somit eine starke Antwort des Tumorgewebes auslösen. Diese komplexe Aufgabe kann nur von wasserlöslichen, biokompatiblen, *in vivo* stabilen und multi-responsiven Nanocarriern gemeistert werden. Um systemische Anwendungen zu ermöglichen, sollten die bereits sehr vielversprechenden Polyvinylphosphonat-mizellen zu stabilen Partikeln weiterentwickelt werden. Diallylvinylphosphonat konnte erfolgreich mit DEVP und 2VP copolymerisiert werden. Die erhaltenen Copolymere wurden durch Thiol-En-Klick-Reaktionen zu stabilen, sphärischen und monodispersen Nanopartikeln verbunden. Dabei variierte ihre Größe in Lösung von 35.6 bis 66.0 nm in Abhängigkeit des 2VP-Gehalts. In vorangegangenen Studien konnte gezeigt werden, dass Partikel mit einer Größe von 30 bis 100 nm das Tumorgewebe, aufgrund einer passiven Anreicherung (EPR-Effekt = engl. enhanced permeability and retention effect), am besten durchdringen. Im Gegensatz dazu durchbrechen sie aber nicht die Wand von normalen Gefäßen. Sind die Vehikel innerhalb dieses Größenbereichs, werden sie meist nicht Opfer unspezifischer Beseitigung durch das Retikulohistiozytäre System und sind zu groß für eine Ausscheidung durch die Nieren.[79, 80] Diese Tatsachen und das gute Beladungs- und Freisetzungsverhalten machte die Nanopartikel zu optimalen Kandidaten für *in-vitro*-Studien.

Die Zytotoxizitätsuntersuchungen belegten eine hohe Biokompatibilität der unbeladenen Transporter und eine effektive Wirkung des Doxorubicins auf die Zellviabilität im Fall der beladenen Proben. Um den Zeitrahmen der Wirkung, sowie die Lokalisierung von DOX im Zellkern zu untersuchen, wurden Fluoreszenzmikroskopiebilder aufgenommen. Diese Bilder zeigten, dass DOX bereits nach einer Stunde Inkubation mit den Partikeln in den Kern migrieren konnte, wo es den zytotoxischen Effekt hervorrufen kann. Sobald DOX den Zellkern erreicht, interkaliert es in die DNS, inhibiert die Topoisomerase II, was zu einer Unterdrückung der Replikation und somit zum Tod der Tumorzellen führt.[83-85] Mit Hilfe von Durchflusszytometrie konnte der Untersuchung der neuen Transportvehikel eine statistische Komponente hinzugefügt werden. Diese Experimente zeigten, dass bereits nach zehn Minuten Inkubationszeit DOX Aufnahme in die Zellen messbar ist. Für eine Probe war das Fluoreszenzsignal sogar stärker als im Fall von freiem DOX. Nach drei Stunden konnte eine hohe Aufnahme detektiert werden, was die erfolgreiche Entwicklung einer neuen Art von Polyvinylphosphonatnanotransportern unterstreicht (Schema 8.3). Alle Daten zu dieser Arbeit werden in den Kapiteln 6 und 9.3 präsentiert.

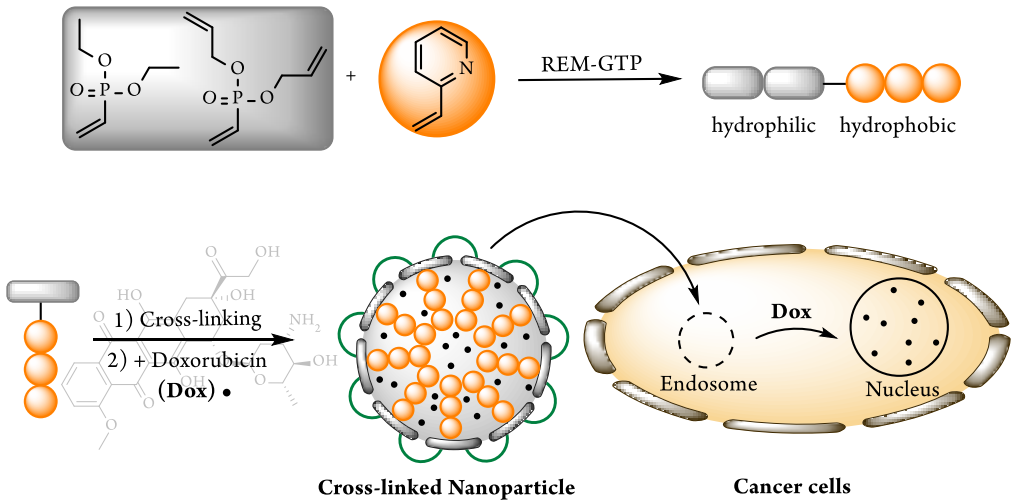

Schema 8.3: Graphische Zusammenfassung der Publikation mit dem Titel: "Synthesis of Next Generation Dual-Responsive Cross-Linked Nanoparticles and their Application to Anti-Cancer Drug Delivery". Diese wird in den Kapiteln 6 sowie 9.3 präsentiert.

Diese Ergebnisse zeigen, dass Polyvinylphosphonatnanotransporter vielversprechende Kandidaten für Wirkstofftransportanwendungen darstellen. Im nächsten Schritt muss ihre Eignung unter verschiedenen *in-vivo*-Bedingungen untersucht werden. Vor allem die Zirkulationszeit, die Biokompatibilität unter diesen komplexen Bedingungen, sowie die Ausscheidung durch die Nieren müssen genau betrachtet werden. Können die pharmakokinetischen Eigenschaften als positiv eingestuft werden, so müssen in einem zweiten Schritt die Zielspezifität und die Dosiseffektivität evaluiert werden.

Eine weitere Aufgabe für die Zukunft dieser Partikel ist die synthetische Optimierung. Durch zusätzliche Experimente könnten noch mehr oder andere Monomere verwendet werden, je nachdem welche Transportereigenschaften benötigt werden. Spezifische Anwendungen könnten andere Anforderungen an die

Charakteristika der Vehikel stellen, wie zum Beispiel ein höherer LCST für Hyperthermiebehandlungen. Einerseits sind für lokale Injektionen weniger stabile Partikel von Vorteil, wohingegen für systemische Applikationen sehr langlebige Transporter benötigt werden. Des Weiteren ist die spezifische Freisetzung am Wirkort noch eine zukünftige Herausforderung. Durch die selektive partielle Thiol-En-Klick-Konjugation ist es möglich, freie Allylseitengruppen zu generieren, die auch nach der Partikelbildung noch zur Verfügung stehen. Diese Seitengruppen können beispielsweise mit Liganden wie Folsäure funktionalisiert werden. Eine solche Modifikation würde dem bereits sehr komplexen und hochentwickelten System eine weitere Dimension hinzufügen.

Zusammenfassend kann festgestellt werden, dass Polyvinylphosphonate responsive Materialien darstellen und als nächste Generation innovativer Vehikel in biomedizinischen Anwendungen gesehen werden können. Mit dieser Arbeit konnte also eine Grundlage für den zukünftigen Einsatz von Polyvinylphosphonaten in der Galenik geschaffen werden.

9 Publications beyond the Scope of this Thesis

9.1 Studies on the Biocompatibility of Poly(diethyl vinylphosphonate) with a New Fluorescent Marker

Title: "Studies on the Biocompatibility of Poly(diethyl vinylphosphonate) with a New Fluorescent Marker"

Status: Communication, Version of Record online: 11 June 2018, Rewarded with Cover Page

Journal: Macromolecular Rapid Communications, 2018, 39, 1800259

Publisher: John Wiley and Sons

Link/DOI: https://doi.org/10.1002/marc.201800259

Authors: Christina Schwarzenböck, Sergei I. Vagin, Werner R. Heinz, Peter J. Nelson, and Bernhard Rieger

Abstract

Utilization of group transfer polymerization for the synthesis of poly(diethyl vinylphosphonate) (PDEVP) allows its controlled end-group functionalization. Thus, a new fluorescent chromophore/PDEVP conjugate was prepared and subjected to biocompatibility tests on two different human cell lines. In contrast to the previous studies, the tagged polymer is not absorbed by cells from the solution and has nearly no impact on cell mortality rate.

9.2 Core-First Synthesis of Three-Armed Star-Shaped Polymers by Rare Earth Metal-Mediated Group Transfer Polymerization

Title: "Core-First Synthesis of Three-Armed Star-Shaped Polymers by Rare Earth Metal-Mediated Group Transfer Polymerization"

Status: Full paper, Publication Date (Web): August 21, 2017

Journal: Macromolecules, 2017, 50, 6569-6576

Publisher: American Chemical Society

Link/DOI https://doi.org/10.1021/acs.macromol.7b01007

Authors: Philipp Pahl, Christina Schwarzenböck, Fabian A. D. Herz, Benedikt S. Soller, Christian Jandl, and Bernhard Rieger

Abstract

Addressing polymer topologies is one of the key methods for tailoring polymer properties. Herein, we report for the first time on the core-first synthesis of three-armed star-shaped polymers with adjustable molecular weights via rare earth metal-mediated group transfer polymerization (REM-GTP). Based on the versatility of REM-GTP, enabling polymerization of a broad variety of functional monomers not accessible via conventional techniques, a novel and fast method toward directed polymeric structures was established. Therefore, the trinuclear catalyst was synthesized by 3-fold C–H bond activation of 1,3,5-tris(3,5-dimethyl-4-pyridinyl)benzene using $Cp_2YCH_2TMS(THF)$ as precursor complex. Kinetic investigations in comparison to monometallic Cp_2Y(*sym*-collidinyl) on the polymerization of diethyl vinylphosphonate (DEVP) and 2-isopropenyl-2-oxazoline (IPOx) evidenced activity of all three metal centers. However, in REM-GTP generally occurring incomplete initiation provoked by the interaction of initiators and monomers, potential impurities, and applied reaction conditions led to a distribution of stars, long linear, and short linear polymers originating from chain growth in three, two, and one direction, respectively. For further visualization PIPOx produced by the trinuclear complex was converted into P(IPOx-*graft*-2-ethyl-2-oxazoline) using living cationic ring-opening polymerization. AFM scans confirmed the occurrence of the three types of polymer. Additionally, comparable solely linear PDEVP and PIPOx were synthesized by dinuclear complexes generated by C–H bond activation of 1,3-bis(3,5-dimethyl-4-pyridinyl)benzene and 1,4-bis(3,5-dimethyl-4-pyridinyl)benzene using $Cp_2YCH_2TMS(THF)$ as precursor. In the case of PDEVP, the mass fraction of the low molecular weight polymer, being formed by chain growth in one direction, was accessible via GPC analysis. Further stochastic examinations on the incomplete initiation for multinuclear complexes corroborated our findings accurately.

9.3 Next Generation Multiresponsive Nanocarriers for Targeted Drug Delivery to Cancer Cells

Title: "Next Generation Multiresponsive Nanocarriers for Targeted Drug Delivery to Cancer Cells"

Status: Full paper, Version of Record online: 19 August 2016

Journal: Chemistry – A European Journal, 2016, 22, 14576-14584

Publisher: John Wiley and Sons

Link/DOI: https://doi.org/10.1002/chem.201601822

Authors: Peter T. Altenbuchner, Patrick D. L. Werz, Patricia Schöppner, Friederike Adams, Alexander Kronast, Christina Schwarzenböck, Alexander Pöthig, Christian Jandl, Martin Haslbeck, and Bernhard Rieger

Abstract

C–H bond activation of 2-methoxyethylamino-bis(phenolate)-yttrium catalysts allowed the synthesis of BAB block copolymers comprised of 2-vinylpyridine (2VP; monomer A) and diethylvinylphosphonate (DEVP; monomer B) as the A and B blocks, respectively, by rare-earth-metal-mediated group-transfer polymerization (REM-GTP). The inherent multi-stimuli-responsive character and drug-loading and -release capabilities were observed to be dependent on the chain length and monomer ratios. Cytotoxicity assays revealed the biocompatibility and nontoxic nature of the obtained micelles toward ovarian cancer (HeLa) cells. The BAB block copolymers effectively encapsulated, transported, and released doxorubicin (DOX) within HeLa cells. REM-GTP enables access to previously unattainable vinylphosphonate copolymer structures, and thereby unlocks their full potential as nanocarriers for stimuli-responsive drug delivery in HeLa cells. The self-evident consequence is the application of these new micelles as potent drug-delivery vehicles with reduced side effects in future cancer therapies.

10 Appendix

10.1 Supporting Information of the Manuscript "Precise Synthesis of Thermoresponsive Polyvinylphosphonate-Biomolecule Conjugates *via* Thiol–ene Click Chemistry"

Electronic Supplementary Material (ESI) for Polymer Chemistry.

Supporting information for the manuscript entitled precise synthesis of thermoresponsive polyvinylphosphonate-biomolecule conjugates *via* thiol–ene click chemistry†

Christina Schwarzenböck,[a] Andreas Schaffer,[a] Philipp Pahl,[a] Peter J. Nelson,[b] Ralf Huss[c] and Bernhard Rieger*[a]

[a] *WACKER-Lehrstuhl für Makromolekulare Chemie, Technische Universität München, Lichtenbergstraße 4, 85748 Garching bei München, Germany. E-Mail: rieger@tum.de*
[b] *Medizinische Klinik und Poliklinik IV, Nephrologisches Zentrum und Arbeitsgruppe Klinische Biochemie, University of Munich, Munich, Germany.*
[c] *Definiens AG, Bernhard-Wicki-Strasse 5, 80636 Munich, Germany.*

Table of contents

1. Material and methods

General Information

All reactions were carried out under argon atmosphere using standard Schlenk or glovebox techniques. All glassware was heat dried under vacuum prior to use. Unless otherwise stated, all chemicals were purchased from Sigma-Aldrich, ABCR, Acros Organics or TCI Europe and used as received. Toluene, THF and diethyl ether were dried using a MBraun SPS-800 solvent purification system. HPLC grade acetonitrile was purchased from VWR Chemicals and dried prior to use. The precursor complexes $Y(CH_2Si(CH_3)_3)_3(THF)_2$ and $LiCH_2TMS$ and the catalyst $Cp_2Y(CH_2TMS)(THF)$ (**6**) are prepared according to literature procedures.[1-4] Diethyl vinyl phosphonate (DEVP) is synthesised according to literature procedures and dried over calcium hydride and distilled prior to use.[5]

Nuclear Magnetic Resonance Spectroscopy

NMR spectra were recorded on a Bruker AVIII-300, AV-500HD and AVIII-500 Cryo spectrometer. ^{1}H- and ^{13}C-NMR spectroscopic chemical shifts δ are reported in ppm relative to the residual proton signal of the solvent. δ (^{1}H) is calibrated to the residual proton signal, δ (^{13}C) to the carbon signal of the solvent. Unless otherwise stated, coupling constants *J* are averaged values and refer to couplings between two protons. Deuterated solvents were obtained from Sigma-Aldrich and dried over 3 Å molecular sieves.

Mass Spectrometry (ESI-MS)

ESI mass spectra were measured on a Varian 500-MS spectrometer in acetonitrile and methanol.

Elemental Analysis (EA)

Elemental analyses were measured on a Vario EL (Elementar) at the Laboratory for Microanalysis at the Institute of Inorganic Chemistry at the Technische Universität München.

Thin-Layer Chromatography (TLC)

Thin-layer chromatography was performed on either silica coated aluminium plates (0.2 mm, F254) from Macherey-Nagel or aluminium oxide coated aluminium plates (0.2 mm, F254) from Macherey-Nagel. The compounds were detected by UV-light (λ = 254 nm, 366 nm) and by staining with a potassium permanganate solution or ninhydrin solution followed by heat treatment (100-150 °C).

$KMnO_4$-staining solution: 0.50 wt% $KMnO_4$ in 1 M sodium hydroxide solution.

Column Chromatography

Purification *via* column chromatography was performed on silica gel (grain size: 60-200 µm) from Acros Organics or aluminium oxide (activated, neutral; grain size: 50-150 µm) from Sigma-Aldrich. The eluent ratios are given for the corresponding procedures.

Flash Chromatography

Flash chromatography was performed on a chromatography system IntelliFlash 310 from *Varian* with PuriFlash cartridges from Interchim filled with silica gel (grain size: 50 µm). Prior to purification the crude product was dry loaded on silica

gel. Gradients of the eluents hexane and ethyl acetate are given for the corresponding procedures. The compounds were detected by UV-light at a wavelength of 254 nm.

Gel Permeation Chromatography

Gel Permeation Chromatography was performed on a *Varian* LC-920 equipped with two PL Polargel M columns with samples of 5 mg/mL. A mixture of 50% THF, 50% water, 9 g/L tetrabutylammonium bromide (TBAB) and 340 mg/L 3,5-Di-*tert*-butyl-4-hydroxytoluene (BHT) as stabilising agent was used as eluent. Absolute molecular weights have been determined by multiangle light scattering (MALS) analysis using a Wyatt Dawn Heleos II in combination with a Wyatt Optilab rEX as concentration source.

Additionally, GPC measurements were carried out on a PL-GPC 50 System (Agilent Technologies) equipped with two PLgel columns with samples of 5 mg/mL. A mixture of 50% THF, 50% water, 9 g/L TBAB and 340 mg/L BHT as stabilising agent was used as eluent. Absolute molecular weights have been determined by a dual-angle light scattering detector in combination with an integrated RI detection unit as concentration source.

Turbidity Measurements

Turbidity measurements were performed on a Cary 50 UV-vis spectrophotometer (Varian). The cloud point of the aqueous polymer solutions was determined by spectrophotometric detection of the changes in transmittance at λ = 500 nm. The samples were heated/cooled at a rate of 1.0 K/min in steps of 1 K followed by a five minutes long period of constant temperature to ensure equilibration. The cloud point was defined as the temperature corresponding to a 10% decrease in optical transmittance.

Centrifugation

Separation of solids *via* centrifugation was carried out with the ultracentrifuge Sorvall MX Plus (Thermo Fisher Scientific) as well as the centrifuges Sorvall RC 6 Plus and Heraeus Megafuge 40 centrifuge series from Thermo Fisher Scientific.

Dialysis

Purification *via* dialysis was performed with a Spectra/Por 1 dialysis tubing (regenerated cellulose) with a molecular weight cut-off (MWCO) of 6-8 kDa (Spectrumlabs). Before use the membranes were treated with deionised water over night and then rinsed with deionised water. A 100:1 ratio of dialysis fluid to sample volume was applied. Specific solvents used as dialysis fluid are given for the corresponding procedures.

2. Syntheses

2.1 Initiator synthesis

2-(4-Vinylphenyl)pyridine (1)[6]

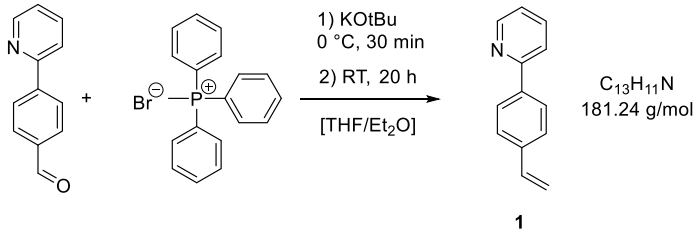

A solution of 4.00 equivalents KO^{t}Bu (6.12 g, 54.5 mmol) in tetrahydrofuran (55.0 mL) was added dropwise to a suspension of methyl triphenylphosphonium bromide (9.72 g, 27.2 mmol, 2.00 eq.) in diethyl ether (250 mL) giving a yellow colored solution and indicating the ylide formation. After stirring for 30 minutes at 0 °C a solution of 4-(pyridin-2-yl)benzaldehyde (2.50 g, 13.6 mmol, 1.00 eq.) in tetrahydrofuran (38.0 mL) was added dropwise. The reaction mixture was stirred over night in the absence of light and then mixed with deionised water (125 mL). After extraction with diethyl ether (three times) the combined organic layers were dried over $MgSO_4$, filtrated and the solvent was removed *in vacuo*. The residue was dissolved in toluene (100 mL), warmed to 40 °C and $MgCl_2$ was added to remove triphenylphosphine oxide. After six hours of stirring the precipitate was removed *via* filtration and the solvent was removed *in vacuo*. The crude product was purified *via* column chromatography (SiO_2, H/EtOAc = 20/1 → 6/1) and lyophilised yielding in a light-yellow oil (1.36 g, 7.53 mmol, 55%).

TLC: R_f = 0.40 (H/Et_2O = 20/1) [UV].

^{1}H-NMR (300 MHz, $CDCl_3$, 300 K): δ (ppm) = 8.70 (d, J_3 = 4.7 Hz, 1H, H_{arom}), 7.98 (d, J_3 = 8.3 Hz, 2H, H_{arom}), 7.83 – 7.69 (m, 2H, H_{arom}), 7.52 (d, J_3 = 8.3 Hz, 2H, H_{arom}), 7.23 (ddd, J = 5.7, 4.8, 2.6 Hz, 1H, H_{arom}), 6.77 (dd, J_3 = 17.9, 10.9 Hz, 1H, H_{vinyl}), 5.83 (d, J_3 = 17.9 Hz, 1H, H_{vinyl}), 5.31 (d, J_3 = 10.9 Hz, 1H, H_{vinyl}).

^{13}C-NMR (76 MHz, $CDCl_3$, 300 K): δ (ppm) = 156.8 (s), 149.5 (s), 138.4 (s), 138.2 (s), 136.9 (s), 136.3 (s), 127.0 (s), 126.6 (s), 122.1 (s), 120.4 (s), 114.5 (s).

ESI-MS: calculated: 182.10 $[M-H]^+$, found: 182.06 $[M-H]^+$.

EA:	calculated:	C 86.15	H 6.12	N 7.73
	found:	C 86.03	H 6.23	N 7.87

2,6-Dimethylpyridine-*N*-oxide[7]

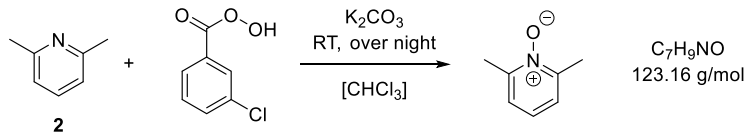

2,6-Dimethylpyridine (**2**) (73.7 mL, 636 mmol, 1.00 eq.) was dissolved in chloroform (250 mL) and then cooled to 0 °C. At this temperature 3-chloroperbenzoic acid (143 g, 636 mmol, 1.00 eq.) was added to the solution and stirred over night at room temperature. The mixture was diluted in chloroform (2000 mL) and K_2CO_3 (352 g, 2.55 mol, 4.00 eq.) was added under vigorous stirring. After 10 minutes, a white solid was separated *via* filtration and washed with 500 mL chloroform. The filtrate was dried over Na_2SO_4, filtrated and the solvent was removed *in vacuo*. The product was obtained as a colorless solid (68.9 g, 559 mmol, 88%).

^{1}H-NMR (500 MHz, $CDCl_3$, 300 K): δ (ppm) = 7.12 (d, J_3 = 7.6 Hz, 2H, H_{arom}), 7.08 – 7.01 (m, 1H, H_{arom}), 2.51 (s, 6H, CH_3).

^{13}C-NMR (126 MHz, $CDCl_3$, 300 K): δ (ppm) = 149.1 (s), 124.8 (s), 124.0 (s), 18.4 (s).

4-Chloro-2,6-dimethylpyridine[8]

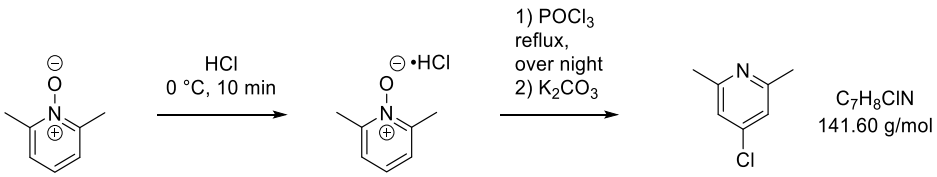

At 0 °C 12 M hydrochloric acid (51.1 mL, 614 mmol, 1.10 eq.) was added dropwise to 2,6-dimethyl-pyridine-*N*-oxide (68.7 g, 558 mmol, 1.00 eq.) and stirred for ten minutes. The solid was separated *via* filtration and washed with *iso*-propanol. The solvent of the yellowish filtrate was removed *in vacuo* and the resulting solid was again washed with *iso*-propanol. Drying of the combined salts yielded in a colorless solid (78.1 g, 489 mmol, 88%), which was used without further purification for the chlorination reaction.

A suspension of 2,6-dimethylpyridine-*N*-oxide hydrochloride (78.0 g, 489 mmol, 1.00 eq.) in 2.50 equivalents of phosphoryl chloride (116 mL, 1.22 mol) was refluxed for 16 hours. Removal of the excess of phosphoryl chloride *in vacuo* resulted in a brown, viscous residue. This residue was slowly added to a mixture of ice and K_2CO_3 at 0 °C under vigorous stirring. By addition of further K_2CO_3 and ice the temperature and an alkaline pH was kept up. The resulting liquid was extracted five times with chloroform and the solvent removed *in vacuo* resulting in a brown oil. The residue was dissolved in ethanol (375 mL), triethylamine (57 mL) was added and the mixture was refluxed for 24 hours. Solvents were removed

in vacuo resulting in a brown oil again. Diethyl ether (250 mL) and water (250 mL) were added to the residue and the aqueous layer was extracted two times with diethyl ether. The combined organic layers were dried over Na_2SO_4, filtrated and the solvent was removed *in vacuo*. Purification of the crude product was performed *via* vacuum distillation (86-88 °C, 54 mbar) yielding in a colorless liquid (41.6 g, 294 mmol, 60%).

^{1}H-NMR (500 MHz, $CDCl_3$, 300 K): δ (ppm) = 6.96 (s, 2H, H_{arom}), 2.47 (s, 6H, CH_3).

^{13}C-NMR (126 MHz, $CDCl_3$, 300 K): δ (ppm) = 159.3 (s), 144.3 (s), 120.6 (s), 24.4 (s).

4-Iodo-2,6-dimethylpyridine (3)[9]

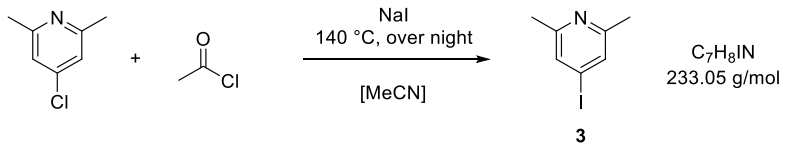

Sodium iodide (19.1 g, 127 mmol, 6.00 eq.) was suspended in a solution of 4-chloro-2,6-dimethylpyridine (3.00 g, 21.2 mmol, 1.00 eq.) in acetonitrile (50.0 mL) in an autoclave (stainless steel). To this suspension 1.50 equivalents of acetyl chloride (2.27 mL, 31.8 mmol) were added dropwise and the mixture was heated to 140 °C and stirred over night. After cooling to room temperature aqueous solutions of K_2CO_3 (25.0 mL, 10.0 wt%), K_2SO_3 (25.0 mL, 5.00 wt%) and $K_2S_2O_3$ (20.0 mL, concentrated solution) were added and ethyl acetate was added until phase separation could be observed. The aqueous phase was extracted with ethyl acetate and the combined organic phase was dried over Na_2SO_4. After filtration, the solvent was removed *in vacuo* giving a brown solid. The combined crude products of four experiments were purified *via* flash chromatography (H → H/EtOAc = 10/1) and yielded in light green crystals (7.82 g, 33.6 mmol, 40%).

TLC: R_f = 0.42 (H/EtOAc = 5/1) [UV].

^{1}H-NMR (500 MHz, $CDCl_3$, 300 K): δ (ppm) = 7.37 (s, 2H, H_{arom}), 2.46 (s, 6H, CH_3).

^{13}C-NMR (126 MHz, $CDCl_3$, 300 K): δ (ppm) = 158.7 (s), 129.6 (s), 106.4 (s), 24.1 (s).

ESI-MS: calculated: 233.98 $[M-H]^+$, found: 233.95 $[M-H]^+$.

EA:	calculated:	C 36.08	H 3.46	N 5.74	I 54.45
	found:	C 36.62	H 3.43	N 6.01	I 52.60

4-(2,6-Dimethylpyridin-4-yl)benzaldehyde (4)

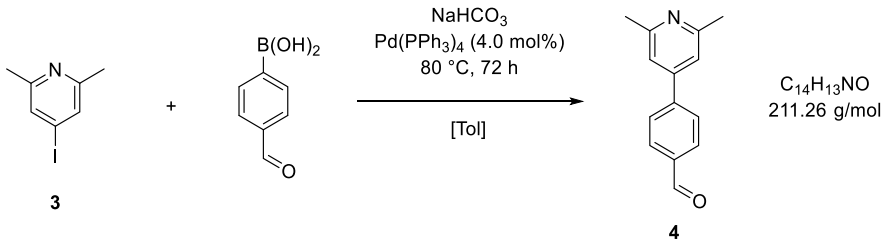

A solution of 4-iodo-2,6-dimethylpyridine (**3**) (3.70 g, 15.9 mmol, 1.00 eq.) in toluene (130 mL) was added to a solution of 4-formylphenylboronic acid (2.62 g, 17.5 mmol, 1.10 eq.) in ethanol (30.0 mL) The solution was degassed *via* drawing vacuum and filling with argon (15 iterations). Afterwards catalytic amounts of $Pd(PPh_3)_4$ (730 mg, 640 µmol, 4.00 mol%) were added and the suspension was heated to 80 °C and stirred for 72 hours. After cooling to room temperature decomposed catalyst residues were removed *via* filtration, the mixture was extracted three times against ethyl acetate, the combined organic layers were dried over $MgSO_4$, filtrated and the solvent was removed *in vacuo*. The crude product was purified *via* column chromatography (Alox, H/EtOAc = 10/1 → H/EtOAc = 2/1) yielding in a colorless solid (2.58 g, 12.2 mmol, 77%).

TLC: R_f = 0.34 (H/EtOAc = 5/1) [UV].

^{1}H-NMR (500 MHz, $CDCl_3$, 300 K): δ (ppm) = 10.08 (s, 1H, $H_{aldehyde}$), 8.07 – 7.90 (m, 2H, H_{arom}), 7.80 – 7.71 (m, 2H, H_{arom}), 7.21 (s, 2H, H_{arom}), 2.61 (s, 6H, CH_3).

^{13}C-NMR (126 MHz, $CDCl_3$, 300 K): δ (ppm) = 191.9 (s), 158.7 (s), 144.8 (s), 136.7 (s), 130.5 (s), 127.9 (s), 118.6 (s), 24.8 (s).

ESI-MS: calculated: 212.11 $[M-H]^+$, found: 212.07 $[M-H]^+$.

EA:	calculated:	C 79.59	H 6.20	N 6.63
	found:	C 79.42	H 6.25	N 6.49

2,6-Dimethyl-4-(4-vinylphenyl)pyridine (5)

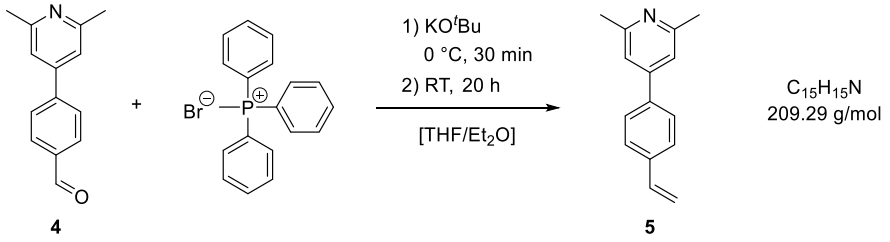

A solution of 4.00 equivalents KO^{t}Bu (11.5 g, 102 mmol) in tetrahydrofuran (103 mL) was added dropwise to a suspension of methyl triphenylphosphonium bromide (18.3 g, 51.2 mmol, 2.00 eq.) in diethyl ether (470 mL) giving a yellow colored

solution and indicating the ylide formation. After stirring for 30 minutes at 0 °C a solution of 4-(2,6-dimethylpyridin-4-yl)benzaldehyde (**4**) (5.40 g, 25.6 mmol, 1.00 eq.) in tetrahydrofuran (70.0 mL) was added dropwise. The reaction mixture was stirred over night in the absence of light and mixed with deionised water (235 mL). After extraction with diethyl ether (three times), the combined organic layers were dried over $MgSO_4$, filtrated and the solvent was removed *in vacuo*. The crude product was purified *via* column chromatography (Alox, H/EtOAc = 10/1) yielding in a colorless solid (3.76 g, 18.0 mmol, 70%).

TLC: R_f = 0.57 (H/EtOAc =5/1) [UV].

^{1}H-NMR (300 MHz, C_6D_6, 300 K): δ (ppm) = 7.38 – 7.25 (m, 4H, H_{arom}), 6.94 (s, 2H, H_{arom}), 6.63 (dd, J_3 = 17.6 Hz, 10.9 Hz, 1H, H_{vinyl}), 5.68 (dd, J_3 = 17.6 Hz, J_2 = 0.9 Hz, 1H, H_{vinyl}), 5.14 (dd, J_3 = 10.9 Hz, J_2 = 0.9 Hz, 1H, H_{vinyl}), 2.52 (s, 6H, CH_3).

^{13}C-NMR (76 MHz, C_6D_6, 300 K): δ (ppm) = 158.6 (s), 148.3 (s), 138.7 (s), 138.2 (s), 136.7 (s), 127.5 (s), 127.1 (s), 118.1 (s), 114.5 (s), 24.7 (s).

ESI-MS: calculated: 210.13 $[M-H]^+$, found: 210.13 $[M-H]^+$.

EA:	calculated:	C 86.08	H 7.22	N 6.69
	found:	C 86.22	H 7.42	N 6.58

2.2 Complex synthesis

$Cp_2YC_{13}H_{10}N$ (7)

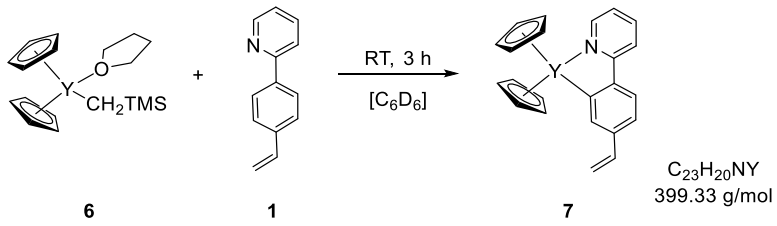

6 **1** **7**

2-(4-Vinylphenyl)pyridine (**1**) (4.78 mg, 26.4 µmol, 1.00 eq.) was dissolved in C_6D_6 (0.50 mL) and added to $Cp_2YCH_2TMS(THF)$ (**6**) (10.0 mg, 26.4 µmol, 1.00 eq.) at room temperature. The solution showed an instant orange coloring. After three hours ^{1}H-NMR spectroscopy showed quantitative conversion. The pure compound (100%) was received after removal of the solvent *in vacuo* as an orange solid.

^{1}H-NMR (500 MHz, C_6D_6, 300 K): δ (ppm) = 8.58 – 8.50 (m, 1H, H_{arom}), 8.05 (d, J_3 = 8.3 Hz, 2H, H_{arom}), 7.30 (dd, J_3 = 8.3, 3.7 Hz, 3H, H_{arom}), 6.83 – 6.50 (m, 2H, H_{arom}, H_{vinyl}), 6.18 (s, 10H, Cp-H), 5.63 (m, J_3 = 18.5 Hz, 1H, H_{vinyl}), 5.10 (d, J_3 = 11.8 Hz, 1H, H_{vinyl}).

EA:	calculated:	C 69.18	H 5.05	N 3.51
	found:	C 68.31	H 5.22	N 3.37

$Cp_2YC_{15}H_{14}N(THF)$ (8)

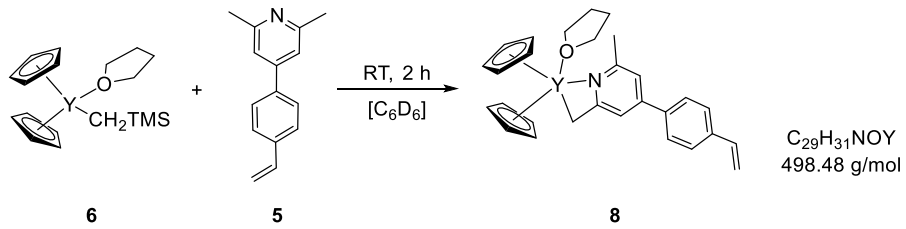

6 **5** **8**

2,6-Dimethyl-4-(4-vinylphenyl)pyridine (**5**) (5.53 mg, 26.4 µmol, 1.00 eq.) was dissolved in C_6D_6 (0.50 mL) and added to $Cp_2YCH_2TMS(THF)$ (**6**) (10.0 mg, 26.4 µmol, 1.00 eq) at room temperature. The solution showed an instant orange coloring. After two hours ^{1}H-NMR spectroscopy showed quantitative conversion. The pure compound (100%) was received after removal of the solvent *in vacuo* as an orange solid.

^{1}H NMR (500 MHz, C_6D_6, 300 K): δ (ppm) = 7.46 (d, J_3 = 8.3 Hz, 2H, H_{arom}), 7.27 (d, J_3 = 8.3 Hz, 2H, H_{arom}), 6.87 (s, 1H, H_{arom}), 6.62 (dd, J_3 = 17.6, 10.9 Hz, 1H, H_{vinyl}), 6.34 (s, 1H, H_{arom}), 6.06 (s, 10H, Cp-H), 5.65 (dd, J_3 = 17.6 Hz, J_2 = 1.0 Hz, 1H, H_{vinyl}), 5.12 (dd, J_3 = 10.9 Hz, J_2 = 1.0 Hz, 1H, H_{vinyl}), 3.48 – 3.37 (m, 4H, THF), 2.41 (s, 2H, CH_2), 2.14 (s, 2H, CH_3), 1.37 – 1.16 (m, 4H, THF).

^{13}C-NMR (126 MHz, C_6D_6, 300 K) δ (ppm) =167.4 (s, C_{arom}), 157.5 (s, C_{arom}), 148.5 (s, C_{arom}), 139.4 (s, C_{arom}), 138.1 (s, C_{arom}), 136.8 (s, C_{vinyl}), 127.4 (s, C_{arom}), 127.0 (s, C_{arom}), 114.0 (s, C_{vinyl}), 110.8 (s, C_{arom}), 110.3 (s, Cp-C), 108.1 (s, C_{arom}), 70.2 (s, THF), 42.7 (d, J_{CY} = 10.7 Hz. CH_2), 25.6 (s, THF), 24.1 (s, CH_3).

EA:	calculated:	C 69.88	H 6.27	N 2.81
	found:	C 69.83	H 6.36	N 2.82

2.3 Synthesis of functionalised biomolecules

Cholesteryl thiocyanate[10]

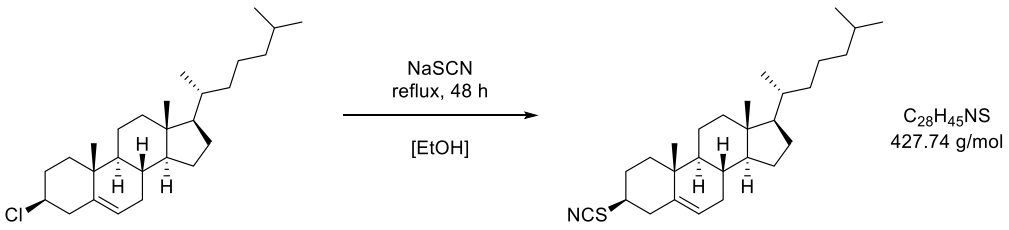

Cholesteryl chloride (12.5 g, 31.0 mmol, 1.00 eq.) was added to a solution of NaSCN (9.40 g, 1.16 mol, 37.4 eq.) in ethanol (600 mL) and was refluxed at 100 °C for 48 hours. Solids were removed *via* hot filtration and washed with warm ethanol. After the product had precipitated from the filtrate it was recrystallised from a 1:1 mixture of ethyl acetate and ethanol and was obtained as light-yellow solid (11.3 g, 26.4 mmol, 85%).

^{1}H-NMR (300 MHz, $CDCl_3$, 300 K): δ (ppm) = 5.41 (d, J_3 = 5.1 Hz, 1H, H_{vinyl}), 3.08 (tt, J_3 = 12.3, 4.2 Hz, 1H, C*H*SCN), 2.61 – 2.36 (m, 2H, chol), 2.09 – 1.74 (m, 6H, chol), 1.62 – 0.98 (m, 23H, chol, CH_3), 0.91 (d, J_3 = 6.5 Hz, 3H, CH_3), 0.87 (s, 3H, CH_3), 0.85 (s, 3H, CH_3), 0.68 (s, 3H, CH_3).

^{13}C-NMR (75 MHz, $CDCl_3$, 300 K): δ (ppm) = 140.1 (s), 123.3 (s), 111.4 (s), 56.8 (s), 56.3 (s), 50.2 (s), 48.2 (s), 42.4 (s), 39.9 (s), 39.8 (s), 39.7 (s), 39.5 (s), 36.6 (s), 36.3 (s), 35.9 (s), 31.9 (s), 31.8 (s), 30.1 (s), 28.4 (s), 28.2 (s), 24.4 (s), 23.9 (s), 22.9 (s), 22.7 (s), 21.0 (s), 19.3 (s), 18.9 (s), 12.0 (s).

EA:	calculated:	C 78.63	H 10.60	N 3.27	S 7.50
	found:	C 78.73	H 10.86	N 3.17	S 7.29

Thiocholesterol[10]

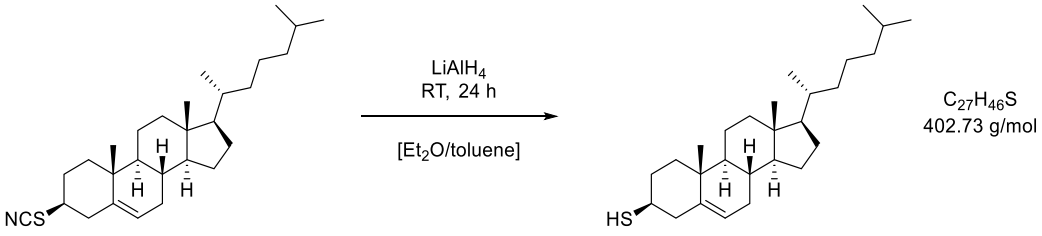

Over a period of two hours a solution of cholesteryl thiocyanate (5.00 g, 11.7 mmol, 1.00 eq.) in toluene (50.0 mL) was added dropwise to a suspension of $LiAlH_4$ (1.00 g, 26.4 mmol, 2.30 eq.) in 100 mL diethyl ether. The suspension was stirred for 24 hours at room temperature and the reaction quenched by slow addition of 50.0 mL 6 N HCl. The organic phase was washed three times with water (150 mL), dried over $MgSO_4$ and filtrated. The solvent was removed *in vacuo*, the crude product was recrystallised from a 3:1 mixture of ethanol and ethyl acetate and thiocholesterol (3.47 g, 8.60 mmol, 74%) was obtained as colorless solid.

^{1}H-NMR (300 MHz, $CDCl_3$, 300 K): δ (ppm) = 5.32 (dd, J_3 = 5.2, 1.6 Hz, 1H, H_{vinyl}), 2.76 – 2.60 (m, 1H, C*H*SH), 2.35 – 2.23 (m, 2H, CH_2CHSH), 2.08 – 1.74 (m, 5H, chol), 1.64 – 1.02 (m, 22H, chol), 1.00 (s, 3H, CH_3), 0.91 (d, J = 6.5 Hz, 3H, CH_3), 0.86 (d, J_3 = 6.6 Hz, 3H, CH_3), 0.86 (d, J_3 = 6.6 Hz, 3H, CH_3), 0.67 (s, 3H, CH_3).

^{13}C-NMR (75 MHz, $CDCl_3$, 300 K): δ (ppm) = 142.1 (s), 121.2 (s), 56.9 (s), 56.3 (s), 50.4 (s), 44.3 (s), 42.5 (s), 40.1 (s), 39.9 (s), 39.7 (s), 39.6 (s), 36.5 (s), 36.3 (s), 35.9 (s), 34.2 (s), 31.9 (s), 28.4 (s), 28.2 (s), 24.4 (s), 24.0 (s), 22.9 (s), 22.7 (s), 21.0 (s), 19.4 (s), 18.9 (s), 12.0 (s).

EA:	calculated:	C 80.53	H 11.51	S 7.96
	found:	C 80.44	H 11.74	S 7.63

Folate-(γ)-NHS[11, 12]

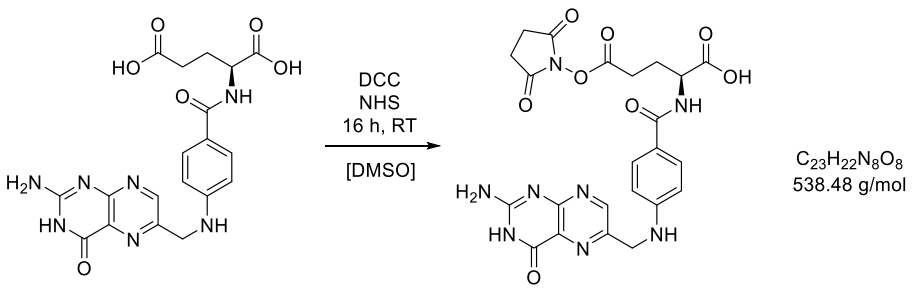

Folic acid (3.00 g, 6.80 mmol,1.00 eq.) was dissolved in dimethyl sulfoxide (50.0 mL) by light heating. After complete dissolution 2.10 g dicyclohexylcarbodiimide (10.2 mmol, 1.50 eq.) and 1.17 g *N*-hydroxysuccinimide (10.2 mmol, 1.50 eq.) were added successively and the mixture was stirred for 16 hours at room temperature. The resulting urea was removed by filtration, the folate derivative was obtained *via* precipitation with excess acetone under vigorous stirring and washed with diethyl ether four times. After drying folate-NHS (3.15 g, 5.85 mmol, 86%) was obtained as a yellow solid.

^{1}H-NMR (400 MHz, DMSO-d_6, 300 K): δ (ppm) = 8.65 (s, 1H, C*H*$_{pteridine}$), 7.79 – 7.53 (m, 2H, H$_{arom}$), 7.04 – 6.83 (br s, 3H, CH$_2$N*H*), 6.71 – 6.53 (m, 2H, H$_{arom}$), 4.88 (dd, J_3 = 7.3 Hz, 1H, C*H*NH(C=O)), 4.49 (d, J_3 = 6.2 Hz, 2H, C*H*$_2$NH), 3.11 – 2.66 (m, 2H, C*H*$_2$CH$_2$CHNH), 2.81 (s, 4H, C*H*$_2$C*H*$_2$), 2.36 – 1.85 (m, 2H, CH$_2$C*H*$_2$CHNH).

^{13}C-NMR (126 MHz, DMSO-d_6, 300 K): δ (ppm) = 172.8 (s, C=O), 170.2 (s, C =O), 170.1 (s, C =O), 166.8 (s, *C*=O), 160.9 (s, C=O$_{pteridine}$), 153.8 (s), 150.9 (s), 148.7(s, *C*H$_{pteridine}$), 129.1 (s), 128.0 (s), 121.2 (s), 111.2 (s), 51.5 (s, CH$_2$CH$_2$*C*H), 45.0 (s, *C*H$_2$NH), 30.5 (s, *C*H$_2$CH$_2$CH), 27.5 (s, CH$_2$*C*H$_2$CH), 25.8 (s, *C*.

3. Polymerisation investigations

3.1 Kinetic measurements of DEVP polymerisations

A solution of the corresponding initiator (21.7 µmol, 1.00 eq.) in 5.00 mL toluene was added to a solution of 21.7 µmol catalyst (1.00 eq.) in 5.00 mL toluene at room temperature and showed an instant orange coloring. The mixture was stirred over night and quantitative conversion was confirmed by ^{1}H-NMR spectroscopy. DEVP (13.0 mmol, 600 eq.) was added in one portion and aliquots were taken from the reaction solution at regular time intervals and quenched by pouring the sample into MeOH. The conversion of DEVP of each aliquot was determined by ^{31}P-NMR spectroscopy. The molecular weight of the polymer samples was determined by GPC-MALS analysis after removal of the solvent *via* drying at ambient temperature.

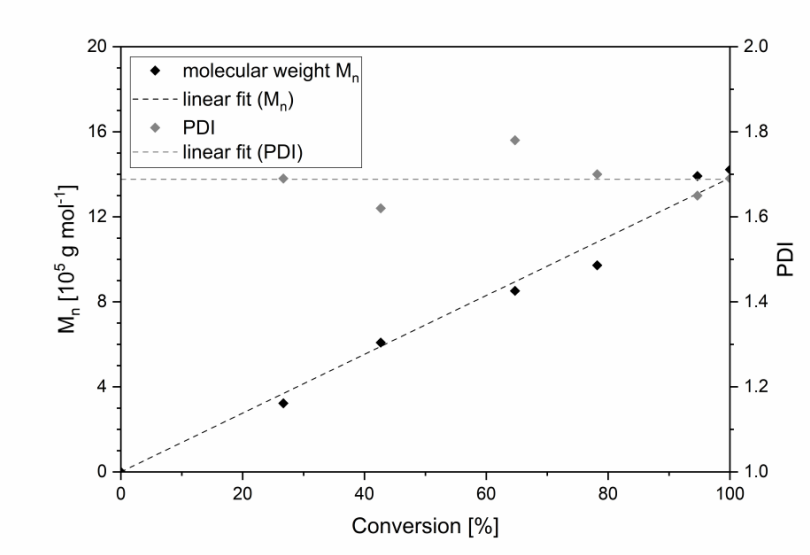

Figure S1: Conversion-dependent plot of M_n and the respective PDI of the polymer aliquots generated during kinetic investigations using *in situ* generated $Cp_2YC_{13}H_{10}N$, (21.7 µmol catalyst, 600 eq. DEVP in 10.0 mL toluene, 30 °C).

3.2 Polymerisation procedure and analysis

A solution of 2,6-dimethyl-4-(4-vinylphenyl)pyridine (65.1 µmol, 1.00 eq.) in 5.00 mL toluene was added to a solution of 65.1 µmol $Cp_2Y(C_2TMS)(THF)$ (1.00 eq.) in toluene (5.00 mL). After quantitative conversion was shown by ^{1}H-NMR spectroscopy, DEVP (6.51 mmol, 100 eq.) was added in one portion and the conversion of DEVP was determined by ^{31}P-NMR spectroscopy after three hours. The reaction was quenched by addition of methanol (0.50 mL) and the polymer was precipitated by pouring the reaction mixture into pentane (150 mL). The clear solution was decanted of, residual solvent was removed by drying at ambient temperature and the polymer was dissolved in water and lyophilised. Molecular weights of the obtained polymers were determined by GPC-MALS and the determination of the cloud points was carried out *via* turbidity measurements.

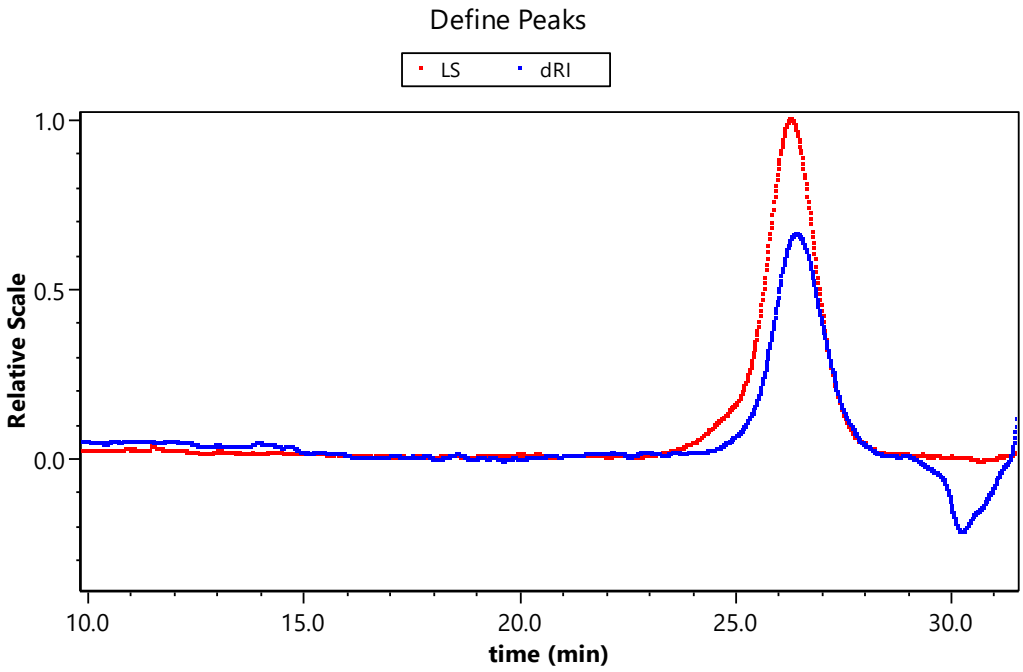

Figure S2: GPC-traces of PDEVP (100 eq. DEVP; entry 1, table 1).

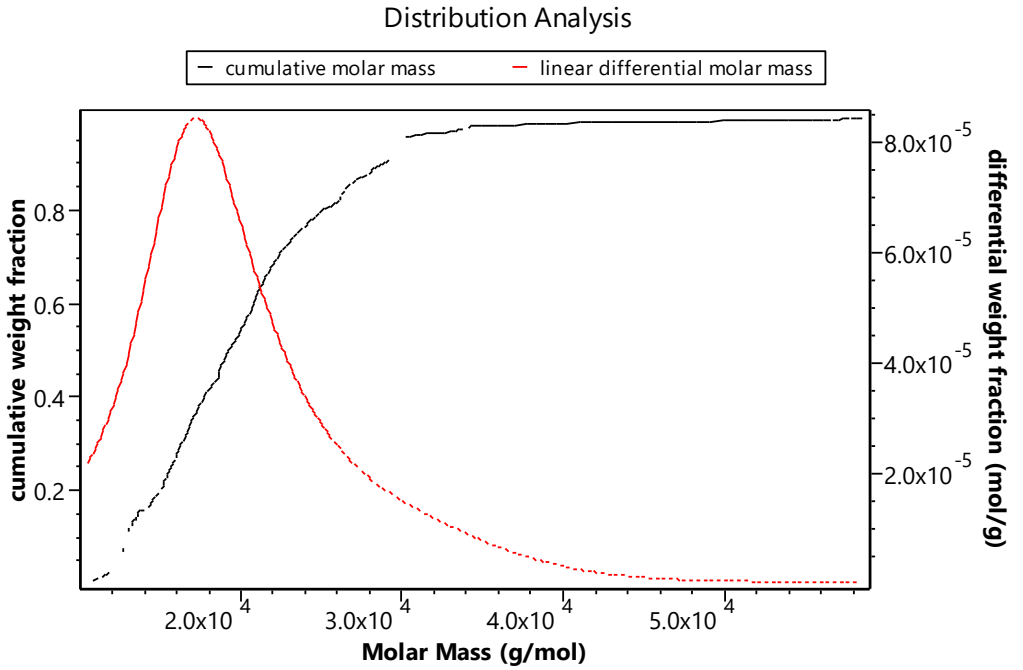

Figure S3: Distribution plot of PDEVP (100 eq. DEVP).

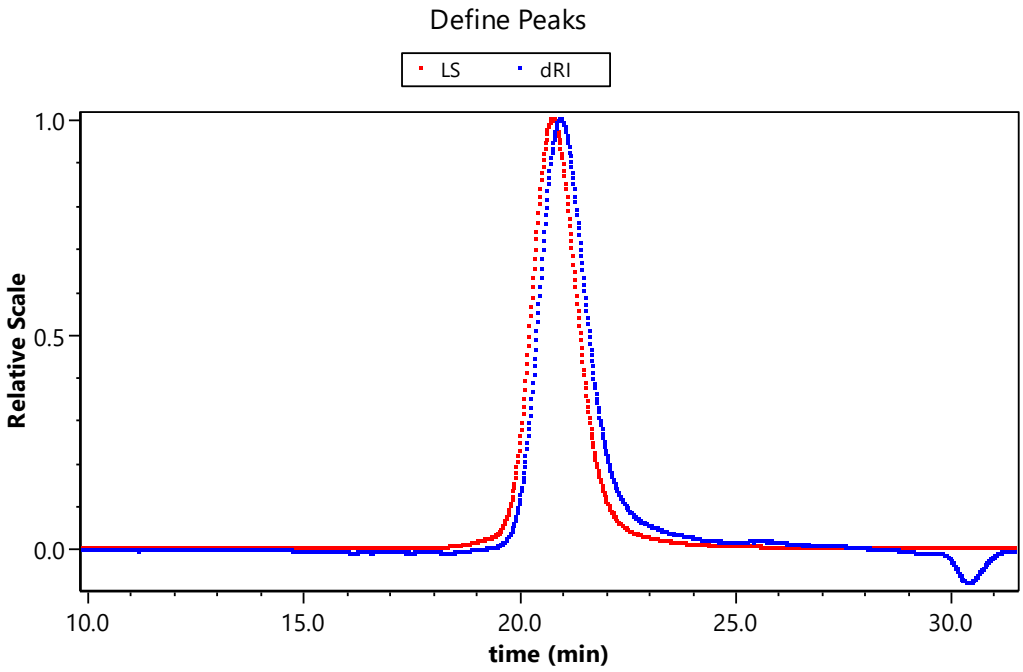

Figure S4: GPC-traces of PDEVP (600 eq. DEVP; entry 2, table 1).

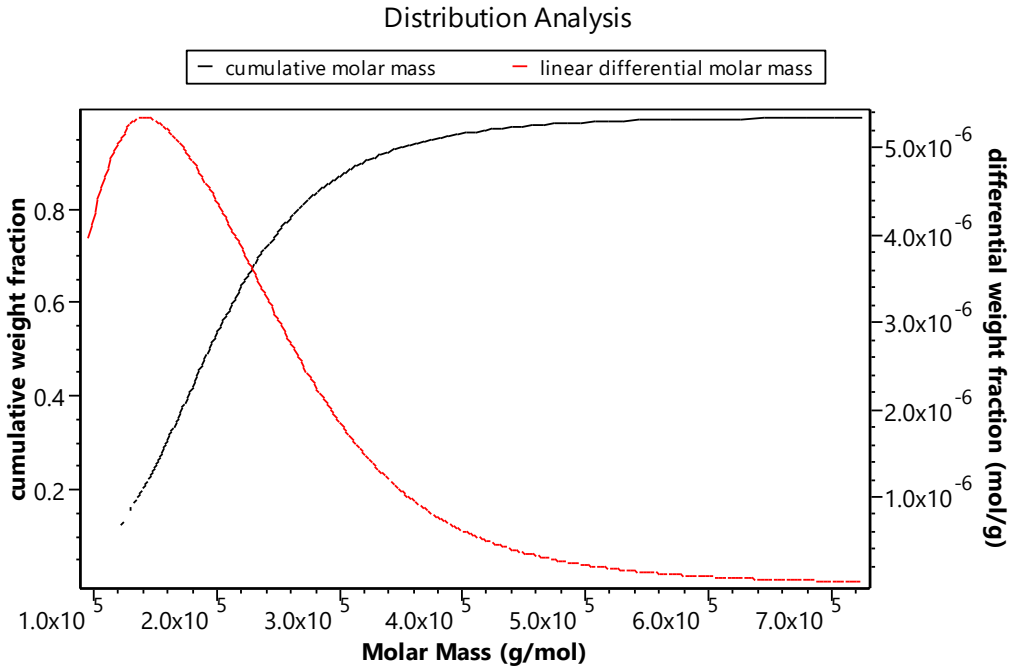

Figure S5: Distribution plot of PDEVP (600 eq. DEVP).

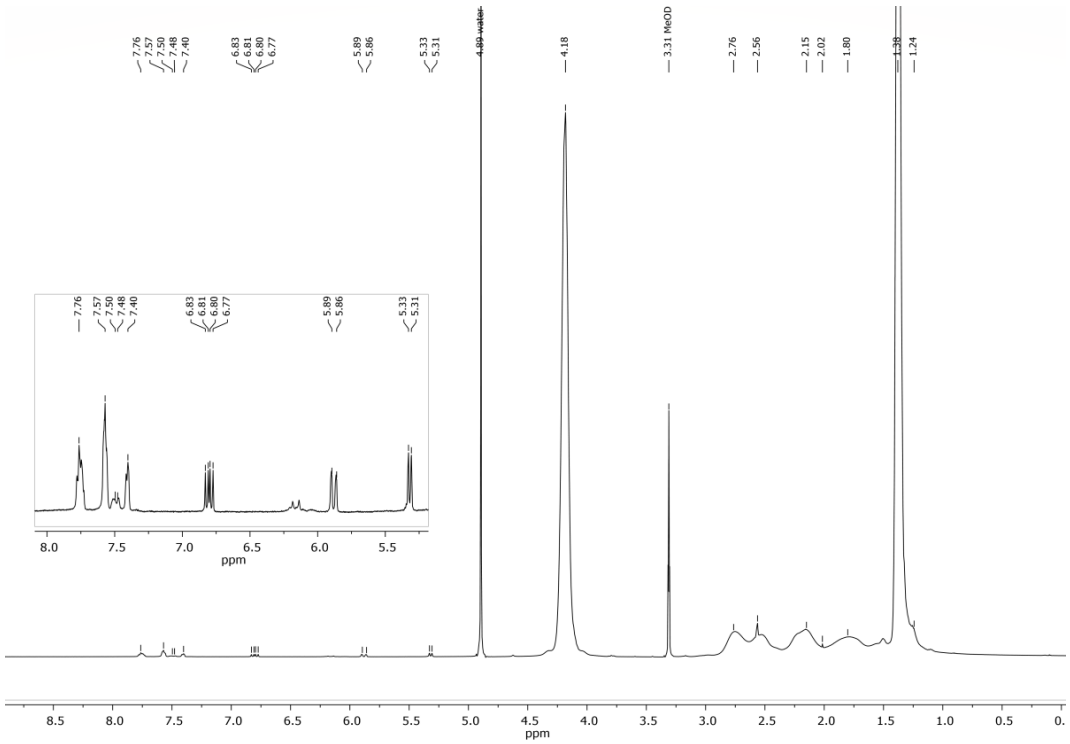

Figure S6: ^{1}H-NMR spectrum of PDEVP (100 eq. DEVP; entry 1, table 1) in MeOD.

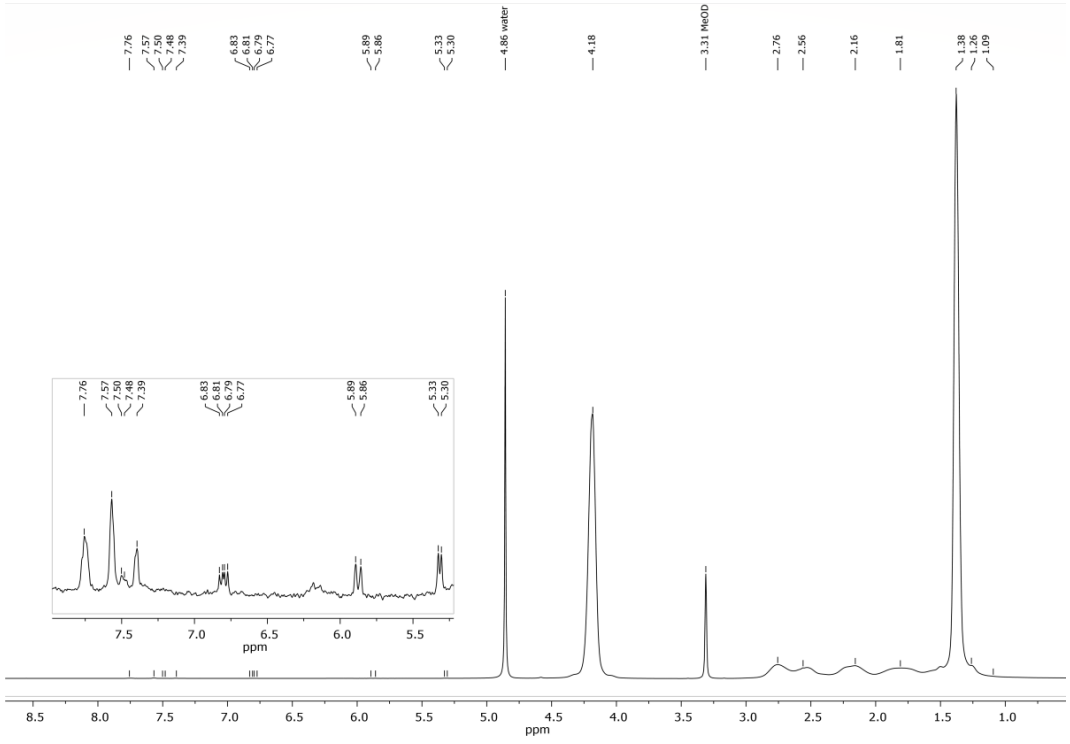

Figure S7: ^{1}H-NMR spectrum of PDEVP (600 eq. DEVP; entry 2, table 1) in MeOD.

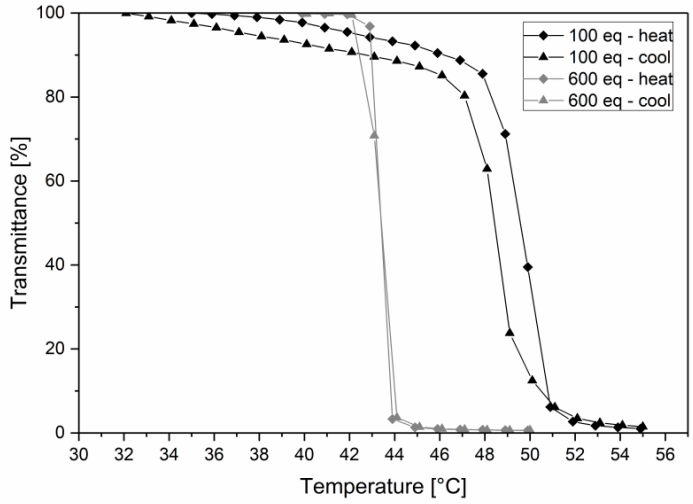

Figure S8: Determination of the LCST of short-chain PDEVP (100 eq.) and long-chain PDEVP (600 eq.). The cloud point was determined at 10% decrease of transmittance for aqueous solutions of PDEVP (2.50 mg/mL).

4. End-group analysis *via* ESI-MS and NMR

For the elucidation of the polymerisation mechanism *via* end-group analysis oligomeric PDEVP was generated: 122 µmol of $Cp_2Y(CH_2TMS)(THF)$ was dissolved in 2.50 mL toluene and was mixed with a solution of the corresponding initiator (122 µmol). After quantitative conversion was confirmed by ^{1}H-NMR spectroscopy 5.00 equivalents of DEVP were added and conversion was determined after two hours *via* ^{31}P-NMR spectroscopy. The signals found by ESI-MS analysis can be attributed to $M_{Initiator}$ + n x M_{DEVP} with either H^+ or Na^+ as charge carrier.

5. Thiol-ene click reactions

General procedure: Thiol-ene coupling of thiocholesterol to poly(diethyl vinylphosphonates)

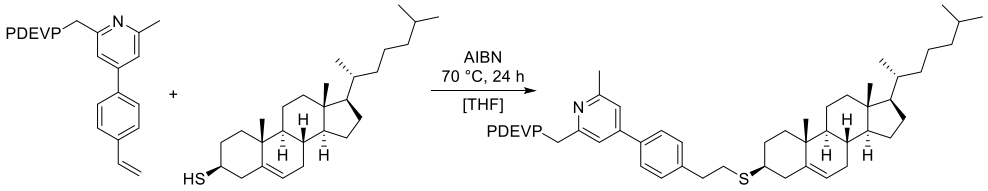

Thiocholesterol (5.00 eq.) and catalytic amounts of azobisisobutyronitrile (0.33 eq.) were added to a solution of 1.00 equivalent of poly(diethyl vinylphosphonate) in tetrahydrofuran (10.0 mL per 1.00 g polymer) in a pressuriseable schlenk flask. The mixture was degassed *via* evacuation and filling with argon (20 iterations) and stirred for 24 hours at

70 °C. After this time period ^{1}H-NMR spectroscopy showed quantitative conversion of the vinyl group. The polymer was purified by precipitation from the reaction solution with excess pentane. The polymeric residue was dissolved in toluene, precipitated with pentane two more times, was dried to remove pentane, dissolved in water and lyophilised.

Table S1: Chemical shifts in ^{1}H- und ^{31}P-NMR of cholesterol-functionalised PDEVP

	Substrate	**^{1}H-NMR (500 MHz, CD_3OD, 300 K) δ [ppm]**	**^{31}P-NMR (203 MHz, CD_3OD, 300 K) δ [ppm]**
1	PDEVP (100 eq.)	7.79 – 7.66 (m, H_{arom}), 7.62 – 7.44 (m, H_{arom}), 7.39 (d, J = 6.3 Hz, H_{arom}), 5.34 (s, chol), 4.20 (s, POCH_2), 2.89 – 2.85 (m, chol), 2.89 – 1.18 (m, PDEVP), 1.40 (m, $POCH_2CH_3$), 1.02 (s, $CH_{3,Chol}$), 0.96 (d, J_3 = 6.5 Hz, $CH_{3,Chol}$), 0.91 (d, J = 6.6 Hz, $CH_{3,Chol}$), 0.90 (d, J_3 = 6.6 Hz, $CH_{3,Chol}$), 0.73 (s, $CH_{3,Chol}$).	33.1
2	PDEVP (600 eq.)	8.09 – 7.21 (m, H_{arom}), 5.36 (s, chol), 4.21 (m, POCH_2), 3.60 (d, J_3 = 7.4 Hz, chol), 2.89 – 1.13 (m, PDEVP), 1.40 (m, $POCH_2CH_3$), 1.05 (s, $CH_{3,chol}$), 0.94 (s, $CH_{3,chol}$), 0.91 (s, $CH_{3,chol}$), 0.90 (s, $CH_{3,chol}$), 0.74 (s, $CH_{3,chol}$).	33.2

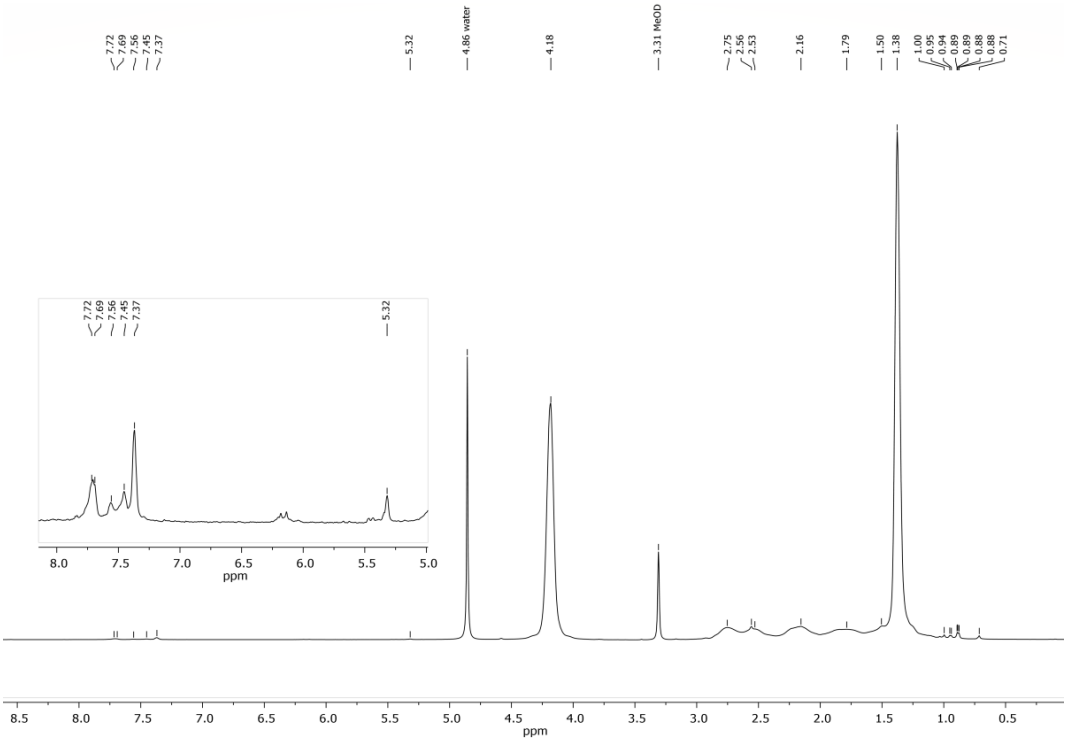

Figure S9: ^{1}H-NMR of PDEVP (100 eq.) after functionalisation with thiocholesterol in MeOD.

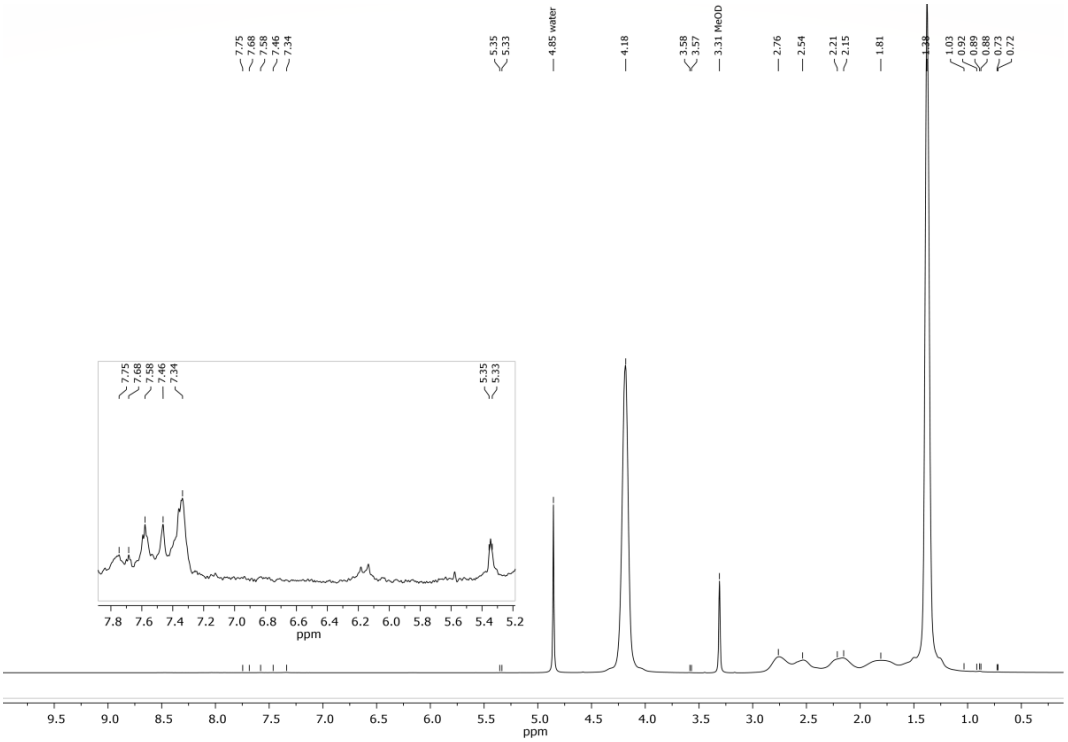

Figure S10: ^{1}H-NMR of PDEVP (600 eq.) after functionalisation with thiocholesterol in MeOD.

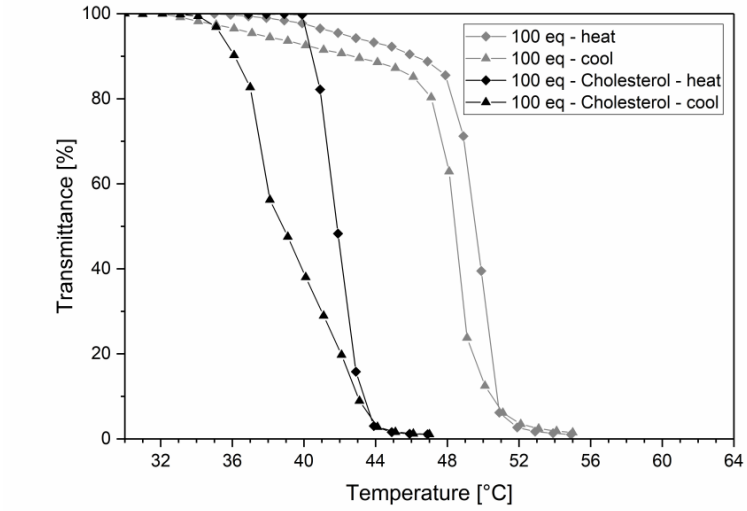

Figure S11: Determination of the LCST of cholesterol-functionalised PDEVP (100 eq.) and the corresponding short-chain PDEVP (100 eq.). The cloud point was determined at 10% decrease of transmittance for aqueous solutions of the polymer substrates (2.50 mg/mL).

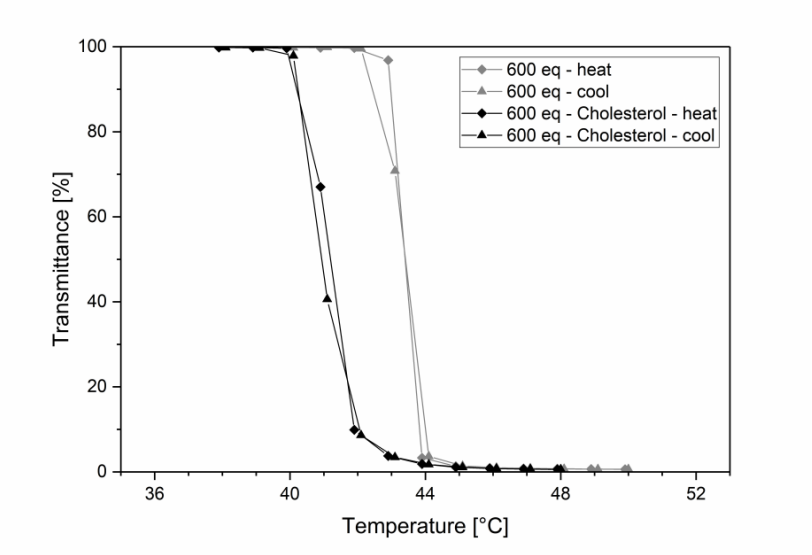

Figure S12: Determination of the LCST of cholesterol-functionalised PDEVP (600 eq.) and the corresponding short-chain PDEVP (600 eq.). The cloud point was determined at 10% decrease of transmittance for aqueous solutions of the polymer substrates (2.50 mg/mL).

General procedure: Thiol-ene coupling of cysteamine hydrochloride to poly(diethyl vinylphosphonates)

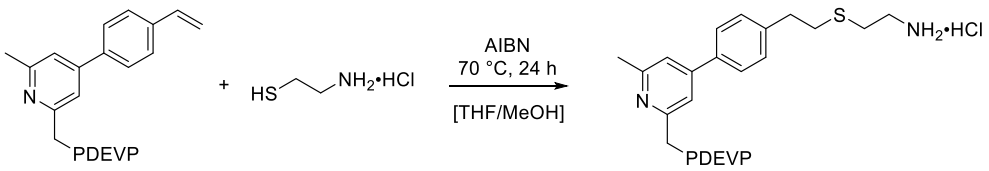

Cysteamine hydrochloride (5.00 eq.) and catalytic amounts of azobisisobutyronitrile (0.33 eq.) were added to a solution of 1.00 equivalent of poly(diethyl vinylphosphonate) in tetrahydrofuran and methanol (10:1, 10.0 mL per 1.00 g polymer) in a pressuriseable schlenk flask. The mixture was degassed *via* drawing vacuum and filling with argon (20 iterations) and stirred for 24 hours at 70 °C. After this time period ^{1}H-NMR spectroscopy showed quantitative conversion of the vinyl group. The polymer was purified *via* dialysis against deionised water. After replacing the dialysate after two and four hours the mixture was dialysed over night and the resulting solution lyophilised.

Table S2: Chemical shifts in ^{1}H- und ^{31}P-NMR of PDEVP after reaction with cysteamine hydrochloride

	Substrate	^{1}H-NMR (500 MHz, CD_3OD, 300K) δ [ppm]	^{31}P-NMR (121 MHz, CD_3OD, 300 K) δ [ppm]	Yield [%]
1	PDEVP (100 eq.)	7.76 – 7.37 (m, H_{arom}), 7.31 – 7.17 (m, H_{arom}), 4.18 (s, POCH_2), 2.98 (t, J_3 = 7.5 Hz, $CH_{2,aliphatic}$), 2.88 (t, J_3 = 5.4 Hz, $CH_{2,aliphatic}$), 2.83 – 1.20 (m, PDEVP), 1.38 (s, $POCH_2CH_3$).	33.2	100
2	PDEVP (600 eq.)	7.86 – 7.43 (m, H_{arom}), 7.30 – 7.12 (m, H_{arom}), 4.18 (s, POCH_2), 2.98 (t, J_3 = 7.1 Hz, $CH_{2,aliphatic}$), 2.93 – 2.87 (m, $CH_{2,aliphatic}$), 2.85 – 1.20 (m, PDEVP), 1.38 (s, $POCH_2CH_3$).	33.2	100

General procedure: Conversion of polymer-bound cysteamine linker with activated folate species

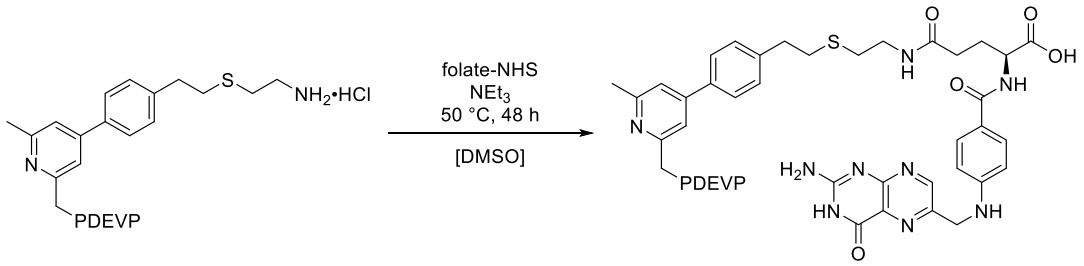

5.00 equivalents of folate-NHS and 6.00 equivalents of triethylamine were added to a solution of 1.00 equivalent of the stated cysteamine-containing poly(diethyl vinylphosphonate) in dimethyl sulfoxide (20.0 mL solvent per 1.00 g polymer). The mixture was stirred for 48 hours at 50 °C and after this period purified *via* dialysis against deionised water. After replacing the dialysate after two and four hours the mixture was dialysed over night and the resulting solution lyophilised.

Table S3: Chemical shifts of folate-containing PDEVP in ^{1}H- und ^{31}P-NMR

	Substrate	^{1}H-NMR (500 MHz, CD_3OD, 300K) δ [ppm]	^{31}P-NMR (203 MHz, CD_3OD, 300 K) δ [ppm]
1	PDEVP (100 eq.)	8.68 (s, pteridine), 7.84 – 6.99 (m, folate, H_{arom}), 6.80 – 6.56 (m, H_{arom}), 4.67 (s, CH_2NH_2), 4.54 (s, CH_2HN), 4.18 (s, POCH_2), 3.14 – 1.06 (m, PDEVP), 1.38 (s, $POCH_2CH_3$).	33.2
2	PDEVP (600 eq.)	8.71 (s, pteridine), 7.77 – 7.51 (m, folate, H_{arom}), 7.55 – 6.98 (m, H_{arom}), 6.79 – 6.60 (m, H_{arom}), 4.60 (s, CH_2NH_2), 4.49 (s, CH_2NH), 4.18 (s, POCH_2), 2.86 – 1.17 (m, PDEVP), 1.38 (s, $POCH_2CH_3$).	33.2

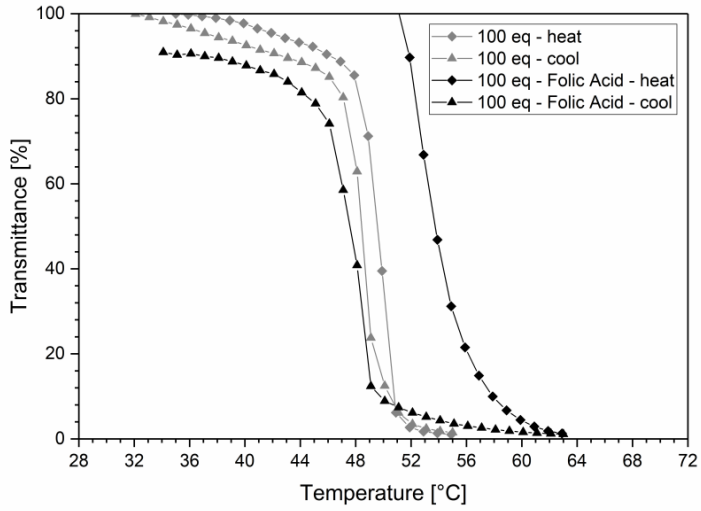

Figure S13: Determination of the LCST of folate-functionalised PDEVP (100 eq.) and the corresponding short-chain PDEVP (100 eq.). The cloud point was determined at 10% decrease of transmittance for aqueous solutions of the polymer substrates (2.50 mg/mL).

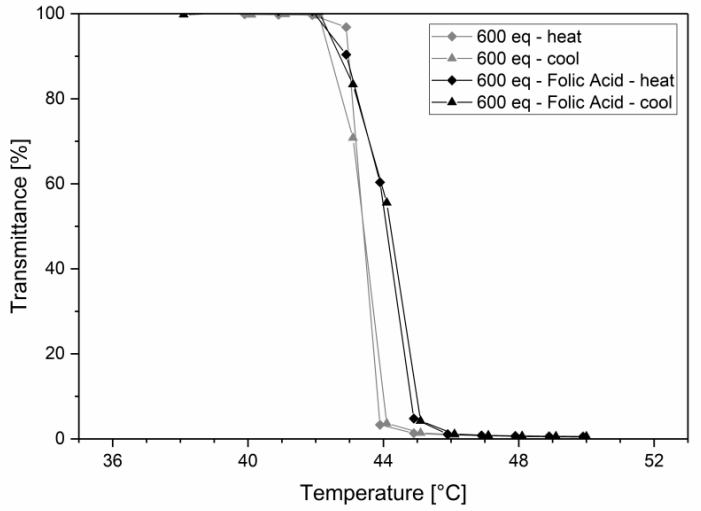

Figure S14: Determination of the LCST of folate-functionalised PDEVP (600 eq.) and the corresponding long-chain PDEVP (600 eq.). The cloud point was determined at 10% decrease of transmittance for aqueous solutions of the polymer substrates (2.50 mg/mL).

6. Cell viability assay

6.1 Cell culture

In vitro studies on polymer samples were performed in HEK and HMEC cells. Cells were cultured in Dulbecco's Modified Eagle Medium (Life Technologies) equipped with 10% (v/v) Fetal Bovine Serum (Biochrom) and 1%

Penicillin/Streptomycin 10000 U/mL /10000 µg/mL (Biochrom) at 37 °C in a humidified atmosphere containing 5% CO_2. For splitting and sub-culturing of cells Trypsin 0.05%/EDTA 0.02% in PBS (PAN Biotech) was used.

6.2 Cell viability studies

The growth inhibition of the polymer samples on HEK and HMEC cells, was determined by analysing their cell viability of in presence of increasing polymer concentrations (0.078 mg/mL to 5.00 mg/mL). Prior to the addition of the polymers the cells were cultured for 24 h in 96 well flat bottom plates (TPP) with a density of 20000 cells/well or 10000 cells/well (for 48 h). After 24 or 48 hours of incubation at 37 °C in a humidified atmosphere with 5% CO_2, the cell viability of the treated cells was determined using the MTT reagent (Sigma Aldrich). Therefore, MTT was dissolved at a concentration of 5 mg/mL in RPMI-1640 without phenol red (Life Technologies). PBS treated cells were used as positive control (100% viability). DMSO treated cells were used as negative control (0% viability). After 3 h of incubation with 50 µL of MTT per well at 37 °C, the blue formazan crystals were dissolved for 15 min on a plate shaker at 550 min^{-1} with 100 µL 0.04 N HCl in isopropanol and exclusion of light. Following the absorbance of each well was measured at 570 nm with 690 nm as background wavelength at a Tecan Genios Plus plate reader.

Shown are mean values of at least three independent biological replicates and the respective standard deviations are indicated.

7. Literature

[1] K. C. Hultzsch, P. Voth, K. Beckerle, T. P. Spaniol, J. Okuda, *Organometallics* **2000**, *19*, 228-243.

[2] G. D. Vaughn, K. A. Krein, J. A. Gladysz, *Organometallics* **1986**, *5*, 936-942.

[3] C.-X. Cai, L. Toupet, C. W. Lehmann, J.-F. Carpentier, *J. Organomet. Chem.* **2003**, *683*, 131-136.

[4] S. Salzinger, B. S. Soller, A. Plikhta, U. B. Seemann, E. Herdtweck, B. Rieger, *J. Am. Chem. Soc.* **2013**, *135*, 13030-13040.

[5] M. Leute, Dissertation thesis, Universität Ulm **2007**.

[6] M. C. DeRosa, D. J. Hodgson, G. D. Enright, B. Dawson, C. E. B. Evans, R. J. Crutchley, *J. Am. Chem. Soc.* **2004**, *126*, 7619-7626.

[7] H. P. Kokatla, P. F. Thomson, S. Bae, V. R. Doddi, M. K. Lakshman, *J. Org. Chem.* **2011**, *76*, 7842-7848.

[8] B. Singh, G. Y. Lesher, P. O. Pennock, *J. Heterocyclic Chem* **1990**, *27*, 1841-1842.

[9] P. Pahl, C. Schwarzenböck, F. A. D. Herz, B. S. Soller, C. Jandl, B. Rieger, *Macromol.* **2017**, *50*, 6569-6576.

[10] G. L. O'Connor, H. R. Nace, *J. Am. Chem. Soc.* **1953**, *75*, 2118-2123.

[11] C. M. Alexander, K. L. Hamner, M. M. Maye, J. C. Dabrowiak, *Bioconjugate Chem.* **2014**, *25*, 1261-1271.

[12] A. F. Trindade, R. F. M. Frade, E. M. S. Macoas, C. Graca, C. A. B. Rodrigues, J. M. G. Martinho, C. A. M. Afonso, *Org. Biomol. Chem.* **2014**, *12*, 3181-3190.

10.2 Supporting Information of the Manuscript "Fluorescent Polyvinylphosphonate Bioconjugates for Selective Cellular Delivery"

CHEMISTRY
A European Journal

Supporting Information

Fluorescent Polyvinylphosphonate Bioconjugates for Selective Cellular Delivery

Christina Schwarzenböck,[a] Andreas Schaffer,[a] Elfriede Nößner,[b] Peter J. Nelson,[c] Ralf Huss,[d] and Bernhard Rieger*[a]

chem_201706034_sm_miscellaneous_information.pdf

Table of Contents

1. Material and methods

General Information

All reactions were carried out under argon atmosphere using standard Schlenk or glovebox techniques. All glassware was heat dried under vacuum prior to use. Unless otherwise stated, all chemicals were purchased from Sigma-Aldrich, Acros Organics or TCI Europe and used as received. Toluene, THF and dichloromethane were dried using a MBraun SPS-800 solvent purification system. The precursor complexes $Y(CH_2Si(CH_3)_3)_3(THF)_2$ and $LiCH_2TMS$ and the catalyst $Cp_2Y(CH_2TMS)(THF)$ are prepared according to literature procedures.[1-4] Diethyl vinylphosphonate (DEVP) is synthesized according to literature procedures, dried over calcium hydride and distilled prior to use.[5]

Nuclear Magnetic Resonance Spectroscopy

NMR spectra were recorded on a Bruker AV-500HD and AVIII-500 Cryo spectrometer. ^{1}H-NMR spectroscopic chemical shifts δ are reported in ppm relative to the residual proton signal of the solvent. δ (^{1}H) is calibrated to the residual proton signal of the solvent. Unless otherwise stated, coupling constants *J* are averaged values and refer to couplings between two protons. Deuterated solvents were obtained from *Sigma-Aldrich* and dried over 3 Å molecular sieves.

Gel Permeation Chromatography

Gel Permeation Chromatography was performed on a *Varian* LC-920 equipped with two PL Polargel M columns with samples of 5 mg/mL. A mixture of 50% THF, 50% water, 9 g/L tetrabutylammonium bromide (TBAB) and 340 mg/L 3,5-Di-*tert*-butyl-4-hydroxytoluene (BHT) as stabilizing agent was used as eluent. Absolute molecular weights have been determined by multiangle light scattering (MALS) analysis using a Wyatt Dawn Heleos II in combination with a *Wyatt* Optilab rEX as concentration source.

Additionally, GPC measurements were carried out on a PL-GPC 50 System (Agilent Technologies) equipped with two PLgel columns with samples of 5 mg/mL. A mixture of 50% THF, 50% water, 9 g/L TBAB and 340 mg/L BHT as stabilizing agent was used as eluent. Absolute molecular weights have been determined by a dual-angle light scattering detector in combination with an integrated RI detection unit as concentration source.

Turbidity Measurements

Turbidity measurements were performed on a Cary 50 UV/Vis spectrophotometer (Varian). The cloud point of the samples was determined by spectrophotometric detection of the changes in transmittance at λ = 500 nm in aqueous solution and λ = 650 nm in mixtures of DMEM (+10% FBS + 1% Penecillin/Streptomycin):PBS (2:1). The samples were heated/cooled at a rate of 1.0 K/min in steps of 1 K followed by a five minutes long period of constant temperature to ensure equilibration. The cloud point was defined as the temperature corresponding to a 10% decrease in optical transmittance.

Centrifugation

Separation of solids *via* centrifugation was carried out with the ultracentrifuge Sorvall MX Plus (Thermo Fisher Scientific) as well as the centrifuges Sorvall RC 6 Plus and Heraeus Megafuge 40 centrifuge series from Thermo Fisher Scientific.

Dialysis

Purification *via* dialysis was performed with a Spectra/Por 1 dialysis tubing (regenerated cellulose) with a molecular weight cut-off (MWCO) of 6-8 kDa (Spectrumlabs). Before use the membranes were treated with deionized water over night and then rinsed with fresh deionized water. A 100:1 ratio of dialysis fluid to sample volume was applied. Specific solvents used as dialysis fluid are given for the corresponding procedures.

UV/Vis Measurements

UV/Vis spectra were recorded on a Varian Cary 50 UV/Vis spectrophotometer in 40 mm × 10 mm × 2 mm quartz glass cuvettes. Deionized water was used as solvent.

Photoluminescence Measurements

Photoluminescence spectra were recorded on a AVA-Spec 2048 spectrometer (AVANTES) with a current controller as 365 nm light source (Prizmatix). A 90° cuvette holder and a 40 mm × 10 mm × 2 mm quartz glass cuvette were used for the measurements. The samples were dissolved in deionized water. Intensity calibration of the spectrometer was performed by an AVANTES DH-Cal calibration light source using the halogen lamp.

2. Polymerization procedure and analysis

A solution of 2,6-dimethyl-4-(4-vinylphenyl)pyridine (65.1 µmol, 1.00 eq.) in 5.00 mL toluene was added to a solution of 65.1 µmol $Cp_2Y(C_2TMS)(THF)$ (1.00 eq.) in toluene (5.00 mL). After quantitative conversion was shown by ^{1}H-NMR spectroscopy, DEVP (6.51 mmol, 100 eq.) was added in one portion and the conversion of DEVP was determined by ^{31}P-NMR spectroscopy after three hours. The reaction was quenched by addition of methanol (0.50 mL) and the polymer was precipitated by pouring the reaction mixture into pentane (150 mL). The clear solution was decanted of, residual solvent was removed by drying at ambient temperature and the polymer was dissolved in water and lyophilized (Vaco 5-II-D from Zirbus technology GmbH). Molecular weights of the obtained polymers were determined by GPC-MALS and the determination of the cloud points was carried out *via* turbidity measurements.

Table S1. Signals of PDEVP substrates in ^{1}H- und ^{31}P-NMRs

	$[M]_0/[Cat]_0$	^{1}H-NMR (500 MHz, CD_3OD, 300K) δ [ppm]	^{31}P-NMR (203 MHz, CD_3OD, 300 K) δ [ppm]
1	100	7.75 (qd, J_3 = 7.7, 4.0 Hz, 2H, H_{arom}), 7.60 – 7.39 (m, 4H, H_{arom}), 6.80 (dd, J_3 = 17.6, 10.8 Hz, 1H, H_{vinyl}), 5.88 (d, J_3 = 17.6 Hz, 1H, H_{vinyl}), 5.32 (d, J_3 = 10.8 Hz, 1H, H_{viynl}), 4.18 (s, POCH_2), 3.07 – 0.97 (m, PDEVP), 1.38 (s, $POCH_2CH_3$)	33.2
2	600	7.79 – 7.70 (m, 2H, H_{arom}), 7.59 – 7.38 (m, 4H, H_{arom}), 6.80 (dd, J_3 = 17.6, 10.9 Hz, 1H, H_{vinyl}), 5.88 (d, J_3 = 17.6 Hz, 1H, H_{vinyl}), 5.32 (d, J_3 = 10.9 Hz, 1H, H_{vinyl}), 4.18 (s, POCH_2), 3.09 – 0.74 (m, PDEVP), 1.38 (s, $POCH_2CH_3$)	33.2

Table S2. Molecular weight M_n, PDI and initiator efficiency I^* of PDEVP

	$[M]_0/[Cat]_0$	M_n [kg/mol]	PDI	I^* [%]
1	100	18.7	1.09	89
2	600	158	1.01	62

3. Functionalization of polyvinylphosphonates

3.1 Introduction of fluorescence to poly(diethyl vinylphosphonates)

General procedure: Partial transesterification of the side-chain groups of poly(diethyl vinylphosphonates)

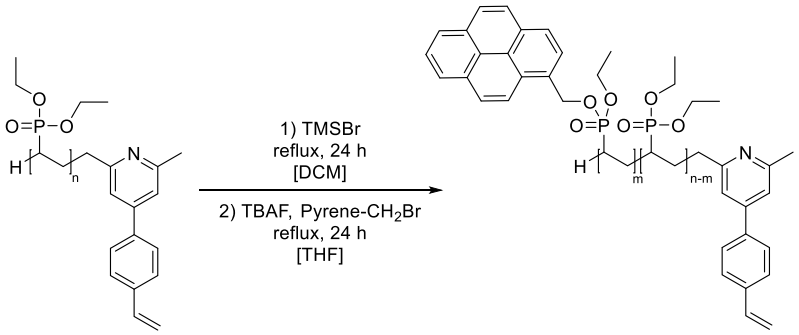

Poly(diethyl vinylphosphonate) was dissolved in absolute dichloromethane (20.0 mL per 1.00 g) and bromotrimethylsilane (2.00 mol-% of corresponding repeating units, 1.00 eq.) was added. The reaction mixture was refluxed for 24 hours, all volatiles were removed *in vacuo* and the residue was dissolved in absolute tetrahydrofuran. 1-(Bromomethyl)pyrene (2.00 eq.) and tetrabutylammonium fluoride (1 M in THF, 2.00 eq.) was added and the mixture was again refluxed for 24 hours. After cooling to room temperature, the solution was concentrated *in vacuo* and the residue was dialyzed against deionized water overnight. The precipitate was removed *via* ultracentrifugation, the supernatant polymer solution was dialyzed against deionized water over night and freeze-dried afterwards.

Table S3. Chemical shifts in ^{1}H- und ^{31}P-NMRs of the fluorescent PDEVP substrates

	Substrate	^{1}H-NMR (500 MHz, CD_3OD, 300K) δ [ppm]	^{31}P-NMR (203 MHz, CD_3OD, 300 K) δ [ppm]
1	PDEVP (100 eq.)	8.42 (d, J_3 = 9.2 Hz, pyrene), 8.29 – 7.95 (m, pyrene), 7.95 – 7.40 (m, pyrene, H_{arom}), 6.81 (dd, J_3 = 17.7, 11.0 Hz, H_{vinyl}), 5.90 (dd, J = 17.7 Hz, J_2 = 4.0 Hz, H_{vinyl}), 5.36 (s, $POCH_2$-*pyrene*), 4.18 (s, $POCH_2$), 2.91 – 1.13 (m, PDEVP), 1.38 (s, $POCH_2CH_3$)	33.2, 32.0
2	PDEVP (600 eq.)	8.42 (d, J_3 = 9.3 Hz, pyrene), 8.28 – 7.94 (m, pyrene), 7.82 – 7.37 (m, H_{arom}), 6.80 (dd, J_3 = 17.7, 10.8 Hz, H_{vinyl}), 5.88 (d, J_3 = 17.7 Hz, H_{vinyl}), 5.36 (s, $POCH_2$-*pyrene*), 4.19 (s, $POCH_2$), 2.89 – 1.17 (m, PDEVP), 1.38 (m, $POCH_2CH_3$)	33.2

Table S4. PDI and degree of pyrene-incorporation of fluorescent PDEVP

	Substrate	PDI	Pyrene-Incorporation [%]
1	PDEVP (100 eq.)	1.07	1.13
2	PDEVP (600 eq.)	1.01	0.38

3.2 Thiol-ene click reactions

General procedure: Thiol-ene coupling of thiocholesterol to poly(diethyl vinylphosphonates)[6]

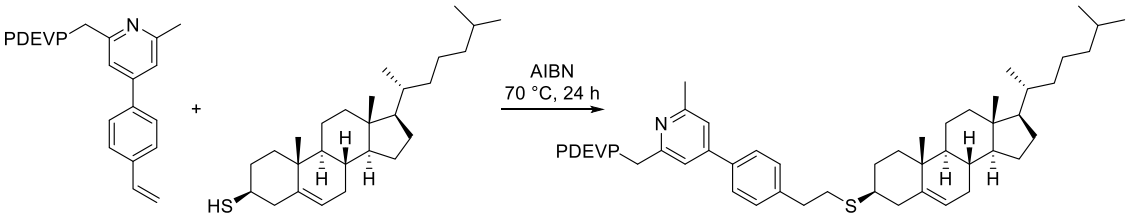

Thiocholesterol (5.00 eq.) and catalytic amounts of azobisisobutyronitrile (0.33 eq.) were added to a solution of 1.00 equivalent of the fluorescent poly(diethyl vinylphosphonate) in tetrahydrofuran (10.0 mL per 1.00 g polymer) in a pressurizeable schlenk flask. The mixture was degassed *via* evacuation and filling with argon (20 iterations) and stirred for 24 hours at 70 °C. After this time period ^{1}H-NMR spectroscopy showed quantitative conversion of the vinyl group. The polymer was purified by precipitation from the reaction solution with excess pentane. The polymeric residue was dissolved in toluene, precipitated with pentane two more times, was dried to remove pentane, dissolved in water and lyophilized.
The non-fluorescent polymer samples were prepared accordingly and their characterization can be found in the corresponding literature.[6]

Table S5. Chemical shifts in ^{1}H- und ^{31}P-NMR of fluorescent, cholesterol-functionalized PDEVP

	Substrate	^{1}H-NMR (500 MHz, CD_3OD, 300 K) δ [ppm]	^{31}P-NMR (203 MHz, CD_3OD, 300 K) δ [ppm]
1	Pyrene-PDEVP (100 eq.)	8.42 (d, J_3 = 9.2 Hz, pyrene), 8.29 – 7.98 (m, pyrene), 7.96 – 7.40 (m, H_{arom}), 5.36 (s, POCH_2-pyrene), 5.34 (s, $H_{vinyl,chol}$), 4.18 (s, POCH_2), 2.96 – 1.13 (m, PDEVP), 1.38 (s, $POCH_2CH_3$), 1.03 (s, $CH_{3,chol}$), 0.95 (d, J = 5.8 Hz, $CH_{3,chol}$), 0.89 (s, $CH_{3,chol}$), 0.88 (s, $CH_{3,chol}$), 0.72 (s, $CH_{3,chol}$)	33.2, 32.0
2	Pyrene-PDEVP (600 eq.)	8.42 (d, J_3 = 9.3 Hz, pyrene), 8.33 – 7.98 (m, pyrene), 7.97 – 7.50 (m, H_{arom}), 5.36 (s, POCH_2-pyrene), 4.18 (s, POCH_2), 2.94 – 1.15 (m, PDEVP), 1.38 (s, $POCH_2CH_3$), 0.96 (s, $CH_{3,chol}$), 0.92 (s, $CH_{3,chol}$), 0.90 (s, $CH_{3,chol}$), 0.72 (s, $CH_{3,chol}$)	33.1

Table S6. PDI and yield of fluorescent, cholesterol-functionalized PDEVP

	Substrate	PDI	Yield [%]
1	Pyrene-PDEVP (100 eq.)	1.11	100
2	Pyrene-PDEVP (600 eq.)	1.14	100

General procedure: Thiol-ene coupling of cysteamine hydrochloride to poly(diethyl vinylphosphonates)[6]

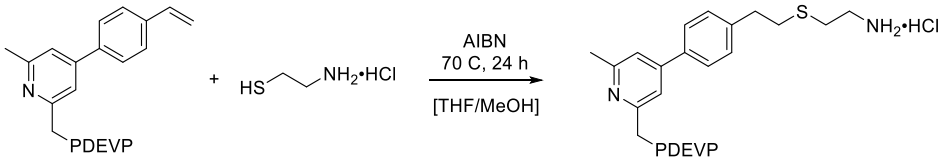

Cysteamine hydrochloride (5.00 eq.) and catalytic amounts of azobisisobutyronitrile (0.33 eq.) were added to a solution of 1.00 equivalent of fluorescent poly(diethyl vinylphosphonate) in tetrahydrofuran and methanol (10:1, 10.0 mL per 1.00 g polymer) in a pressurizeable schlenk flask. The mixture was degassed *via* drawing vacuum and filling with argon (20 iterations) and stirred for 24 hours at 70 °C. After this time period ^{1}H-NMR spectroscopy showed quantitative conversion of the vinyl group. The polymer was purified *via* dialysis against deionized water. The dialysate was replaced after two and four hours. Subsequently, the mixture was dialyzed over night and the resulting solution was lyophilized.

The non-fluorescent polymer samples were prepared accordingly and their characterization can be found in the corresponding literature.[6]

Table S7. Chemical shifts in ^{1}H- und ^{31}P-NMR of PDEVP after reaction with cysteamine hydrochloride

	Substrate	^{1}H-NMR (500 MHz, CD_3OD, 300K) δ [ppm]	^{31}P-NMR (121 MHz, CD_3OD, 300 K) δ [ppm]	Yield [%]
1	Pyrene-PDEVP (100 eq.)	8.44 (d, J_3 = 9.5 Hz, pyrene), 8.32 – 7.70 (m, pyrene, H_{arom}), 7.63 – 7.35 (m, H_{arom}), 5.36 (s, POCH_2-pyrene), 4.20 (s, POCH_2), 3.00 (t, J_3 = 7.5 Hz, $CH_{2,aliphatic}$), 2.91 (t, J_3 = 7.5 Hz, $CH_{2,aliphatic}$), 2.88 – 1.17 (m, PDEVP), 1.40 (s, $POCH_2CH_3$)	33.2, 32.0	100
2	Pyrene-PDEVP (600 eq.)	8.48 – 7.69 (m, pyrene, H_{arom}), 7.64 – 7.35 (m, H_{arom}), 5.35 (s, POCH_2-pyrene), 4.18 (s, POCH_2), 2.88 – 1.19 (m, PDEVP), 1.38 (s, $POCH_2CH_3$)	33.2	100

General procedure: Conversion of polymer-bound cysteamine linker with activated folate species[6]

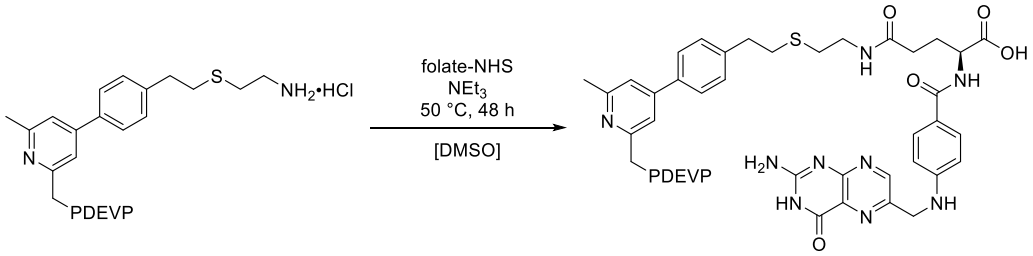

5.00 equivalents of folate-NHS and 6.00 equivalents of triethylamine were added to a solution of 1.00 equivalent of the stated cysteamine-containing poly(diethyl vinylphosphonate) in dimethyl sulfoxide (20.0 mL solvent per 1.00 g polymer). The mixture was stirred for 48 hours at 50 °C and subsequently purified *via* dialysis against deionized water. The dialysate was replaced after two and four hours. Following, the mixture was dialyzed over night and the resulting solution was lyophilized. The non-fluorescent polymer samples were prepared accordingly and their characterization can be found in the corresponding literature.[6]

Table S8. Chemical shifts of fluorescent, folate-containing PDEVP in ^{1}H- und ^{31}P-NMR

	Substrate	^{1}H-NMR (500 MHz, CD_3OD, 300K) δ [ppm]	^{31}P-NMR (203 MHz, CD_3OD, 300 K) δ [ppm]
1	Pyrene-PDEVP (100 eq.)	8.70 (s, pteridine), 8.42 – 7.24 (m, pyrene, folic acid, H_{arom}), 6.78 – 6.63 (m, H_{arom}), 5.39 – 5.31 (m, POCH_2-pyrene), 4.66 (s, CH_2NH$_2$), 4.43 (s, CH_2NH), 4.18 (s, POCH_2), 3.10 – 1.02 (m, PDEVP), 1.41 – 1.35 (m, POCH$_2$CH_3)	33.2, 32.3
2	Pyrene-PDEVP (600 eq.)	8.70 (s, pteridine), 8.62 – 7.82 (m, pyrene, folic acid, H_{arom}), 7.76 – 7.41 (m, pyrene, folic acid, H_{arom}), 6.79 – 6.64 (m, H_{arom}), 5.38 – 5.31 (m, POCH_2-pyrene), 4.60 (s, CH$_2$NH$_2$), 4.42 (s, CH_2NH), 4.18 (s, POCH_2), 3.18 – 1.18 (m, PDEVP), 1.38 (s, POCH$_2$CH_3)	33.2

Table S9. PDI and yield of fluorescent, folate-containing PDEVP

	Substrate	PDI	Yield [%]
1	Pyrene-PDEVP (100 eq.)	1.11	74
2	Pyrene-PDEVP (600 eq.)	1.11	73

3.3 Investigation of thermoresponsive behavior of the polymer substrates

In the following the LCST measurements in aqueous solution of the non-fluorescent (Figure S1) and the fluorescent substrates (Figure S2) are shown. The corresponding measurements of the fluorescent and non-fluorescent polymer samples in DMEM/PBS (2:1) are illustrated analogously in figures S3 and S4. In all cases the short-chain substrates (100 eq.) are compared to the analogous long-chain polymers (600 eq.).

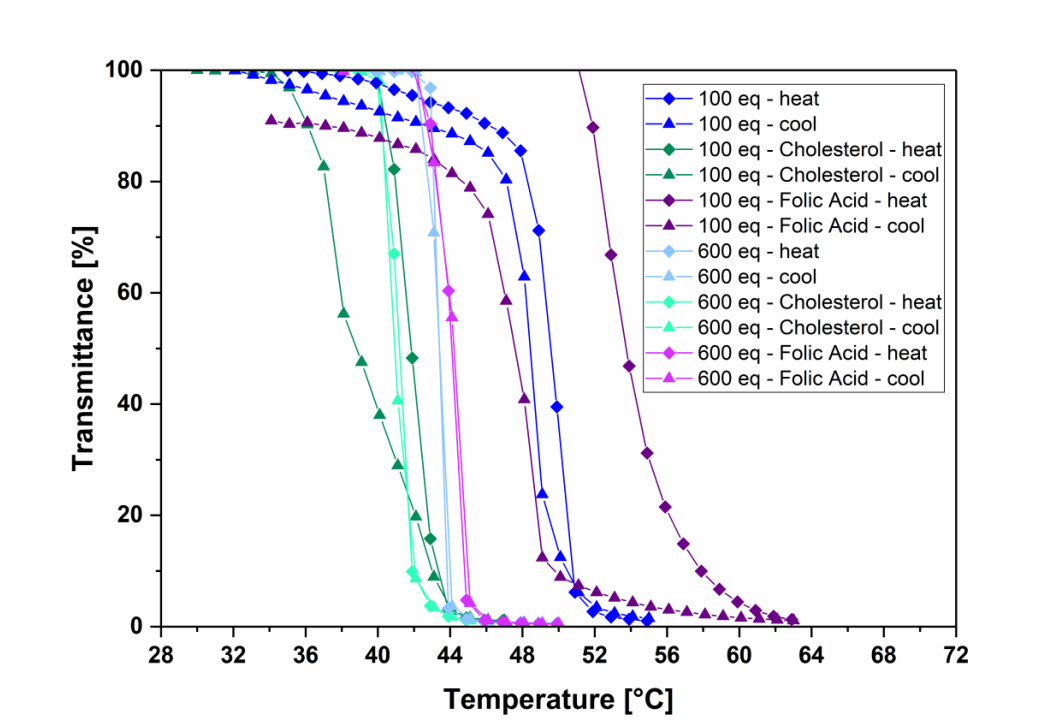

Figure S1. Determination of the cloud points of the non-fluorescent PDEVP samples in aqueous solution. The cloud point was determined at 10% decrease of transmittance for aqueous solutions of the polymer substrates (2.50 mg/mL).

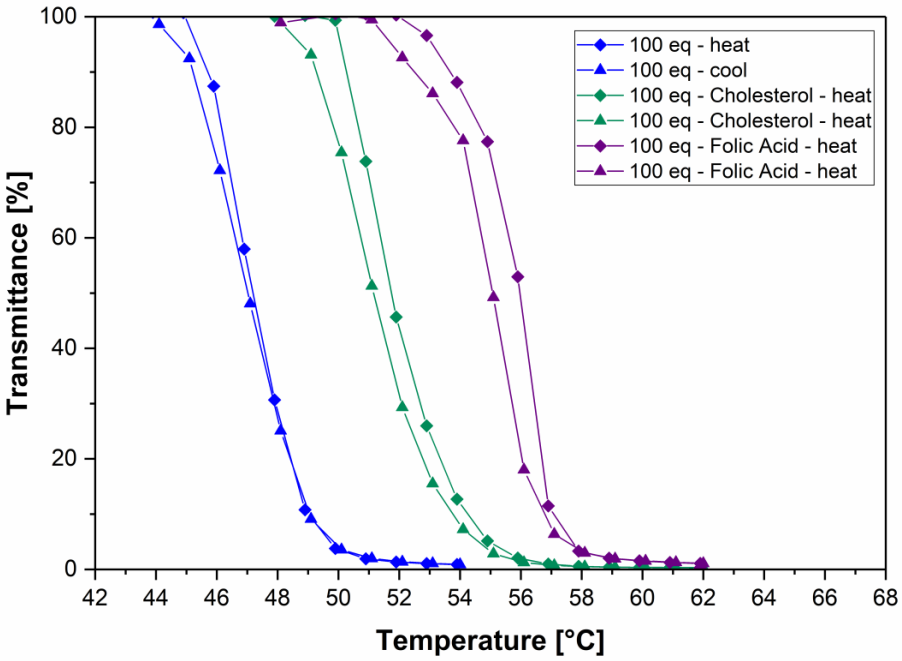

Figure S2. Determination of the cloud points of the fluorescent PDEVP samples in aqueous solution. The cloud point was determined at 10% decrease of transmittance for aqueous solutions of the polymer substrates (2.50 mg/mL).

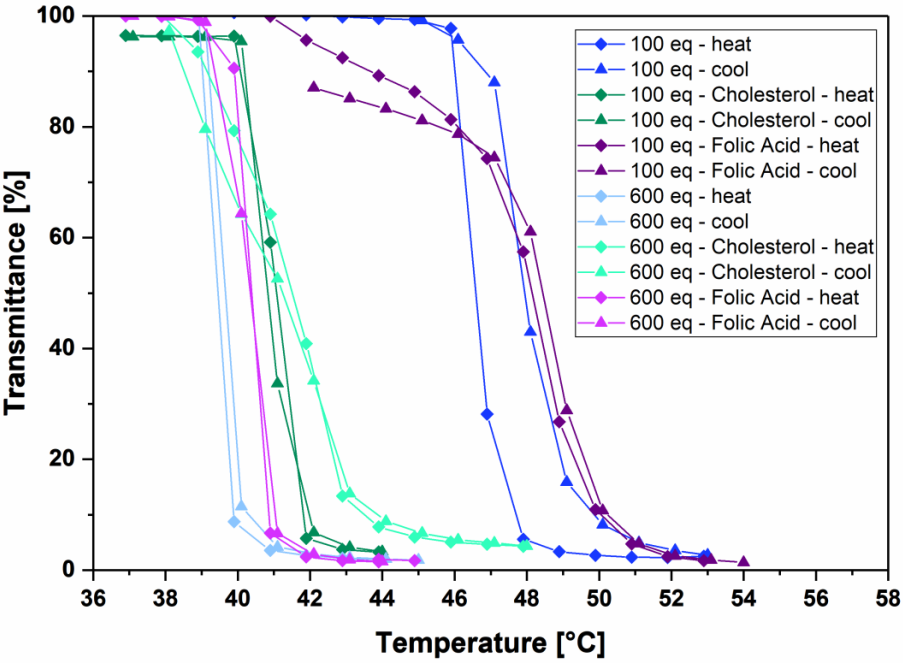

Figure S3. Determination of the cloud points of the non-fluorescent PDEVP samples in DMEM/PBS (2:1). The cloud point was determined at 10% decrease of transmittance for DMEM/PBS solutions of the polymer substrates (2.50 mg/mL).

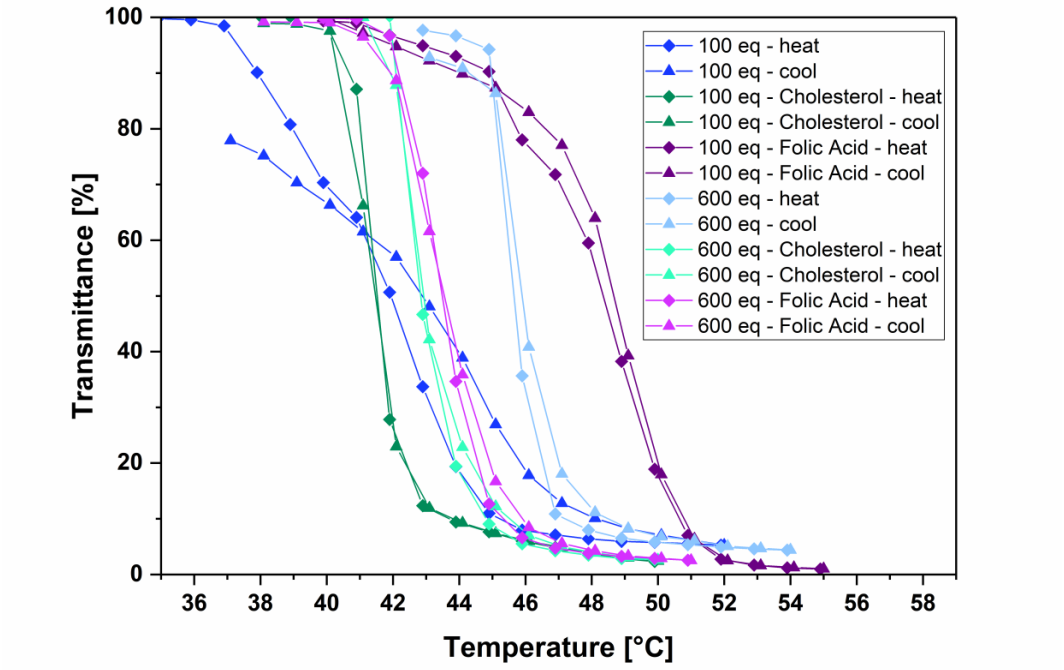

Figure S4. Determination of the cloud points of the fluorescent PDEVP samples in DMEM/PBS (2:1). The cloud point was determined at 10% decrease of transmittance for DMEM/PBS solutions of the polymer substrates (2.50 mg/mL).

4. *In vitro* experiments

4.1 Cell culture

In vitro studies on polymer samples were performed in HEK-293 and HMEC cells (ATCC). Cells were cultured in Dulbecco's Modified Eagle Medium (Life Technologies) equipped with 10% (v/v) Fetal Bovine Serum (Biochrom) and 1% Penicillin/Streptomycin 10000 U/mL /10000 µg/mL (Biochrom) at 37 °C in a humidified atmosphere containing 5% CO_2. For splitting and sub-culturing of cells Trypsin 0.05%/EDTA 0.02% in PBS (PAN Biotech) was used.

4.2 Cell viability studies

The growth inhibition of the polymer samples on HEK-293 and HMEC cells, was determined by analyzing their cell viability in presence of increasing polymer concentrations (0.078 mg/mL to 5.00 mg/mL). Prior to the addition of the polymers, the cells were cultured for 24 h in 96 well flat bottom plates (TPP) with a density of 20000 cells/well or 10000 cells/well (for 48 h). After 24 or 48 hours of incubation at 37 °C in a humidified atmosphere with 5% CO_2, the cell viability of the treated cells was determined using the 3-(4,5-Dimethyl-2-thiazolyl)-2,5-diphenyl-2*H*-tetrazolium bromide reagent (MTT) (Sigma Aldrich). Therefore, MTT was dissolved at a concentration of 5 mg/mL in RPMI-1640 without phenol red (Life Technologies). PBS treated cells were used as positive control (100% viability). DMSO treated cells were used as negative control (0% viability). After 3 h of incubation with 50 µL of MTT per well at 37 °C, the blue formazan crystals were dissolved for 15 min on a plate shaker at 550 min^{-1} with 100 µL 0.04 N HCl in isopropanol and exclusion of light. Following the absorbance of each well was measured at 570 nm with 690 nm as background wavelength at a Tecan Genios Plus plate reader. Shown are mean values of at least three independent biological replicates and the respective standard deviations are indicated.

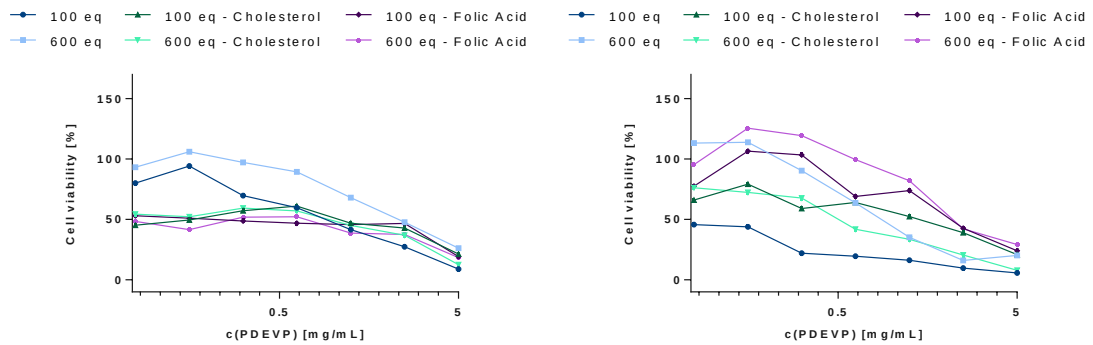

Figure S5. Cell viability of HEK-293 cells after 24 h (left) and 48 h (right) of incubation with fluorescent polymer samples.

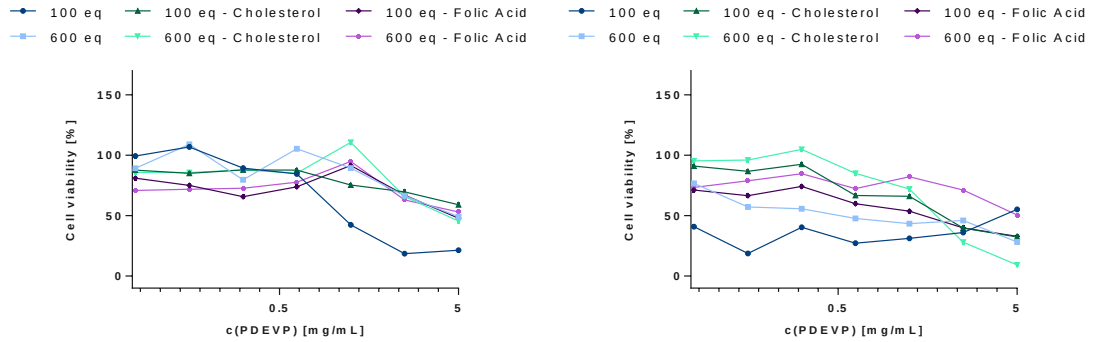

Figure S6. Cell viability of HMEC cells after 24 h (left) and 48 h (right) of incubation with fluorescent polymer samples.

4.3 Viability studies on the impact of heat shock treatment with LCST polymers on cells

In preparation for the MTT assay, the cells were treated as mentioned under 6.2. After the incubation for 24 h with the polymer samples, the cells were heated to 42 °C for 1.5 h. Half of the plates were then measured as described before and the second half was cooled and stored at 37 °C for regeneration for 24 h. After these 24 h, the MTT assay was performed as usual.

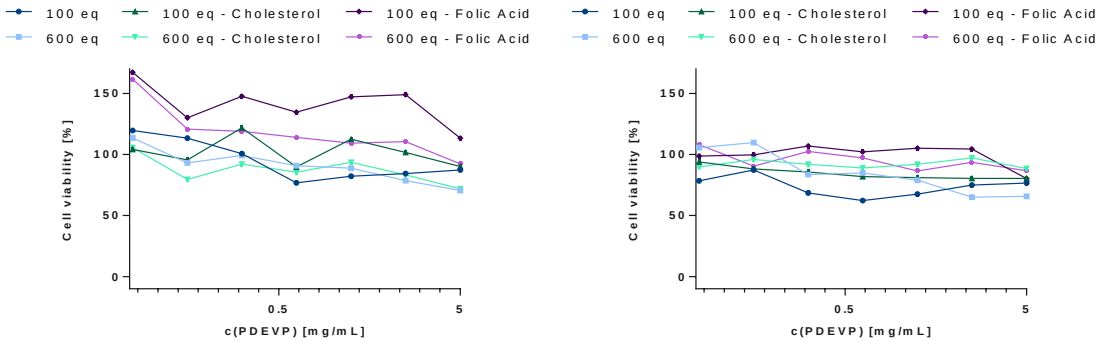

Figure S7. Cell viability of HEK-293 cells after 24 h incubation with polymer samples, followed by 1.5 h heat shock (left) and 1.5 h heat shock with 24 h regeneration at 37 °C (right).

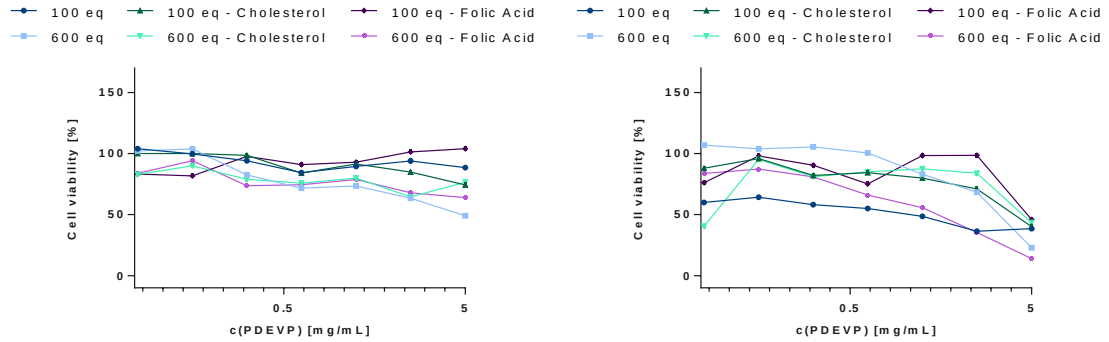

Figure S8. Cell viability of HMEC cells after 24 h incubation with polymer samples, followed by 1.5 h heat shock (left) and 1.5 h heat shock with 24 h regeneration at 37 °C (right).

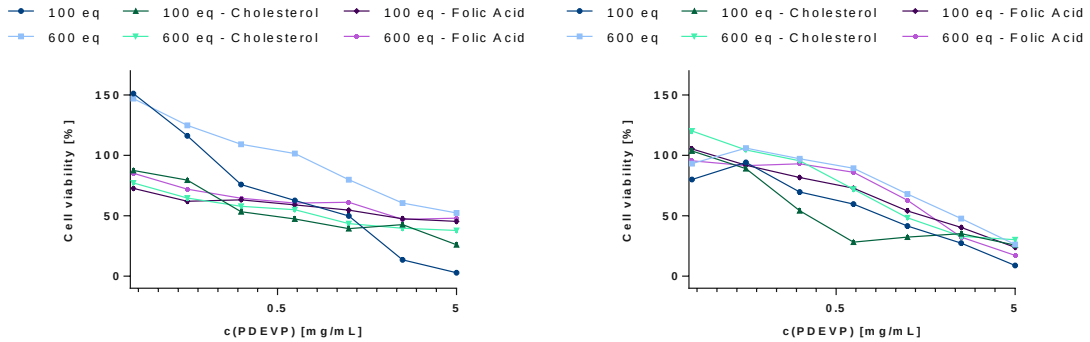

Figure S9. Cell viability of HEK cells after 24 h incubation with fluorescent polymer samples, followed by 1.5 h heat shock (left) and 1.5 h heat shock with 24 h regeneration at 37 °C (right).

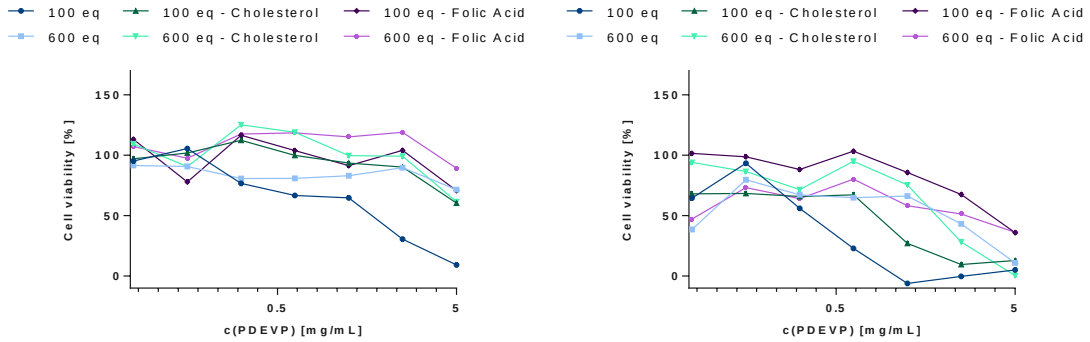

Figure S10. Cell viability of HMEC cells after 24 h incubation with fluorescent polymer samples, followed by 1.5 h heat shock (left) and 1.5 h heat shock with 24 h regeneration at 37 °C (right).

4.4 Confocal microscopy

For microscopic studies, the HMEC-1 cells were cultured for 24 h in 8-well glass chamber slides (Nunc). Subsequently, they were treated with a total concentration of 1.25 mg/mL of fluorescent polymer sample, dissolved in PBS, for 4 h at 37 °C. After this incubation time the polymers were removed, the cells were washed with PBS and fixed with 4% Paraformaldehyd in PBS for 10 min. Thereafter, the cells were washed with DMEM/FBS for 10 min for blocking and twice with PBS. The first staining step was 30 min CMFDA (Molecular Probes) leading to global cytoplasma staining and mouse anti-human HLA-class I antibody W6/32 (Professor Nößner's lab) leading to plasma membrane staining, dissolved in serum-free medium at 37 °C. To remove free stain and antibody three PBS washing steps were conducted, followed by the addition of the rhodamine red™-x-conjugated goat anti-mouse IgG antibody (RRX from Jackson Immuno Research Laboratories, INC.) for 30 min in serum-free medium at 37 °C. After three more washing steps, the chambers were removed, Vectashield (Vector Laboratories, Inc.) and the cover slip were put on top of the microscope slide. The measurements were performed on a Leica TCS SP5 confocal microscope with 63x magnification, using the sequential acquisition mode for CMFDA and RRX.

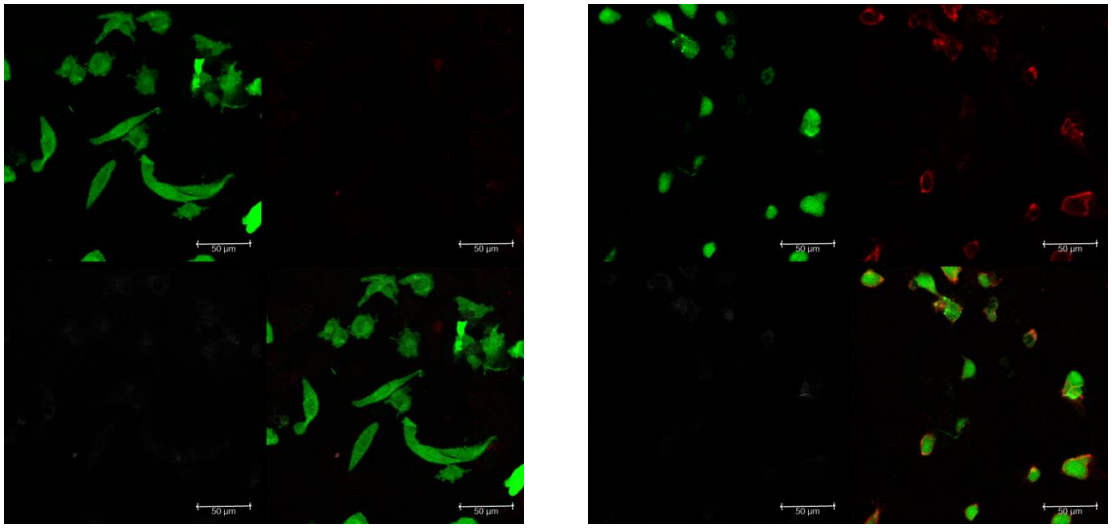

Figure S11. Confocal microscopy images of CMFDA only without W6/32 antibody (left), and CMFDA plus W6/32 antibody with RRX (right) stained HMEC-1 cells all without polymer addition as control samples. The four panels show the CMFDA (top left), the RRX (top right), the polymer channel (bottom left) and the merge of all three detection channels (bottom right).

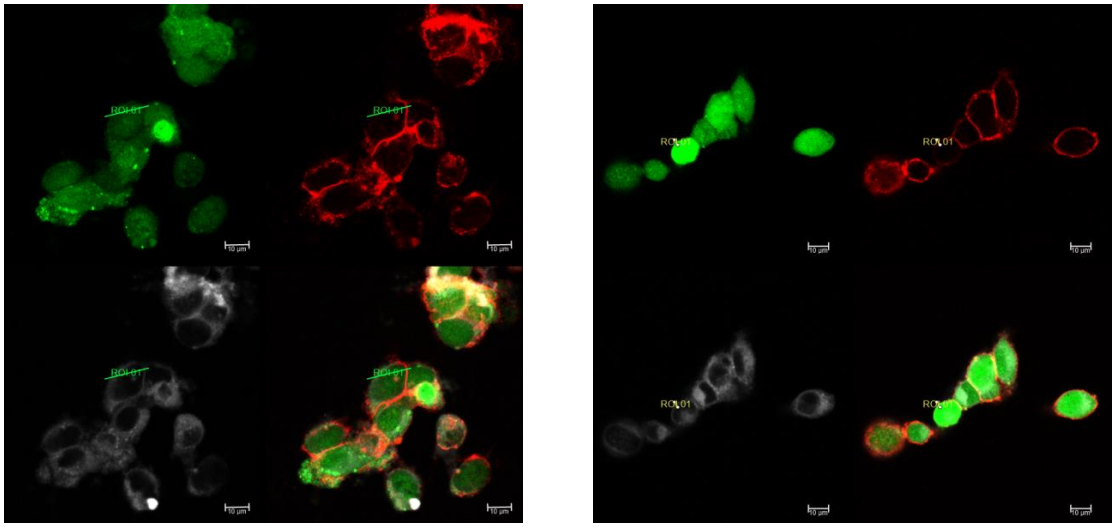

Figure S12. Confocal microscopy images of whole cell region of interest analysis (ROI) (left) and of single cell wall ROI analysis (right). HMEC-1 cells were stained with CMFDA, anti-HLA-class I antibody (RRX) and cholesterol-anchored fluorescent PDEVP.

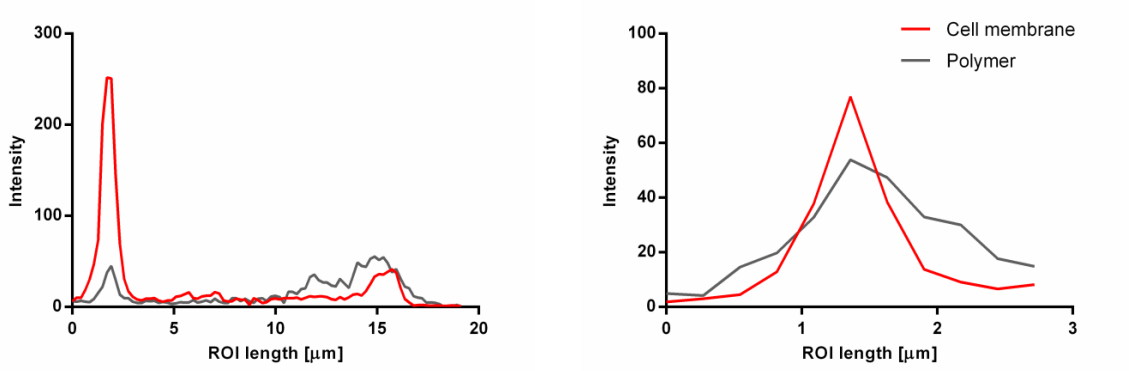

Figure S13. Fluorescence intensity of the ROI analysis shown in Figure S12 (CMFDA was omitted for clarity).

5. References

[1] K. C. Hultzsch, P. Voth, K. Beckerle, T. P. Spaniol, J. Okuda, *Organometallics* **2000**, *19*, 228-243.

[2] G. D. Vaughn, K. A. Krein, J. A. Gladysz, *Organometallics* **1986**, *5*, 936-942.

[3] C.-X. Cai, L. Toupet, C. W. Lehmann, J.-F. Carpentier, *J. Organomet. Chem.* **2003**, *683*, 131-136.

[4] S. Salzinger, B. S. Soller, A. Plikhta, U. B. Seemann, E. Herdtweck, B. Rieger, *J. Am. Chem. Soc.* **2013**, *135*, 13030-13040.

[5] M. Leute, PhD thesis, University of Ulm **2007**.

[6] C. Schwarzenböck, A. Schaffer, P. Pahl, P. J. Nelson, R. Huss, B. Rieger, *Polym. Chem.* **2017** , DOI: 10.1039/C7PY01796K.

10.3 Supporting Information of the Manuscript "Synthesis of Next Generation Dual-Responsive Cross-Linked Nanoparticles and their Application to Anti-Cancer Drug Delivery"

Electronic Supplementary Material (ESI) for Nanoscale.

Supporting Information for the Manuscript Entitled Synthesis of Next Generation Dual-Responsive Cross-Linked Nanoparticles and their Application in Anticancer Drug Delivery†

Christina Schwarzenböck,[a] Peter J. Nelson,[b] Ralf Huss[c] and Bernhard Rieger*[a]

[a] *WACKER-Lehrstuhl für Makromolekulare Chemie, Technische Universität München, Lichtenbergstraße 4, 85748 Garching bei München, Germany. E-Mail: rieger@tum.de*

[b] *Medizinische Klinik und Poliklinik IV, Nephrologisches Zentrum und Arbeitsgruppe Klinische Biochemie, University of Munich, Munich, Germany.*

[c] *Definiens AG, Bernhard-Wicki-Strasse 5, 80636 Munich, Germany.*

Table of Contents

1. Material and methods

General Information

All reactions were carried out under argon atmosphere using standard Schlenk or glovebox techniques. All glassware was heat dried under vacuum prior to use. Unless otherwise stated, all chemicals were purchased from Sigma-Aldrich, ABCR, Acros Organics or TCI Europe and used as received. Toluene and dichloromethane (DCM) were dried using a MBraun SPS-800 solvent purification system. The precursor complexes $Y(CH_2Si(CH_3)_3)_3(THF)_2$, $LiCH_2TMS$ and the catalyst $Cp_2Y(CH_2TMS)(THF)$ were prepared according to literature procedures.[1-4] Diethyl vinylphosphonate (DEVP) as well as 2-bromoethylphosphonic dichloride were synthesised according to literature procedures.[5-7] All monomers were dried over calcium hydride and distilled prior to use.

Nuclear Magnetic Resonance Spectroscopy

NMR spectra were recorded on a Bruker AVIII-300, AV-500HD and AVIII-500 Cryo spectrometer. ^{1}H-NMR spectroscopic chemical shifts δ are reported in ppm relative to the residual proton signal of the solvent. δ (^{1}H) is calibrated to the residual proton signal of the solvent. Deuterated solvents were obtained from Sigma-Aldrich and dried over 3 Å molecular sieves.

Elemental Analysis (EA)

Elemental analyses were measured on a Vario EL (Elementar) at the Laboratory for Microanalysis at the Institute of Inorganic Chemistry at the Technische Universität München.

Gel Permeation Chromatography

Gel Permeation Chromatography was performed on a *Varian* LC-920 equipped with two PL Polargel M columns with samples of 5 mg/mL. A mixture of 50% THF, 50% water, 9 g/L tetrabutylammonium bromide (TBAB) and 340 mg/L 3,5-Di-*tert*-butyl-4-hydroxytoluene (BHT) as stabilising agent was used as eluent. Absolute molecular weights have been determined by multiangle light scattering (MALS) analysis using a Wyatt Dawn Heleos II in combination with a Wyatt Optilab rEX as concentration source.

Turbidity Measurements

Turbidity measurements were performed on a Cary 50 UV/Vis spectrophotometer (Varian) in 40 mm × 10 mm × 2 mm quartz glass cuvettes with a magnetic stirring bar. The cloud point of the aqueous polymer solutions was determined by spectrophotometric detection of the changes in transmittance at λ = 500 nm, respectively 650 nm in case of the DMEM/PBS samples. The samples were heated/cooled at a rate of 1.0 K/min in steps of 1 K followed by a 5 min long period of constant temperature to ensure equilibration. The cloud point was defined as the temperature corresponding to a 10% decrease in optical transmittance.

Dialysis

Purification *via* dialysis was performed with a Spectra/Por 1 dialysis tubing (regenerated cellulose) with a molecular weight cut-off (MWCO) of 6-8 kDa (Spectrumlabs). Before use the membranes were treated with deionised water over night and then rinsed with deionised water. A 100:1 ratio of dialysis fluid to sample volume was applied. Specific solvents used as dialysis fluid are given for the corresponding procedures.

DLS Measurements

The samples were dissolved in water at a concentration of 2.5 mg/mL. The measurement was performed at a Zetasizer Nano ZS (Malvern). The diameter was averaged over three independent values consisting each of 10 measurements.

Transmission Electron Microscopy

The nanoparticle solutions were added onto a copper grid with a continuous carbon film for one minute and stained with a 2% uranyl acetate solution. Microscopy was done with a JEM 1400 plus microscope (JEOL, Tokyo) with a LaB6 filament operated at 120 kV. Images were collected with a Ruby (JEOL) CCD camera with a pixel size of 0.332 nm.

Surface Tension Measurements

For the surface tension analysis, the samples were dissolved in deionised water and then a dilution series was prepared (0.025 mg/mL to 1.000 mg/mL). The measurements were performed on a Drop Shape Analyzer DSA100 (Krüss). The surface tension of each concentration was averaged over the values of three independent droplets.

Photoluminescence Measurements

Photoluminescence spectra were recorded on a AVA-Spec 2048 spectrometer (AVANTES) with a current controller as 365 nm light source (Prizmatix). A 90° cuvette holder and a 40 mm × 10 mm × 2 mm polystyrene cuvette (VWR) were used for the measurements. Intensity calibration of the spectrometer was performed by an AVANTES DH-Cal calibration light source using the halogen lamp.

2. Syntheses

2.1 Monomer synthesis[8]

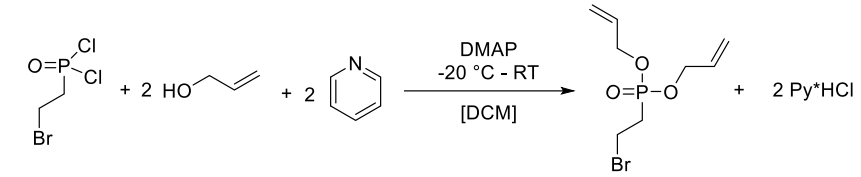

$C_2H_4BrCl_2OP$ 225.83 g/mol | C_3H_6O 58.08 g/mol | C_5H_5N 79.10 g/mol | $C_8H_{14}BrO_3P$ 269.07 g/mol

Allylic alcohol (2.1 eq., 93.0 mmol, 6.3 mL), pyridine (2.1 eq., 93.0 mmol, 7.5 mL) and a catalytic amount of DMAP were dissolved in anhydrous DCM. This solution was cooled to -10 °C, kept at this temperature for 30 min and cooled further to -20 °C. 2-Bromoethylphosphonic dichloride (1.0 eq., 44.3 mmol, 5.9 mL) was dissolved in DCM and added dropwise. After full addition the solution was kept 1 h at -20 °C and was slowly warmed to RT overnight. The resulting white solid is filtered off and the solution is washed three times with water. After drying with $MgSO_4$ the evaporation of the solvent under reduced pressure followed. The product was obtained as a clear slightly yellow liquid (95.6%, 42.3 mmol, 11.4 g).

^{1}H-NMR (300 MHz, $CDCl_3$, 300 K) δ [ppm] 5.99-5.87 (m, 2 H, 2 x $POCH_2CH$=CH_2), 5.39-5.25 (m, 4 H, 2 x $POCH_2CH$=CH_2), 4.57-4.53 (m, 4 H, 2 x $POCH_2CH$=CH_2), 3.58-3.49 (m, 2H, PCH_2CH_2-Br), 2.49-2.37 (m, 2H, PCH_2CH_2-Br).

^{31}P-NMR (121 MHz, $CDCl_3$, 300 K) δ [ppm] 26.51.

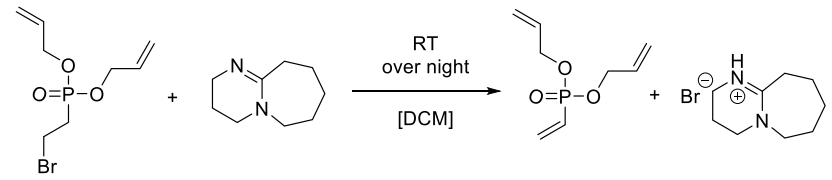

$C_8H_{14}BrO_3P$ 269.07 g/mol | $C_9H_{16}N_2$ 152.24 g/mol | $C_8H_{13}O_3P$ 188.16 g/mol

1,8-Diazabicyclo[5.4.0]undec-7-ene (DBU, 2.8 eq.) was added dropwise to a stirred solution of diallyl-2-bromoethyl phosphonate in DCM. The resulting dark solution was washed three times with 2 M HCl and dried over $MgSO_4$. The solvent was evaporated under reduced pressure which resulted a viscous brown raw product. After testing varying purification methods the most successful one was vacuum distillation with addition of 1000 ppm phenothiazin to inhibit radical side reactions. The product was obtained as a clear liquid.

^{1}H-NMR (300 MHz, $CDCl_3$, 300 K) δ [ppm] 6.26-5.74 (m, 5 H, PCH=CH_2, PCH=CH_2, 2 x $POCH_2CH$=CH_2), 5.25-5.08 (q, 4 H, 2 x $POCH_2CH$=CH_2), 4.56-4.50 (t, 4 H, 2 x $POCH_2CH$=CH_2).

^{31}P-NMR (121 MHz, $CDCl_3$, 300 K) δ [ppm] 17.90.

2.2 Copolymerisation procedure and analysis

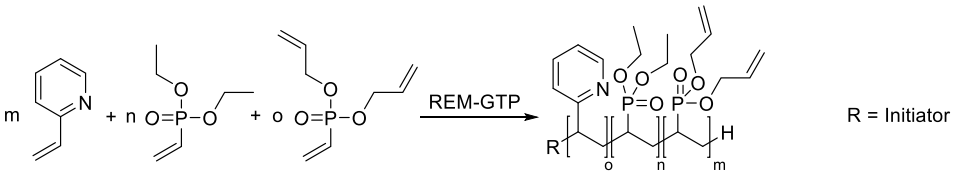

2,4,6-Trimethylpyridine (1.00 eq.) was added to a solution of $Cp_2Y(CH_2TMS)(THF)$ (1.00 eq.) in toluene (6 mg catalyst pro mL). After quantitative conversion was shown by ^{1}H-NMR spectroscopy, the respective equivalents of 2-vinylpyridine were added in one portion. The reaction mixture was stirred overnight. One aliquot (0.1 mL) was taken and quenched by the addition of 0.4 mL CD_3OD (calculation of conversion of 2-vinylpyridine *via* ^{1}H-NMR) in an NMR-tube while the calculated amount of DEVP was added to the reaction solution. The conversion of DEVP was determined by ^{31}P-NMR spectroscopy after 90 min. The DEVP procedure was repeated with DAlVP (5 eq.). The reaction was quenched by addition of methanol (0.50 mL) and the polymer was precipitated by pouring the reaction mixture into pentane (150 mL). The clear solution was decanted of, residual solvent was removed by drying at ambient temperature and the polymer was dissolved in water and lyophilised.

Molecular weights and molecular weight distributions of the first polymerisation sequence were measured *via* GPC-MALS analysis of the first aliquot. Composition A/BB' [2VP/DEVP DAlVP] is determined *via* ^{1}H-NMR-spectroscopy of the dried block copolymer. The molecular weight of the block copolymer is determined with the help of the composition A/BB' and the molecular weight of the first block. Molecular weight distributions are determined *via* GPC-MALS analysis.

Table S1 Composition, molecular weight (M_n) and $Đ$ of blockcopolymer substrates

	Feed A_{eq}/B_{eq}	Composition A/B [2VP/DEVP]	$Eq_{,NMR}$ (B')/Chain	M_n (A) [* 10^4 g/mol]	$M_{n,NMR}$ (AB) [* 10^4 g/mol]	$Đ$
AB1	$2VP_{100}/DEVP_{100}$	1/1.3	6	1.3	4.1	1.17
AB2	$2VP_{100}/DEVP_{200}$	1/2.2	5	1.2	5.4	1.12
AB3	$2VP_{200}/DEVP_{200}$	1/1.4	5	2.5	7.9	1.10

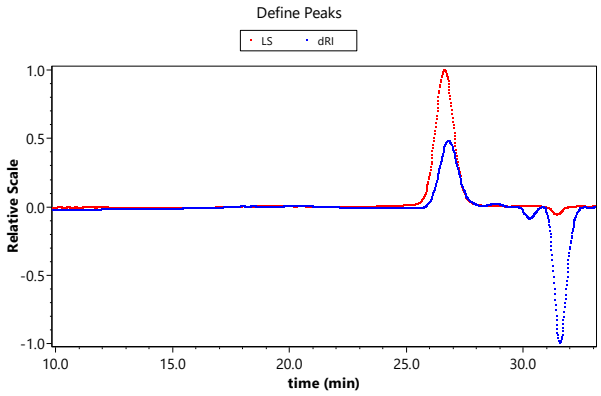

Fig. S1 GPC-traces of P2VP block of AB1.

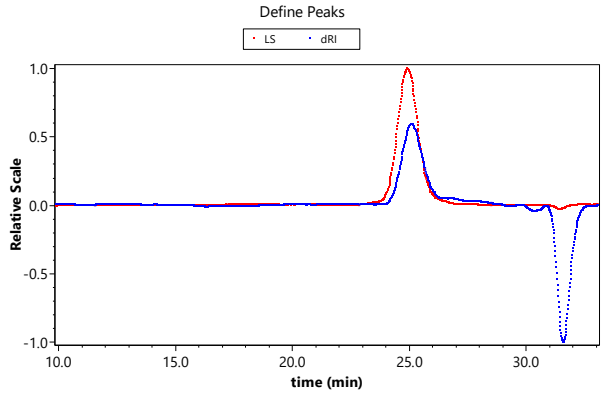

Fig. S2 GPC-traces of 2VP/DEVP blocks of AB1.

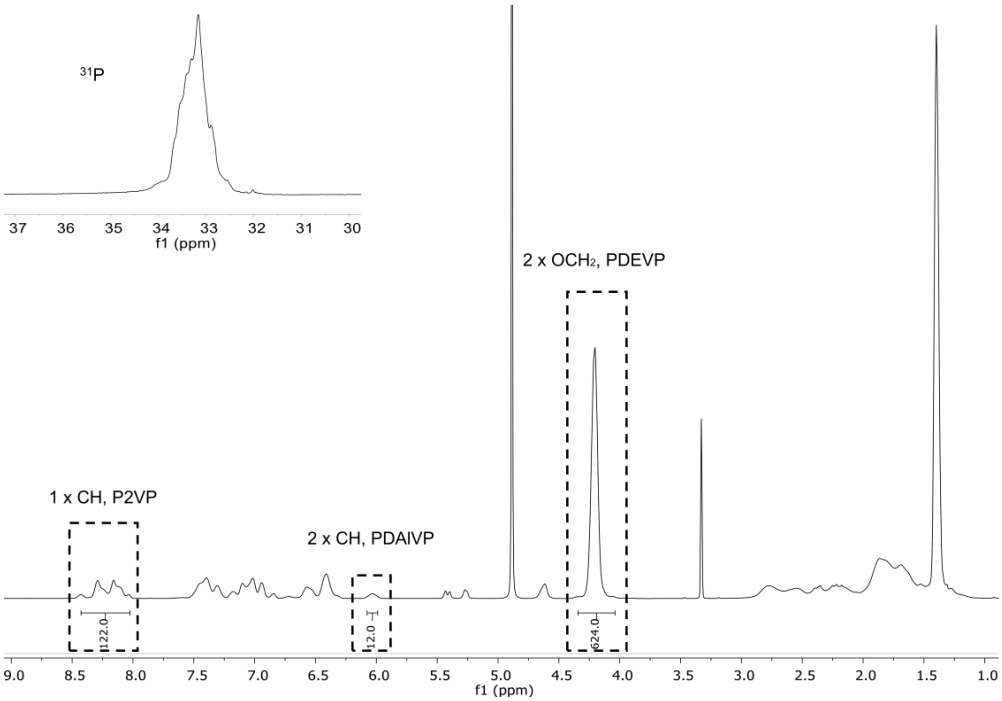

Fig. S3 ^{1}H- and ^{31}P-NMR spectrum of AB1 in MeOD.

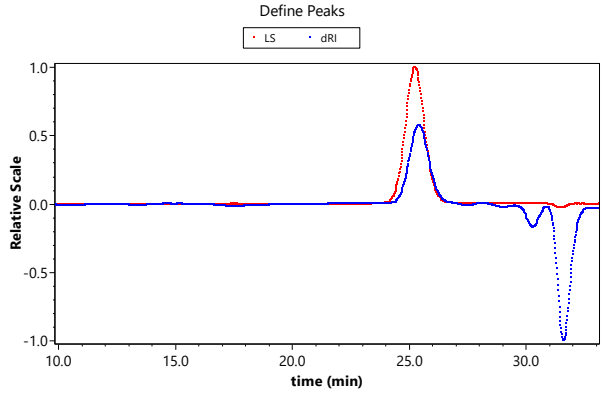

Fig. S4 GPC-traces of P2VP block of AB2.

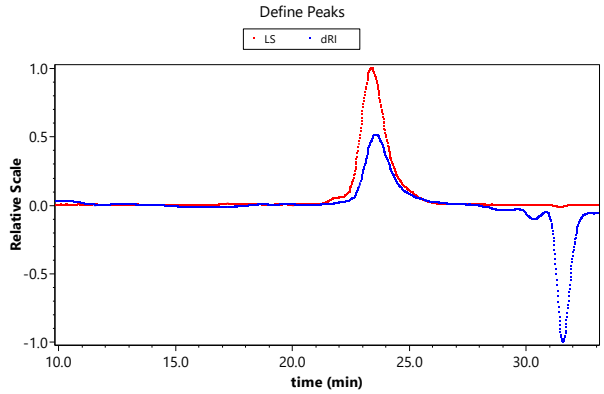

Fig. S5 GPC-traces of 2VP/DEVP blocks of AB2.

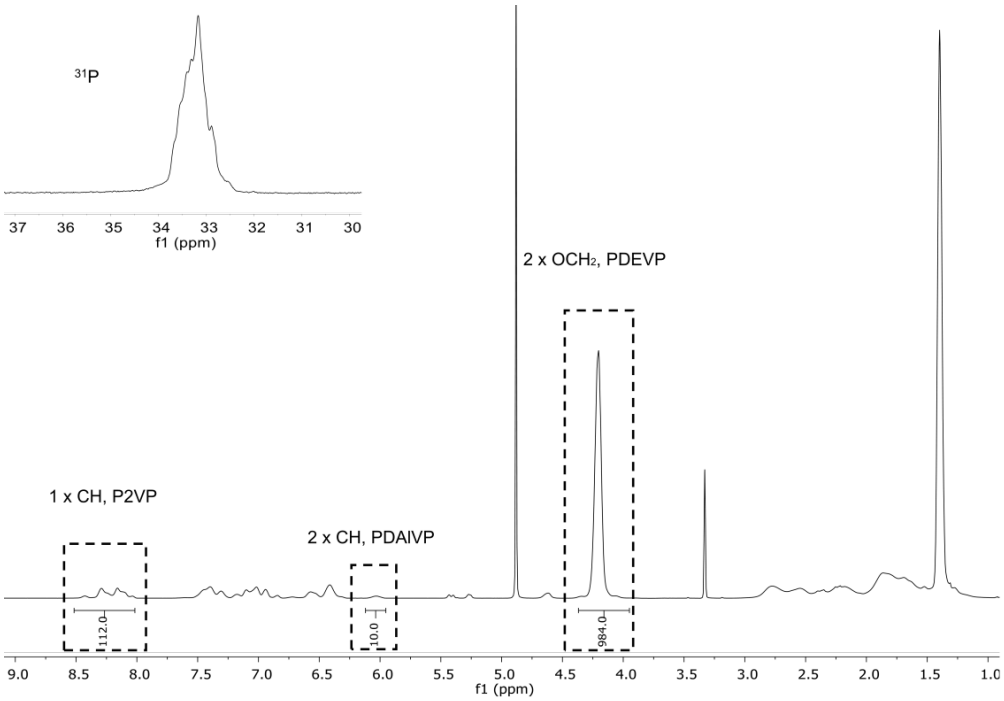

Fig. S6 ^{1}H- and ^{31}P-NMR spectrum of AB2 in MeOD.

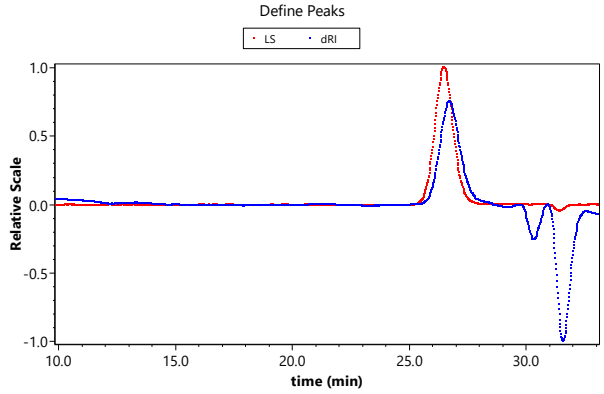

Fig. S7 GPC-traces of P2VP blocks of AB3.

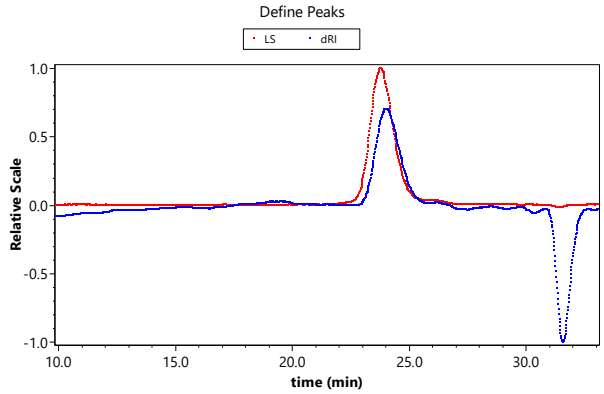

Fig. S8 GPC-traces of 2VP/DEVP block of AB3.

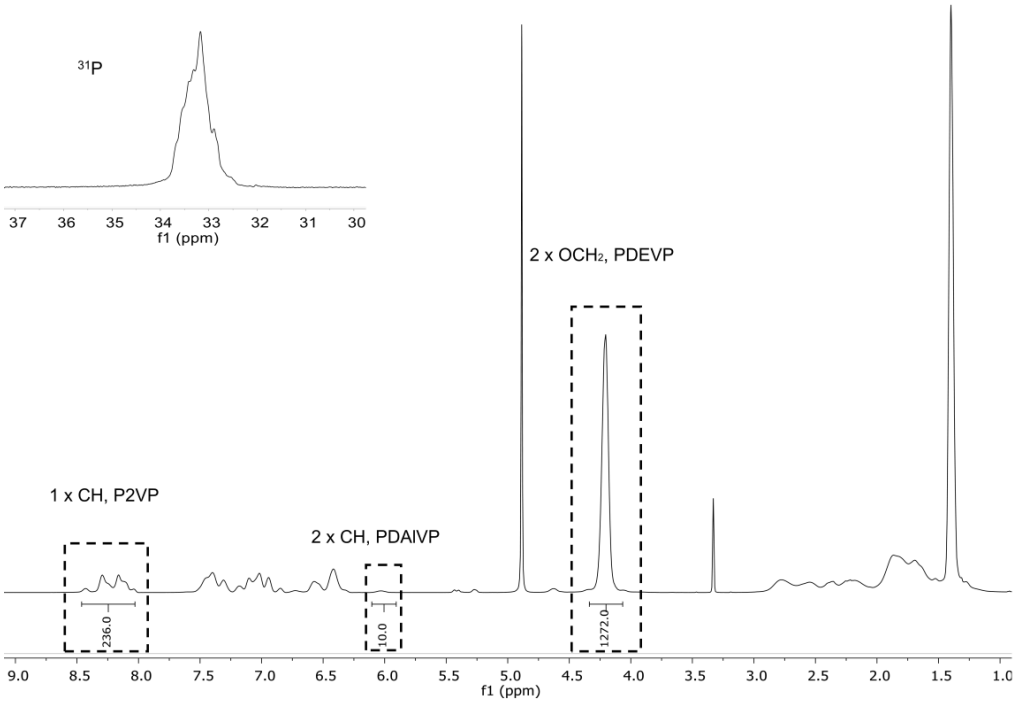

Fig. S9 ^{1}H- and ^{31}P-NMR spectrum of AB3 in MeOD.

2.3 Nanoparticle synthesis *via* thiol-ene click reactions

General procedure: Thiol-ene coupling of polymer micelles towards stable nanoparticles

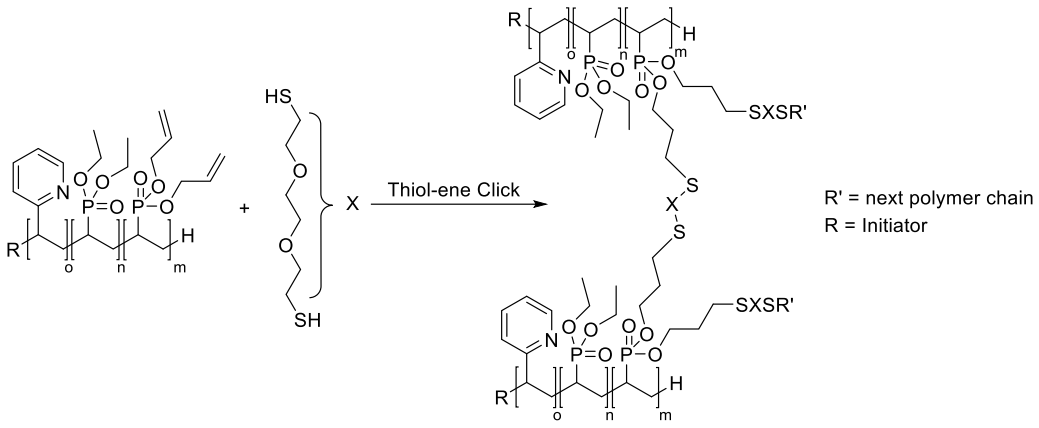

4.5 eq of 3,6-dioxa-1,8-octanedithiol corresponding to each double bond in the polymer are dissolved in DCM and added to the chosen polymer dissolved in DCM to reach an overall concentration of polymer in DCM of 4.6 mg/mL. After the addition of a catalytic amount of azobisisobutyronitrile (AIBN) the reaction mixture was degassed and heated to reflux for 16 h. The solvent was fully evaporated under reduced pressure and the resulting nanoparticles were dissolved in water, dialysed overnight and lyophilised to obtain a white powder.

Following NMR and elemental analysis were used to proof the full conversion of all double bonds and the presence of the according amounts of sulphur in the nanoparticles.

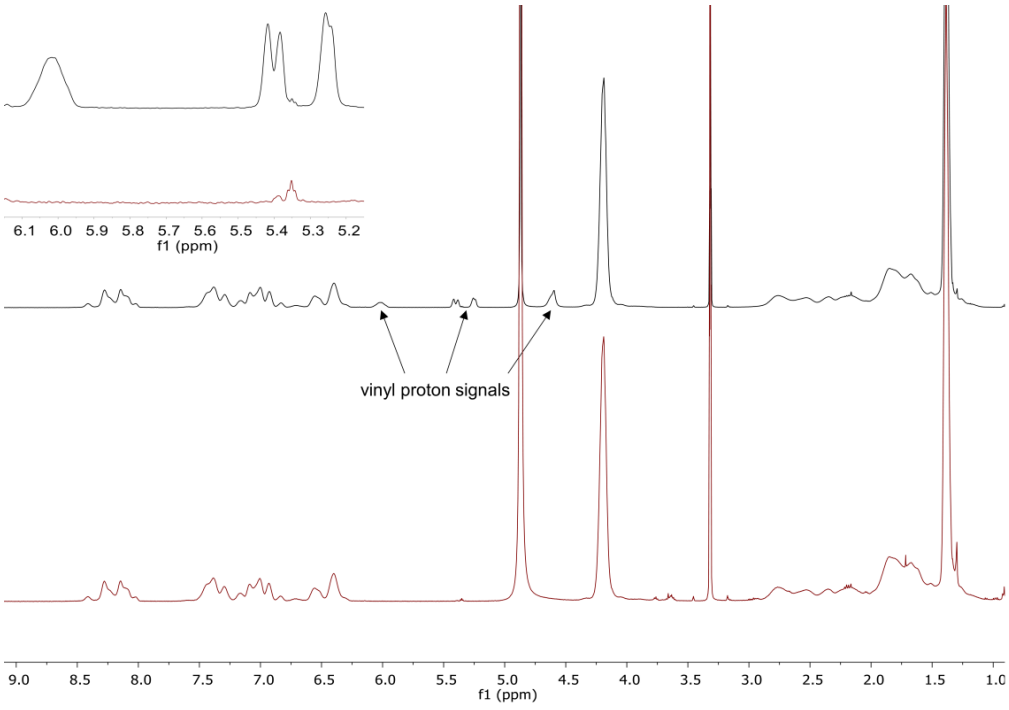

Fig. S10 ^{1}H-NMR spectra of AB1 and NP1 in MeOD.

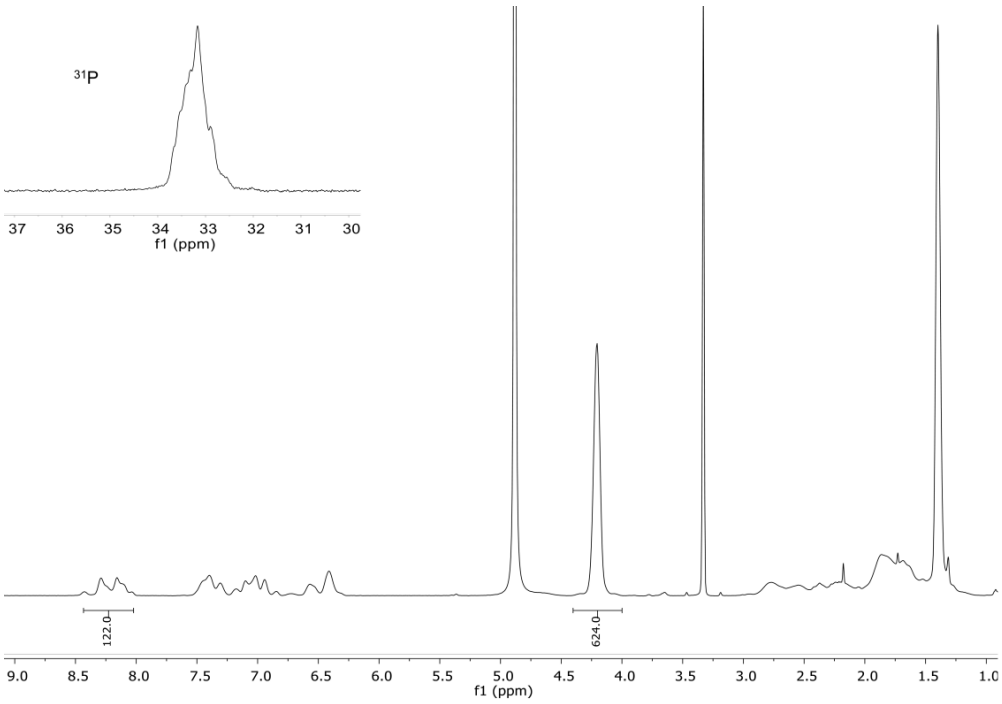

Fig. S11 ^{1}H- and ^{31}P-NMR spectrum of NP1 in MeOD.

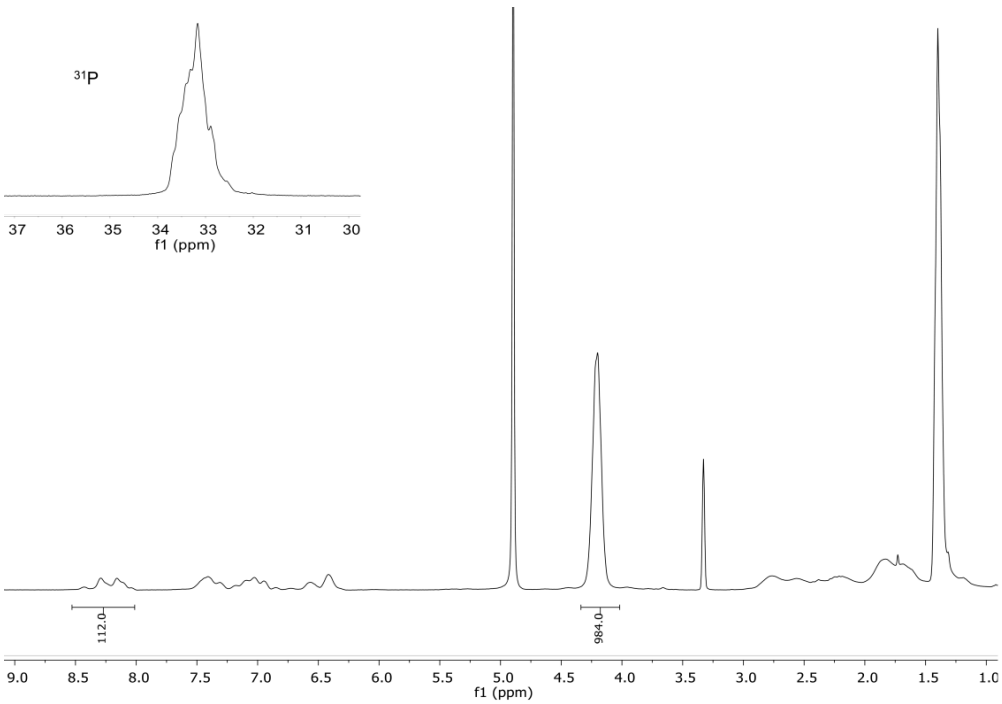

Fig. S12 ^{1}H- and ^{31}P-NMR spectrum of NP2 in MeOD.

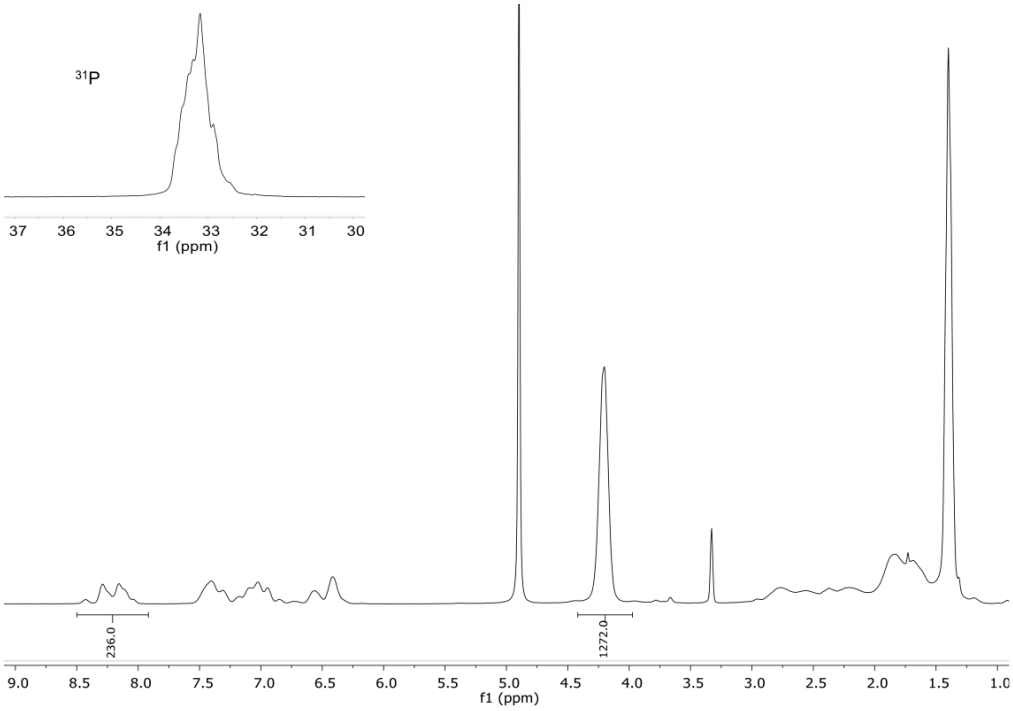

Fig. S13 ^{1}H- and ^{31}P-NMR spectrum of NP3 in MeOD.

Table S2 Elemental analysis of nanoparticle samples

		C	H	N	S
NP1	**calculated**	55.43	7.57	4.23	0.94
NP1	**found**	54.95	7.63	4.11	1.02
NP2	**calculated**	51.83	7.71	2.93	0.59
NP2	**found**	51.50	7.77	2.91	0.42
NP3	**calculated**	55.31	7.58	4.20	0.41
NP3	**found**	54.85	7.72	4.14	0.43

3. Characterisation of polymer micelles and nanoparticles

3.1 Lower critical solution temperature

Table S3 Cloud points (T_c) of blockcopolymer substrates and nanoparticles

	Substrate	T_C [°C] (H_2O)	T_C [°C] (DMEM)
AB1	-	40.0	36.0
AB2	-	40.0	36.0
AB3	-	37.0	32.0
NP1	**AB1**	46.0	37.5
NP2	**AB2**	45.0	37.0
NP3	**AB3**	39.5	33.0

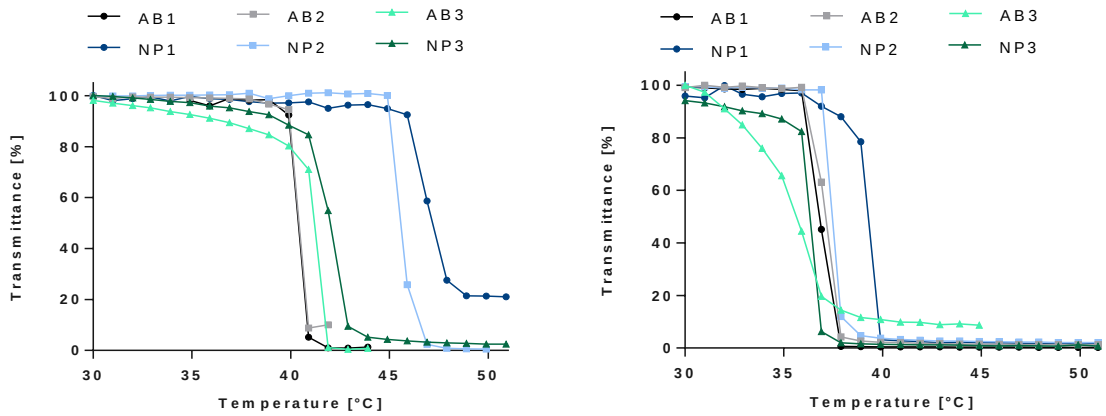

Fig. S14 Determination of the LCST of the samples AB1, AB2, AB3, NP1, NP2 and NP3 in water (left) and DMEM/PBS (2/1) (right) (2.50 mg/mL). The cloud point was determined at 10% decrease of transmittance.

3.2 Critical micelle concentration studies

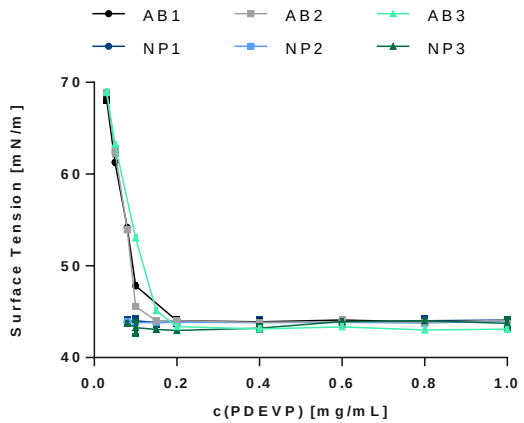

Fig. S15 Surface tension plot of the polymers AB1, AB2, AB3 and the particles NP1, NP2 and NP3

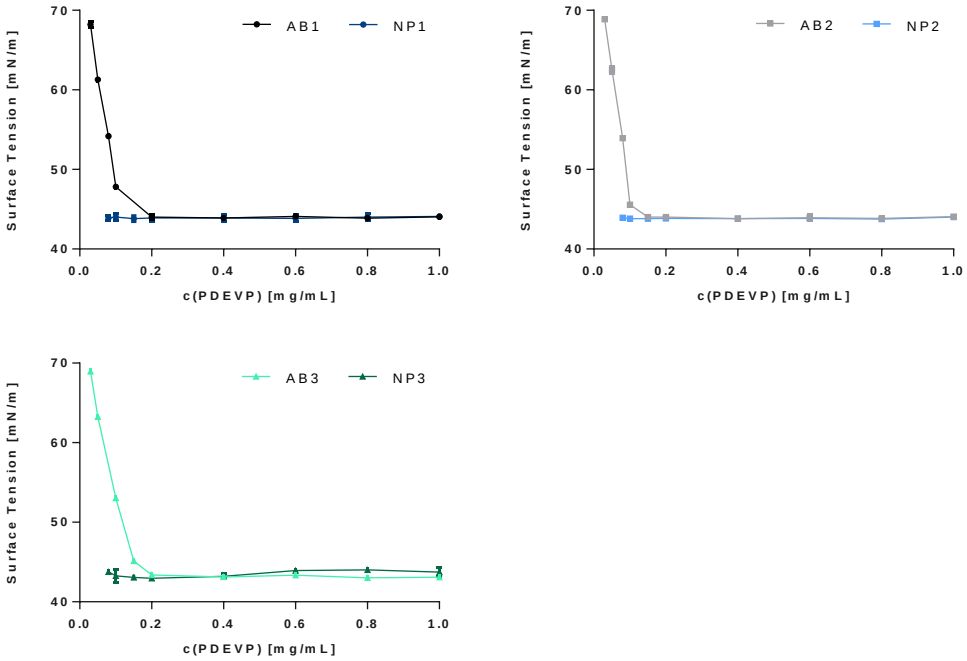

Fig. S16 Surface tension plots of AB1, NP1 (top left), AB2, NP2 (top right) and AB3, NP3 (bottom left).

3.3 Dynamic light scattering

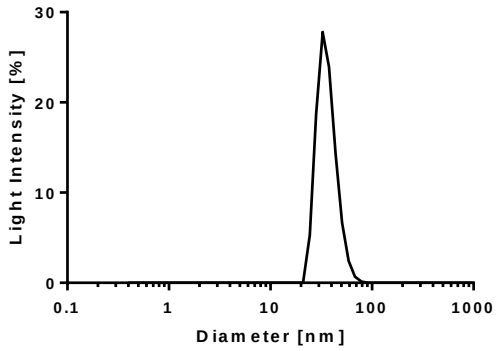

Fig. S17 Size distribution of NP1 determined *via* DLS measurement at a concentration of 2.5 mg/mL in water.

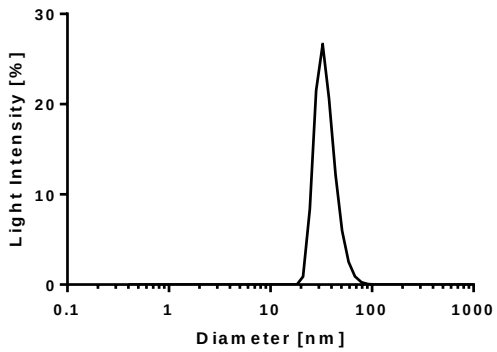

Fig. S18 Size distribution of NP2 determined *via* DLS measurement at a concentration of 2.5 mg/mL in water.

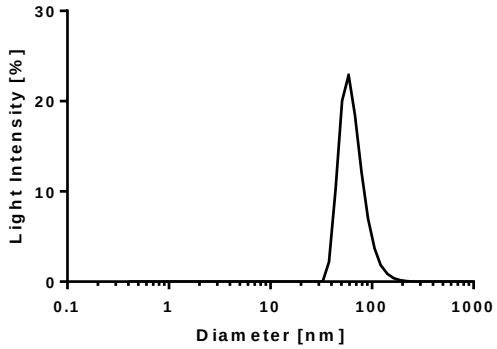

Fig. S19 Size distribution of NP3 determined *via* DLS measurement at a concentration of 2.5 mg/mL in water.

3.4 Transmission electron microscopy

The following figures S20-22 show the TEM images and their analysis. For each histogram plot with Gaussian regression fit fifty particles were measured. The mean sizes are depicted in the following table also in comparison to the DLS data.

Table 4 Diameter, polydispersity and zeta potential ζ of nanoparticles

	d [nm] (DLS)	PDI (DLS)	ζ [mV]	d [nm] (TEM)	PDI (TEM)
NP1	36.39 ± 1.09	0.030	-5.02 ± 0.10	32.54 ± 1.89	0.058
NP2	35.57 ± 2.31	0.065	-5.30 ± 0.35	28.70 ± 1.64	0.057
NP3	65.99 ± 7.65	0.116	-3.97 ± 0.21	53.19 ± 2.70	0.051

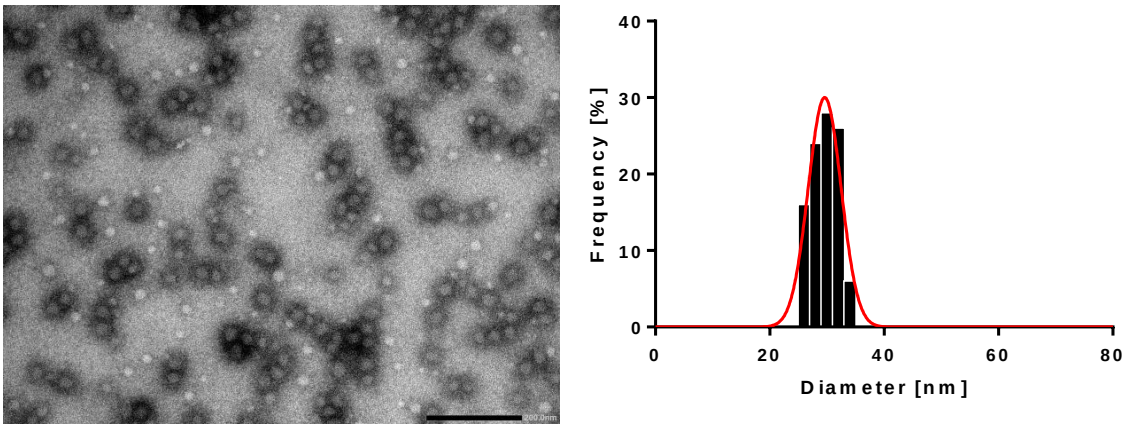

Fig. S20 TEM image of NP1 (left) and histogram plot with gaussian regression fit (right).

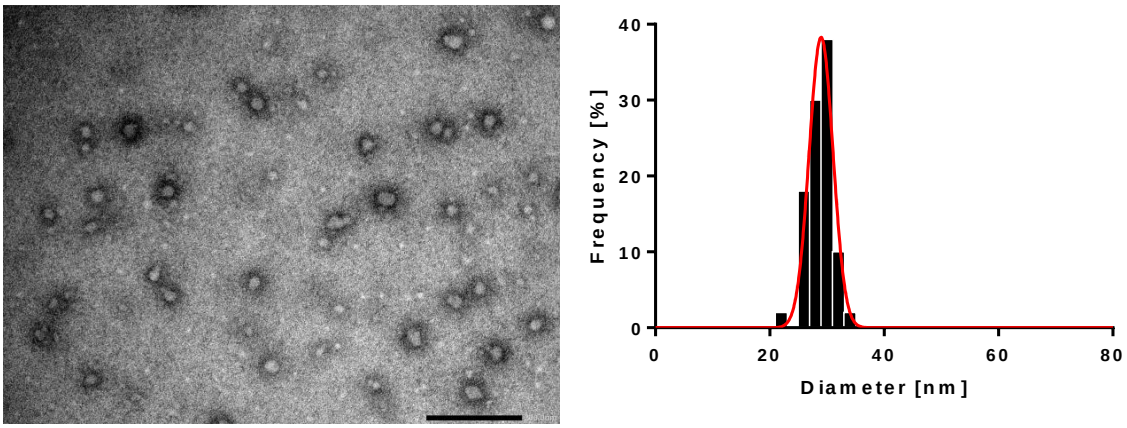

Fig. S21 TEM image of NP2 (left) and histogram plot with gaussian regression fit (right).

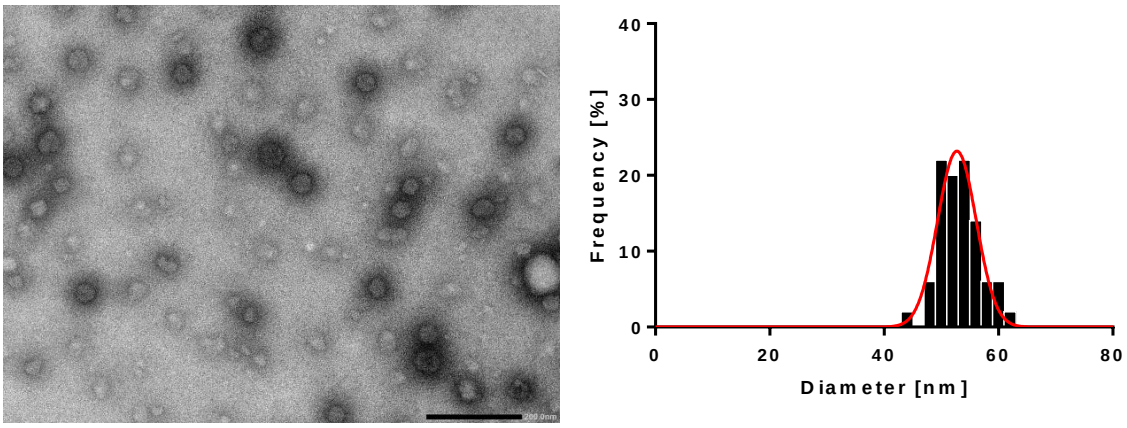

Fig. S22 TEM image of NP1 (left) and histogram plot with gaussian regression fit (right).

3.5 Loading and release properties

To obtain fluorescein loaded vehicles, firstly fluorescein was dissolved in DMSO (c = 0.3 mg/mL). Under continuous stirring the fluorescein solution was added dropwise to an ice cooled polymer solution (Polymer/Fluorescein = 12/1). The mixture was then stirred for 1 h on ice and 90 min at ambient temperature, followed by overnight dialysis against water (MWCO: 6000 – 8000).

The next day the dialysis tubes were placed in separate beakers and the release study was started. The first sample (reference) was put into 90 mL deionised water, the second, third and fourth samples into 90 mL deionised water and put into a preheated water bath (37 °C, 42 °C + 44 °C) (temperature release), and the fifth and sixth samples were put into 90 mL citrate buffer (pH = 4.3 + 6.0) (pH release). Samples of 2 mL were drawn regularly for 48 h and the beaker refilled with the appropriate amount of fresh water/buffer. The samples were then measured *via* fluorescence spectrometry and quantitatively analysed against a freshly prepared calibration curve consisting of 10 known concentrations.

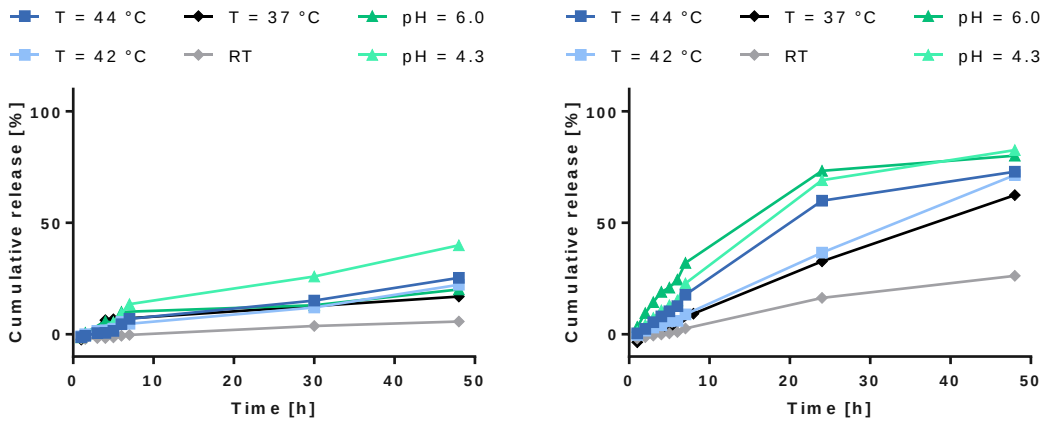

Fig. S23 Cumulative release of fluorescein from the AB1 (left) and NP1 (right) under varying conditions.

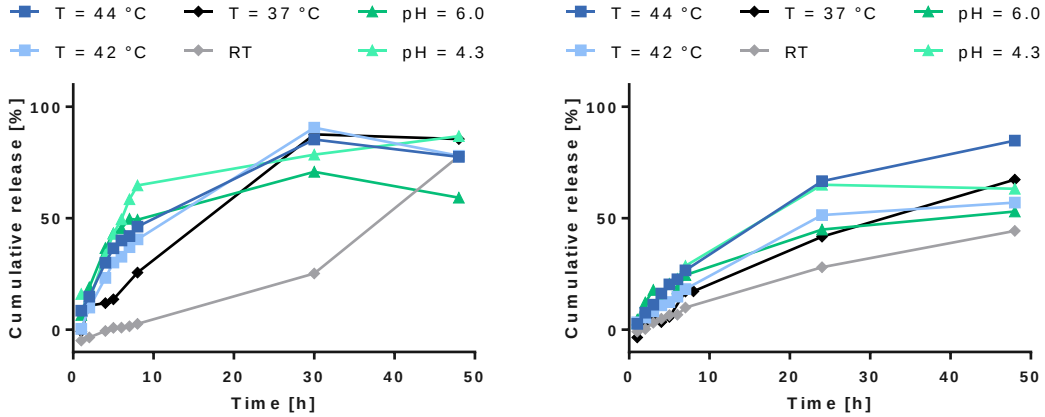

Fig. S24 Cumulative release of fluorescein from the AB2 (left) and NP2 (right) under varying conditions.

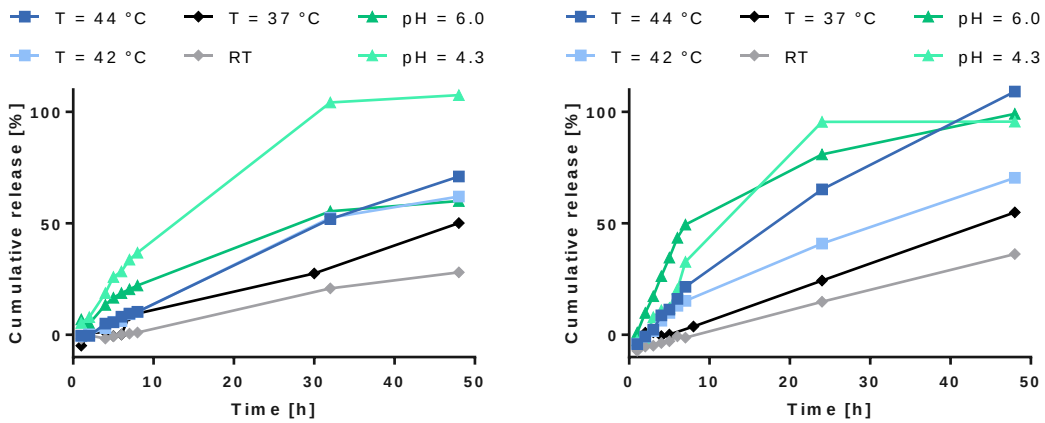

Fig. S25 Cumulative release of fluorescein from the AB3 (left) and NP3 (right) under varying conditions.

4. In vitro experiments

4.1 Cell culture

In vitro studies on nanoparticle samples were performed in HeLa and MCF-7 cells (ATCC). Cells were cultured in Dulbecco's Modified Eagle Medium (Life Technologies) equipped with 10% (v/v) Fetal Bovine Serum (Biochrom) and 1% Penicillin/Streptomycin 10000 U/mL /10000 µg/mL (Biochrom) at 37 °C in a humidified atmosphere containing 5% CO_2. For splitting and sub-culturing of cells Trypsin 0.05%/EDTA 0.02% in PBS (PAN Biotech) was used.

4.2 Cell viability studies

The growth inhibition of the nanoparticle samples on HeLa and MCF-7 cells, was determined by analysing their cell viability in presence of increasing polymer concentrations (0.08 to 5.00 mg/mL) or increasing doxorubicin (Dox) concentrations (0.09 to 6.00 µg/mL) incorporated into the particles. Prior to the addition of the samples, the cells were cultured for 24 h in 96 well flat bottom plates (TPP) with a density of 10000 cells/well. After 3 or 24 h of incubation at 37 °C in a humidified atmosphere with 5% CO_2, the cell viability of the treated cells was determined using the 3-(4,5-Dimethyl-2-thiazolyl)-2,5-diphenyl-2*H*-tetrazolium bromide reagent (MTT) (Sigma Aldrich). Therefore, MTT was dissolved at a concentration of 5 mg/mL in RPMI-1640 without phenol red (Life Technologies). PBS treated cells were used as positive control (100% viability). DMSO treated cells were used as negative control (0% viability). After 3 h of incubation with 50 µL of MTT per well at 37 °C, the blue formazan crystals were dissolved for 15 min on a plate shaker at 550 min^{-1} with 100 µL 0.04 N HCl in isopropanol and exclusion of light. Following the absorbance of each well was measured at 570 nm with 690 nm as background wavelength at a Tecan Genios Plus plate reader. Shown are mean values of at least three independent biological replicates and the respective standard deviations are indicated.

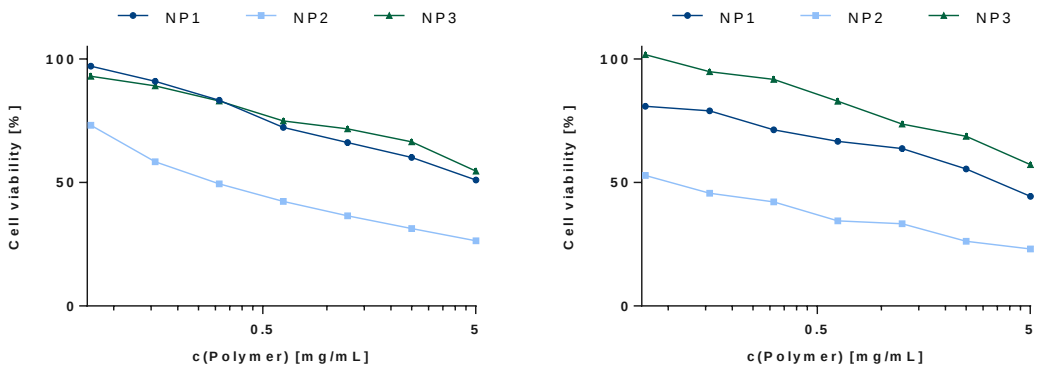

Fig. S26 Cell viability of HeLa (left) and MCF-7 cells (right) after 24 h of incubation with unloaded nanoparticle samples (measured in triplicate, standard error of the mean indicated).

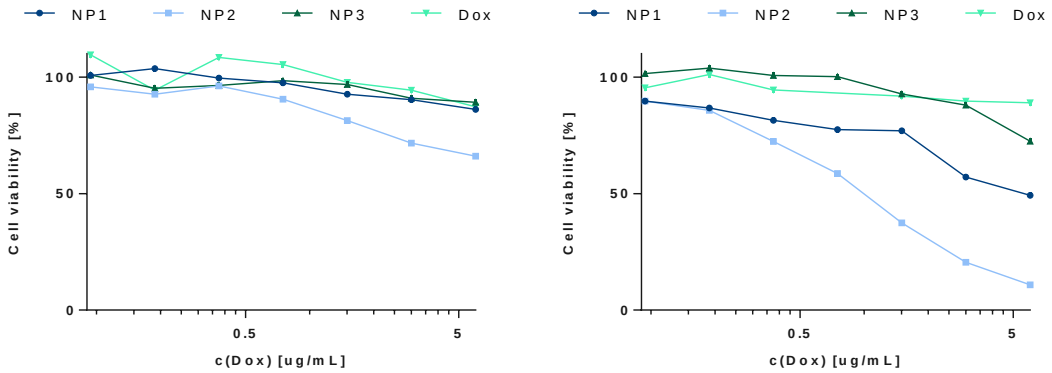

Fig. S27 Cell viability of HeLa (left) and MCF-7 cells (right) after 3 h of incubation with doxorubicin loaded nanoparticle samples (measured in triplicate, standard error of the mean indicated).

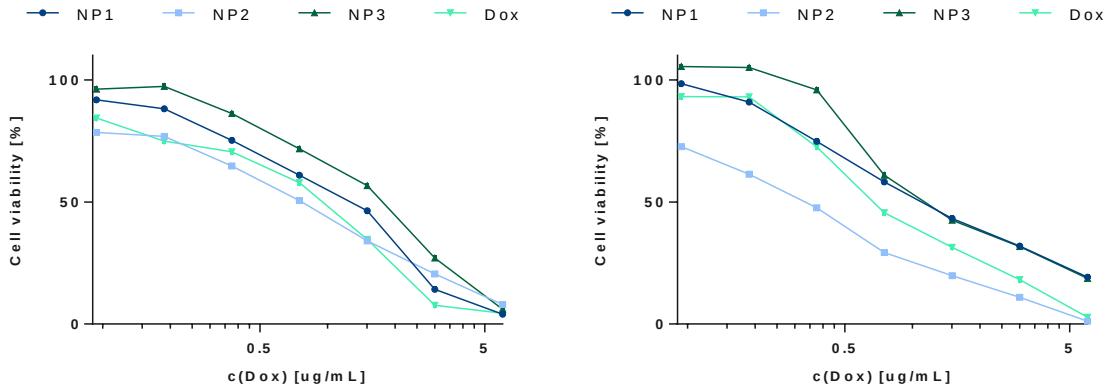

Fig. S28 Cell viability of HeLa (left) and MCF-7 cells (right) after 24 h of incubation with doxorubicin loaded nanoparticle samples (measured in triplicate, standard error of the mean indicated).

4.3 Fluorescence microscopy

For microscopic studies HeLa and MCF-7 cells were cultured for 24 h in 8-well glass chamber slides (BD Falcon). Following they were treated with a total concentration of 3.0 µg/mL of doxorubicin or particles loaded with the respective dox amount, dissolved in PBS, for 1 or 3 h at 37 °C in a humidified atmosphere with 5% CO_2. After this incubation time the samples were removed, the cells were washed with PBS and fixed with 4% Paraformaldehyd in PBS for 10 min. After three more washing steps, the chambers were removed, Vectashield (Vector Laboratories, Inc.) and the cover slip were put on top of the microscope slide. The measurements were performed on a Leica DM IL inverted fluorescence microscope with 20x magnification (scale bar = 50 µm).

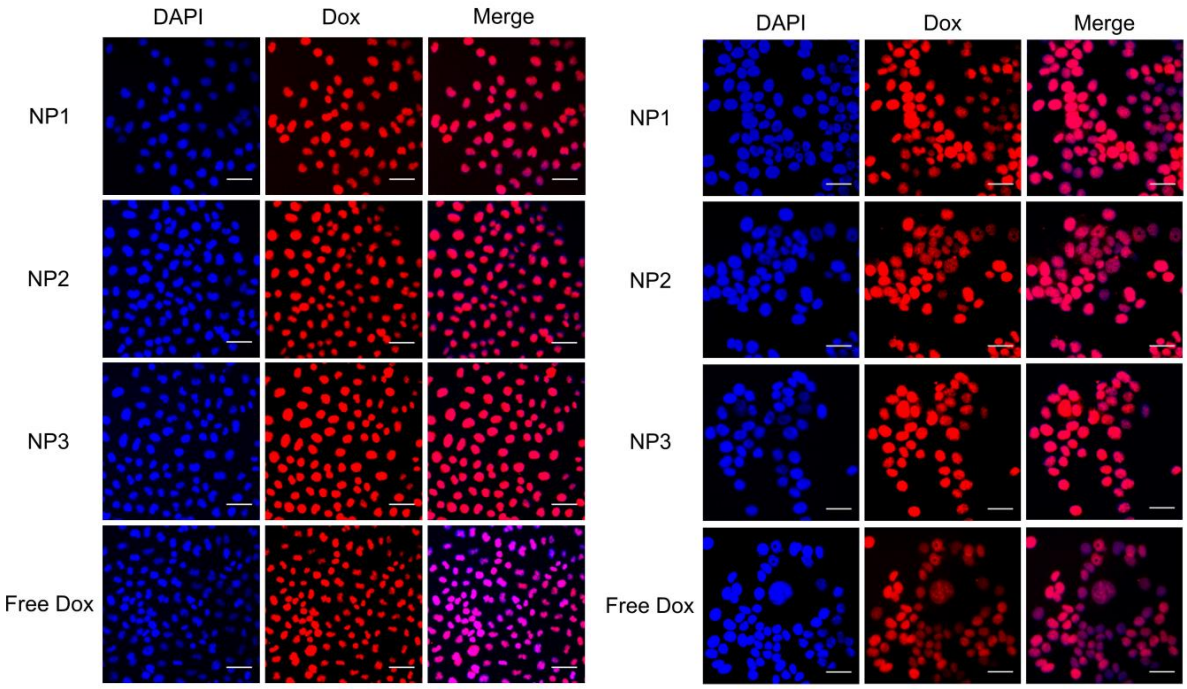

Fig. S29 Fluorescence microscopic pictures of HeLa (left) and MCF-7 (right) cells incubated with NP1, NP2, NP3 and doxorubicin for 1 h at 37 °C

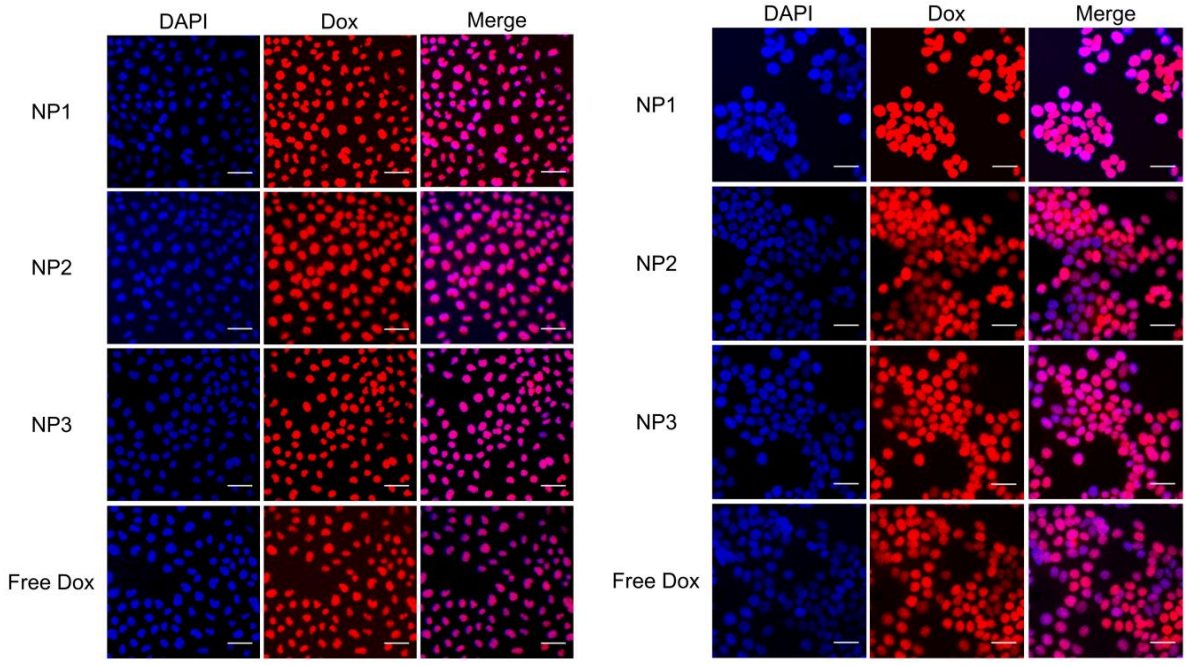

Fig. S30 Fluorescence microscopic pictures of HeLa (left) and MCF-7 (right) cells incubated with NP1, NP2, NP3 and doxorubicin for 3 h at 37 °C.

4.4 Fluorescence activated cell sorting

For flow cytometry HeLa and MCF-7 cells were cultured for 24 h in 6-well flat bottom plates (TPP) with a density of 500000 cells/well at 37 °C in a humidified atmosphere with 5% CO_2. Following they were treated with a total concentration of 3.0 µg/mL of doxorubicin or particles loaded with the respective dox amount, dissolved in PBS, for 10 min or 3 h. After this incubation time the samples were removed, the cells were washed with PBS and scraped from the plates' surface. Suspended in 0.5 mL PBS the cells were transferred to an Eppendorf tube, centrifuged, the supernatant was removed and the pellet was resuspended in 0.2 mL ice cold PBS. The measurements were performed with a FACSCanto II (BD Biosciences) and a FACSCalibur (BD Biosciences) and the data were analysed with the help of the software FlowJo.

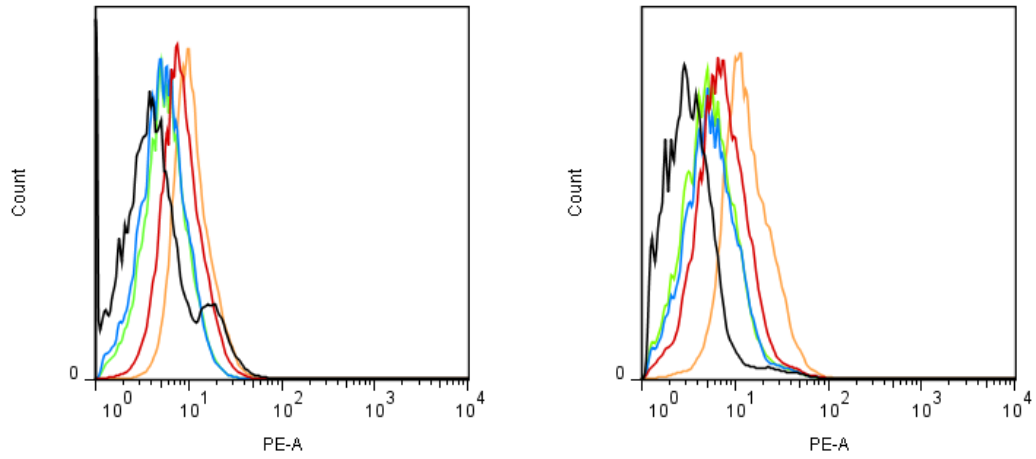

Fig. S31 Mean fluorescence intensity of HeLa (left) and MCF-7 cells (right) incubated with PBS (black) NP1 (blue), NP2 (green), NP3 (orange) and doxorubicin (red) for 10 min at 37 °C.

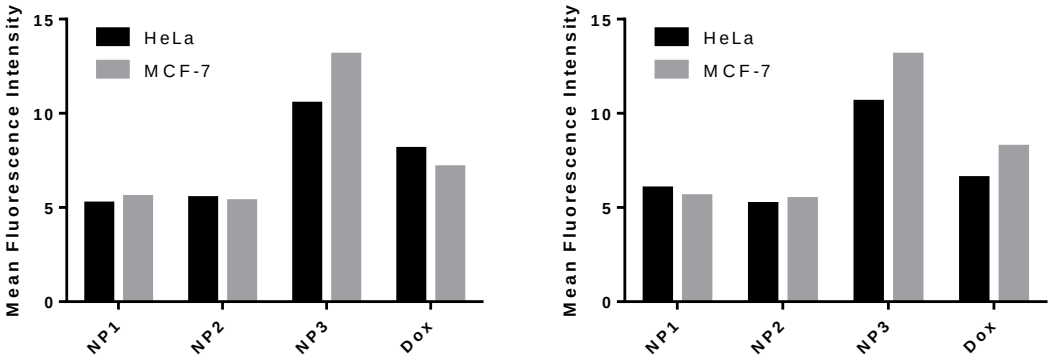

Fig. S32 Mean fluorescence intensity comparison of HeLa (black) and MCF-7 cells (grey) incubated with NP1, NP2, NP3 and doxorubicin for 10 min at 37 °C (left) and 42 °C (right).

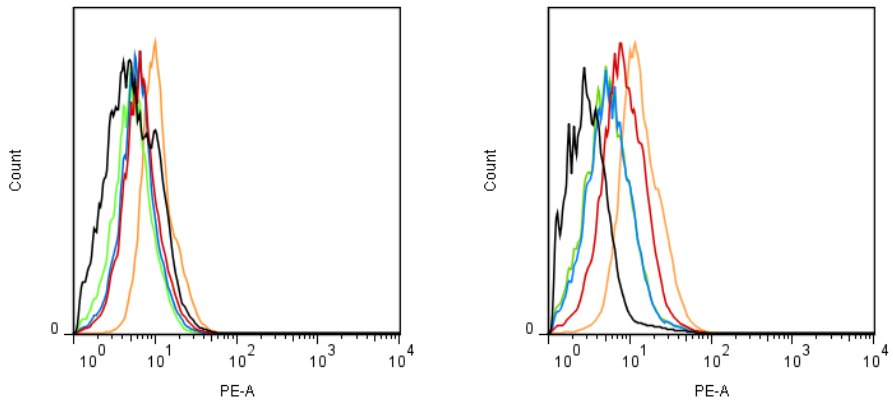

Fig. S33 Mean fluorescence intensity of HeLa (left) and MCF-7 cells (right) incubated with PBS (black) NP1 (blue), NP2 (green), NP3 (orange) and doxorubicin (red) for 10 min at 42 °C.

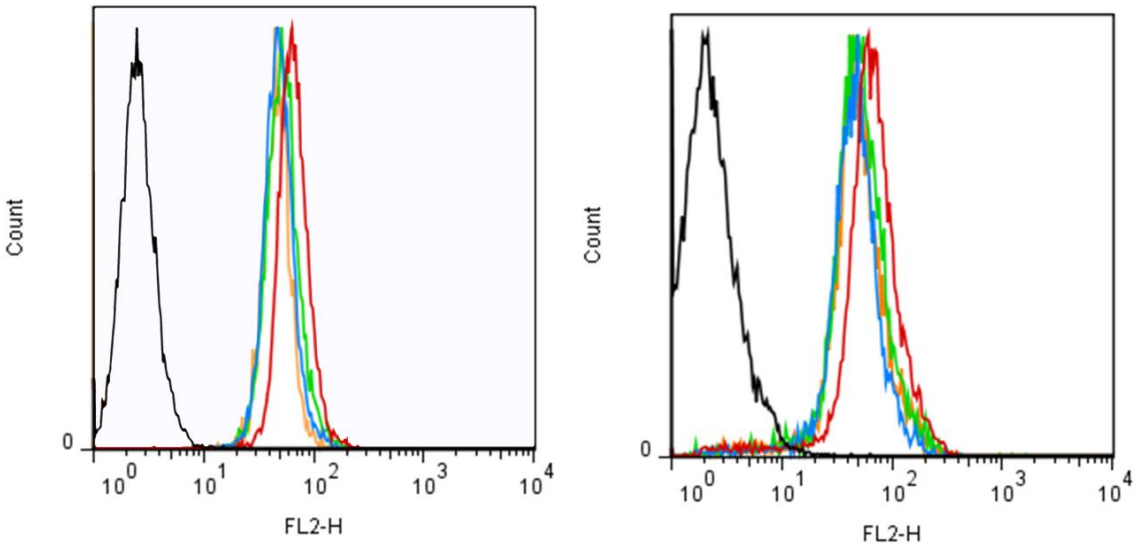

Fig. S34 Mean fluorescence intensity of HeLa (left) and MCF-7 cells (right) incubated with PBS (black) NP1 (blue), NP2 (green), NP3 (orange) and doxorubicin (red) for 3 h at 37 °C.

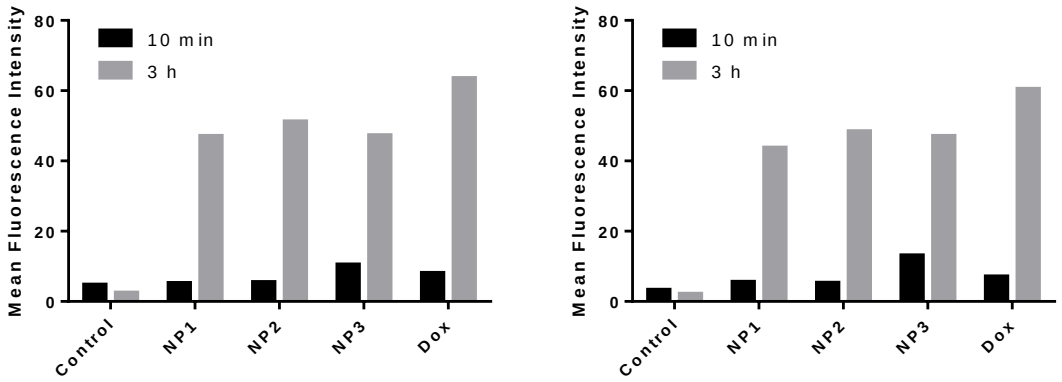

Fig. S35 Mean fluorescence intensity comparison of HeLa (left) and MCF-7 cells (right) incubated with NP1, NP2, NP3 and doxorubicin for 10 min (black) and 3 h (grey) at 37 °C.

5. Literature

[1] K. C. Hultzsch, P. Voth, K. Beckerle, T. P. Spaniol, J. Okuda, *Organometallics* **2000**, *19*, 228-243.

[2] G. D. Vaughn, K. A. Krein, J. A. Gladysz, *Organometallics* **1986**, *5*, 936-942.

[3] C.-X. Cai, L. Toupet, C. W. Lehmann, J.-F. Carpentier, *J. Organomet. Chem.* **2003**, *683*, 131-136.

[4] S. Salzinger, B. S. Soller, A. Plikhta, U. B. Seemann, E. Herdtweck, B. Rieger, *J. Am. Chem. Soc.* **2013**, *135*, 13030-13040.

[5] M. Leute, Dissertation thesis, Universität Ulm **2007**.

[6] M. A. Pudovik, G. A. Chmutova, L. K. Kibardina, S. A. Terent'eva, R. K. Bagautdinova, N. A. Khailova, R. M. Kamalov, A. N. Pudovik, *Russ. J. Gen. Chem.* **2006**, *76*, 376-380.

[7] J. Kainz, Dissertation thesis, Technische Universität München **2015**.

[8] L. Rigger, R. L. Schmidt, K. M. Holman, M. Simonović, R. Micura, *Chem. Eur. J.* **2013**, *19*, 15872-15878.

11 References

[1] *J. Chem. Edu.* **1986**, *63*, 743.

[2] R. Mülhaupt, *Angew. Chem. Int. Ed.* **2004**, *43*, 1054-1063.

[3] http://www.nobelprize.org/nobel_prizes/chemistry/laureates/1953/, **2014**, (accessed March 2018).

[4] B. S. Soller, S. Salzinger, B. Rieger, *Chem. Rev.* **2016**, *116*, 1993-2022.

[5] http://www.plasticseurope.org/application/files/5715/1717/4180/Plastics_the_facts_2017_FINAL_for_website_one_page.pdf, **2018**, (accessed March 2018).

[6] https://www.plasticseurope.org/de/resources/publications/196-plastics-facts-2013, **2013**, (accessed March 2018).

[7] https://www.plasticseurope.org/de/resources/publications/189-plastics-facts-2014, **2015**, (accessed March 2018).

[8] O. Webster, W. Hertler, D. Sogah, W. Farnham, T. V. RajanBabu, *J. Am. Chem. Soc.* **1983**, *105*, 5706-5708.

[9] M. Rikkou-Kalourkoti, O. W. Webster, C. S. Patrickios, in *Encyclopedia of Polymer Science and Technology*, **2013**.

[10] A. H. E. Müller, G. Litvinenko, D. Yan, *Macromolecules* **1996**, *29*, 2339-2345.

[11] A. H. E. Müller, G. Litvinenko, D. Yan, *Macromolecules* **1996**, *29*, 2346-2353.

[12] P. M. Mai, A. H. E. Müller, *Macromol. Rapid Commun.* **1987**, *8*, 247-253.

[13] R. P. Quirk, J. Ren, *Macromolecules* **1992**, *25*, 6612-6620.

[14] F. Adams, P. Pahl, B. Rieger, *Chem. Eur. J.* **2018**, *24*, 509-518.

[15] O. W. Webster, *J. Polym. Sci. A* **2000**, *38*, 2855-2860.

[16] O. W. Webster, in *New Synthetic Methods*, Springer Berlin Heidelberg, Berlin, Heidelberg, **2004**, pp. 1-34.

[17] Y. Zhang, M. Schmitt, L. Falivene, L. Caporaso, L. Cavallo, E. Y.-X. Chen, *J. Am. Chem. Soc.* **2013**, *135*, 17925-17942.

[18] K. Fuchise, Y. Chen, T. Satoh, T. Kakuchi, *Polym. Chem.* **2013**, *4*, 4278-4291.

[19] M.-T. Popescu, C. Tsitsilianis, C. M. Papadakis, J. Adelsberger, S. Balog, P. Busch, N. A. Hadjiantoniou, C. S. Patrickios, *Macromolecules* **2012**, *45*, 3523-3530.

[20] Y. Chen, K. Takada, N. Kubota, O.-T. Eric, T. Ito, T. Isono, T. Satoh, T. Kakuchi, *Polym. Chem.* **2015**, *6*, 1830-1837.

[21] K. Takada, T. Ito, K. Kitano, S. Tsuchida, Y. Takagi, Y. Chen, T. Satoh, T. Kakuchi, *Macromolecules* **2015**, *48*, 511-519.

[22] W. R. Hertler, *J. Polym. Sci. A* **1991**, *29*, 869-873.

[23] B. S. Soller, S. Salzinger, C. Jandl, A. Pöthig, B. Rieger, *Organometallics* **2015**, *34*, 2703-2706.

[24] H. Yasuda, H. Yamamoto, K. Yokota, S. Miyake, A. Nakamura, *J. Am. Chem. Soc.* **1992**, *114*, 4908-4910.

[25] S. Collins, D. G. Ward, *J. Am. Chem. Soc.* **1992**, *114*, 5460-5462.

[26] H. Yasuda, H. Yamamoto, M. Yamashita, K. Yokota, A. Nakamura, S. Miyake, Y. Kai, N. Kanehisa, *Macromolecules* **1993**, *26*, 7134-7143.

[27] H. Yasuda, *J. Organomet. Chem.* **2002**, *647*, 128-138.

[28] F. H. Westheimer, *Science* **1987**, *235*, 1173-1178.

[29] S. C. Kamerlin, P. K. Sharma, R. B. Prasad, A. Warshel, *Q. Rev. Biophys.* **2013**, *46*, 1-132.

[30] M. V. Chaubal, A. S. Gupta, S. T. Lopina, D. F. Bruley, *Crit. Rev. Ther. Drug Carrier Syst.* **2003**, *20*.

[31] D.-P. Chen, J. Wang, *Macromolecules* **2006**, *39*, 473-475.

[32] C.-S. Xiao, Y.-C. Wang, J.-Z. Du, X.-S. Chen, J. Wang, *Macromolecules* **2006**, *39*, 6825-6831.

[33] S. Zhang, J. Zou, F. Zhang, M. Elsabahy, S. E. Felder, J. Zhu, D. J. Pochan, K. L. Wooley, *J. Am. Chem. Soc.* **2012**, *134*, 18467-18474.

[34] F. Zhang, S. Zhang, S. F. Pollack, R. Li, A. M. Gonzalez, J. Fan, J. Zou, S. E. Leininger, A. Pavía-Sanders, R. Johnson, *J. Am. Chem. Soc.* **2015**, *137*, 2056-2066.

[35] U. B. Seemann, J. E. Dengler, B. Rieger, *Angew. Chem. Int. Ed.* **2010**, *49*, 3489-3491.

[36] S. Salzinger, B. Rieger, *Macromol. Rapid Commun.* **2012**, *33*, 1327-1345.

[37] N. Zhang, S. Salzinger, B. Rieger, *Macromolecules* **2012**, *45*, 9751-9758.

[38] A. Ford-Moore, J. H. Williams, *J. Chem. Soc.* **1947**, 1465-1467.

[39] G. M. Kosolapoff, *J. Am. Chem. Soc.* **1948**, *70*, 1971-1972.

[40] M. Leute, Dissertation thesis, Universität Ulm **2007**.

[41] J. Kainz, Dissertation thesis, Technische Universität München **2015**.

[42] D. Lanzinger, S. Salzinger, B. S. Soller, B. Rieger, *Ind. Eng. Chem. Res.* **2015**, *54*, 1703-1712.

[43] R. H. Herpel, P. Vedantham, D. L. Flynn, P. R. Hanson, *Tetrahedron Lett.* **2006**, *47*, 6429-6432.

[44] N. B. Orm, Y. Dkhissi, S. Daniele, L. Djakovitch, *Tetrahedron* **2013**, *69*, 115-121.

[45] M. Essahli, M. El Asri, A. Boulahna, M. Zenkouar, M. Viguier, Y. Hervaud, B. Boutevin, *J. Fluor. Chem.* **2006**, *127*, 854-860.

[46] B. Bingöl, G. Hart-Smith, C. Barner-Kowollik, G. Wegner, *Macromolecules* **2008**, *41*, 1634-1639.

[47] T. Sato, M. Hasegawa, M. Seno, T. Hirano, *J. Appl. Polym. Sci.* **2008**, *109*, 3746-3752.

[48] S. V. Shulyndin, Y. A. Levin, B. E. e. Ivanov, *Russ. Chem. Rev.* **1981**, *50*, 865.

[49] M. H. Bride, W. A. W. Cummings, W. Pickles, *J. Appl. Chem.* **1961**, *11*, 352-357.

[50] C. Blomberg, *J. Organomet. Chem.* **1972**, *45*, 1-137.

[51] T. Wagner, A. Manhart, N. Deniz, A. Kaltbeitzel, M. Wagner, G. Brunklaus, W. H. Meyer, *Macromol. Chem. Phys.* **2009**, *210*, 1903-1914.

[52] D. M. Paisley, C. Marvel, *J. Polym. Sci. A* **1962**, *56*, 533-538.

[53] B. S. Soller, N. Zhang, B. Rieger, *Macromol. Chem. Phys.* **2014**, *215*, 1946-1962.

[54] J. E. Dengler, Diploma Thesis thesis, Technische Universität München **2007**.

[55] S. Salzinger, U. B. Seemann, A. Plikhta, B. Rieger, *Macromolecules* **2011**, *44*, 5920-5927.

[56] S. Salzinger, B. S. Soller, A. Plikhta, U. B. Seemann, E. Herdtweck, B. Rieger, *J. Am. Chem. Soc.* **2013**, *135*, 13030-13040.

[57] E. Y.-X. Chen, *Chem. Rev.* **2009**, *109*, 5157-5214.

[58] H. Nguyen, A. P. Jarvis, M. Lesley, W. M. Kelly, S. S. Reddy, N. J. Taylor, S. Collins, *Macromolecules* **2000**, *33*, 1508-1510.

[59] P. L. Watson, *J. Am. Chem. Soc.* **1983**, *105*, 6491-6493.

[60] P. L. Watson, *Chem. Comm.* **1983**, 276-277.

[61] D. Steinborn, in *Grundlagen der metallorganischen Komplexkatalyse*, Springer, **2010**, pp. 283-313.

[62] R. Waterman, *Organometallics* **2013**, *32*, 7249-7263.

[63] B.-J. Deelman, M. Booij, A. Meetsma, J. H. Teuben, H. Kooijman, A. L. Spek, *Organometallics* **1995**, *14*, 2306-2317.

[64] R. Duchateau, C. T. van Wee, J. H. Teuben, *Organometallics* **1996**, *15*, 2291-2302.

[65] R. Duchateau, E. A. Brussee, A. Meetsma, J. H. Teuben, *Organometallics* **1997**, *16*, 5506-5516.

[66] S. N. Ringelberg, A. Meetsma, S. I. Troyanov, B. Hessen, J. H. Teuben, *Organometallics* **2002**, *21*, 1759-1765.

[67] V. F. Quiroga Norambuena, A. Heeres, H. J. Heeres, A. Meetsma, J. H. Teuben, B. Hessen, *Organometallics* **2008**, *27*, 5672-5683.

[68] H. Kaneko, H. Nagae, H. Tsurugi, K. Mashima, *J. Am. Chem. Soc.* **2011**, *133*, 19626-19629.

[69] Y.-J. Kim, Y. T. Matsunaga, *J. Mater. Chem. B* **2017**, *5*, 4307-4321.

[70] C. Weber, R. Hoogenboom, U. S. Schubert, *Prog. Polym. Sci* **2012**, *37*, 686-714.

[71] J.-F. Lutz, Ö. Akdemir, A. Hoth, *J. Am. Chem. Soc.* **2006**, *128*, 13046-13047.

[72] C. E. Hoyle, C. N. Bowman, *Angew. Chem. Int. Ed.* **2010**, *49*, 1540-1573.

[73] A. B. Lowe, *Polym. Chem.* **2010**, *1*, 17-36.

[74] G. M. Miyake, E. Y.-X. Chen, *Macromolecules* **2008**, *41*, 3405-3416.

[75] N. Zhang, S. Salzinger, B. S. Soller, B. Rieger, *J. Am. Chem. Soc.* **2013**, *135*, 8810-8813.

[76] F. Adams, P. Altenbuchner, P. Werz, B. Rieger, *RSC Adv.* **2016**, *6*, 78750-78754.

[77] P. T. Altenbuchner, P. D. Werz, P. Schöppner, F. Adams, A. Kronast, C. Schwarzenböck, A. Pöthig, C. Jandl, M. Haslbeck, B. Rieger, *Chem. Eur. J.* **2016**, *22*, 14576-14584.

[78] T. Sun, Y. S. Zhang, B. Pang, D. C. Hyun, M. Yang, Y. Xia, *Angew. Chem. Int. Ed.* **2014**, *53*, 12320-12364.

[79] Y. Matsumura, K. Kataoka, *Cancer Sci.* **2009**, *100*, 572-579.

[80] J. Wang, W. Mao, L. L. Lock, J. Tang, M. Sui, W. Sun, H. Cui, D. Xu, Y. Shen, *ACS Nano* **2015**, *9*, 7195-7206.

[81] M. Alibolandi, F. Sadeghi, K. Abnous, F. Atyabi, M. Ramezani, F. Hadizadeh, *Eur. J. Pharm. Biopharm.* **2015**, *94*, 521-531.

[82] L. Qiu, C.-Y. Hong, C.-Y. Pan, *Int. J. Nanomed.* **2015**, *10*, 3623-3640.

[83] Y.-M. Li, T. Jiang, Y. Lv, Y. Wu, F. He, R.-X. Zhuo, *Colloids Surf., B* **2015**, *132*, 54-61.

[84] W. Chen, F. Meng, R. Cheng, C. Deng, J. Feijen, Z. Zhong, *J. Control. Release* **2015**, *210*, 125-133.

[85] E. S. Kim, C. Durairaj, R. S. Kadam, S. J. Lee, Y. Mo, D. H. Geroski, U. B. Kompella, H. F. Edelhauser, *Pharm. Res.* **2009**, *26*, 1155-1161.

[86] C. D. Magnusson, D. Liu, E. Y.-X. Chen, M. A. Kelland, *Energy Fuels* **2015**, *29*, 2336-2341.

[87] C. Schwarzenböck, A. Schaffer, P. Pahl, P. J. Nelson, R. Huss, B. Rieger, *Polym. Chem.* **2018**, *9*, 284-290.

[88] C. Schwarzenböck, A. Schaffer, E. Nößner, P. J. Nelson, R. Huss, B. Rieger, *Chem. Eur. J.* **2018**, *24*, 2584-2587.

[89] D. J. O'Shannessy, E. B. Somers, E. Albone, X. Cheng, Y. C. Park, B. E. Tomkowicz, Y. Hamuro, T. O. Kohl, T. M. Forsyth, R. Smale, *Oncotarget* **2011**, *2*, 1227.

[90] S. Gorle, M. Ariatti, M. Singh, in *2nd International Conference on Geological and Environmental Sciences IPCBEE: Hong Kong*, **2013**.

[91] P. L. Yeagle, *Biochim. Biophys. Acta, Biomembr.* **1985**, *822*, 267-287.

[92] P. Yeagle, *Biochimie* **1991**, *73*, 1303-1310.

[93] L. Rigger, R. L. Schmidt, K. M. Holman, M. Simonović, R. Micura, *Chem. Eur. J.* **2013**, *19*, 15872-15878.

[94] C. Schwarzenböck, P. J. Nelson, R. Huss, B. Rieger, *Nanoscale* **2018**, *10*, 16062-16068.

[95] P. T. Altenbuchner, B. S. Soller, S. Kissling, T. Bachmann, A. Kronast, S. I. Vagin, B. Rieger, *Macromolecules* **2014**, *47*, 7742-7749.

[96] T. Yoshikawa, L. P. Ruhr, W. Flory, D. Giamalva, D. F. Church, W. A. Pryor, *Toxicol. Appl. Pharmacol.* **1985**, *79*, 218-226.